Synthesis and characterisation of molecularly imprinted nanoparticles with enzyme-like catalytic activity for the Kemp elimination

Servant, Ania

UNIVERSITY OF LONDON

SYNTHESIS AND CHARACTERISATION OF MOLECULARLY IMPRINTED NANOPARTICLES WITH ENZYME-LIKE CATALYTIC ACTIVITY FOR THE KEMP ELIMINATION

A thesis presented in part fulfilment of the Degree of Doctor of Philosophy at the University of London

BY

ANIA SERVANT, MSc in Polymer Sciences, Ecole Nationale Superieure de Chimie de Paris (France)

June 2010

School of Biological and Chemical Sciences

Queen Mary University of London

THESIS ABSTRACT

The development of new efficient catalysts with more economical processes and lower environmental impact has now become a major challenge in chemical research. Although it is now well-established that catalysis employs nanoscale processes, the concept of using nanomaterials as new potential catalysts is very recent. This new area of research has today found its place as *nanocatalysis*. The global aim of this work is to generate synthetic materials capable of behaving like enzymes, with high catalytic efficiency and good selectivity. These materials would supplement enzymes in conditions where these natural catalysts are not utilisable. Our focus is on the synthesis of molecularly imprinted nanogels with catalytic activity for hydrolytic and carbon-carbon bond formation reactions. The advantages of using nanogels as polymer matrix for the generation of catalytic imprinted polymers have been intensively studied and proven in our group and led to two major publications. However, since the dimensions of the nanogels prepared are over the length scale of a single active site, it is essential to investigate the impact of their size, their morphology along with their behaviour in different solvent systems as these parameters will have an effect on their catalytic efficiency and selectivity. The knowledge gained from these studies will lead us to the generation of tailor-made imprinted nanogels with more understanding of their dynamic nature.

This thesis has focussed on the rationalisation of the effects of different experimental parameters on the catalytic activity and imprinting efficiency of molecularly imprinted nanogels, using the Kemp elimination as a model reaction. The correlation between the morphology and the structure of the particles and their catalytic behaviour was investigated. This consisted of altering polymerization parameters such as initiator content and monomer-template ratio, and also external stimuli such as organic solvent content, surfactants and temperature alterations, that can play a role in the swelling of the particles.

The non-covalent complex formation between the functional monomer (4-vynilpiridine) and the template (indole) was studied ^{1}H-NMR. The optimal interaction between both molecules is found to be in non-polar solvents. Soluble nanogels synthesized in a suitable solvent using high dilution radical polymerization, were obtained with a good yield. The size of the particles was characterized by dynamic light scattering nm and Electronic Microscopy and was found to be around 15 nm. The number of the active sites was determined by an acid-base titration of pyridine moieties inside the polymer, allowing an accurate determination of the kinetic parameters such as k_{cat} and K_M. The imprinted nanoparticles show significant catalytic activity with 617-fold enhancement over the background reaction. The use of surfactant shows a significant improvement of the catalytic activity, imprinting efficiency and affinity of the polymers towards the substrate. This is in correlation with the effect of surfactant in the size of the nanogels that is decreased from 15 nm to 7 nm. The imprinted nanoparticles also display good selectivity properties when using different substrates.

DEDICATED TO MY LATE GRAND-MOTHER

Annette JACQUENS (1922-2007)

ACKNOWLEDGMENTS

I would like to thank deeply my supervisor Dr. Marina Resmini for her constant help throughout my PhD and her helpful advices that allowed me to gain so much experience and confidence.

I would like to thank all the members of NASCENT network for their help and friendship. Being a member of NASCENT made me feel like being a part of a family for four amazing years.

I would like to thank Prof. Karsten Haupt, for his friendly welcome in France during my two week secondement.

I would like to thank Prof. Alice Sullivan and Dr. Ali Zarbakhsh for their helpful comments and advices as members of my panel.

I would like to thank all the member of Marina Resmini research group, past and present for their friendship, help and support during hard times.

I would like to thank everybody in the Joseph Priesley Building for their friendship and support.

I would like to thank Mr Alan Bradshaw for his endless patience with my mistakes in my orders, the technical staff of Joseph Priesley Building, and all the members of the store.

I would like to thank the European Union and Marie Curie Actions for funding this project, and Queen Mary University of London.

I would like to thank Mark for his great help in this thesis and his endless patience and my family for their constant support and faith in me.

LIST OF ABBREVIATIONS

AIBN = Azobisisobutyronitrile

ACN = Acetonitrile

C_M = Monomer concentration

CLC = Critical gelation conentration

DCE = 1,2-dichloroethane

DLS = Dynamic Light Scattering

DMF = Dimethylformamide

DMSO = Dimethylsulfoxide

EGDMA = Ethylene Glycol Dimethacrylate

HPLC = High Performance Liquid Chromatography

k_{cat} = rate constant of the catalysed reaction

K_M = Michaelis-Menten constant

MIP = Molecularly Imprinted Polymer

NIP = Non-imprinted polymer

NPs = Nanoparticles

SANS = Small Angle Neutron Scattering

TEM = Transmission Electron Microscopy

Tris = 2-amino-2-hydroxymethyl-1,3-propandiol

4-VP = 4-vinylpyridine

V_{Max} = Maximum velocity

CONTENTS

TABLE OF FIGURES

CHAPTER 1

INTRODUCTION

1 Introduction

1.1 General objectives and overview

The global aim of this work is to generate synthetic materials capable of behaving like enzymes with potential industrial applications. Enzymes are known to be powerful catalysts that can recognize specifically a substrate and tremendously accelerate the reaction rate by lowering the activation energy of the crucial intermediate of the reaction. However due to their nature, enzymes cannot be employed under harsh conditions such as organic solvents or at high temperature since, as proteins, they are easily denatured. There is an increasing necessity today in chemical research to create new efficient catalysts capable of complementing the work of enzymes in a wider range of conditions. In response to these needs, huge efforts have been put in to the generation of synthetic materials referred to as *enzyme mimics*; catalytic antibodies and catalytic imprinted polymers are good examples of these[1].

The objectives of this work are to develop a systematic method to improve the catalytic efficiency of imprinted nanogels towards a model reaction and to contribute to the understanding of how these complex systems behave. The ultimate goal is to successfully exploit nanogel material properties and to be able to design and tailor-make catalytic imprinted nanogels for specific reactions. In our group, we study the application of microgels and nanogels as polymer format in combination with the molecular imprinting approach for the development of novel catalysts. This has resulted in two major publications, where imprinted nanogels demonstrated good results and great potential[2-3].

The focal point of this thesis was the optimization of the catalytic activity and imprinting efficiency of imprinted nanogels for a model reaction. The correlation between morphology and structure changes of the particles with their catalytic behaviour was also investigated. This consisted of altering certain polymerization

parameters such as initiator content or monomer-template ratio, and also external stimuli such as organic solvent content, use of surfactants and temperature which play a role in the swelling of the particles. Most of the work was carried out at Queen Mary University of London; however some characterization experiments were performed at University of Technology of Compiègne (U.T.C.) in France under the supervision of Prof. Karsten Haupt in partnership with the NASCENT European network.

The imprinting approach was used for the generation of specific three-dimensional cavities inside a nanogel-like polymer matrix. The model system chosen to perform all the kinetic studies was based on the Kemp elimination reaction, which is the base-catalyzed isomerisation of benzisoxazoles resulting in the formation of cyanophenols[4]. This reaction has been intensively studied in the past and still today much effort is put into the development of catalysts since there is no enzyme for this reaction[5]. Its mechanism is therefore well established. In addition, which is very convenient for data collection, this system offers the possibility to work under a variety of conditions, making it versatile. The choice of the template molecule and functional monomer was made based on the transition state analogue approach following the pathway determined for the targeted reaction.

The specificity of the nanogels was investigated by studying the catalytic and imprinting efficiency of the nanoparticles with using another substrate molecule notably with the presence of a nitro group. Another approach to evaluate the selectivity of the polymer matrix was to prepare nanogels imprinted with another template such as nitro-indole and to investigate the catalytic activity with both substrates, benzisoxazole and 5-nitrobenzisoxazole.

Different types of techniques were employed to study and characterize the morphology of the nanogel particles. Dynamic Light Scattering measurements, using a Zetasizer instrument, were performed to determine the average diameter of the particles. The data were confirmed by imaging the polymers using Transmission Electron Microscopy (T.E.M.). Both instruments were available at Queen Mary University of London, although some images were collected at the University of

Technology of Compiègne in France. Further characterizations of size and morphology of the nanoparticles were conducted using Small Angle Neutron Scattering (S.A.N.S.) at Isis laboratories in Rutherford facilities in Oxfordshire. The determination of the number of active sites, which is the number of pyridine residues incorporated inside the nanogel matrix, was also carried out as it allows an accurate calculation of the kinetic parameters such as k_{cat}. This was performed using a back-titration procedure of the pyridine moieties inside the nanogels.

1.2 Advances in nanotechnologies

"A macrophysics phenomenon is a fact observable directly and a microphysics phenomenon is a fact which we have to admit the existence without being able to observe it directly"
Louis de Bröglie, 1929 (Physics Nobel Price)

Nanoscience and nanotechnology have become the focal point of many areas in scientific research over the last 20 years and has generated considerable changes in our day to day life. More than just an enormous scientific advance it has now turned into a social matter. Incredible progress in microelectronics, data storage and optoelectronics are good examples of the versatility of this new science. How can we define and identify this new gigantic science-technology field? How can the word nano make such a difference? Numerous definitions of nanoscience are available in the literature but they all seem to converge towards a unique definition:

"*Nanoscience is the study of phenomena and manipulation of materials at atomic, molecular and macromolecular scales, where properties differ significantly from those at larger scales*"[6].

It is now possible to manipulate and use atoms[7], molecules[8], clusters and nanoparticles[9-10] as primary blocks for the construction of advanced and novel phases of condensed matter on the nanometre scale. At this scale a new world arises where

chemistry and physics come together and novel properties of matter are being discovered and developed. A notorious scheme of this convergence is shown in **Figure 1**. Mastering these properties can direct us to new science as well as innovative products, devices and technologies. This exponential growth of nanoscience and technology could possibly be explained by the development of novel methods to synthesize nanomaterials but beyond all doubt by the discovery of new tools for characterization and manipulation[11]. Around 50 years ago, Richard Feynmann in his notorious speech "*there is plenty of room in the bottom*"[12] claimed that nanoscale science and engineering would necessitate the development of accurate experimental tools and techniques that could visualize the nanoworld, and potentially alter it, indeed it has.

This trend towards miniaturization is inspired by a similar phenomenon that appeared in the semi-conductor industry during the late 20th century, with the aim of developing smaller and faster computers to the current ultimate goal of creating the quantum computer[13-15]. However, the need to create smaller and smaller objects is also encouraged by the desire to develop novel devices of other types in different areas of research such as micro and nano-electromechanical systems, gas and chemical sensors or biomedical equipment. Numerous innovative methods for the synthesis of nanoparticles and nanotubes, and their assemblies, are now well-developed and established. Moreover novel methods of fabricating ordered nanostructures, along with new devices and concepts, are being currently discovered. Examples including nanostructured biomaterials for tissue engineering[16] and mechanical devices that operate at sub-micron length scales are now described in the literature.

For all these reasons, it can be predicted that nanotechnology will have a similar or stronger impact on our modern society than the silicon integrated circuit (which led to the "electronic revolution" of the 20th century), especially when its effects have consequences on such different fields of human activity as medicine, security and telecommunication[17]. Some concepts in nanoscience are not new; a lot of current technologies function with nanoscale processes, catalysis and photography are good examples of these. Nevertheless our ability to generate, structure and tailor-

make materials at nanoscale is very recent. Therefore the next step and goal of the science and technology of nanomaterials should be to completely master the production of isolated nanostructures and their assemblies with the desired properties; to investigate and establish concepts of nanodevices; to build new classes of high performance materials, including biologically-inspired systems; and to invent more instruments for the characterisation of nanostructures[11].

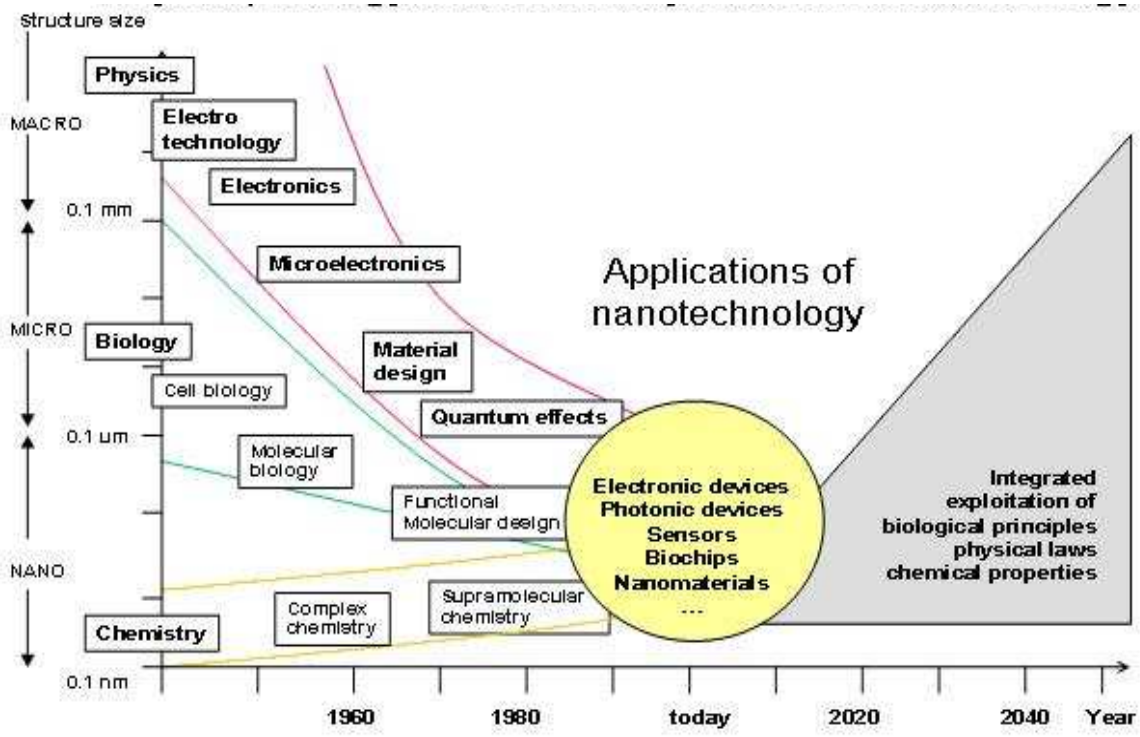

Figure 1: Research approach in nanotechnology: Convergence of the different science fields in one[18].

1.3 Nanomaterials and catalysis

Catalysis has always constituted a fundamental and central field of nanoscience and nanotechnology[19], the ultimate goal being to develop more economical processes with a lower environmental impact. The development of many compounds, now indispensable for our modern society, would not have been possible without the existence of catalysts. Catalysts are able to regulate the pathways of chemical

reactions, lowering the activation energy of the crucial intermediate of the reaction, making possible the formation of targeted products at a rate that is commercially viable. Nowadays, the main focus in the search for new efficient and tailor-made catalysts is to fully understand the steps of catalysis at the nanoscopic scale. This could lead us to the generation of a new class of catalysts with more activity and specificity.

Currently most industrial catalysts are found to be high-surface-area active solids, scattered in the form of very small particles. The dimension of these entities ranges from 1 to 20 nm. This tendency to use smaller and smaller catalysts was initiated by the need to maximize the surface area and therefore of reducing the specific cost per function[20]. The size of the particles is a critical parameter for the functioning of catalysts and has encouraged researchers to invest in the development of highly active nanoparticles (NPs) as novel active species. The fact that nanomaterials exhibit properties that differ from their bulk counterparts can be explained partly by surface effect. Atoms located at the surface of particles are in contact with fewer atoms than their bulk counterpart. Due to this low coordination and unsatisfied bonds, these atoms exhibit higher activity and their average binding energy is increased. When the particles or clusters are smaller, the number of atoms at the surface is higher. The atoms located on the edge and corners of particles are even less coordinated than those on surfaces and therefore display tighter bonding to foreign atoms and molecules[21]. In fact, nanomaterials are not well-defined cubes or spheres and possess numerous defects that expose more atoms on the edges and on corners. The enhancement of reactivity of these low coordination sites may be to a large extent responsible for the enhanced catalytic activity of nanoparticles compared to the bulk materials.

The application of nanomaterials and more specifically nanoparticles (NPs) in catalysis appeared first in the 19th century with photography with the use of silver-NPs (Ag-NPs) and the decomposition of hydrogen peroxide (Pt-NPs)[22]. Innovative catalytic applications of NPs were then communicated in 1940 by Nord on nitrobenzene reduction[23], followed by Parravano in 1970 where hydrogen-atom transfer between benzene and cyclohexane and oxygen-atom transfer between CO and CO_2 were

catalyzed using gold-NPs (Au-NPs)[24]. The real breakthrough appeared with Haruta's original studies on oxide-supported gold-NP-catalyzed CO oxidation by O_2 at low temperatures[25-26]. This decade has witnessed an exponential growth of catalytic studies with NPs in the fields of redox-catalysis, photo-catalysis, hydrogenation of unsaturated substrates and oxidations. In the mid-1990s, preliminary studies of palladium-NPs (Pd-NPs) catalysis were described by Reetz for Heck Carbon-Carbon coupling[27]. This example of Pd-NPs usage will be described in greater details later in section 1.3.1.1.1.

The beginning of the 21st century saw an explosive growth in the research field of nanomaterials for catalysis with the ultimate aim of improving catalytic activities and selectivity and studying the catalytic mechanisms with more understanding[28]. Therefore the utilisation of nanomaterials in catalysis has become an area of great interest and a vast variety of nanomaterials are currently being developed as described in **Figure 2**.

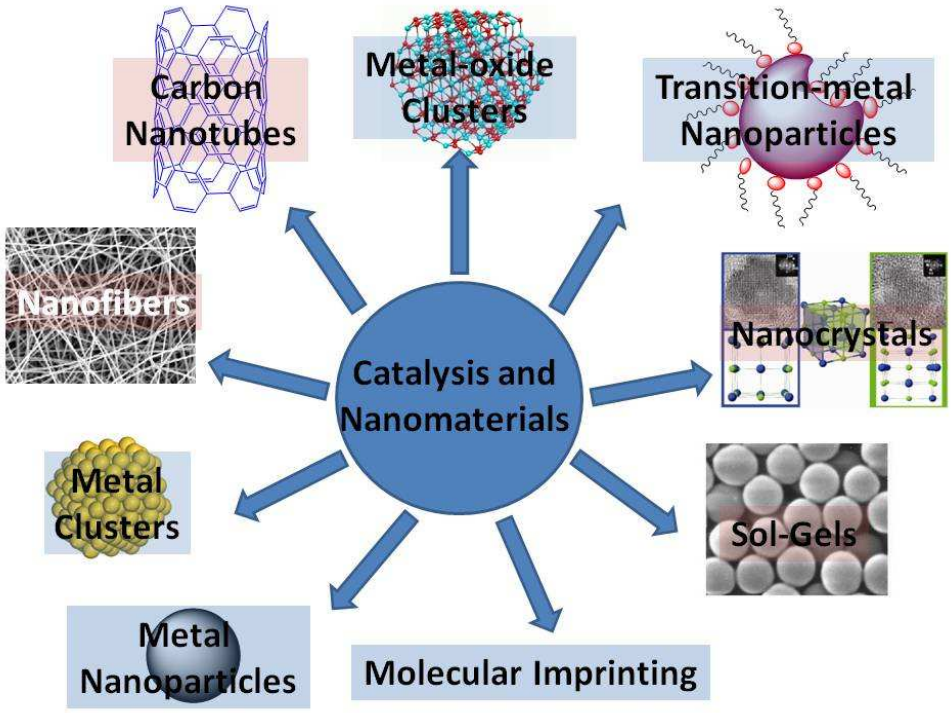

Figure 2: Scheme describing the different types of nanomaterials used for catalysis

This trend towards the production of new catalysts using nanotechnology is referred as a new field called *nanocatalysis*. This new field of *nanocatalysis* stands in parallel with the traditional catalysis but differs from it simply by the fact that the materials generated are explicitly designed and tailor-made over length scales greater than a single active site[20]. As a consequence, extensive studies of the physical chemistry of nanomaterials are highly required in particular mass diffusion, transport in pores, and structure of the surface as they will certainly have an effect on the catalytic activity. The knowledge gained from these studies will lead us to the development of new synthetic strategies for the production of the next catalyst generation, along with more understanding of their dynamic nature.

In this thesis, only a few examples of catalytic nanomaterials are presented and the work more specifically relates to the use of nanoparticles in catalysis. First, the use of catalytic metal and transition metal based NPs is described as it represents a very important part in the field of *nanocatalysis*. Then the use of sol-gels as organic-inorganic metal carriers and their application in catalysis is presented in the second part of this introduction. The use of the molecular imprinting approach for the development of catalysts is described last and represents a major part of this introduction as this technique is directly related to the work presented in this thesis.

1.3.1 Towards the use of Nanoparticles (NPs)

1.3.1.1 Transition-Metal NPs

The development and application of transition-metal NPs have shown a considerable progress over the last 10 years especially in terms of their preparation, structure determination, and applications[22, 29]. The size of these particles goes from 1 to 50 nm dimension where metals display typically size-dependent properties. When the cluster of atoms is small enough, the percentage of atoms that are on the surface becomes higher. Atoms at the surface of solids exhibit special properties that are of great interest for catalysis[30-31]. The metal atoms that compose the NPs are generated

by a large range of methods often including chemical reduction of a metal salt, as described in **Figure 3**, thermal, photochemical, or sono-chemical decomposition of a metal (0) complex, hydrogenation of a coordinating olefin moiety, vapour phase deposition, and electrochemical reduction of higher valence species of the metal[22, 32].

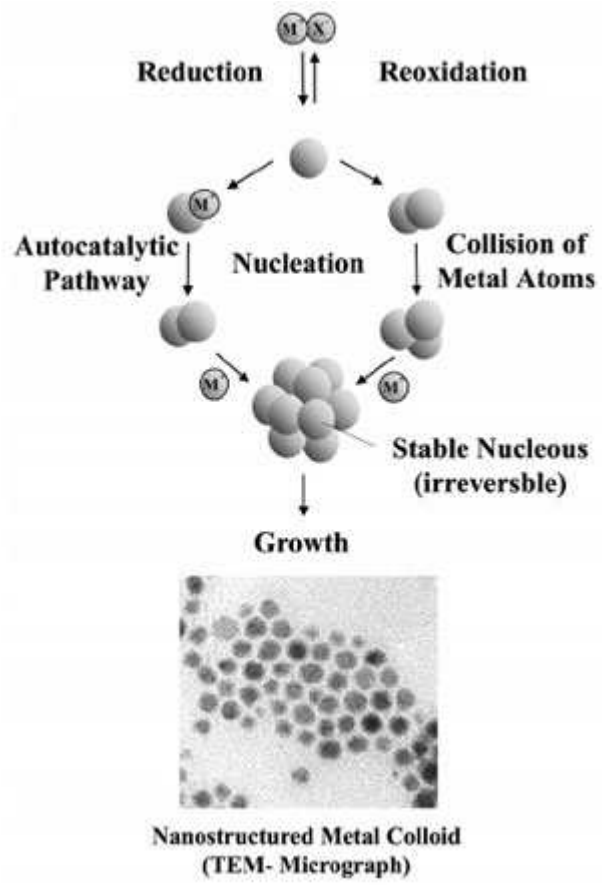

Figure 3: Schematic representation of formation of metal colloids by chemical reduction of a metal salt[33]

The synthesis of transition metal-NPs is divided in several steps. Following the generation of the metal atoms as explained earlier, a nucleation occurs to form an initial cluster of atoms. The cluster then grows until it reaches a certain volume. In order to prevent aggregation, the particles are grown in presence of a protecting agent. There are two types of protections: protection by electrostatic stabilization or steric stabilization as described in **Figure 4**. The electrostatic stabilization consists in the formation of a double electric layer where ions of the same sign are adsorbed onto the surface of the NP. The counter ions create a second layer in situ that repels the neighbouring particles. Steric stabilization occurs through the adsorption of molecules

with a long alkyl chain. The volume of these protecting molecules keeps away the other metal-NPs and as a result prevents aggregation. Polymers such as (poly(vinylpyrrolidone)(PVP))[34], cyclodextrines[35], dendrimers[36] are some of the most popular protecting agents.

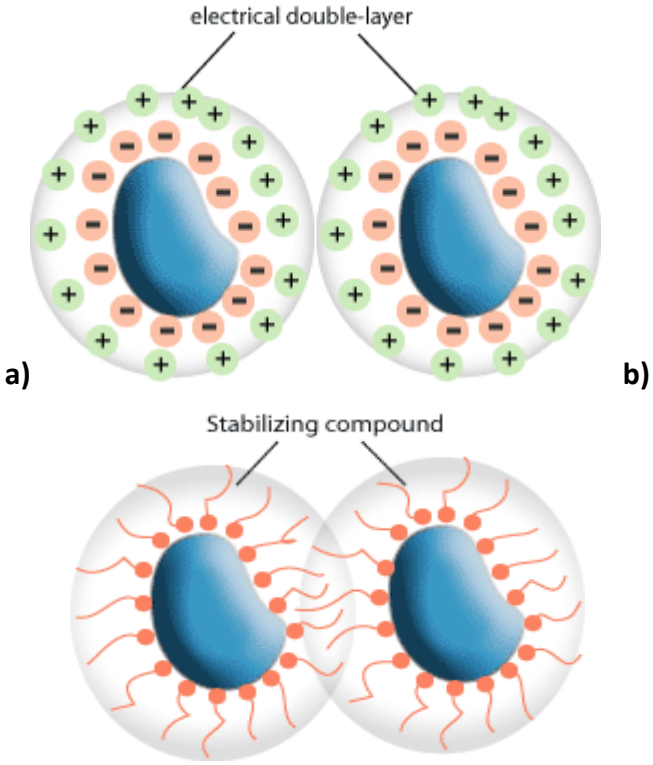

Figure 4: a) Electrostatic stabilization of NPs by a double electric layer and b) steric stabilization[37].

Other common stabilizers are ionic surfactants such as sodium dodecyl sulfate (SDS) and lauryl trimethylammonium chloride or heavily fluorinated compounds[38]. These compounds protect nanoparticles from aggregation by both electrostatic and steric mechanisms.

The most common transition metal NPs found in the literature and studied for catalysis are palladium-NPs (Pd-NPs). The next section will be dedicated to these Pd-based catalysts and their applications.

1.3.1.1.1 Palladium-NPs (Pd-NPs)

The discovery of the catalytic formation of C-C and C-N bonds by palladium-NP catalysts marked a definite progress in the field of catalysis. The problems of catalyst recovery and pollution by phosphines are now resolved mostly by the use of supported NP catalysts which can be removed by simple filtration and recycled. Among several reactions, Pd-NPs are well-known to catalyze the Heck reaction. This reaction is one of the key reactions in the production of fine chemicals. Therefore the utilisation of NP catalysts for this system is of great interest[39]. The Heck reaction is employed, among a vast quantity of products, for the production of the herbicide prosulfuron[40], the anti-inflammatory naproxen[41], or the anti-asthma singular[42]. This reaction is based on the arylation of olefins as indicated in **Scheme 1**.

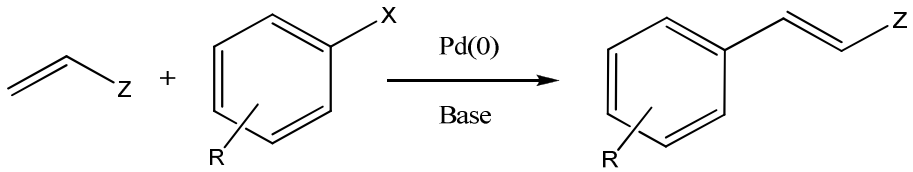

1a: Z = COOR
1b: Z = Ph
1c: Z = CN

2a: X = I
2b: X = Br
2c: X = Cl

3a,b,c

Scheme 1: Mizoroki-Heck reaction is arylation of olefins **1a,b,c** from aryl halides **2a,b,c**[39].

As of today, the development of Pd-NPs is directed towards the resolution of main issues which are i) to find a system that is able to activate C-Cl bonds and in the meantime to find cheaper leaving groups, ii) to recover and re-use the catalysts without losing the catalytic activity and iii) to develop phosphine-free palladium catalysts. Few examples of palladium-NPs application for the catalysis of the Heck reaction can be found in the literature. Reetz and co-workers demonstrated that Pd-NPs stabilized with tetraalkylammonium with diameter of 3 nm display catalytic activity towards the reaction of butyl acrylate as shown in **Scheme 1** (**1a)** with iodobenzene to allow the formation of butyl cinnamate[43]. These palladium-based NPs were prepared electrochemically or by thermolysis of palladium acetate. This group

also established the catalysis of the same system with different substrates using Pd-NPs of different sizes with an electrostatic stabilization. All these reactions are summarized in **Scheme 1**[44-45]. Following these results, the use of Pd-NPs was developed and others groups reported methods where Pd-NPs were synthesized by different ways: i) reduction of Palladium (II)[46-48] ii) sono-chemical decomposition of $Pd_2(dba)_3$[49] (dba - dibenzylacetone), and iii) hydrogenation of the coordinating olefins of $Pd_2(dba)_4$[50]. In the previous cases, very high turnover numbers were obtained.

Other types of reactions can be catalyzed using Pd-NPs. The Suzuki cross-coupling is one of them. This reaction, as described in **Scheme 2**, is well-known to generate biphenyls **3** by coupling aryl boronic acids **1** with aryl halides **2**[51].

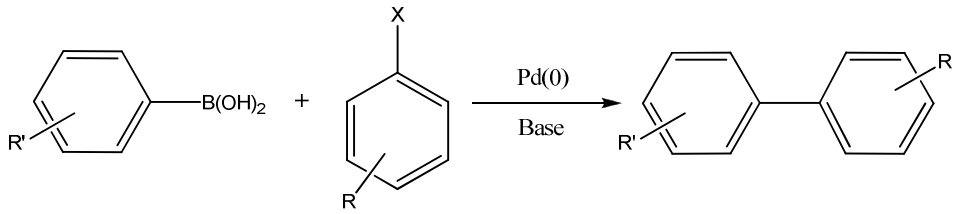

4 **5** **6**

Scheme 2: The Suzuki cross-coupling reaction between arylboronic acids **4** and aryl halides **5** results in the formation of biphenyls **6**[51].

Other groups reported the application of Pd-NPs for the catalysis of this reaction. Reetz and co-workers described the formation of biphenyl from aryl bromide or even from aryl chloride with electron-attracting groups[43]. Gladyzs et al. communicated Suzuki couplings using fluorous sulfide[52]. Many other examples are available in the literature where many different substrates are investigated.

1.3.1.1.2 Other transition metal-NPs

A large variety of other transition metal based NPs are used for catalysis and are available in the literature. Suzuki cross-coupling can for instance be catalyzed by other transition metal NPs such as copper-NPs (Cu-NPS) and Ruthenium-NPs (Ru-NPs) or NPs based combinations of transition metals. These novel NPs with another transition metal than Palladium represented a definite advance in the field. Other

useful reactions are known to be catalyzed by Cu-NPs or Ru-NPs such as acetylene polymerization and ring-opening metathesis polymerisations[53].

1.3.1.2 Precious-Metal NPs

1.3.1.2.1 Gold-NPs

While bulk gold is chemically inert, gold divided into small particles (10 nm or less) and scattered onto metal oxides or activated carbon surfaces has attracted tremendous attention for its catalytic properties. In this state, gold can be used as a catalyst that can perform at low temperatures for many reactions including CO oxidation and propylene epoxidation. The catalytic properties of gold particles were first discovered in the 1970s. Bond and Sermon described the catalytic hydrogenation of alkenes and alkynes at 473 K with gold small particles deposited onto silicates[54]. Then Pavano and coworkers studied the catalysis of oxygen and hydrogen transfer reactions over Au/MgO and Au/Al_2O_3[24, 55]. Many studies into the catalytic properties of gold particles followed, and the real breakthrough appeared in 1987 with the discovery of the high catalytic activity of composite oxides of gold when combined with 3d transition metals for CO oxidation at low temperatures[25]. Later, the same research group reported that these active gold catalysts constituted of Au-NPs dispersed on metal oxide surfaces such as Fe_2O_3, Co_3O_4, and NiO[26, 56] as shown on **Figure 5**.

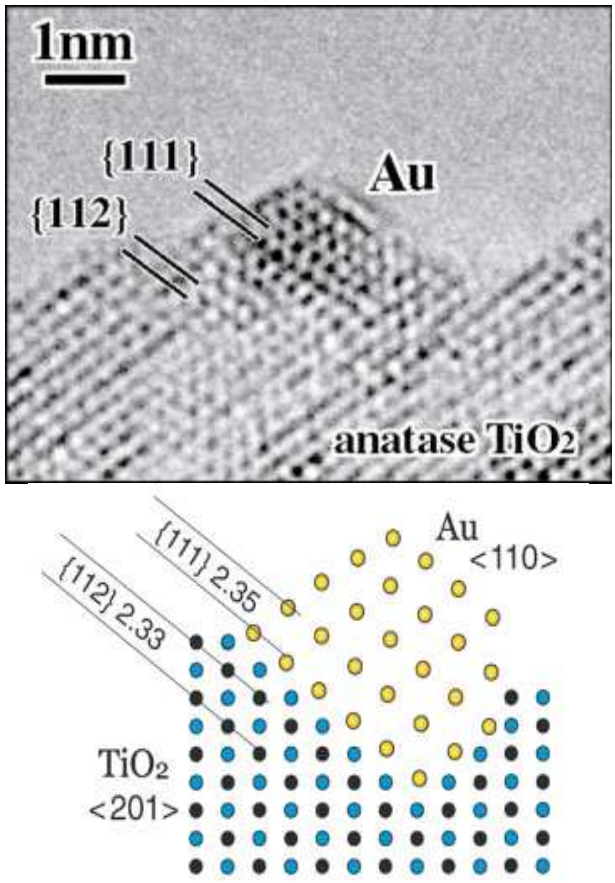

Figure 5: Transition electron micrograph of Au-TiO_2 nanoparticles prepared by deposition-precipitation and calcinations in air at 673K[57].

The first commercial application of gold-NPs was developed in 1992 for a toilet deodorizer[58].

Various techniques are reported in the literature in relation with the deposition of Au-NPs onto metal oxide surfaces and can be divided into three categories. The first technique is based on the following: precursors such as hydroxide, oxide or metal mixtures of gold are mixed together with the metal that composes the support by co-precipitation or amorphous alloying among other techniques. This precursor mixture is then transformed into metallic Au-NPs in air at high temperatures that strongly tights to crystalline metal oxides such as α-Fe_2O_3, Co_3O_4, and ZrO_2[25]. The second technique is the deposition or adsorption of gold compounds by deposition-precipitation (DP), by gas-phase grafting, liquid phase grafting[59-60] and Chemical Vapour Deposition (CVD)[61]. The third technique is based on the use of mono-dispersed gold colloids that are stabilized by organic compounds or polymers[62].

The performance of gold-NPs depends on three important parameters: strong contact between gold particles and the support, the type of support and the size of the particles. Two typical reactions, CO oxidation and propylene epoxidation are well-known to be structure-sensitive over gold catalysts suggesting that the reactions might occur at the perimeter interfaces around the gold NPs[57]. Many other reactions are catalyzed by gold-NPs including oxidative decompositions[63], reduction or decomposition of NO_x[64] and selective hydrogenations resulting in the formation of ethylene[65], butenes[54], or allylalcohol[66]. Gold catalysts display many advantageous features including excellent structure sensitivity to reactions, catalytic activity even at low temperatures, and moisture activation. For all these reasons gold catalysts are expected to be developed in the next few decades especially in industrial environments.

The use of precious metals for the generation of efficient catalysts is not only limited to gold. In the field of electro-catalysis, platinum has been extensively employed and the development of platinum based nanomaterials has marked a real improvement in the production of electrodes.

1.3.1.2.2 Platinum-NPs

The use of platinum blacks for the construction of electrodes used to be common and is still carried out by the reduction of platinum salt into particles with an average size around 10 nm and a surface area about 25 to 30 m^2g^{-1} [67]. This method is employed in particular for the commercialisation of fuel-cell electrodes, where the Pt-particles are joined together with polytetrafluoroethene (PTFE) to form an active layer of a gas-diffusion electrode. Depending on platinum content in the electrode, this operation is quite expensive. Therefore the generation of Pt-NPs with higher active surface area is a high priority in the research area of fuel-cell related electro-catalysis. For the commercialization of these types of catalysts, three important requirements need to be met: high performance based on a high surface area, low cost involving

small particles and thin layers, and longevity, which is characterized by a high resistance to corrosive acid environment[68]. As platinum is generally resistant to corrosive environment, the main challenge is to master the synthesis of high surface area platinum catalysts.

For the construction of electrodes other than for gas-phase reactions, a conducting substrate is needed; carbon black is found to be the material of choice[69]. Thus, platinum and platinum-alloy NPs are dispersed on different types of carbon supports such as powders, nanoparticles, fibers, nanotubes or solid or porous sheets and are employed for reactions such as Hydrogen Oxidation Reaction (HOR). The first example of platinum-alloy NPs deposited onto a carbon support was reported in 1980. This system was named PtV/C and demonstrated higher catalytic activity than pure platinum for oxidation reactions. Since then many other binary platinum alloys and even tertiary platinum alloys have been developed, and have demonstrated higher activity than pure platinum. **Figure 6** shows an example of dispersion of platinum NPs and platinum alloy NPs on carbon nanohorns, which are carbon nanotubes with irregular hornlike shapes.

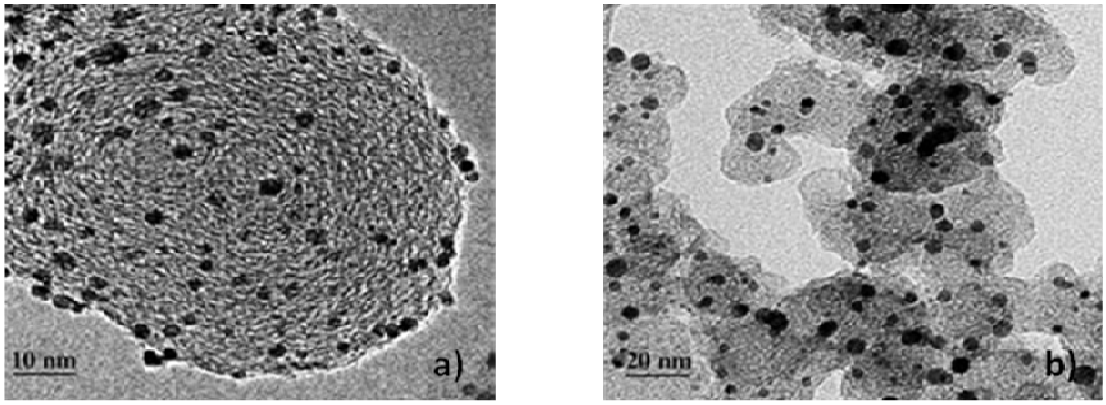

Figure 6: Low-magnification HREM micrograph of a) Pt/Vulcan and b) PtCo/Vulcan (Vulcan is a carbon nanotube with irregular hornlike shape support[68]

All the examples listed in this section, from transition-metal NPs to precious metal-NPs, suggests that nanoparticles with a size ranging from 2-10 nm are attractive for many applications from development of drugs to commercialisation of electrodes and industrial catalysts. The list above is far from exhaustive but the main areas of research in the application of metal based NPs have been presented. The following

section focuses on another type of nanomaterial also very used in catalysis and also used as metal carriers.

1.3.2 Sol-gel as a metal-containing catalytic material

Colloidal silica particles are obtained from the hydrolysis of a metal alkoxide followed by condensation and polymerization reactions[70-71]. They are organic-inorganic compounds that provide distinctive possibilities for generating versatile materials. Different structures of colloidal particles can be obtained, ranging from mono-dispersed spherical particles to agglomerates of complex structures as shown in **Figure 7**.

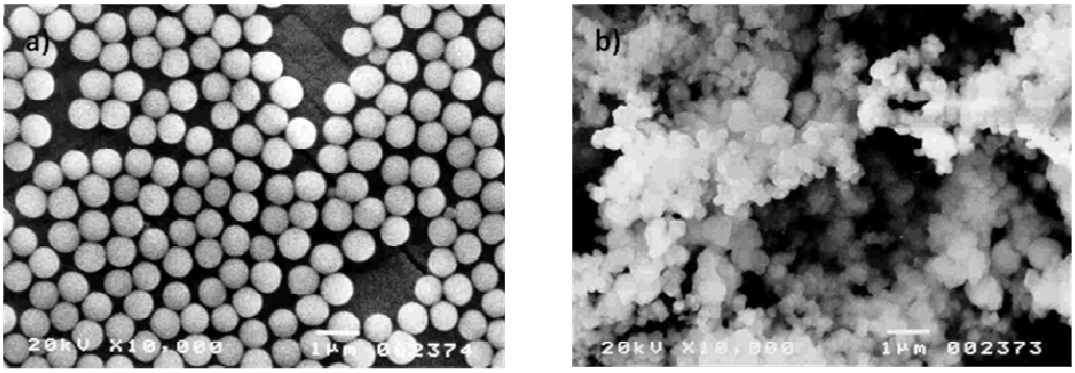

Figure 7: a) TEM picture of a) silica particles; b) silica aggregates[72]

This depends on the choice of synthesis process parameters[72]. Nowadays, various precursors can be synthesised leading to the generation of hybrid silica with specific properties. The sol-gel process has attracted attention in the development of novel catalysts since the pore structure can be easily controlled. In particular, sol-gels have been used over the last decade for the preparation of heterogeneous supported metal and metal-oxide catalysts[73-74]. The sol-gels method offers the possibility of controlling the pore structure, the pore size, the composition and surface polarity of metal oxides[75]. The new supported metal and metal oxides materials are obtained by introducing organic or organometallic precursors during the sol-gel polycondensation. This technique allows the adjustment of the catalyst loading and the sol-gel matrix is built around the metal complex resulting in good catalyst stability; the porosity of the

matrix allows the substrate to reach the active sites. The selectivity of these types of materials can be improved by the use of molecular imprinting, which technique is developed in section 1.4.

There are some examples of immobilization of metal inside a sol-gel matrix such as rhenium, ruthenium, platinum and also transition metal such as nickel and cobalt in the literature[76]. Promising results on the immobilization of titanium in a silica matrix with a high dispersion of titanium were also described and demonstrated a high catalytic activity for some epoxidations[77]. This technique could provide an alternative to dispersing metal NPs on carbon supports, as the metal is incorporated inside a sol-gel matrix with a tunable pore size.

The capacity of a catalyst for recognizing a specific substrate is an important parameter that plays a significant role in its selectivity and/or its catalytic activity. It is therefore necessary to adjust the environment of the catalytic site in order to generate recognition specificity and to induce selectivity. This remains quite challenging for catalytic metal-based nanomaterials and the number of studies is limited. The molecular imprinting approach seems to be a good alternative for the creation of recognition sites inside a polymer matrix as a cavity complementary in shape and size to a target molecule is generated. The next part of this introduction focuses on the use of nanomaterials based polymers for the generation of novel catalysts where selectivity can be introduced using the molecular imprinting approach.

1.4 Molecular imprinting

Since the pioneer studies of Poliakov in the 1930s[78], in which some unusual adsorption properties in silica particles were reported, the concept of molecular imprinting has evolved to become a well-established field with a vast array of applications. The concept of molecular imprinting is based on the self-assembly of functional monomers around a target molecule, called template molecule. Once the polymerization process in presence of a cross-linker is achieved, the imprint molecule

is extracted under suitable conditions. As a result, a cavity with a complementary size, shape and functionality is left inside a three dimensional matrix. This process is illustrated in **Figure 8**. The highly cross-linked matrix that is generated keeps the functional groups fixed in place inside the cavity and allows a selective recognition of the template molecule.

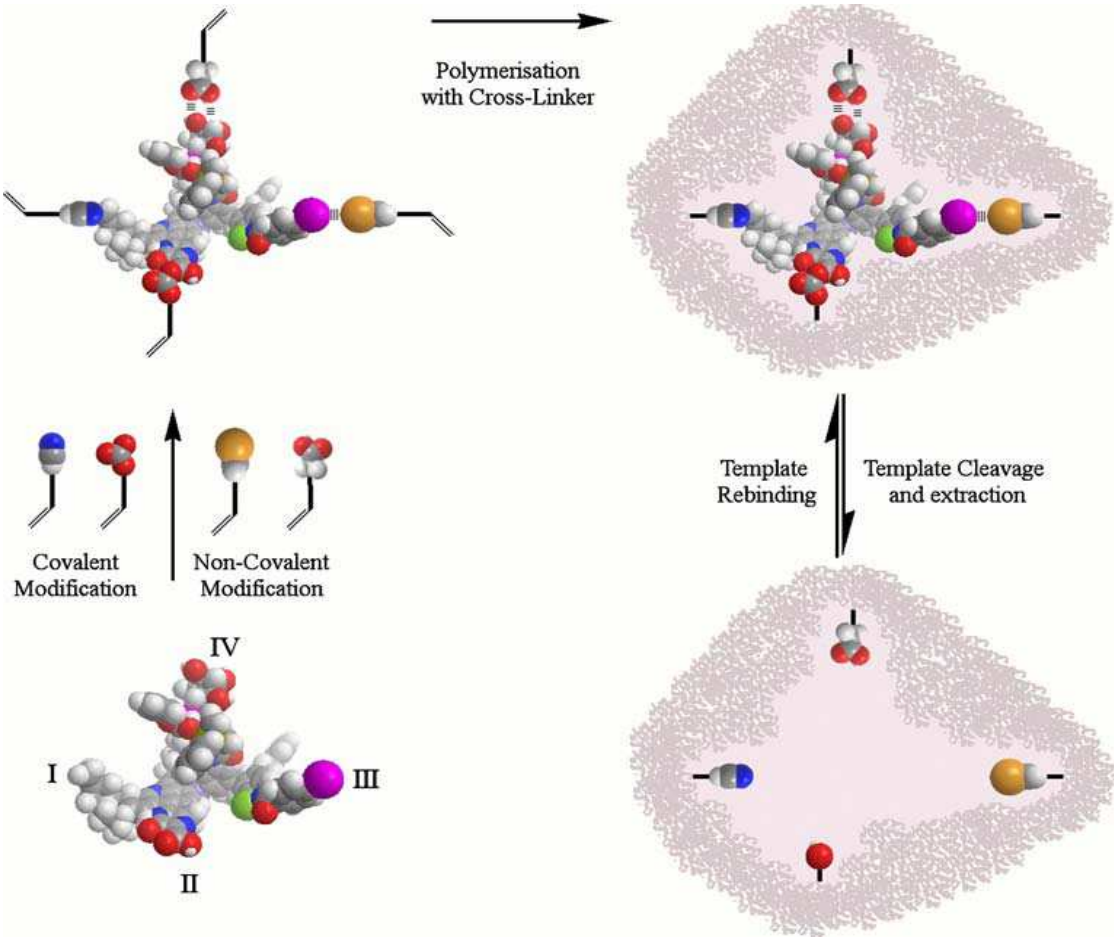

Figure 8: Scheme of the molecular imprinting process, where a cavity is formed after the removal of the template molecule[79]

A wide range of applications in different fields of research has arisen from the molecular imprinting technique including sensors, biosensors, solid phase extraction, and chromatographic separations. Imprinted polymers also demonstrated potential as scavengers to eliminate undesirable compounds from foods or biological fluids, and as screening tools in drug delivery[80]. Different types of polymer matrices have been explored for the creation of imprinted polymers with high selectivity, including

nanowires, carbon nanotubes, sol-gels, dendrimers, polymer particles or bulk polymers[79].

In the following part, a few examples of polymer formats developed with the molecular imprinting approach are presented; however this list does not cover the extensive literature that is now available[79].

1.4.1 Imprinting in nanomaterials

Since the first example of molecular imprinted bulk polymers in 1972 reported by Wulff and Sarhan for the separation of a racemic mixture using the covalent approach[81], a large range of polymer formats have been produced and this contributed to a marked enlargement in the potential applications of the molecular imprinting approach. However, free radical polymerization of vinyl-based monomers remains the common method employed for the creation of molecularly imprinted polymers, mainly due to its ease of processing but also the commercial availability of a broad range of monomers. Besides the imprinting in sol-gels matrices, there are only a few reports of unusual or novel types of polymerization[82]. Some of them such as dendrimers nanofibers and nanowires are reported here.

1.4.1.1 Dendrimers

The first example of polymer matrix that is reported in this thesis is the preparation of a single macromolecule with a single recognition. This idea was initially introduced and realized by Zimmerman et al. in 2002[83], where a porphyrin template was imprinted into a single macromolecule, specifically a dendrimer. This allowed the preparation of homogeneous hosts with a single recognition site. The covalent approach was used in this study, where the porphyrin was bound through ester linkages to eight third generation dendrons. The extraction of the template molecule was performed by hydrolysis. The resulting imprinted dendrimer was found to be selective, and could rebind porphyrins with four hydrogen bond donor/acceptor sites

in toluene. However the template molecule due to its great size could not rebind, only smaller porphyrins could be accepted making the matrix size-selective.

Following these studies, the same group developed another type of imprinted dendrimer using a template with a lower symmetry with the ultimate aim of producing an amine-selective sensor[84]. The resulting imprinted polymer was found to be highly selective through three-point interaction, which binding induced a change of colour.

This type of molecular imprinting into a single macromolecule displays many advantages such as a high imprinting efficiency, quantitative template extraction, and solubility in usual solvents. However, the synthesis of dendrimers is well known to be difficult and time-consuming and this excludes the use of this method from the production of imprinting polymers with industrial applications. Furthermore, many templates are found to be incompatible with this imprinting approach.

1.4.1.2 Nanowires, nanotubes, and nanofibres

As mentioned previously, a vast variety of polymer formats is used for the generation of molecular imprinted polymers and among them stand nanotubes and nanowires. Wang et al. was the first group that reported the successful preparation of imprinted nanowires using a nanomolding process. This process allows the creation of recognition sites at the surface of the nanowires and is based on the use of alumina membranes functionalized with the template molecule[85]. Subsequently the nanopores of the membrane are filled with the pre-polymerisation mixture. After polymerisation, in the presence of suitable cross-linker content, the membrane is dissolved chemically leading to the generation of polypyrrole nanowires with glutamic acid binding sites located at the surface. This method, described in **Figure 9**, was notably employed for the imprinting of a TNT template molecule using 70 nm pore size alumina membrane[86] and also for the imprinting of many proteins such as albumin, haemoglobin, and cytochrom *c* [87]. In the latter, the isolated nanowires demonstrated a considerable imprinting factor, around seven-fold difference between imprinted and non-imprinted nanowires. A significant binding capacity that can be correlated with the high surface area of the nanowires was also reported. The capability of quantitatively removing the

template molecule also represents the main advantages compared to other imprinting systems.

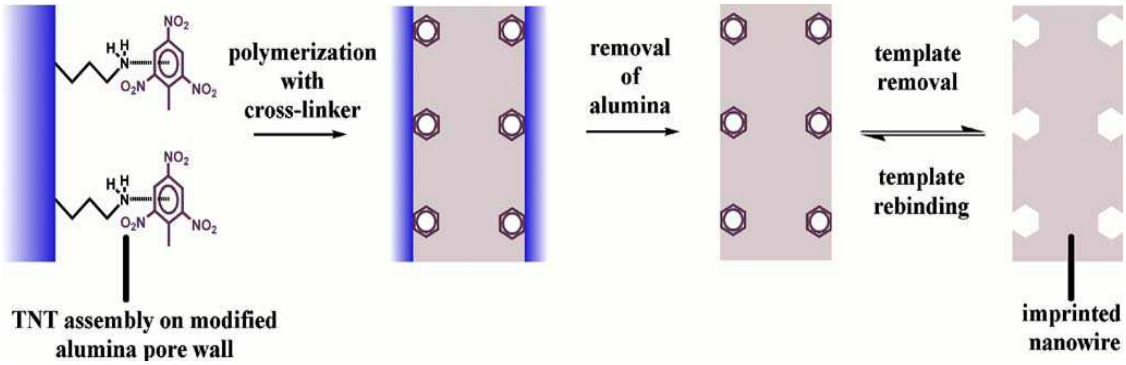

Figure 9: Process scheme of TNT-imprinted acrylic-based nanowires using a non-covalent molecular imprinting approach[86].

Other studies reported the use of nanotubes as polymer matrix. Nanotubes differ from nanowires by the fact that they are hollow nanowires and show higher surface to volume ratio. Imprinted nanotubes, along with efficient recognition elements, were found to be very useful in the chemical separation of many hormones[88]. It was also reported that magnetic properties could be explored using nanotubes. This could lead to novel applications in drug delivery as biochemical sensors among others.

The use of nanofibres with the molecular imprinting approach was reported by Ye et al. where they generated imprinted nanofibres by incorporating imprinted nanoparticles into electrospun nanofibres[89-91]. This group also managed to generate recognition sites inside the nanofibres[92]. These imprinted nanomaterials have displayed significant imprinting efficiencies and this could lead to potential applications such as the development of new recognition materials for solid phase extraction and novel sensing elements.

1.4.1.3 Nanoparticles

There are many methods available in the literature for the synthesis of nanoparticles. For the preparation of imprinted nanoparticles, the most common approaches remain the emulsion and precipitation polymerization methods. There are

a number of examples available in the literature of the emulsion polymerization process using molecular imprinting. Emulsion polymerization is a radical polymerization technique based on the water-in-oil or oil-in-water emulsion, in which polymerization occurs inside the droplets formed, and where aggregation is stabilized by the amphiphilicity of particles (charged groups introduced by initiators). This technique leads to the formation of narrow particles, which have an internal structure comparable to macroscopic networks. Perez et al. described the successful synthesis of cholesterol-imprinted core-shell nanoparticles, where core nanoparticles were subsequently imprinted via covalent imprinting approach in a second stage polymerization[93-94]. The size of these resulting nanoparticles was found to be around 30-40 nm. The cholesterol-template molecule was removed by hydrolytic cleavage from the shell of the nanoparticles. The synthesis of imprinted nanoparticles following this method using the non-covalent approach was also reported; in this case caffeine was imprinted in polymeric core-shell nanoparticles in an aqueous media[95]. The NPs were found to be highly selective allowing the recognition of the template molecule caffeine and leaving theophylline unbound.

Other techniques such as mini-emulsion and micro-emulsion polymerization have been employed also for the production of imprinted nanoparticles with a template-directed method of imprinting. This approach gives rise to the creation of an imprinted recognition site at the surface of the particle by using a target molecule as the head of a surfactant. The template molecule is then led to the inner surface of the micelle. Markowitz et al. developed this technique to imprint an α-chymotrypsin transition state analogue (TSA) at the surface of silica nanoparticles[96]. This concept is described in **Figure 10**. This example will developed more in detail in section 1.4.2.

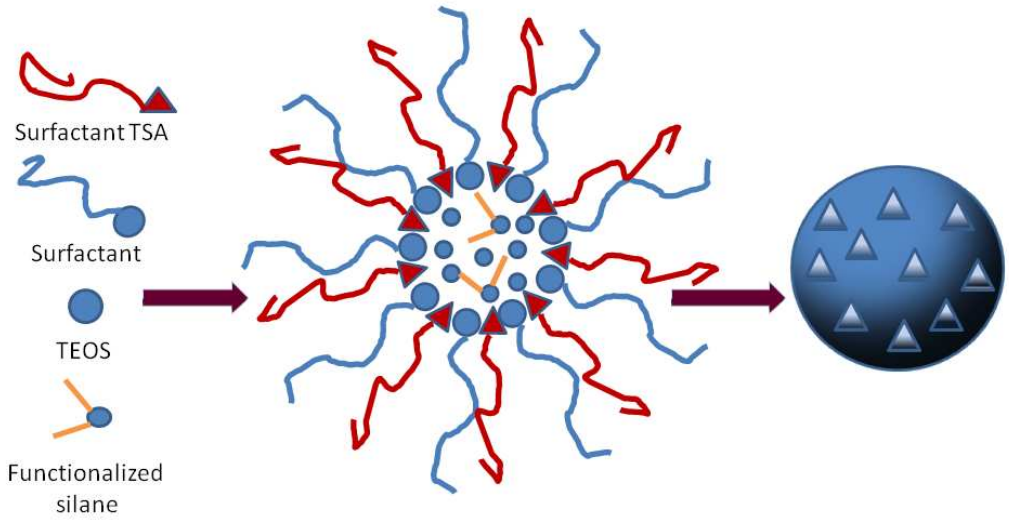

Figure 10: Template-directed imprinting procedure of silica nanoparticles. Particle formation and surface-imprinting is started by mixing an anionic surfactant, the TSA surfactant with cyclohexane, ammoniated ethanol and water in a water-in-oil emulsion following by the addition of TEOS and functionalized silanes[96].

Precipitation polymerization is a common technique to generate nanoparticles, in which the polymerization process occurs in a homogeneous media and where all the monomers and initiators are mixed in a dilute solution of porogen. During the polymerization process, primary particles are initially formed and aggregate to each other to generate bigger particles. The latter are stabilized against coagulation by steric hindrance or by the high rigidity of their cross-linked surfaces. The first application of this technique along with the molecular imprinting approach was reported by Ye and co-workers, who successfully imprinted hydrophobic and hydrophilic template molecules following this polymerization route[97]. Subsequently, the use of this technique generated imprinted nanoparticles with many applications in sensing[98], capillary electrochromatography[99] and drug delivery[100].

1.4.2 Catalytic imprinted polymers

1.4.2.1 The transition state analogue approach (TSA) and first studies

Although considerable efforts have been invested in the production of a variety of imprinted nanomaterials for different types of applications, the most intriguing and challenging utilization of the molecular imprinting approach remains for catalysis and

development of enzyme mimics. Molecularly imprinted polymers (MIPs) have attracted a lot of attention in the field of catalysis over the few decades, as they offer the possibility of generating a three dimensional recognition site inside a polymer matrix and could theoretically adopt an enzyme-like behaviour. MIPs as active materials are unlikely to outperform enzymes or even catalytic antibodies; however they have the advantages of being utilisable under harsh conditions and in organic solvents. Contrary to binding MIPs, the production of catalysts following the molecular imprinting approach necessitates the imprint of the matrix with a template molecule that obeys the transition state analogue (TSA) approach. This concept is based on the selection of a template molecule that resembles closely to the crucial intermediate of the uncatalyzed reaction in order to stabilize its formation and reduce its activation energy[101]. As well-established, the transition state of the reaction itself cannot be employed to imprint the matrix because of its instability. Instead a TSA is carefully selected with the view of obtaining a chemical structure extremely similar to the transition state or at least similar functionalities in the appropriate region.

The first attempt to synthesize catalytic imprinted polymers using the TSA approach was reported by Mosbach et al. in 1989[102]. In this study, imprinted polymers with catalytic activity for the hydrolysis of p-nitrophenylacetate (**8**) were prepared. The choice of the imprint molecule was based on the TSA approach and p-nitrophenol methylphosphonate (**7**) was selected as template, as described in **Scheme 3**. Vinylimidazole-based polymers were synthesized in presence of cobalt (II) in order to create a metal binding site. This method consisted of the formation of a complex between the metal, two polymerisable imidazole units and the TSA and was used in previous studies[103]. The choice of vinylimidazole as functional monomer was based on the fact that imidazole units were previously found to be catalytically active in ester hydrolysis. The resulting polymers showed good catalytic activity with a rate enhancement over 60-fold compared to the non-imprinted polymers.

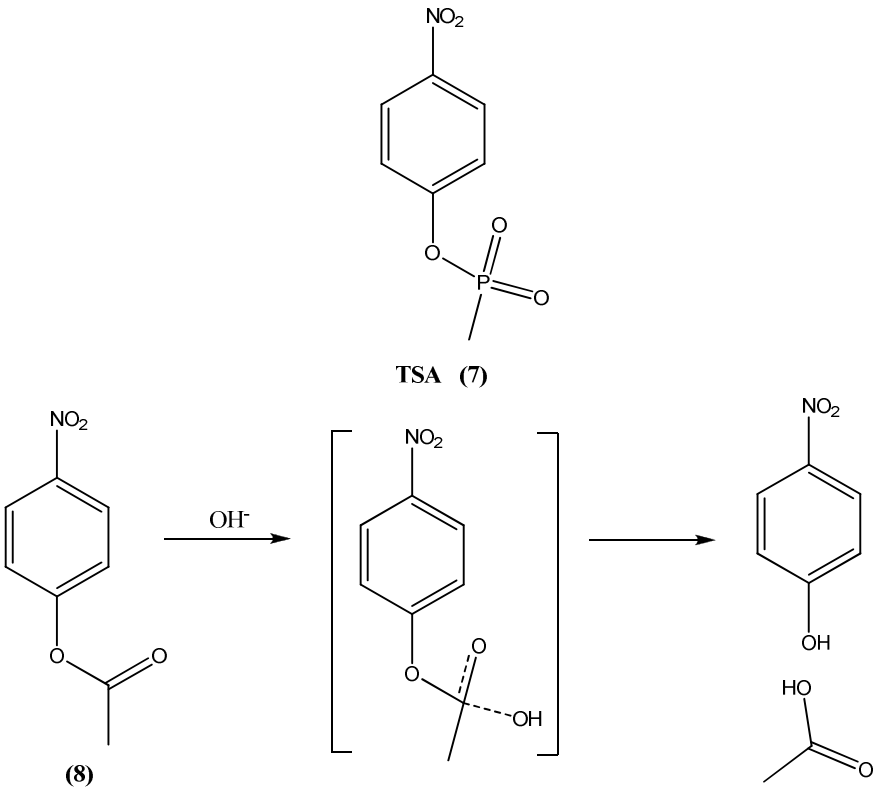

Scheme 3: Chemical structure of the TSA molecule p-nitrophenol methylphosphonate (**7**); Reaction scheme of the hydrolysis of p-nitrophenolate (**8**)

Inspired by this pioneer study, several attempts in the production of esterolytic imprinted polymers were carried out based on the same transition state analogue[104]. Ohkubo et al. investigated the full kinetic profile of this system and demonstrated that the imprinted polymer followed the Michaelis and Menten model and therefore ascertained the enzyme-like behaviour of these synthetic entities[105].

1.4.2.2 Catalytic 'bulk' imprinted polymers

The TSA approach has been widely applied and several groups have started to develop catalytic imprinted polymers for a large array of chemical reactions. Generally the preparation of MIPs has been via the route of "bulk" polymerization. This type of polymerisation includes the mixture of vinylic monomers and cross-linkers with a free radical initiation. Subsequently, the material formed requires grinding in order to obtain particles in the range of micro/nanometre and usually irregular and

polydisperse particles are obtained after grinding. Mosbach et al. reported the synthesis of artificial Diels-Alderase using molecular imprinted polymers for the catalysis of the cycloaddition of tetrachlorothiophene dioxide (**9**) with maleic anhydride (**10**) as shown in **Scheme 4**[106].

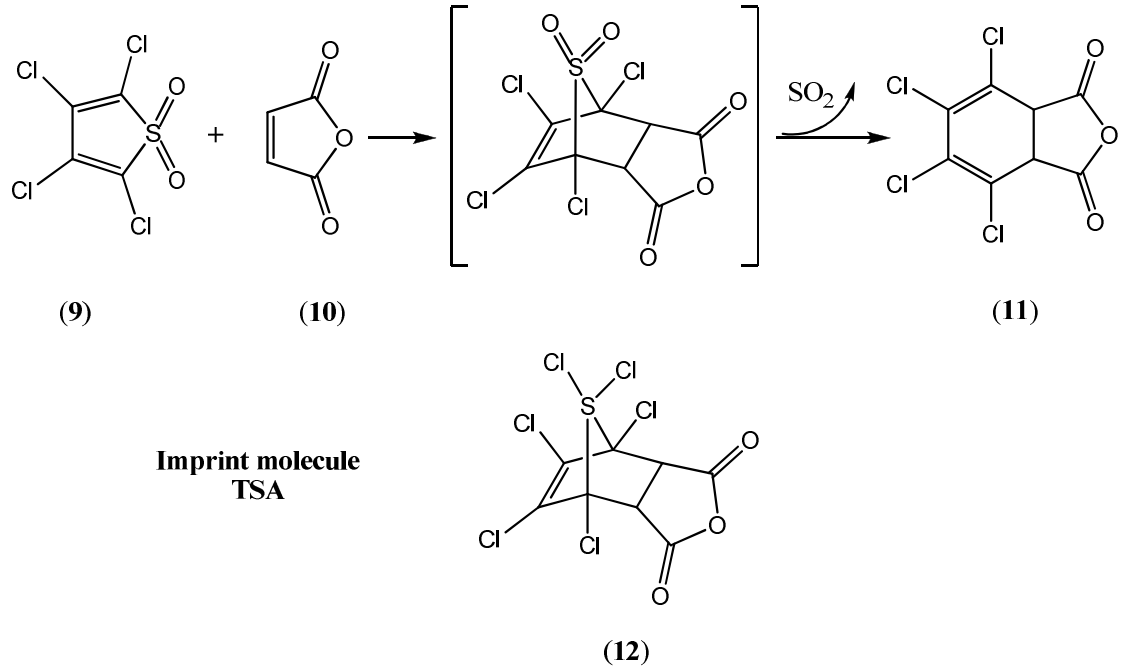

Scheme 4: Diels-Alder reaction between tetrachlorothiophene dioxide (**9**) and maleic anhydride (**10**) resulting in the formation of (**11**), 4,5,6,7-tetrachloroisobenzofuran-1,3(3aH,7aH)-dione, the Diels-Alder product of the reaction. The imprint molecule (**12**), chlorendic anhydride used follows the TSA approach[106].

In this study, the polymer matrix was imprinted with (**12**), chlorendic anhydride, which template molecule follows the TSA approach. The imprinted polymers formed displayed a significant catalytic activity with a rate enhancement of around 270-fold over the uncatalyzed reaction (k_{cat}/k_{uncat}) in acetonitrile at 82°C. They were found to follow a Michaelis-Menten model with rate constant k_{cat} of 3.82×10^{-2} min^{-1} and a Michealis-Menten constant K_M of 42.7 mM. The Michaelis-Menten constant K_M quantifies the affinity of an enzyme towards the substrate. Generally, the affinity is the highest when the value of K_M is the lowest. The constant found by Mosbach et al. for the catalysis of the Diels-alder reaction is quite high, which means a low affinity between the polymer matrix and the substrate. The same group also developed imprinted bulk polymers capable of accelerating the isomerisation of benzisoxazoles,

reaction known as Kemp elimination[107]. The imprinted polymers demonstrated a catalytic activity following also the Michaelis-Menten model with a rate constant k_{cat} of 0.205 min^{-1} with rate acceleration (k_{MIP}/ $k_{control}$) over 7-fold compared to the control polymer which was not imprinted.

Other examples of catalytic bulk MIPs using the TSA approach have been reported in the literature, notably for mimicking a class II aldolase enzyme. The polymers were prepared by imprinting a complex of dibenzoylmethane (**13**) and a cobalt (II) ion in a 4-vinylpyridine-styrene-divinylbenzene copolymer in a non-covalent imprinting[108]. The selected monomers were assumed to interact with the template molecule (**13**) by Van der Waals and π-π stacking interactions. The imprinting process is shown in **Figure 11**.

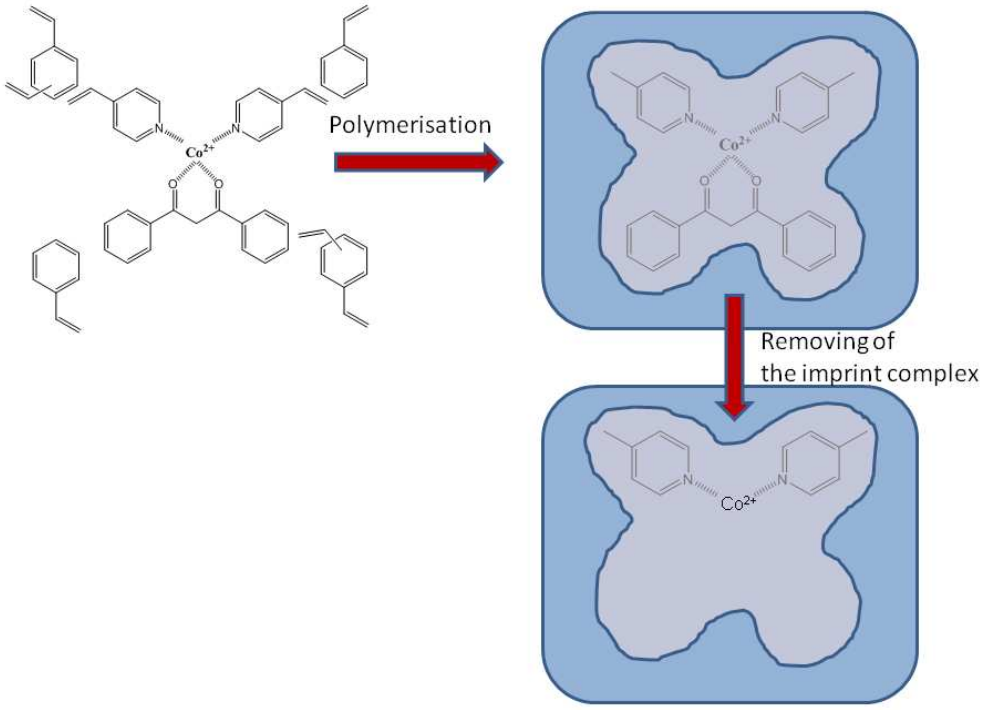

Figure 11: Imprinting process for the aldolase type II system[108].

This MIP was prepared to catalyze the aldol condensation of acetophenone (**14**) with benzaldehyde (**15**) and results in the formation of a chalcone (**16**). This reaction is shown in **Scheme 5**. The TSA approach was applied and as a result dibenzoylmethane (**13**) was selected as template molecule. This is shown in **Scheme 5**.

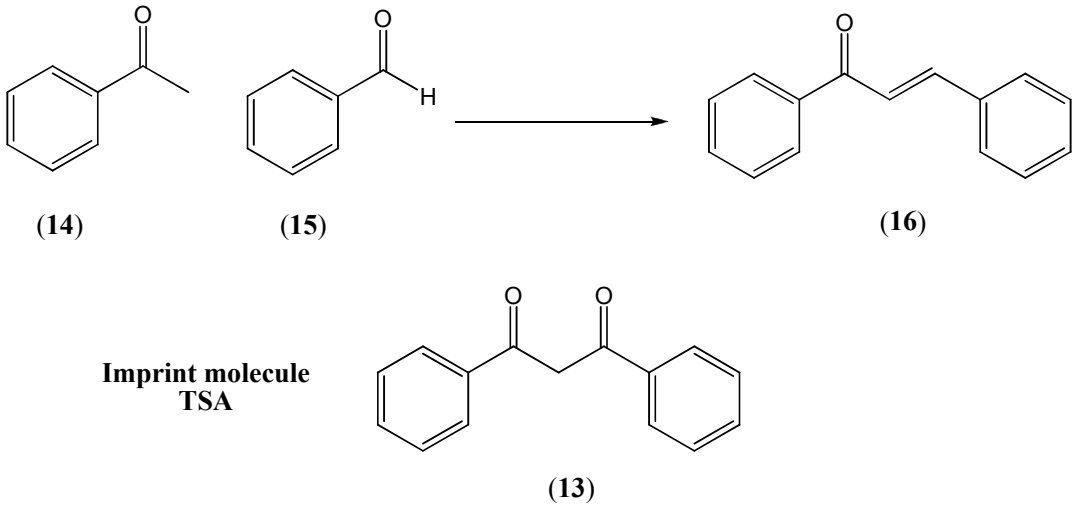

Scheme 5: Aldol condensation of acetophenone (**14**) and benzaldehyde (**15**) resulting in the formation of chalcone (**16**). The TSA molecule used to imprint the polymer matrix is dibenzoylmethane (**13**)[108].

The resulting active polymers were able to selectively catalyze the reaction with an 8-fold rate enhancement compared to the uncatalyzed reaction. The polymers also demonstrated good turnover and selectivity towards the substrate and turnover, and could perform under harsh conditions such as high temperature and organic solvent for several weeks. This marked a definite advance in the field of enzyme mimics and catalytic 'bulk' imprinted polymers.

An interesting system was reported by Wulff and co-workers, concerning the synthesis of catalytic imprinted polymers for hydrolysis reactions using a process that they named "*stoichiometric non-covalent imprinting*"[109]. The basic principle of "stoichiometric imprinting" is the complex formation between the template molecule and the different functional monomers with an association constant K_a above 10^3 M^{-1}. This ensures that the equilibrium of the complex formation is well pushed toward the complex[104]. The choice of the functional monomers, polymerisable N,N'-di-ethyl-amidine units was based on the strong interaction that this molecule displays towards the TSA, phosphonate ester. As described in **Figure 12**, the ratio between functional monomer and template was 2:1.

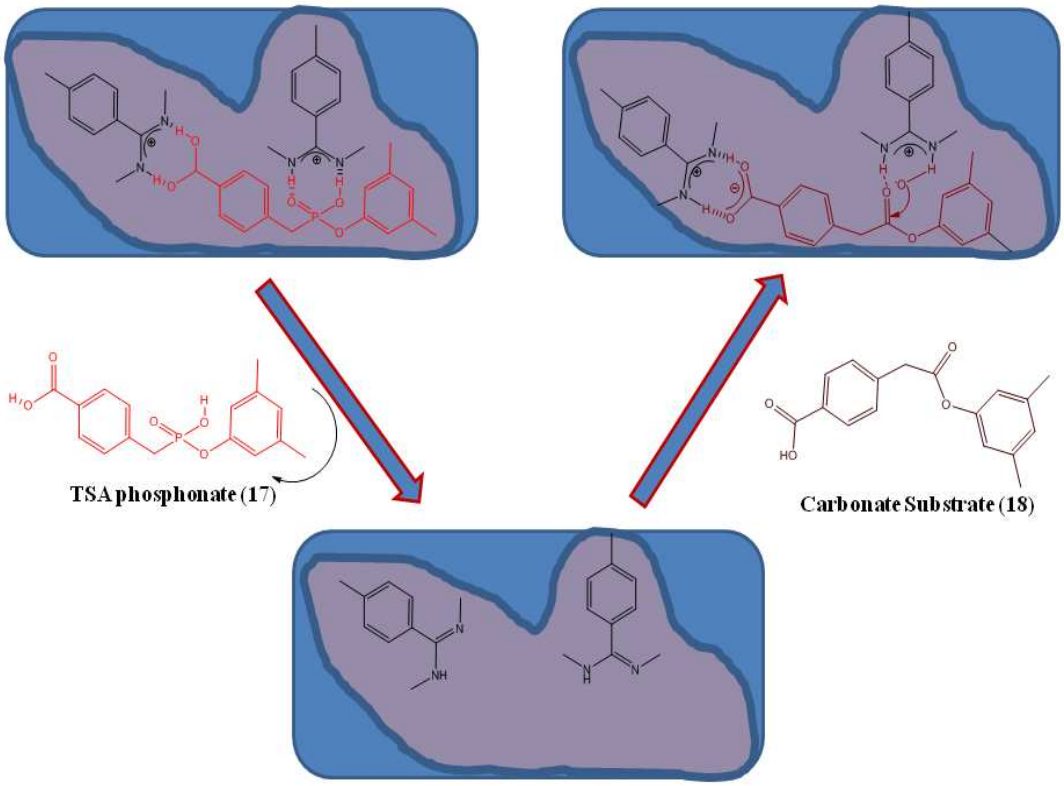

Figure 12: Imprinting process for the production of imprinted polymers for carbonate hydrolysis. After the extraction of the TSA, phosphonate ester (**17**), the polymer matrix is left with a specific cavity capable of recognizing the substrate molecule 4-(2-3,5-dimethylphenoxy)-2-oxoethyl)benzoic acid (**18**)[109].

Following this approach, bulk polymers and polymer beads *via* suspension polymerization were prepared with the aim of catalyzing the hydrolysis of di-aryl esters. The resulting polymers displayed a relatively good rate enhancement; however evidence of product inhibition was reported. Surprisingly, the same polymers were found to be much more active towards carbonates and carbamates due to the absence of product inhibition. A rate enhancement over 1000-fold relatively to the uncatalyzed reaction was reported. There was no significant improvement in catalytic activity between the imprinted bulk polymers and the imprinted polymer beads[109].

In order to avoid the issue of product inhibition, some groups started developing imprinted polymers for the catalysis of elimination reactions where the product displays less affinity to the polymer matrix than the substrate or template molecule. Several reactions have been studied and amongst them stand the dehydrofluorination of 4-fluoro-4-nitrophenylbutan-2-one (**19**), shown in **Scheme 6**.

The catalysis of this reaction was previously investigated by Schultz et al. using catalytic antibodies[110].

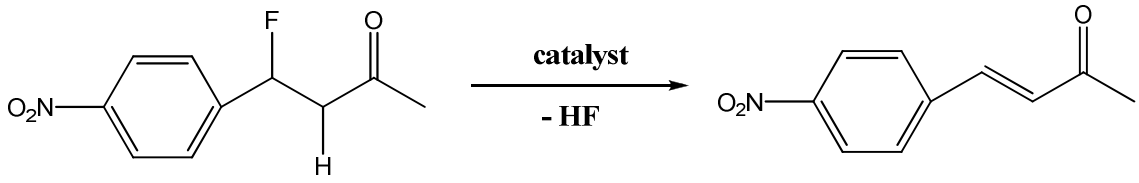

(**19**)

Scheme 6: Reaction scheme of the dehydrofluorination of 4-fluoro-4-nitrophenylbutan-2-one (**19**).

Two research groups described the synthesis of an imprinted 'bulk' polymer capable of catalyzing the latter reaction. The design of the system for the imprint of the matrix was inspired by previous studies carried out with catalytic antibodies[110]; in both studies, ethylene dimethacrylate and methacrylic acid were used as cross-linker and backbone monomers respectively[111-112]. Methacrylic acid is in fact often used to form ionic-type bond with amino groups and also to generate hydrogen bonding with polar functionalities that are present in the template molecule. The benzenemalonic acid-imprinted polymers showed a rate enhancement over 10-fold compared to the uncatalyzed reaction. The kinetic studies carried out by Shea and co-workers were performed in benzene using a ratio 10:1 of active sites to substrate (**19**). The imprinting process of the system is shown in **Figure 13**.

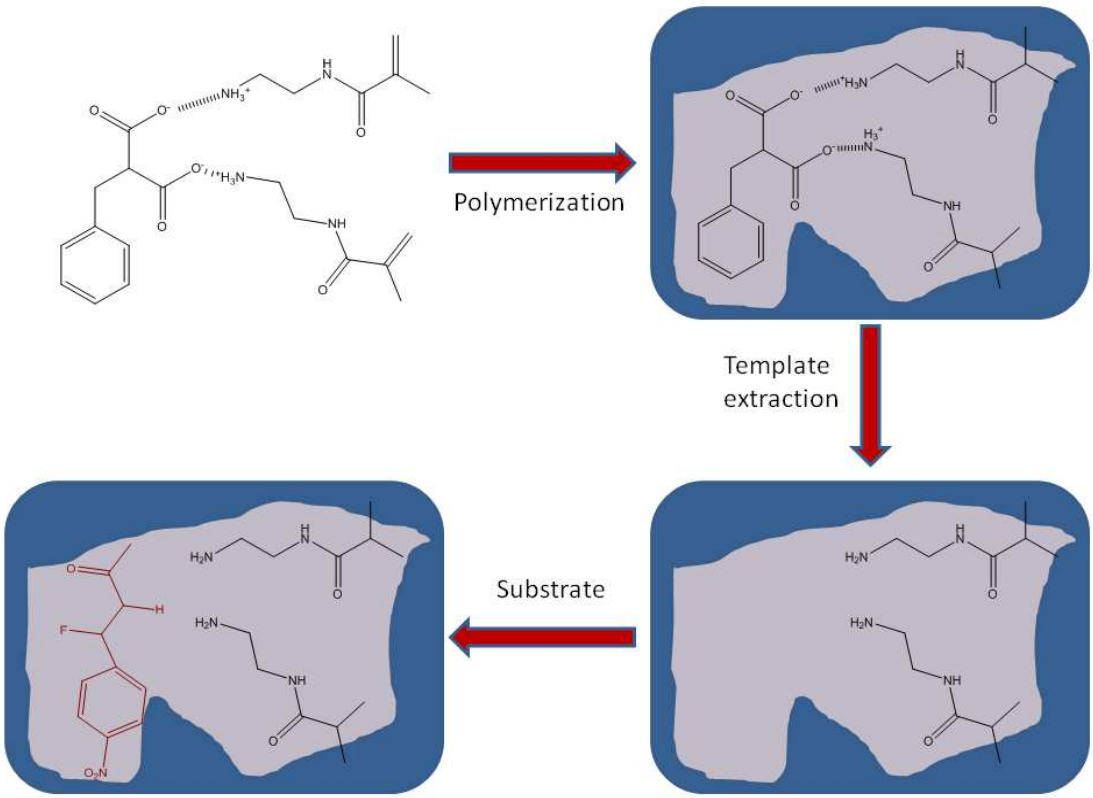

Figure 13: Imprinting process for the generation of catalytic imprinting polymers for the dehydrofluorination of 4-fluoro-4-nitrophenylbutan-2-one (**19**). The polymer matrix was imprinted with benzenemalonic acid[111-112].

As suggested in **Figure 13**, the catalytic activity is dependent on the hydrogen bonding strength between the polymer matrix and the substrate. As a consequence, the polarity of the solvent has an effect on the performance of the polymers. These studies confirmed the fact that molecular imprinting is a potential alternative for the generation of tailor-made catalysts.

More recently Wulff and co-workers developed an imprinted bulk polymer with carboxypeptidase A type activity[113]. The design of this system was based on previous investigations carried out by the same group on the development of imprinted polymers for carbonate hydrolysis presented in a previous section. The TSA was therefore tetrahedral phosphonates that allowed a stable complex with the functional monomer N,N'-di-ethyl-amidine (cf **Figure 12**). The novelty in this system was to introduce another catalytic entity, which was constituted of amidinium residues 3-fold coordinated with metal such as Zn^{2+} or Cu^{2+}. This led to a stoichiometric non-covalent

based imprinting process with stronger interactions between the template molecule and the functional monomers. The metal centres were introduced during the polymerisation process. The imprinting process is shown in **Figure 14**.

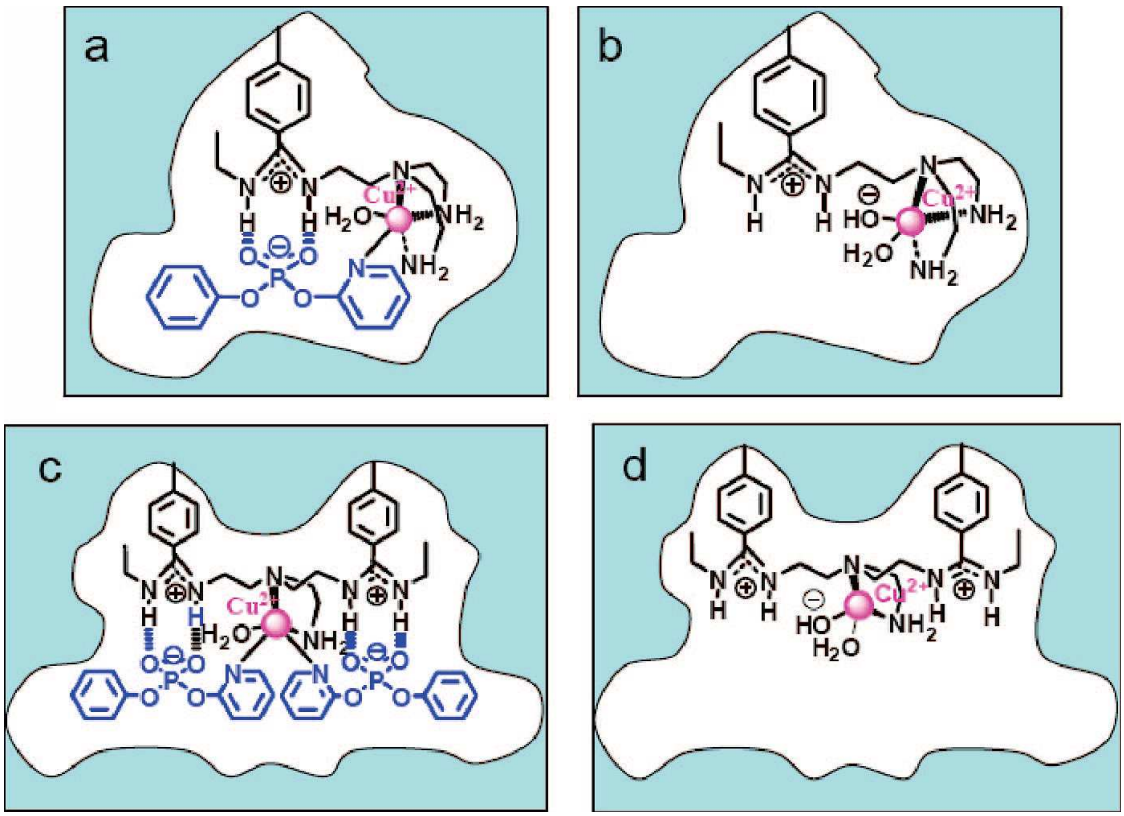

Figure 14: The 4 steps of the imprinting process for the synthesis of imprinted 'bulk' polymers with caboxypeptidase A activity: a) imprinting of the polymer with the template molecules in presence of the metal centre and functional monomers, b) extraction of the template leaving unchanged the functionalities inside the cavity; c) Imprinting of polymer with a different functional monomer allowing the incorporation of two template molecules; d) extraction of the templates molecules leaving the active site with in place the different functional groups[113].

The imprinted polymers displayed tremendous catalytic activity with an extraordinary rate enhancement about 10^5-fold compared to the uncatalyzed reaction. The activity of the polymers was even greater when the cavity contained two amidinium moieties around 410 000- fold compared to the background reaction (cf **Figure 14**). So far this has been the highest value of rate constant obtained by imprinted polymers and they are comparable to those obtained by catalytic antibodies. This marked a definite advance in the field of catalytic imprinted polymers.

Other examples of catalytic imprinted 'bulk' polymers are available in the literature. The examples presented previously however show a good range of chemical reactions that have been investigated with the use of molecular imprinting approach. The use of bulk polymers might not be appropriate for a good enzyme mimic due to the high rigidity of the polymer matrix, and the insolubility of the particles generated via grinding and sieving. Furthermore, the grinding process leads to significant heterogeneity of the active sites and hindered access to the active cavity and this limits the efficiency of the catalysts. In an effort to respond to these issues, several research groups investigated the use of other polymer formats for the production of a new class of catalytic imprinted polymers. The next section discusses a few examples of catalytic imprinted polymers with different polymer formats.

1.4.2.3 Sol-gels and Surface imprinted polymer catalysts

The TSA approach has also been reported on silica sol-gel systems although these types of polymer matrix have been exploited much less for the generation of catalysts. In 1988, the first generation of TSA imprints in the surface of alumina-containing silica gels was reported by Morihara et al.[114]. The concept of this type of imprinting is based on 'footprinting', which is the surface modification of commercially available silica gels using alumina ions and the TSA molecule. The imprinted gel was prepared for the catalysis of the butanolysis of benzoic anhydride and demonstrated enzyme-like catalytic activity, although evidence of substrate inhibition was found. Following this pioneer study from Morihara and co-workers, Maier et al. prepared a silica-based imprinted polymer with the aim of catalyzing the trans-esterification of ethyl phenylacetate (**20**) with n-hexanol resulting in the formation of hexyl phenylacetate (**21**), as described in **Scheme 7**[115].

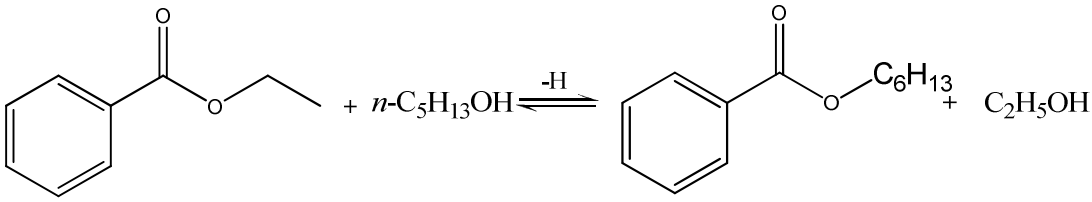

(**20**) (**21**)

Scheme 7: Trans-esterification of ethyl phenylacetate (**20**) resulting in the formation of hexyl phenyl acetate (**21**).

A phosphonate (**23**) was used as TSA molecule to mimic the established transition state as described below in **Figure 15**.

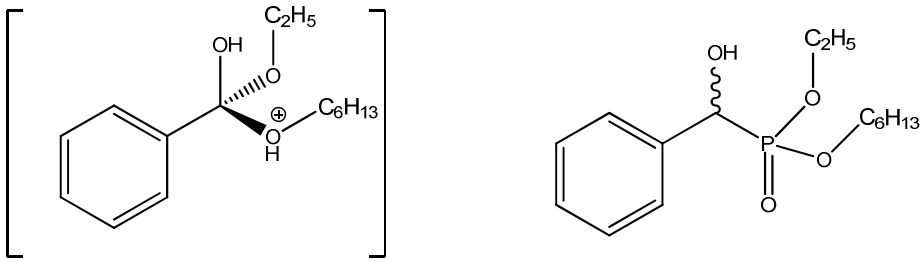

(**22**) (**23**)

Figure 15: Silica gel matrix was imprinted with the TSA phosphonate (**23**) in order to mimic the established transition state

The imprinted silica-based polymer displayed good catalytic activity characterized by a value of V_M of 3.75 µM and K_M of 3.6 mM. The polymers demonstrated higher activity than the previous studies from Morihara et al.; however optimization of the selectivity and turnover remain necessary for the industrial application of this technique. Markowitz et al. applied this technique to generate catalytic imprinted sol-gels for the enantioselective hydrolysis of amides[96], where the recognition sites were located at the surface of the polymer particles as described in **Figure 10** in section 1.4.1.3. The imprinted particles demonstrated a good catalytic activity and selectivity, and were found to be selective towards the trypsin substrate over the chrymotrypsin molecule. Furthermore, the formation of the D-isomer of the trypsin product seems to be favoured over the formation of the L-isomer.

This '*foot-printing*' concept developed by Morihara and co-workers has now been investigated in close detail and has been particularly developed for the imprint of metal oxide. A good example of surface molecular imprinting technique was reported

by Suzuki and co-workers, where imprinted polymers for ester hydrolysis were prepared[116]. The TSA template was initially absorbed onto a pre-cleaned surface of Al_2O_3. An imprinted silica layer was formed around this target molecule via chemical vapour deposition (CVD) of tetramethoxisilane (TMOS). Subsequently the TSA template molecule was removed by repetitive ethanol washes. The resulting polymer was utilised to catalyse the hydrolysis of a library of alkyl esters. Encouraging catalytic activities were obtained from the polymers and notably the highest rate constant for the hydrolysis of ethyl isobutyrate was reached. This technique was extended to other systems notably for the catalysis of alkene hydrogenation using chemisorbed rhodium species[117]. The metal compound in the form of $Rh_2Cl_2(CO)_4$ was initially adsorbed onto the silica surface SIO_2. Following this step, the template ligands $P(OCH_3)_3$ were then coordinated to the metal to form SiO_2-O-Rh-$(P(OCH_3)_3)_2$. Subsequently controlled CVD and hydrolysis of TMOS were carried out to generate a silica over-layer around the metal centre as shown in **Figure 16**.

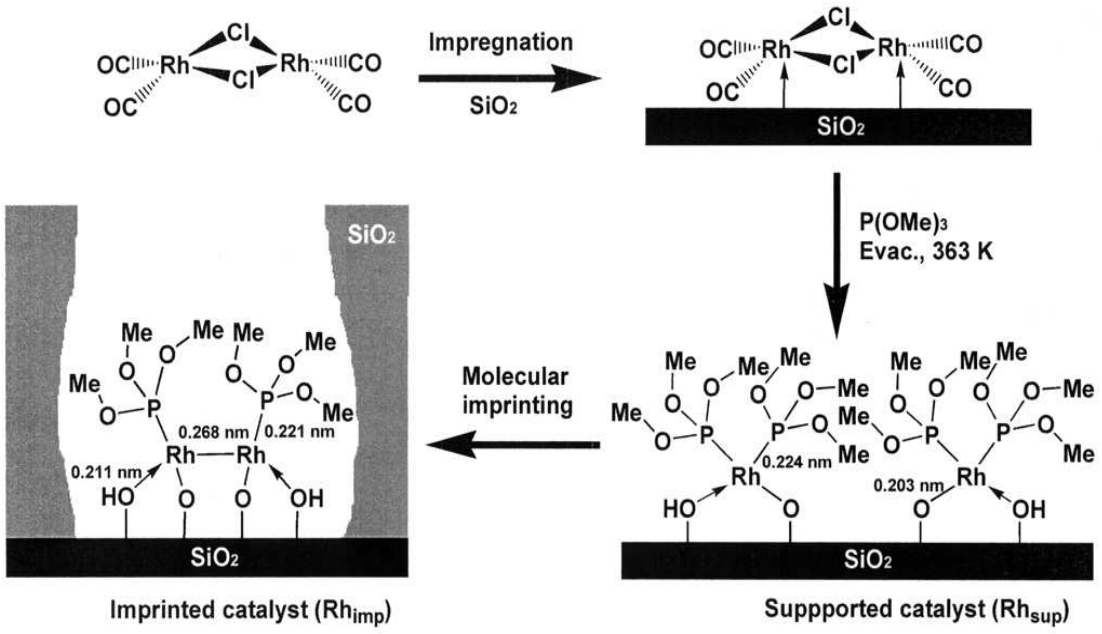

Figure 16: Imprinting process for Wilkinson-type imprinted polymers for alkene hydrogenation[117].

Catalytic studies demonstrated that Rh centres in the matrix were highly active with 51-fold and 31-fold rate enhancement respectively in the hydrogenation of 3-methylpent-2-ene and 3-ethylpent-2-ene compared to the non-imprinted Rh catalyst.

Evidence of selectivity were found as alkenes with longer chains or larger branched alkenes displayed lower rate enhancement around 10-fold compared to the non-imprinted polymer.

Overall, these studies permitted the development of new protocols for imprinting at surfaces and the production of a new class of catalysts with high activities and accessible sites. Many ingenious methods of imprinting polymers are currently being investigated and developed with the ultimate goal of developing tailor-made catalysts that are able to display an enzyme-like behaviour[104]. The production of enzyme mimics using the molecular imprinting approach necessitates a careful consideration of the polymer format and matrix. Good rigidity is required to preserve the shape of the cavity generated during the imprinting process as well as a high flexibility of the matrix to ease the uptake or release of target molecules. A good balance of these two contradictory features is needed to achieve a good enzyme-like behaviour. The porosity of the matrix is also of great importance as the active sites have to be accessible and available[1].

In the next section of this thesis, the focus will be on particular polymer formats used for the catalytic imprinted materials such as microgel and nanogel particles. These materials have attracted considerable attention over the last decade in many fields and especially in the development of catalysts via the molecular imprinting approach.

1.4.2.4 Catalytic imprinted nanogels

Microgels and nanogels are defined as intra-molecularly cross-linked particles, which are able to swell in the appropriate solvent and to aggregate in bad solvent as displayed in **Figure 17**[118]. They are also found to be intermediate branched and macroscopic cross-linked networks. Microgel particles were first identified and named by Baker in 1949[119], although the synthesis of microgels was initially reported by Staudinger and Husemann in 1935[120]. In this study, divinylbenzene (DVB) was polymerized in high dilution in a good solvent to generate swollen polymer particles. The typical size attributed to microgels has been extensively discussed in the literature

and was established in the range of 60 nm to 200 nm by Antonietti et al.[121] while in other papers it was determined to be over 1000 nm[122]. Nanogels differ from microgels in terms of size and they are defined to be smaller typically below 50 nm.

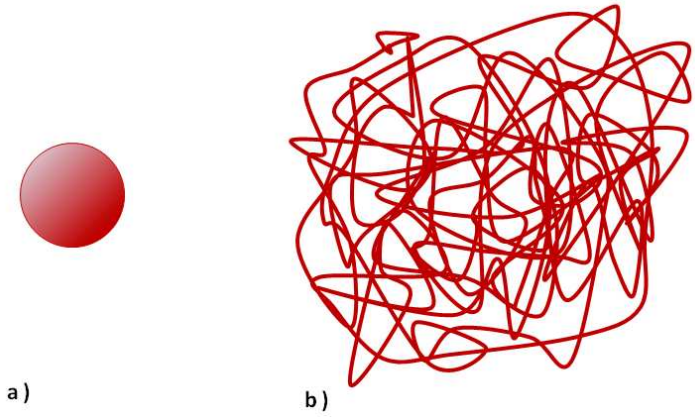

Figure 17: Scheme of microgels swelling in **a)** a bad solvent and **b)** in a good solvent[118].

A large array of common monomers used in radical polymerisation including methacrylic acid, methacrylate, acrylamide, styrene or DVB can be used to obtain microgel particles[122-124]. Microgels display colloidal properties in solution and a low viscosity in correlation with their assumed compact nature. There are currently two ways of obtaining nanogels, one is the emulsion polymerisation (explained in a previous section) and the other one is high dilution radical polymerisation. The latter is the method employed in this work to synthesise nanogels. This technique consists of mixing the monomers and initiator in dilute solution of solvent. At high dilution, according to the Ziegler dilution law, intramolecular cross-links are found to be favoured leading to the formation of nanogels or microgels without evidence of macro-gelation[124]. The presence of unreacted double bonds at the surface of the particles can engender further inter-particle cross-linking and give rise to aggregates with a greater size. If the concentration of all the monomers present in the pre-polymerisation mixture is kept under a certain value determined experimentally, called the Critical Monomer Concentration C_{MC}, microgels and nanogels particles can be obtained. Above this value, macrogelation occurs. These phase diagrams (shown in section 1.2 of the results and discussion part) describing nanogels and microgels

formation are dependent on all the polymerisation parameters including temperature, polymerisation solvent, type of monomers, initiator, cross-linker content, etc..

Due to their good properties of solubility in appropriate solvents and a high degree of flexibility of the matrix, microgels and nanogels are utilised in a large variety of applications including coating and rubber industry, immobilising enzymes and bioassays, or drug delivery. Combining the molecular imprinting technology and nanogel synthesis would yield a material with suitable features for a good enzyme mimic. Therefore, over the last decade imprinted nanogels has attracted great attention for the generation of a novel class of catalysts and enzyme mimics with potential industrial applications and were developed for the catalysis of diverse reactions. In the next paragraph, few examples of reactions catalysed by imprinted nanogels and microgels will be presented. Two major types of reactions have been used to apply and investigate imprinted nanogels catalytic efficiency notably hydrolysis reactions and Carbon-Carbon bond formation reactions.

1.4.2.4.1 Hydrolytic reactions

Hydrolytic reactions are commonly used to investigate catalytic activity and efficiency of imprinted polymers due to their versatility and the ease of monitoring product formation. The rate of hydrolytic reactions is generally higher than those where a carbon-carbon bond formation is involved. The first example of catalytic imprinted microgels was reported by Resmini et al. for carbonate hydrolysis[125]. In this study, soluble imprinted microgels containing two different amino acid side chains, arginine and tyrosine were prepared. These two amino acids were found to be highly involved in the catalysis of several hydrolytic reactions[126-127]. The design of these novel 'soluble' microgels was based on the TSA approach, the template molecule selected for the hydrolysis of carbonate (**24**) was the phosphate (**25**) (shown in **Figure 18**). The hydrolysis of *p*-nitrophenyl carbonate (**24**) is described on **Scheme 8**.

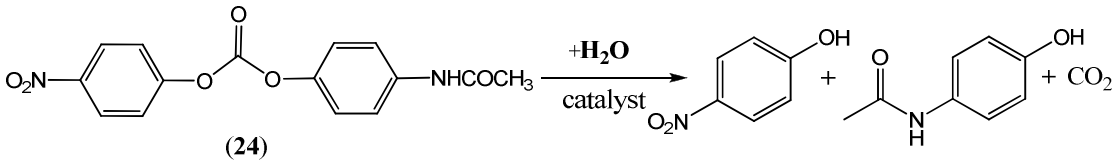

(**24**)

Scheme 8: Reaction scheme for the hydrolysis of the *p*-nitrophenyl carbonate (**24**)

Polymerisable derivatives of arginine (**27**) and tyrosine (**26**) were used as functional monomers that interact non-covalently with the TSA molecule (**25**) as shown in **Figure 18**. Acrylamide and N, N'-ethylenebisacrylamide were utilised as backbone monomers to form the microgel matrix.

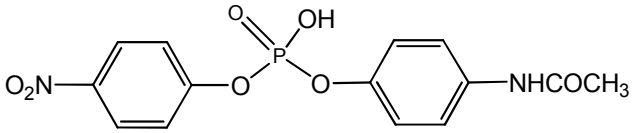

(**25**)

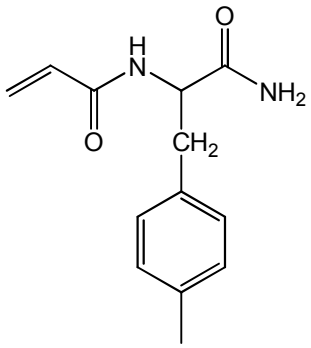

(**26**)

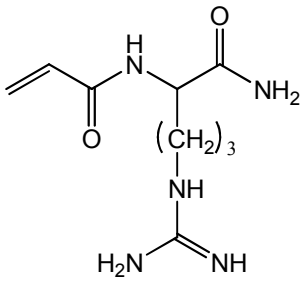

(**27**)

Figure 18: Structures of phosphonate TSA (**25**), polymerisable tyrosine (**26**) and arginine (**27**) as functional monomers[125].

The imprinted microgels were synthesized using high dilution radical polymerisation in DMSO, which technique is described in section 1.4.2.4. The cross-linker content and the monomer concentration C_m were fixed at 70% in mol and 0.5% in mass respectively, which conditions ensure the generation of microgels without evidence of macrogelation. The imprinted polymers demonstrated good catalytic activity with a significant rate enhancement compared to uncatalyzed reaction and were found to follow the Michaelis and Menten saturation model. The catalytic efficiency of the polymers was given by an estimate of the ratio k_{cat}/k_{uncat}, which value was around 530.

The selectivity of the cavity was also investigated by using another substrate structurally related to (**24**) but with the nitro group located in the *ortho* position instead of the *para* position. Although there is a moderate rate enhancement with this substrate, no difference in catalytic activity was found between the imprinted polymer and the non-imprinted polymer, ensuring the specificity of the cavity formed by imprinting.

Following this study, the same group investigated the catalytic activity of imprinted microgels synthesized with a cross-linker content ranging from 70% to 90% in mol[2]. All the polymers demonstrated catalytic activity with significant rate enhancement compared to the background reaction without the presence of any catalyst. However, only the imprinted polymer with a cross-linker content of 70% followed a Michaelis and Menten saturation curve with a higher catalytic efficiency; the ratio of k_{cat}/k_{uncat} was around 53. Physical chemical characterizations were performed on the polymers and the microgel form was confirmed by coil viscosity measurements. Size characterizations were also carried out using a Zetasizer instrument, which established that the an average size of the particles was under 1000 nm, with two types of particle populations, one ranging from 20 nm to 70 nm and the other from 100 nm to 800 nm.

In line with this work, Wulff et al. developed imprinted nanogels with catalytic activity for carbonate hydrolysis[128]. The preparation of imprinted single-molecule nanogels containing only one active site per particle was reported. This was achieved with using high dilution radical polymerisation with an extra step based on the '*post-dilution*' technique. This method involves starting the polymerisation process at high monomer concentration such as C_m around 5% or 10% in weight and just prior to macrogelation diluting the system to the desired concentration for instance 0.1% in weight. This was established based on previous studies on microgel formation, where it was reported that the degree of cross-linking is the highest just prior to macrogelation during the polymerisation process[129]. In addition, the temperature was increased stepwise from 60°C to 80°C during the polymerisation. As a result, highly compact nanogel particles were obtained with an average size around 20 nm as shown in **Figure 19** this gave clear colloidal solutions in the majority of organic solvents.

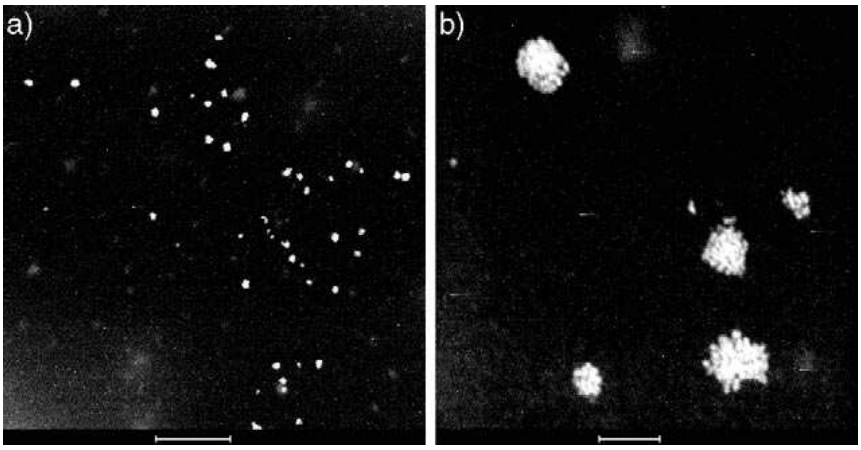

Figure 19: STEM pictures of imprinted nanogels: a) Ru-O_4 stained imprinted nanogels with a scale of 200 nm; b) Ru-O_4 stained imprinted nanogels with a scale of 20 nm[128].

The average mass M_N and M_W of the polymers were also determined using two different techniques, osmometric membrane and Gel Permeation Chromatography (GPC). The average mass M_N was found to be around 44 kDa, which is similar to their natural counterparts, the enzymes. Along with these studies, the number of active sites per particle was investigated. The presence of one active site per particle was reported for one of the imprinted nanogels synthesized with the 'post-dilution' method. This result marked a definite progress for the development of enzyme mimics.

The design of the system was based on the TSA approach and the template selected was dipheny phosphonate that could form a complex (**28**) with the functional monomer N,N'-diethyl-4-vinylbenzamide as shown in **Figure 20**.

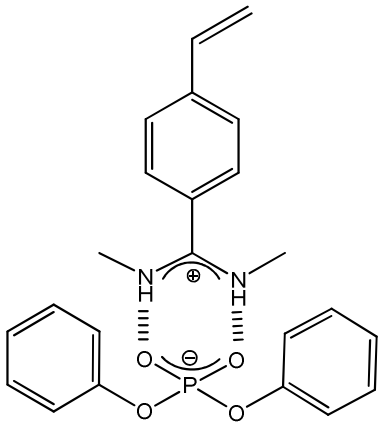

(**28**)

Figure 20: Structure of the complex (**28**) formed between the TSA molecule, diphenyl phosphonate and the functional monomer, N,N'-diethyl-4-vinyllbenzamide

The imprinted particles demonstrated good catalytic activity with a 291-fold rate enhancement compared to the uncatalyzed reaction and 18-fold rate enhancement compared to the non-imprinted nanogels, which attests a successful imprinting.

Taking this approach of developing catalytic imprinted nanogels to the next level, some groups invested a great deal of effort into production of imprinted nanogels for the catalysis of more challenging reactions such as carbon-carbon bond formation.

1.4.2.4.2 Carbon-carbon bond formation

Imprinted polymers with catalytic activity for carbon-carbon bond formation reactions have been developed much less than those for hydrolytic reactions. This is due to the fact that the development of such systems is in general more challenging. While many examples of 'bulk' imprinted polymers for these types of reactions are available in the literature (some were presented in a previous section), there are to date only few examples of imprinted nanogels for the catalysis of carbon-carbon bond formation. Li et al. reported first the preparation of soluble imprinted nanogels with a peroxidise-like activity[130]. The design of the system was based on the knowledge of the high activity of metallo-porphyrin coupled with a protein moiety in natural peroxidase. Thus imprinted nanogels were prepared for the catalysis of the homovanillic acid (HVA) oxidation. These studies followed previous work carried out by the same group

on the insoluble imprinted 'bulk' polymers for the catalysis of the same reaction[131]. The latter polymers demonstrated efficient catalysis with considerable substrate specificity in the presence of hydrogen peroxide. In this study, soluble imprinted nanogels were synthesized in presence of a catalytic entity consisting of Fe-porphyrin (*hemin*), 4-vinylpyridine, acrylamide, and ethylene glycol dimethacrylate (EGDMA) as cross-linker via a high dilution radical polymerisation. The TSA molecule was HVA, which served also as substrate. The resulting nanogels were characterized by GPC, transmission electronic microscopy (TEM) (shown in **Figure 21**), Dynamic Light Scattering (DLS) and the average diameter of the particles was found to be around 200 nm in DMSO. The imprinting system is described in **Figure 22.**

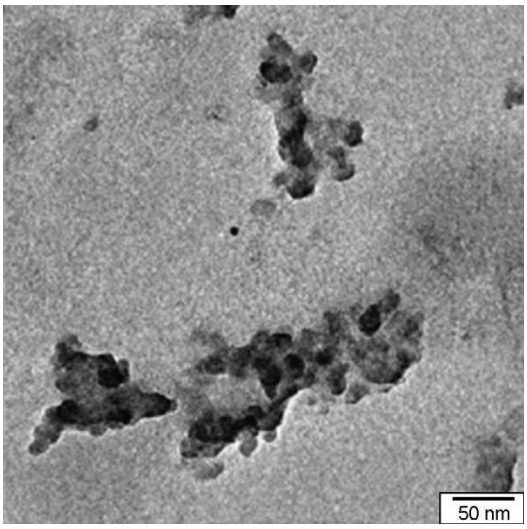

Figure 21: TEM picture of imprinted nanogels[130]

The kinetic studies in presence of the nanogels demonstrated a good catalytic activity that was higher in a mixture of DMSO-buffer where the nanogels gives completely clear solutions than in buffer alone. The kinetic profile follows the Michaelis and Menten model. A rate enhancement about 7-fold compared to the results obtained for the 'bulk' polymers was also noticed. This suggested the higher efficiency of the nanogel matrix compared to ground bulk polymers due to their smaller size and the greater degree of flexibility of the polymer matrix.

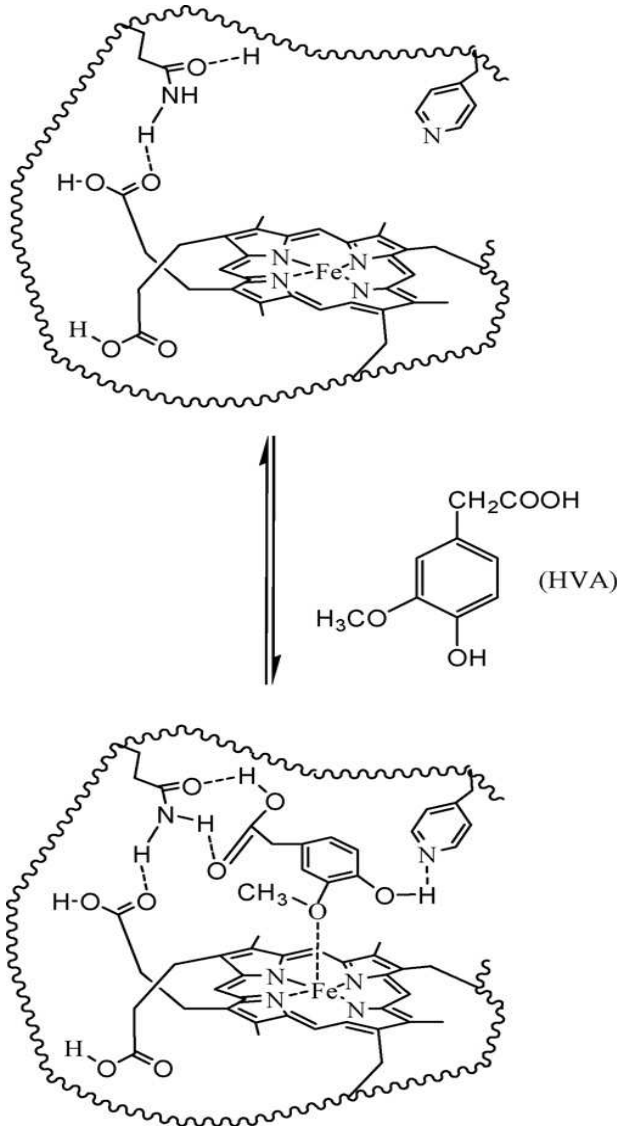

Figure 22: Imprinting process for imprinted nanogels with peroxidise-like activity with HVA as template and substrate[130].

The second example of catalysis of carbon-carbon bond formation reactions by imprinted nanogels was reported by Carboni et al.[3]. Imprinted nanogels with aldolase type I like activity were prepared. The reaction used to test the efficiency of these nanoparticles was a cross-aldol reaction between 4-nitrobenzaldehyde (**29**) and acetone resulting in the formation of the corresponding β-OH-ketone (**30**) as shown in **Scheme 9**.

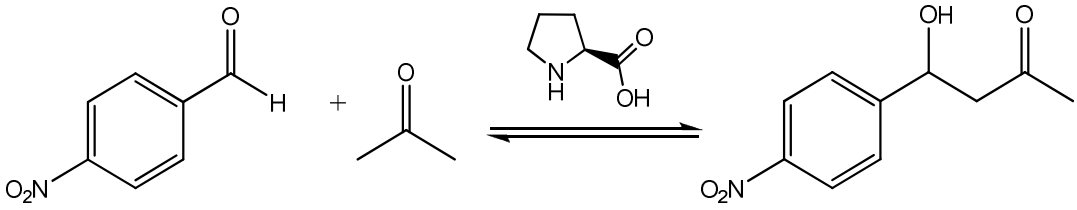

(**29**) (**30**)

Scheme 9: Cross-aldol reaction between 4-nitrobenzaldehyde (**29**) and acetone resulting in the formation of the corresponding β-OH-ketone (**30**)

The aldol condensation is a very important reaction in organic chemistry leading to the formation of a new chiral centre supporting a hydroxyl group that allows the generation of other functionalities. The control of the reaction stereo-selectivity is of a high interest for its practical applications. The use of natural enzymes, such as aldolase type-I, gives the opportunity of forming the desired product at viable rate but is limited in terms of range of conditions which can be utilised. Extensive work has been done on catalytic antibodies to overcome this issue[132]. The creation of polymerisable derivatives of amino-acids as functional monomers would yield to the generation of a new class of catalytic imprinted polymers. This was done previously by Resmini et al. to create enzyme mimics that could catalyse carbonate hydrolysis[2] as described in section 1.4.2.3.1. In this work, a polymerisable derivative of L-proline was synthesized and used as functional monomer. The selection of the template molecule (**31**) was inspired by the TSA approach and allowed the formation of a covalent template with the polymerisable proline derivative (**32**) as described in **Scheme 10**.

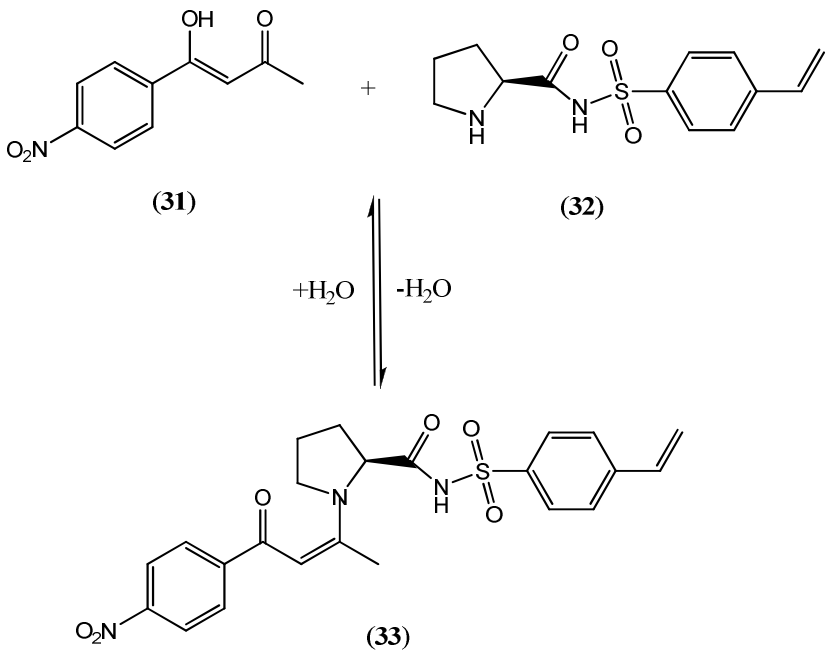

Scheme 10: Reaction scheme of the formation of the covalent complex (**33**) between the TSA molecule (**31**) and the polymerisable proline derivative (**32**)[3]

After the formation of the complex, all the monomers and initiator are added in situ in presence of the porogen. Imprinted nanogels are then generated by a standard protocol of high dilution radical polymerisation. Soluble acrylamide-based nanogels were obtained and characterized by standard techniques such as DLS, GPLC and Electronic microscopy. The average size of the nanoparticles was found to be around 20 nm and this was confirmed by TEM pictures shown in **Figure 23**. The number of active sites, which represents the number of proline moieties incorporated inside the nanogel matrix was determined and was evaluated to be 54% and 47% of proline for the imprinted and non-imprinted polymers respectively. This knowledge is crucial for the accurate determination of the kinetic parameters.

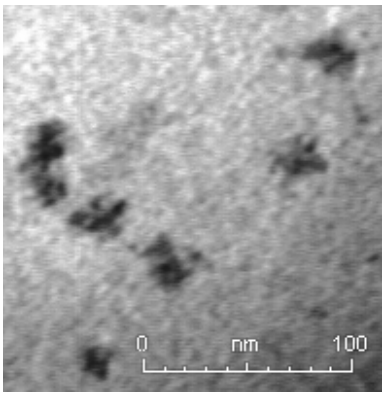

Figure 23: TEM picture of imprinted nanogels with aldolase type-I like activity, where the average size of the particles is around 20 nm^3

The catalytic activity of the nanogels was studied by monitoring the formation of the product, β-hydroxyketone by HPLC. The imprinted nanogels demonstrated good catalytic activity and turnover with a Michaelis and Menten kinetic profile giving a value for the rate constant k_{cat} (calculated using V_M/[active sites]) of 0.25×10^{-2} min^{-1} for the imprinted nanogels, which was comparable with the catalytic antibodies. The imprinting efficiency established by the ratio between the rate constant from the imprinted polymers and the rate constant of the non-imprinted polymers was found to be 18.8. This value stands among the highest values of imprinting factor ever obtained. Along with these remarkable results, the enantio-selectivity of the polymer matrix was investigated using a chiral HPLC column. This potential enantio-selectivity was introduced by the chiral centre from the polymerisable proline derivative as functional monomer. The enantiomeric excess determined was about 63 %, which is higher ever achieved in the generation of catalytic imprinted polymers.

The list of the previous examples describing the combination of the molecular imprinting approach along with a nanogel-type polymer matrix demonstrates the superiority in catalytic and imprinting efficiency of these materials compared to imprinted 'bulk' polymers and makes them a good alternative to biochemical catalysts. They also allow the possibility of creating tailor-made efficient catalysts that are more and more required by our modern industry.

The optimisation of catalytic imprinted nanogels performance for a model system, the Kemp elimination, for the developing enzyme-mimics is one of the

objectives of this work and the next chapter is focusing on the design of the imprinting system and the kinetic and physical chemical characterisations of the resulting imprinted nanogels.

CHAPTER 2

RESULTS AND DISCUSSION

POLYMER SYNTHESIS

2 RESULTS AND DISCUSSION

2.1 RESULTS AND DISCUSSION: POLYMER SYNTHESIS

2.1.1 Project rationale

2.1.1.1 Introduction:

Since the discovery of the interesting properties of materials at nano-range scale, there has been growing interest towards this new field of technology, known as nanotechnology, notably for the use of these materials for innovative products and devices. One particular application that has considerable potential is the development of new catalysts. The discovery of more efficient and environmentally friendly catalysts would contribute to the development of new economical processes, increasingly a requirement in our modern society, where innovation, respect of the environment, and the use of renewable sources of energy are constantly searched for[133].

Catalysts play a fundamental role in chemical research. The quality and efficiency of these entities have great impact in fields such as organic chemistry as they allow new synthetic strategies leading to considerable progress in drug development and processing[1]. Therefore, there is an increasing need of catalysts with high specificity and turnover, but also high substrate and stereo-selectivity. The possibility of obtaining new catalysts with dimensions comparable to enzymes would yield to new class of tailor-made catalysts that can perform on a wider range of reactions. The outcome from this is not to outperform enzymes but to generate synthetic entities capable of acting under harsh conditions such as organic solvent or high temperature and/or to create catalysts for reactions, for which there are no enzymes.

As explained in the section 1.4 of the introduction, the molecular imprinting approach offers the advantage of producing three-dimensional recognition sites inside

a polymer matrix, as a result of the imprint of a target molecule. In addition, the Transition State Analogue (TSA) approach, which consists of imprinting the polymer matrix with a molecule that closely resembles to the reaction intermediate, gives the opportunity of generating sites that can lower the activation energy of the transition state and as a result accelerate the reaction. This approach has been used for the generation of polymers with catalytic activity although mainly using the 'bulk' polymer format, where small particles are obtained by grounding and sieving the solid material. This gave interesting results, however the catalytic efficiency of these materials, with some exceptions, was not comparable to enzymes. Enzymes are known to exhibit considerable conformation fluctuations generally located in the substrate-binding region. These structural properties, which are responsible of the opening/closing substrate binding pockets, arise from and are facilitated by the high flexible of the enzyme matrix as shown in **Figure 24**.

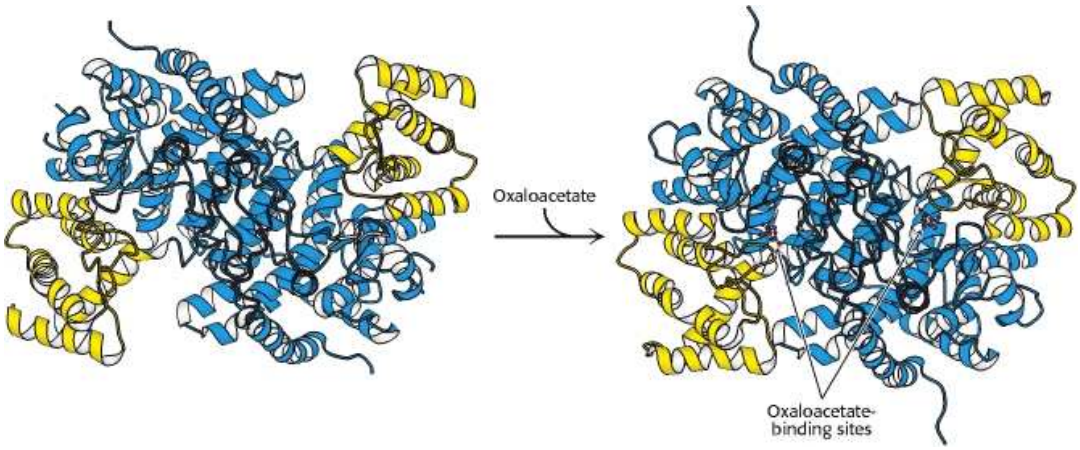

Figure 24: Conformation changes in citrate synthase on binding oxalo-acetate where the unbound enzyme is in its opened form (left) and the liganded enzyme is in its closed formed (right)[134]

Analysis and computational modelisations of enzyme mechanism of action appear to indicate that these large concerted motions along with a set of organised interactions contribute strongly to an enhanced catalytic activity and efficiency[135-136]. The high rigidity of 'bulk' polymer matrix presents therefore a disadvantage by preventing conformation fluctuations, which are essential especially for a fast equilibrium between release and up-take of molecules such as template or substrate.

Furthermore, the heterogeneity of the active sites and of the size of the particles resulted in limited catalytic activity, turnover and specificity.

The research group in which this work was carried out acquired significant knowledge on catalytic antibodies and developed the hypothesis that the rigidity of the polymer matrix was limiting considerably the efficiency of catalytic sites[126, 137-138]. It was assumed that the polymer matrix was required to possess a good balance of essential features for a closer resemblance with enzyme behaviour: i) high flexibility of the matrix, to ease the equilibrium between the uptake and the release of molecule inside the matrix; ii) rigidity to maintain a fix position of the functional groups that ensures good molecular recognition; iii) high porosity of the matrix that enables a fast access of the molecules to the active sites. The optimal combination of these contradictory features remains very challenging to achieve and many efforts are invested for this purpose. An alternative to the usage of 'bulk' polymers appeared to be necessary for the development of efficient catalytic imprinted polymers.

Micro/nanogels are intra cross-linked macromolecules that, in response of external stimuli, are able to swell and de-swell in the appropriate solvent, conferring high flexibility to the polymer matrix. An example of microgel swelling in function of pH is illustrated in **Figure 25**.

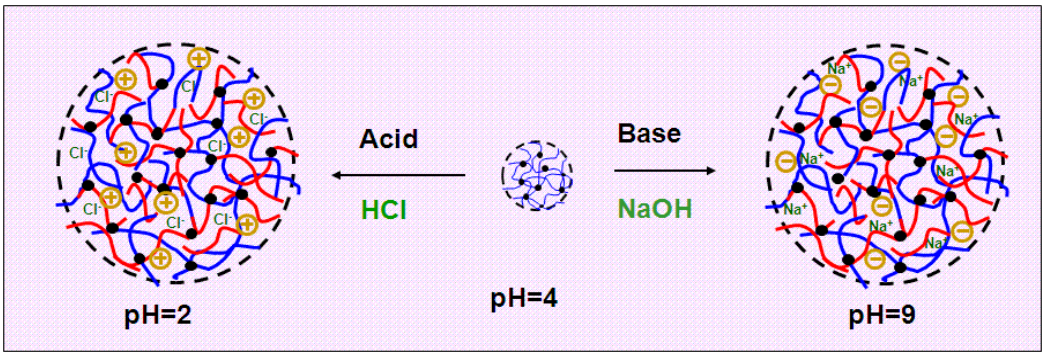

Figure 25: Example of a pH-responsive microgel system, where swelling of the polymer matrix is obtained at high or low pH[139]

This high flexibility is more likely to allow the polymer matrix to adopt different structural conformations than 'bulk' polymers. Micro/nanogels seemed therefore to be good candidate to outperform 'bulk' polymers as 'artificial enzymes'. Furthermore,

nanogels with a size that can reach the one of enzymes and with a low polydispersity were synthesised using a wide range of monomers. This insures a high surface to volume ratio and reduces the diffusion time for the substrate to access the active sites.

In our group, the use of micro/nanogels as polymer matrix has been extensively investigated and applied to catalyse different types of reactions such as the hydrolysis of carbonate and a cross-aldol reaction. In these two systems, nanogels clearly demonstrated superiority in the catalytic efficiency and specificity in comparison with previous studies performed on the same type of reactions using imprinted 'bulk' polymers. The imprinted nanogels with hydrolase activity were the first reported example of application of the nanogel format for the generation of catalytic imprinted polymers[2]. Other studies on imprinted nanogels for carbonate hydrolysis succeeded this pioneer attempt improving the catalytic efficiency and the morphology of the material.

In these types of catalytic systems, the dimension scale of these particles overpasses the one of a single active site. Therefore, parameters such as mobility, confinement effects, solution behaviour, and interfacial properties of these nanoscale materials have to be taken into consideration. More specifically, the different behaviour adopted by nanogels in different solvents systems and the possible impact of these morphology changes in the catalytic activity remains still unknown. Thus, intensive investigations on the physical chemistry of these materials such as mass diffusion, swelling, aggregation or surface structure and their effects on the activity are highly necessary and require careful attention.

2.1.2 Objectives

The objectives of this work are to contribute to the understanding of how the physical chemistry of nanogels particles is correlated to the catalytic activity and to attempt the identification of the parameters that affect the catalytic and imprinting efficiency of the particles. A complete understanding of the nanogel behaviour has so far not been reported and is essential for their application in catalysis, as it would yield

new synthetic strategies for their development as new class of tailor-made catalysts. In this thesis, the modification of polymerisation parameters including initiator content and template/functional monomer ratio, as well as the effect of external stimuli such as organic solvent content, pH, and use of surfactant on the catalytic activity of the imprinted nanogels was investigated. These studies were carried out with the view of implementing the synthesis and the development of more active and efficient imprinted nanogels.

2.1.3 Model reaction: The Kemp Elimination

In order to investigate the catalytic activity of imprinted nanogels by altering the conditions of kinetic experiments and/or the formulation of the nanoparticles, the choice of an appropriate system was of great importance. This required the identification of a model reaction that was suitable for the investigation of the catalytic activity of the nanoparticles under various conditions. The selection of such reaction would provide a system that is versatile and for which the kinetic conditions such as solvent, pH or temperature could be easily altered and optimised. The search for this ideal system was also directed towards a model reaction that does not require any complex organic synthesis of substrate or monomer and to possess a well-established mechanism. In addition, a reaction based on elimination mechanism would be more advantageous in order to prevent any issues of product inhibition that often arise during the catalysis process with imprinted polymers.

In this view, the Kemp elimination was selected as a model reaction. The reaction scheme is described in **Scheme 11**.

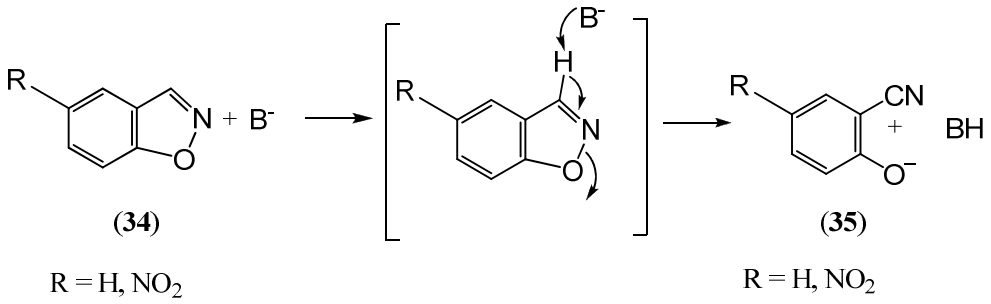

Scheme 11: Base-catalysed isomerisation of benzisoxazoles (**34**) resulting in the formation of cyanophenols (**35**) known as Kemp elimination[4].

The Kemp elimination is the base-catalysed isomerisation of benzisoxazoles (**34**) resulting in the formation of cyanophenols (**35**)[4]. This reaction has been extensively studied in the past and its mechanism is now well-established. There is no enzyme catalysing this reaction, making the design of enzyme-like catalysts for this reaction even more challenging. Several research groups used this reaction as a model for the creation and development of new catalytic systems. Kirby and co-workers demonstrated the catalytic activity and efficiency of set of water-soluble polymers prepared by alkylation of polyethylenimine (PEI). They named this novel type of catalysts 'synzymes'. These 'synzymes' were found to be very active in water with rate enhancements as high as 10^6 compared to the uncatalysed reaction and at least 1000 turnover per active sites[5]. Holffeder et al. reported the catalysis of the Kemp elimination by Bovine Serum Albumin (BSA) and other serum albumins. More specifically, it was demonstrated the high catalytic activity of lysine moieties towards this reaction along with other factors[140]. The catalytic activity of natural coils towards the Kemp elimination was described by Shulman *et al.*[141]. The development of catalytic antibodies was also reported by Muller *et al.*, where it was described the significant and complementing activity of the side chains of three different polar residues Asp(H35), His(H95) and Glu(L34) as shown in **Figure 26**[142].

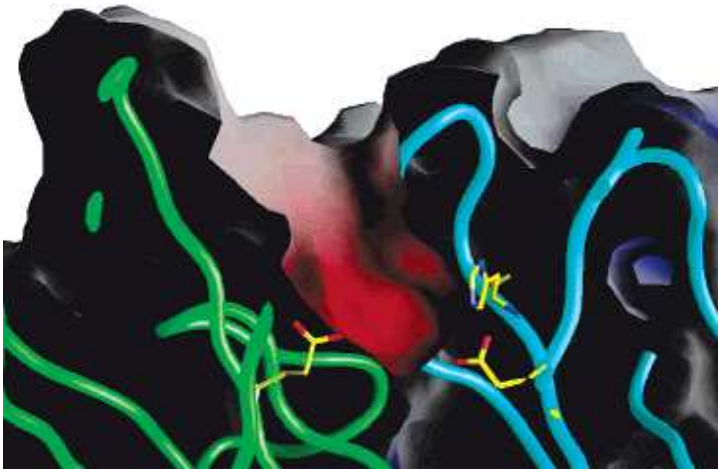

Figure 26: Active site of antibody 13G5 in the absence of ligands. A slice of the binding pocket is shown. The heavy and light chains are displayed in cyan and green coils respectively. The side chains of the three polar residues Asp(H35), His(H95) and Glu(L34) are highlighted and project into an hydrophobic cavity[142].

The real breakthrough in the development of enzyme mimics for the Kemp elimination was reported by Röthlisberger and co-workers in 2008[143], where the design of eight enzymes was achieved by means of computational design methodology. Quantum mechanical transition state calculations were used to model an idealised active site with protein-based functional groups. These groups were positioned in a way to maximise transition state stabilisation. The base-catalysed deprotonation of the carbon atom in the Kemp elimination mechanism inspired the design of the active site. These artificial enzymes were constituted of two different base catalytic motifs: the first one was based on the carboxylic group of an aspartate or glutamate side chain, and the second shown in **Figure 27** was the imidazole of a histidine positioned and polarised by the carboxyl group of aspartate or glutamate referred as a His-Asp dyad. The catalytic parameters of the new designed enzymes reported in this paper, displayed comparable catalytic efficiency to the most active catalysts of the Kemp elimination of 5-nitrobenzisoxazole reported so far, which are the catalytic antibodies. This work carried out by Röthlisberger *et al.* marked an important progress in the development of new tailor-made catalysts and provided further insights into the making of enzyme mimics.

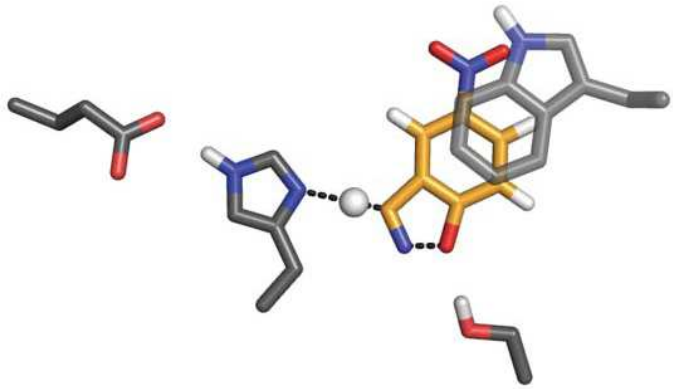

Figure 27: Example of active site motif highlighting a His-Asp dyad used for deprotonation, and a π-stacking aromatic residue for transition state stabilisation[143].

The development of enzyme mimics for the Kemp elimination using the molecular imprinting approach was also previously investigated. As mentioned in section 1.4.2.2 of the introduction, Mosbach *et al.* reported the synthesis of imprinted 'bulk' polymers[107]. The imprinted and non-imprinted polymers were prepared in anhydrous dichloromethane. The solid material obtained after polymerisation was ground and sieved to obtain polydispersed particles with a size that range from 25 µm to 75 µm. The kinetic studies of the imprinted polymer demonstrated relatively good catalytic activity following the Michaelis-Menten saturation model. Nevertheless, the determination of active site numbers, which corresponds to the concentration of pyridine moieties incorporated in the polymer matrix, was not carried out. The knowledge of this parameter is important as it allows an accurate calculation of the rate constant k_{cat} of the catalysed reaction. Furthermore, the Michaelis-Menten model can only be applied if the concentration of catalyst does not overpass 30% of substrate concentration. This verification was not carried out on this paper, questioning the validation of this model. In addition, the inhibition studies demonstrated a decrease of only about 10% of the catalytic activity when the template indole was added to the imprinted polymers. This decrease could be explained by the fact that indole by filling the cavity prevented the access of the substrate into the active sites. A low decrease around 10% in catalytic activity clearly demonstrated that the catalysis of the reaction was initiated by the pyridine moieties located at the surface of the particles outside the imprinted cavities and therefore that the catalysis was not specific. This result was

not surprising considering the large excess of functional monomer incorporated in the matrix compared to the template, which is expected to favour the formation of non-specific active sites. Overall in this work, the use of the imprinted 'bulk' polymers as enzyme mimics was not as thorough and detailed as it could be expected.

Another study using liquid crystalline imprinted materials (LCIM) was reported for the catalysis of the Kemp elimination as shown in **Figure 28**[144]. This approach consisted in replacing chemical cross-linking by physical cross-linking due to the interactions between the mesogens. Different LCIM were prepared from polysiloxanes or polyacrylates with low cross-linker content.

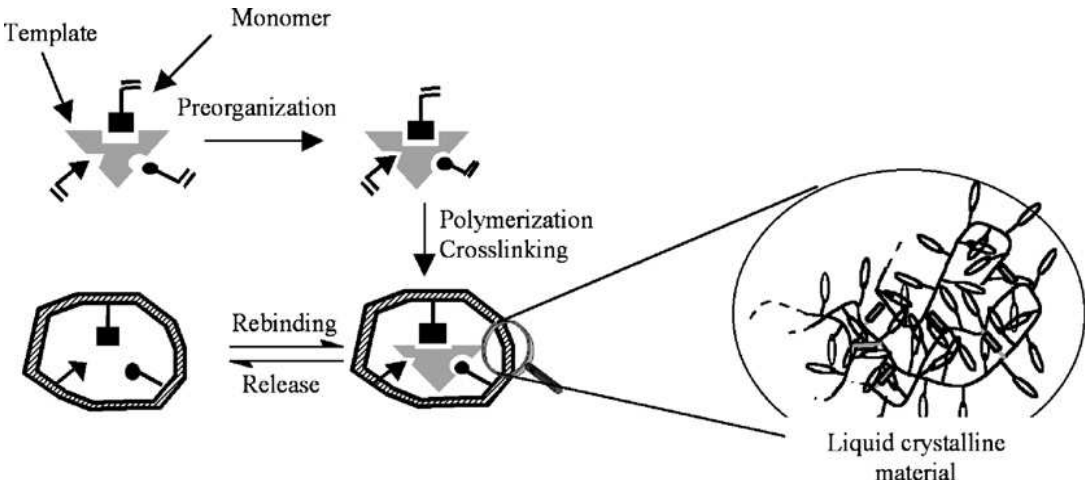

Figure 28: The molecular imprinting approach using liquid crystalline materials[144]

The imprinted materials demonstrated remarkable properties of molecular recognition. This was attributed to the mesomorphic order that provided significant enhancement to the bonding between the template and the liquid crystalline network. Although a good imprinting efficiency was demonstrated by a higher activity of the imprinted polymer compared to the non-imprinted polymer, the polymers did not show however greater catalytic activity than with Mosbach's system described in the previous paragraph. Similarly to the work of Mosbach's group, the number of active sites was not determined, which prevents an accurate calculation of the kinetic parameters.

Despite considerable interests in the Kemp elimination, the development of imprinted nanogels has not been reported for this system. The use of this model

reaction to develop new methodologies for generating catalysts is in fact very recent. The Kemp elimination possesses many features that are advantageous for kinetic studies. The product formed during the reaction, cyanophenol, has a strong characteristic band detectable by UV-Visible spectroscopy, allowing an easy data collection. The shape of the transition state of the reaction is known and therefore the TSA approach can be applied to design an appropriate template molecule. The popular use of this reaction demonstrated that this system is a model of choice to evaluate or develop new catalysts. It is worth noticing that the use of this reaction for the development of catalytic imprinted nanogels was investigated in the first stage of this project in 2006 before the Nature paper was published in 2008[143].

2.1.4 Design of the system

Previously in our group, the preparation of imprinted nanogels was performed on systems that involved the formation of a tight complex between the template molecule and the functional monomer resulting from strong interactions. In fact, in the hydrolase system, the interactions were ionic with a high association constant K_a leading to an imprinting process with a stoichiometric non-covalent approach[2]. In the aldolase-type system, the imprinting process was based on a reversible covalent interaction between the template and the functional monomer. The complex formed was an enaminone that could be reversed by simple hydrolysis to give the initial template molecule and the functional monomer[3]. In both cases, the interactions between the template and the functional monomer were very strong and led to the generation of three dimensional cavities with good properties of molecular recognition and specificity.

Pauling and Haldane in 1946 suggested that the enhanced catalytic activity of enzyme was related to a well-organised network of weak interactions such as hydrogen bonding or hydrophobic interactions capable of stabilising a transition state[145]. Therefore, for a general understanding of how this environment could be reproduced using imprinted nanogels, the choice of interactions between the template

molecule and the functional monomer was directed towards non-covalent interactions such as H-bonding or hydrophobic interactions.

In the early stage of the project, it was important to design a system that fulfilled different criteria to increase the possibility of creating specific cavities. Three important parameters had to be taken into consideration: i) the choice of the couple template/functional monomer that can form a tight complex, ii) the nature and content of cross-linker to obtain a good balance of rigidity and flexibility and iii) the choice of a polymerisation solvent that favoured the interactions between the molecules of the system. The conception of this finalised system would lead to a successful imprinting by reducing the formation of non-specific binding sites. This also would have a great effect on the generation of cavities that would be able to interact well with the substrate and lower the activation energy of the transition state.

2.1.4.1 Choice of the template and functional monomer couple

The design of the system was based on the TSA approach applied to a non-covalent imprinting approach. This method, as explained in section 1.4.2.1, consisted in imprinting the polymer matrix with a molecule that resembled closely to an important intermediate of the reaction. Designing 'artificial enzymes' is a very challenging and daunting task that involves a series of requirements including a precise knowledge of the geometry of transition state, and the tools to correctly position crucial functional group at the right place[146].

The mechanism of the Kemp elimination has been well-established. The identification of a suitable template molecule with the correct molecular and electronic geometry could be easily done by simple analysis of the shape of the transition state of the reaction as shown in **Figure 29**.

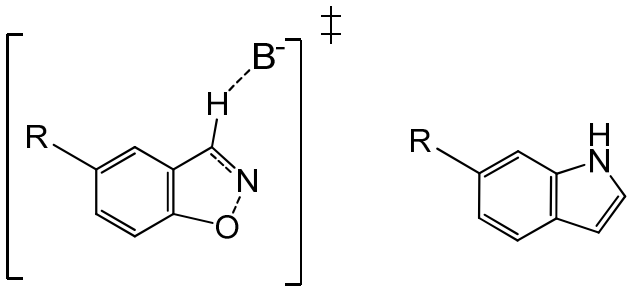

(36) **(37)**

$R = H, NO_2$

Figure 29: Choice of the template molecule following the TSA approach, where (**36**) represents the transition state of the Kemp elimination and (**37**) the template molecule, indole.

The selection of a template molecule that displays the ability of forming interaction with a unique direction point was also of great important for the generation of cavity with a unique way of fitting. This was expected to reduce the heterogeneity of the cavity formed during the imprinting process. Thus, after careful consideration indole was selected as template as its shape resembled closely to the one of the transition state of the reaction and presented one possible point of interaction.

The functional monomer chosen was 4-vinylpyridine. This monomer is commonly used in molecular imprinting since it displays good rate of polymerisation at 80°C in a wide range of solvents, compared to the styrene monomer[147]. This molecule displays good properties of basicity (pK_a of the nitrogen proton around 5.4), which was an essential feature for the catalysis of the Kemp elimination. This vinylic monomer is also a well-established hydrogen bonding acceptor. The indole proton attached to the nitrogen is known to be slightly acidic (pK_a around 16 in water) and it can act as a hydrogen bond donor. The removal of this proton necessitates indeed the use of a very strong base such as sodium hydride. The utilisation of 4-vinylpyridine as functional monomer would therefore not induce the deprotonation of indole. Our approach was to form a complex between indole and 4-vinylpyridine via a hydrogen bond with the nitrogen proton of the indole in the appropriate solvent. This type of interaction between two conjugated π-electrons systems has already been investigated in the

past. In 1983, Mataga *et al.* studied the fluorescence quenching of amino-pyrene with adding increasing equivalents of pyridine[148]. This is shown in **Figure 30**.

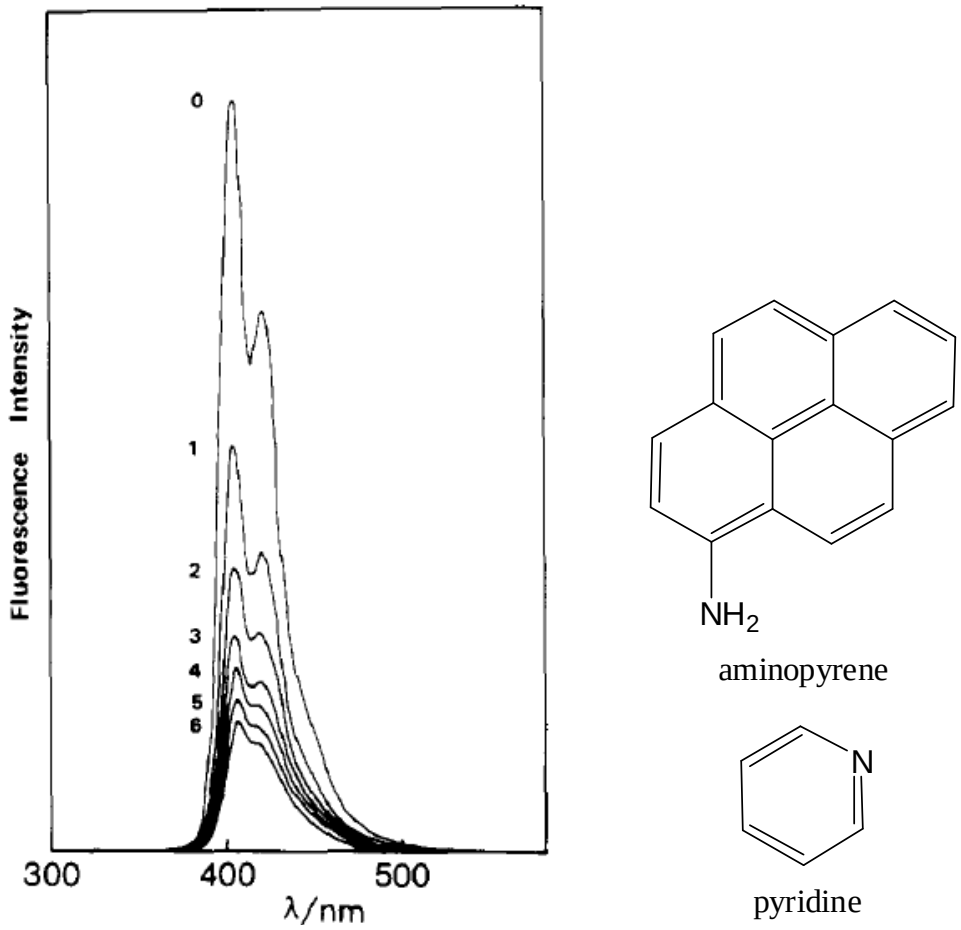

Figure 30: Fluorescence quenching of aminopyrene AP in presence of different pyridine P concentrations; [AP] = 5×10^{-5} M, [P]: (1) 0.0052 M; (2) 0.0103 M; (3) 0.0155 M; (4) 0.0207 M; (5) 0.0258 M; (6) 0.0310 M[148]

In agreement with these observations, it was established the formation of two types of interactions between the molecules, a hydrogen bond (D*-H---A) from the donor D amino-pyrene and the acceptor A pyridine, and charge transfer (D^--H---A^+). It was also demonstrated that the charge transfer from the amino-pyrene to the pyridine molecule was the cause of the fluorescent quenching. However, the methylation of the amino-pyrene was found to suppress the quenching meaning that the hydrogen bond between both molecules was crucial for the charge transfer to occur.

Hidalgo *et al.* reported the same type of fluorescence quenching of betacarboline (**38**) (9H-pyrido-[3,4-*b*]indole), shown in **Figure 31** in presence of pyridine[149].

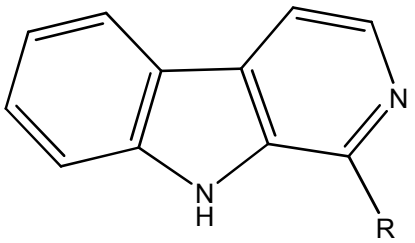

(**38**)

R = H
R = CH_3

Figure 31: Structure of betacarboline (**38**)[149]

A charge transfer was also causing the fluorescence quenching, however the formation of the hydrogen bond was characterised by UV-Visible spectroscopy, characterised by a shift towards the red in the absorbance spectra. The methylation of the nitrogen from the indole moiety gave rise to the suppression of the fluorescence quenching similarly to the previous study of Malaga *et al.* It is worth noting that for both studies, the hydrogen bond formation was only occurring in non-polar solvents such as methylene chloride and was not observed in polar solvents.

For our system, a hydrogen bond was envisaged between indole and 4-vinylpyridine. The strength of this interaction was expected to be weak and highly dependent on the nature of the solvent, in which the polymerisation would be carried out. Interaction studies needed to be investigated in order to optimise the conditions of polymerisation.

In order to avoid any competition between monomers with the template molecule during the polymerisation process, the use of a co-monomer was not considered. This type of competition is often the cause of a reduction of active sites resulting in a lower catalytic and imprinting efficiency. The influence of a co-monomer on the binding capacity of non-covalent theophilline-imprinted polymers was studied in previous work by Tunc and co-worker[150]. More specifically, it was reported the

effect of adding 2-hydroxymethyl methacrylate (HEMA) or acrylamide (ACM) as co-monomer to a MAA/EGDMA polymer backbone. The preparation of the different imprinting systems is shown in **Figure 32**. In both case, the binding capacity of the imprinted polymer towards theophilline was reduced from 61% (without co-monomer) to 41% using HEMA as a co-monomer and 40% using ACM as co-monomer. This decrease was explained by monomer-monomer associations and morphological differences between monomers. It was also demonstrated that the use of co-monomers induced a heterogeneous distribution of binding sites.

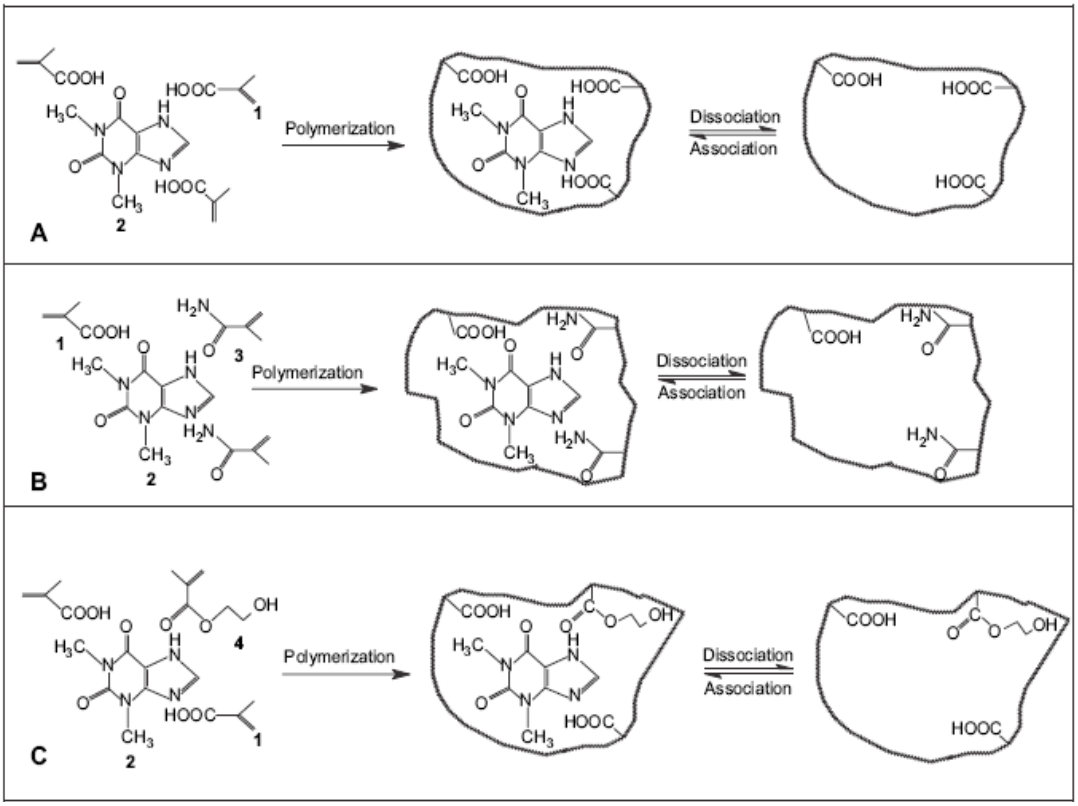

Figure 32: Representation of possible interactions between theophilline and functional monomers to obtain specific cavities: A) MAA/EGDMA; B) MAA/ACM/EGDMA; C) MAA/HEMA/EGDMA[150].

This reduction of activity was also described by Mosbach et al. in the preparation of catalytic imprinted 'bulk' polymers for the Kemp elimination, where it was found that the addition of methyl methacrylate as co-monomer in the pre-polymerisation mixture decreased considerably the catalytic efficiency of the polymers[107]. As a result, 4-vinylpyridine would be used as functional monomer as well as backbone monomer for our system.

2.1.4.2 Choice of the cross-linking agent

The type of cross-linkers used for the preparation of molecularly imprinted polymers are various, but the most common found in the literature includes divinylbenzene (DVB), ethylene glycol dimethacrylate (EGDMA), *N, N'*-ethylene-bis-acrylamide. The first parameter to take into consideration for the selection of a particular cross-linker is its reactivity compared to the reactivity of the functional monomer during the polymerisation process. The reactivity of both compounds needs to be similar in order to achieve a good incorporation of the functional monomer inside the polymer matrix. In the opposite case, a phase separation is observed due to a fast polymerisation of the molecules of cross-linker leaving out the molecules of functional monomer. As a consequence, the functional monomer is not or to a very small extent incorporated into the polymer matrix leading to the failure of the imprinting process. Tables of reactivity of common monomers and cross-linkers are available in the literature[151].

The second important parameter in the choice of a suitable cross-linker was the physical-chemical properties of the polymer matrix resulting from a particular cross-linker after polymerisation. Wulff and co-workers in the early studies, compared a series of different types of styrenic-based and methacrylate-based cross-linkers, commercially available or custom-made[152]. In their system, EGDMA was found to be the best cross-linking agent compared to DVB and its tetramethylene analogue. This ranking was established based on the selectivity of the polymer matrix towards the separation of a racemate mixture of the template. This was attributed to the rigidity and prochiral character of the methacrylate groups of EGDMA. Other cross-linkers with more than two (meth)acrylate groups such as trimethylolpropane trimethacrylate (TRIM)[153], pentaerythritol triacrylate (PETRA)[154] or pentaerythritol tetraacrylate (PETEA)[155], which structures, shown on **Figure 33,** were found to be even superior to EGDMA in the preparation of selective imprinted polymers in some applications.

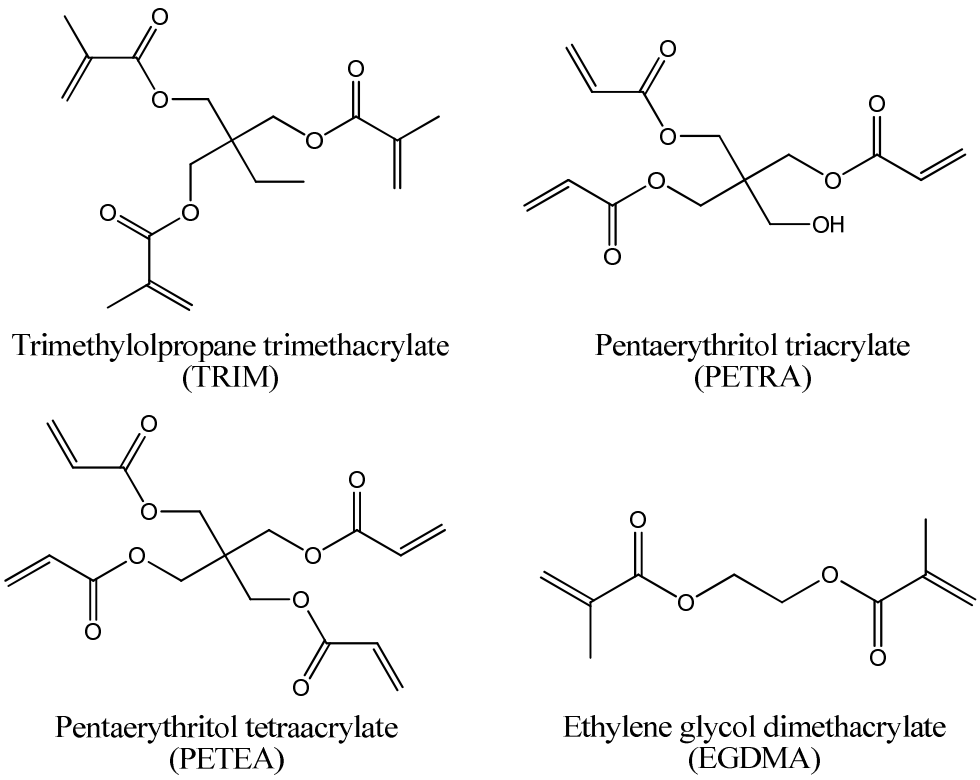

Figure 33: Structures of the different acrylate-based cross-linkers used in the preparation of imprinted polymers.

The couple acrylamide/bisacrylamide is widely use in the preparation of soluble polymer gels. In our group, this couple has been employed for the generation of catalytic imprinted microgels and nanogels[2-3]. The reason of the popularity of this couple resides in the ability of the amide functional groups to interact well with amino acids or other polar groups and to prevent or minimise non-polar interactions that might occur during the polymerisation process and affect the solubility of the monomers in the medium.

Ethylene glycol dimethacrylate (EGDMA) (**41**) was selected as cross-linker in our system in association with 4-vinylpyridine. This cross-linker does not contain any hydroxyl or amine moieties. Therefore, it was not expected to prevent and/or minimise any interaction between the template and 4-vinylpyridine. In addition, EDGMA is soluble in a wide range of non-polar solvents including chloroform, methylene chloride and polar solvents such as DMF or DMSO.

The final design of the imprinting system is described in **Figure 34**.

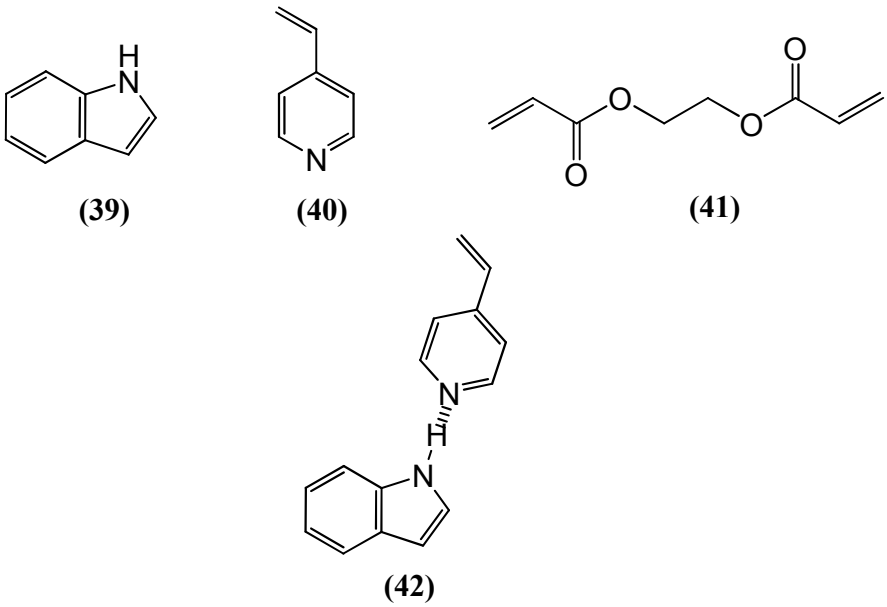

(39) **(40)** **(41)** **(42)**

Figure 34: Choice of the template (**39**), indole, the functional monomer (**40**), 4-vinylpyridine, the cross-linker (**41**) EGDMA and the theoretical non-covalent complex (**42**) formed between indole and 4-vinylpyridine via hydrogen bonding to imprint the polymer matrix.

2.1.4.3 Choice of the polymerisation solvent

The polymerisation solvent plays an important role in the imprinting process. The strength of the interactions between the template and the functional monomer depends strongly on the nature of the solvent more specifically its polarity, its proticity, and its ability of dissolving all the components of the system. As a general rule, the solubility properties of the solvent chosen have to match with those of all the components of the polymerisation mixture. This is due to the fact that compound with certain properties are better solvated in solvents exhibiting similar properties. All the molecules of our system are soluble in most of the organic solvents. Water was discarded as polymerisation solvent since indole and EGDMA are not soluble in aqueous media. However, the selection of solvent cannot be achieved without a thorough study of the interactions between the template and the functional monomer as it influences strongly the strength of these interactions.

The study of the interactions between the template indole and the functional monomer 4-vinylpyridine are required prior the synthesis of the imprinted nanoparticles. The outcomes of these studies would provide useful information about the conditions for an optimal interaction between both molecules, which interaction is crucial for the generation of specific cavities. This knowledge would also indicate the nature of solvent that must be used during the polymerisation process.

2.1.5 Study of template-monomer interactions

The strength of interaction between the template molecule and the functional monomer was a parameter of great importance in the synthesis of imprinted nanoparticles as it controls the specificity and the molecular recognition ability of the imprinted sites. Strong interactions that are able to undergo the polymerisation process ensure that the functional groups will be maintained in the right place and kept in place inside the cavity after removal of the template molecule. When the interactions are weak, they are more likely to be distroyed during the polymerisation process. As a consequence, the position of the functional groups is altered limiting the formation of a specific cavity and leading to the formation of non-specific sites. The imprinting efficiency is then reduced. It becomes clear that the study of these interactions was a key step in the preparation of imprinted polymers. It is worth noting however that this step was rarely reported in a majority of publications, where imprinted polymers were prepared and studied.

2.1.5.1 Towards the formation of the complex template-monomer

As explained in the introduction, several approaches have been used and are available in the literature for the formation of a tight template/functional monomer complex to imprint the polymer matrix. They differ from each other depending on the nature of interactions used to link both molecules during the imprinting process. To date, the different imprinting approaches reported are non-covalent, stoichiometric non-covalent, covalent and semi-covalent.

In the covalent approach, the template is covalently bound to one or several polymerisable units. After polymerisation the template is extracted by cleavage of the bound leaving the functional groups in place. The cavity formed by this process is able to recognize and re-bind the template molecule by re-establishment of the covalent bound. The advantages of this approach is that the functional groups are only associated with one template molecule and the complex formed is very stable, which ensures a control of the shape of the cavity. Unfortunately, only a limited number of suitable molecules can be imprinted via this method such as alcohols (diols), aldehydes, amines, or carboxylic acids. A famous example of covalent molecular imprinting was reported by Wulff *et al.* in 1977 for the imprint of sugar into a 'bulk' polymer matrix[156]. The imprinting process is described on **Figure 35**.

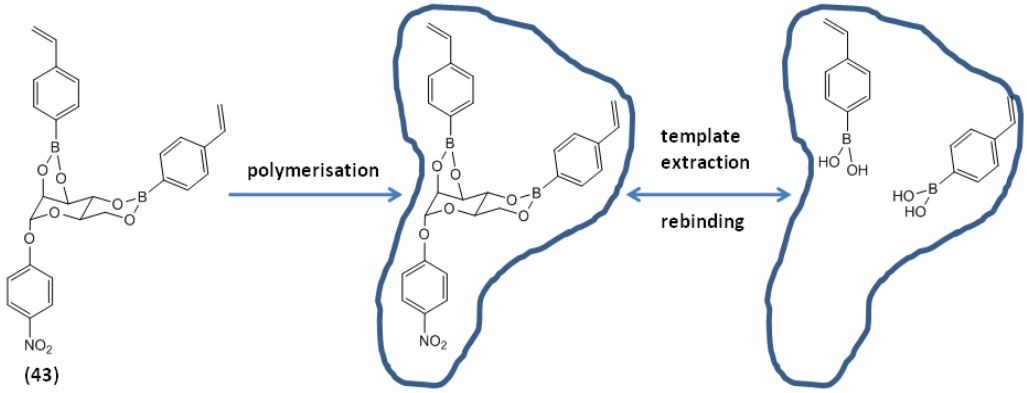

Figure 35: Covalent imprinting process for the imprint of a sugar molecule using a condensation vinylboronic acid with a sugar template. The covalent template - monomer complex (**43**) is polymerised in presence of a cross-linking agent to give an imprinted 'bulk' polymer where the template is removed by hydrolytic cleavage[156].

The semi-covalent approach is based on the formation of a covalent template-monomer complex as described previously but after extraction of the template the target molecule is re-bound onto the polymer matrix by non-covalent association. This can be achieved by linking the template and the polymerisable units directly or by the use of a spacer group such as a carbonyl group[157].

The stoichiometric non-covalent approach, which has been used in our group, is based on the formation of an equimolar template-monomer complex with strong electrostatic interactions and high affinity between complementary groups. The

affinity constant associated stands generally above 10^3 M^{-1}. Wulff *et al.* were the first to report this approach, where the TSA phosphate template was tightly bound to the polymerisable unit for the generation of imprinted 'bulk' polymer for the hydrolysis of carbonates[158].

The formation of a non-covalent template-monomer complex remains the approach which is the most widely employed. The interactions are based on hydrogen bonds, ion pairing or dipole-dipole interactions. The target molecule is then re-bound to the polymer matrix through the same type of interactions. This technique is used mainly because it is very convenient. A large variety of functional monomers and template molecules can indeed be utilised with this approach. The major disadvantage resides however in the lack of control on the self-assembly of the functional polymerisable units around the template molecule, leading to different spatial arrangements than expected. As a result, cavities with different shapes and binding capacity are created giving rise to heterogeneous active sites. In response to these issues, molecular modelling techniques were carried out by Karim *et al.* allowing a tailored selection of functional monomers based on the structure of the template[159]. In this work, a large database of functional monomers was created along with the best conditions for maximising the interactions and lowering the number of self-assembly modes.

The formation of tight complexes appears to be essential for the generation of imprinted cavities with good properties of selectivity. In the case of weak interactions, such as in non-covalent imprinting systems, where it is difficult to control the self assembly between the template and the polymerisable units, the study of the template-monomer complex formation is essential to identify conditions where the assembly is optimal.

2.1.5.2 Investigation of the monomer-template association

In the present system, the interactions between the template indole and the functional monomer, 4-vinylpyridine are non-covalent and the association between

both molecules is expected to be occurring via a hydrogen bond between the nitrogen proton from the indole to the nitrogen of 4-vinylpyridine. The ability of indole to form a hydrogen bond-based complex with a hydrogen bond acceptor similar to 4-vinylpyridine, for instance isoquinoline, was investigated in previous work using mass spectroscopy[160]. In this study, an intermolecular compound of 1:1 molecular ratio of indole-isoquinoline were isolated as crystals, upon crystallisation from mixtures of the two compounds. This was performed after demonstrating the evidence of the association of both molecules via hydrogen bond using the nuclear Magnetic Resonance (NMR) spectroscopy. From the mass spectroscopy analysis, clusters of indole - isoquinoline at equimolecular ratio were found to be the predominant species. This suggested that the hydrogen bonded complex formed between the two species worked as a unit species for the nucleation of intermolecular compounds. This is explained in **Figure 36**.

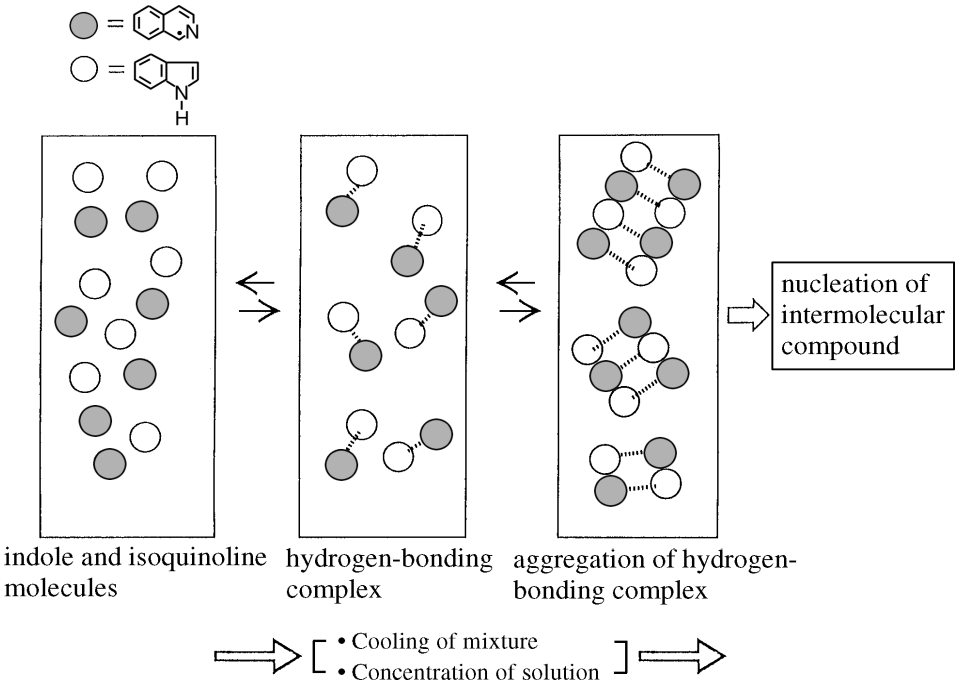

Figure 36: Schematic illustration of aggregation of the hydrogen bonded complex between indole and isoquinoline[160].

Isoquinoline is an isomer of quinoline, which compound belongs to the family of the benzopyridines. Being structurally related to pyridine, isoquinoline displays similar basicity, rather weak, with a pK_a around 5.4 very close to that of pyridine. This

previous work confirmed therefore the strong possibility of a hydrogen bonded complex between indole and 4-vinylpyridine in our system.

Thus, it was decided to investigate closely the interactions between indole and 4-vinylpyridine by analysing the formation of the hydrogen bond or other types of non-covalent associations using standard analytical techniques with the view of determining a binding constant for the complex.

2.1.5.3 Nuclear Magnetic Spectroscopy (NMR) technique for the determination of binding constant

One of the methods commonly employed to monitor hydrogen bond formation is by using Nuclear Magnetic Resonance (NMR) spectroscopy. This technique has been extensively used in the past for the determination of binding constants and has proven to be a very powerful technique for investigating complex formation between molecules. Proton NMR chemical shifts are found to be very sensitive to the environment of the proton and as a result it varies even when non-covalent association occurs[161]. A good example of this technique was reported for the analysis of the AAA-DDD pattern of hydrogen bond acceptors (A) and donors (D) in the arrangement of three contiguous hydrogen bonding centres. This arrangement, shown in **Figure 37** was proven to be the strongest association between two species and the binding constant K_a was found to be in the range of 10^7 M^{-1} [162].

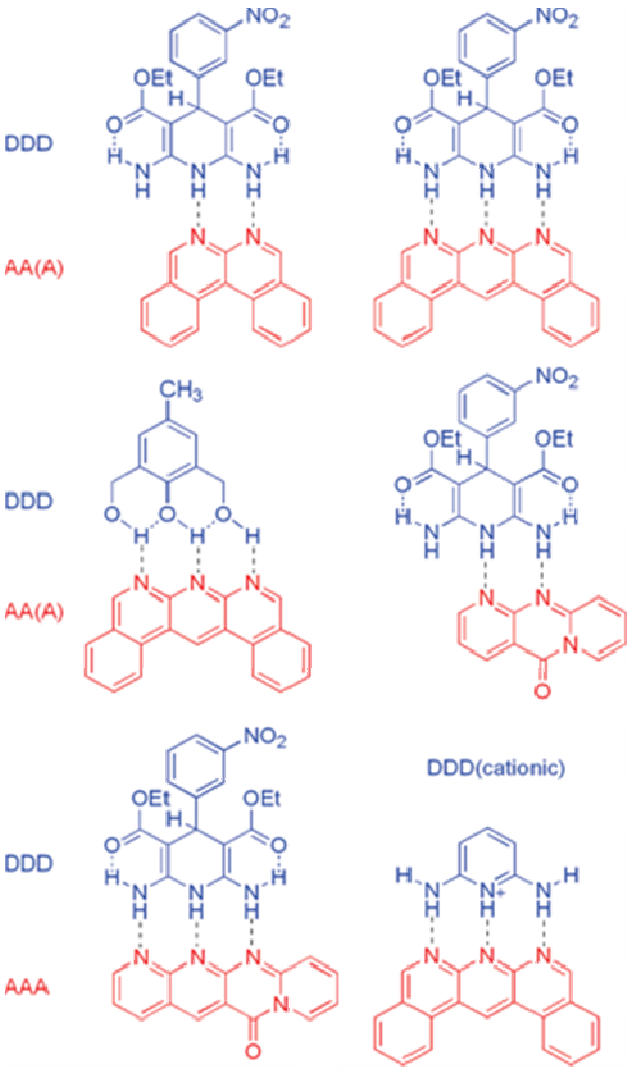

Figure 37: Examples of systems AAA-DDD studied by Leigh *et al.*[162]

A large part of our existing knowledge of non-covalent interactions and the resulting complex formation between a guest (G) and a host (H) resides in the determination of binding constants. A measurement of binding constant permits indeed a quantitative analysis of the association between two molecules. In our system, in correlation with the research results of Yamamoto and co-workers, explained in the previous paragraph[160], it was expected that one molecule of indole would bind one molecule of 4-vinylpyridine. This would suggest that there would be only one binding site per molecule of host H. Thus, the stoichiometry of the resulting complex would not have an impact on the constant determination and the reaction of complex formation can be written as follow:

$$\mathbf{H} + \mathbf{G} \rightleftharpoons \mathbf{HG} \qquad \textbf{(Eq 1)}$$

Where H is the host, G the guest and HG the complex formed.

The dissociation constant K_D can therefore be described as follow:

$$K_D = \frac{[H][G]}{[HG]} \qquad \textbf{(Eq 2)}$$

Where K_D is the dissociation constant, [H] the concentration of host H molecules, [G] the concentration of guest G molecules and [HG] the concentration of complex formed.

It is thus possible to establish the fraction of total binding sites occupied θ, as follow:

$$\theta = \frac{[G]_{bound}}{[H]_{total}} = \frac{[HG]}{[H]+[HG]} \qquad \textbf{(Eq 3)}$$

Where θ is the fraction of total binding sites occupied, $[G]_{bound}$ the concentration of G complexed to H and $[H]_{total}$ the total concentration of host H.

Given the definition of θ, we can use **Eq 2** to substitute the value of [HG] in **Eq 3** to obtain as follow:

$$\theta = \frac{[G]}{K_D + [G]} \qquad \textbf{(Eq 4)}$$

Determining θ is often easy using spectrophotometric methods. In the case of NMR, two cases needs to be distinguished.

- Case 1: The host-guest complexation equilibrium has a slow exchange rate compared to the time scale of the NMR instrument.

In this case, the chemical shifts which are assigned to the host parts in complex and those to the free host are separated and observed individually. By simple integration of the peaks, the determination of θ becomes trivial and a plot of θ versus the different concentrations of guest G allows the measurement of K_D.

- Case 2: The host-guest complexation has a very fast exchange rate compared to the time scale of the NMR instrument.

In this case, the chemical shifts which are assigned to the host parts in the complex and those to the free host are fused into a same peak and appear at the weight average between the chemical shift of the free host and the chemical shift of the complexed host. The relationship between the apparent chemical shift δ, the chemical shift of the free host δ_H and the chemical shift of the complexed host δ_C can be written as follow:

$$\delta = \delta_H \times (1-\theta) + \delta_C \times \theta \qquad \textbf{(Eq 5)}$$

Where θ is the fraction of total binding sites occupied, δ the apparent chemical shift, δ_H the chemical shift of the free host and δ_C the chemical shift of the complexed host.

The latter case is the one that is the most frequent for the determination of binding constant using the NMR spectroscopy. When the value of θ obtained in **Eq 5** is substituted in **Eq 4**, the equation becomes as follow:

$$\frac{(\delta - \delta_H)}{(\delta_C - \delta_H)} = \frac{[G]}{K_D + [G]} \qquad \textbf{(Eq 6)}$$

The dissociation constant K_D can then be determined by plotting the apparent chemical shift δ in function of the concentration of guest added.

The idea was then to determine the binding constant between indole and 4-vinylpyridine using the NMR instrument applying this method.

2.1.5.4 Study of indole-4-vinylpyridine complex

The interactions between indole and 4-vinylpyridine needed to be investigated in order to maximize the association of these two molecules in the pre-polymerisation mixture. This consisted of studying the variation of the chemical shift δ_{Hi} of the nitrogen proton from the indole molecule in presence of increasing equivalents of 4-vinylpyridine in different solvent systems. This would allow the identification of the most suitable solvent, in which to process the polymerisation. The nitrogen proton of indole H_i was in fact susceptible of being involved in a hydrogen bonding with the nitrogen from 4-vinylpyridine as described in **Figure 38**. The variation of chemical shift

of this proton when adding different equivalents of 4-vinylpyridine in the media compared to that of free indole would provide the information necessary to determine the binding constant and therefore the strength of interaction.

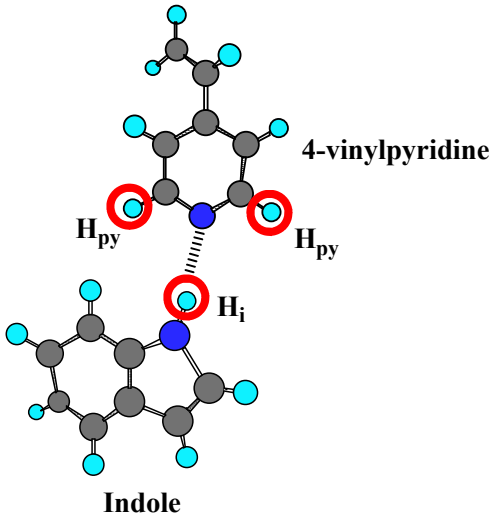

Figure 38: Non-covalent association via hydrogen bonding between indole and 4-vinylpyridine and the protons H_i and H_{Py} susceptible to have their chemical shift affected.

Preliminary studies of the interactions between indole and 4-vinylpyridine with using ^{1}H-NMR (270 MHz) in non-polar deuterated solvents such as chloroform ($CDCl_3$) were first carried out. The association of indole and 4-vinylpyridine was monitored with adding increasing equivalents of 4-vynilpyridine ranging from 0.2 equivalent (1.71×10^{-2} M) to 2 equivalents (1.71×10^{-1} M) to an indole solution in $CDCl_3$ at concentration of 85.4 mM. Spectra of indole alone and in presence of 4-vinylpyridine were recorded. The different chemical shifts δ_{Hi} and δ_{Py} of the nitrogen proton of indole H_i and of the vicinal protons of the nitrogen atom of 4-vynilpyridine H_{Py} respectively were identified for each concentration of 4-vinylpyridine and the values are shown in **Table 1**.

Table 1: Values of the chemical shifts of δ_{Hi} and δ_{HPy} in function of the concentration of 4-vinylpyridine in $CDCl_3$ using ^{1}H-NMR (270 MHz). The chemical shifts are in ppm and relative to TMS (tetramethylsilane).

[4-vinylpyridine] (M)	δ_{Hi} in $CDCl_3$ (ppm)	δ_{Hpy} in $CDCl_3$(ppm)	$\Delta\delta_{Hi}$ (ppm) in $CDCl_3$	$\Delta\delta_{Hpy}$ (ppm) in $CDCl_3$
0	8.13	8.48	0	0
1.71×10^{-2}	8.20	8.50	0.07	0.02
3.42×10^{-2}	8.27	8.53	0.14	0.05
5.12×10^{-2}	8.32	8.54	0.19	0.06
8.54×10^{-2}	8.42	8.55	0.29	0.07
1.28×10^{-1}	8.50	8.56		0.08
1.71×10^{-1}	8.70	9.57	0.57	0.09

As described in **Table 1**, the values of the chemical shift δ_{Hi} as well as δ_{Py} were increased as the concentration of 4-vinylpyridine was increased. The shift was however less important for the protons H_{py}. These data suggested that there was an interaction, which became stronger as the concentration of 4-vinylpyridine increased between both molecules in chloroform. The values of the chemical shifts $\Delta\delta_{Hi}$ and δ_{HPy} were plotted versus the concentration of 4-vinylpyridine and the plots are shown in **Figure 39**.

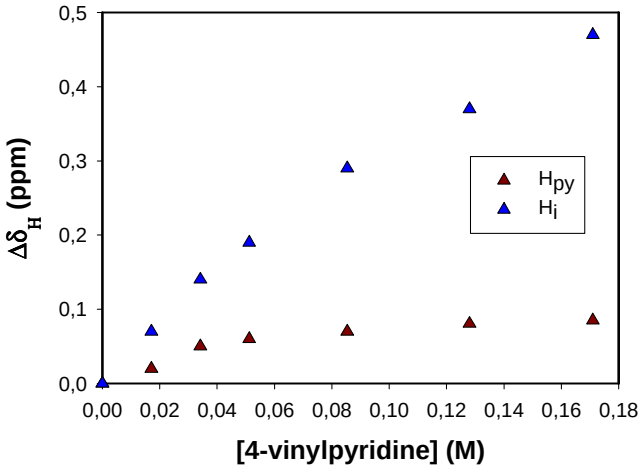

Figure 39: Plots of the variation of chemical shifts $\Delta\delta_{Hi}$ and $\Delta\delta_{HPy}$ of the protons H_i and H_{py} versus the concentration of 4-vinylpyridine. $\Delta\delta_{Hi}$ and $\Delta\delta_{HPy}$ are defined by the value of chemical shift with 4-vynilpyridine corrected by the one of indole alone and 4-vinylpyridine alone respectively.

For both types of protons H_i and H_{Py}, a curvature was noticeable and in the case of the protons H_{Py} a plateau was reached. The chemical shift of the protons H_{py}, δ_{HPy}, displayed a less important variation from 0.02 ppm (0.2 equivalent) to 0.08 ppm (2 equivalents) than the one of the proton H_i, that reached a plateau after 1 equivalent of 4-vinylpyridine. This lower variation of chemical shift $\Delta\delta_{HPy}$ could be explained by the fact that these protons are not directly involved in the hydrogen bond. In opposition, the proton H_i, which was directly involved in the hydrogen bond, displayed a more significant change down field in its chemical shift from 0.07 ppm at 1 equivalent of 4-vinylpyridine to 0.57 ppm at 2 equivalents. The light curvature of the plot of $\Delta\delta_{Hi}$ in function of the concentration of 4-vinylpyridine indicated the formation of an equilibrium between the complex and the two species. The increase of chemical shift for both types of protons demonstrated the formation of a hydrogen bond between indole and 4-vinylpyridine, which association seemed rather weak.

The same experiment was repeated in a similar non-polar solvent, deuterated methylene chloride (CD_2Cl_2). For an easier determination of indole signals in the spectra and more specifically the signal of H_i, deuterated pyridine, *d*5-pyridine, was used instead of 4-vinylpyridine. The latter differ from 4-vinylpyridine only by the absence of the vinyl group in *para* position, which should not generate significant

change in the association of both molecules and provide similar alterations in the chemical shift of the proton H_i as for 4-vinylpyridine. The protons H_{Py} from 4-vinylpyridine did not display indeed a variation in their chemical shift as significant as the proton H_i and therefore could be discarded from the spectra. The spectra of indole alone for each equivalents of pyridine were recorded as shown on **Figure 40**.

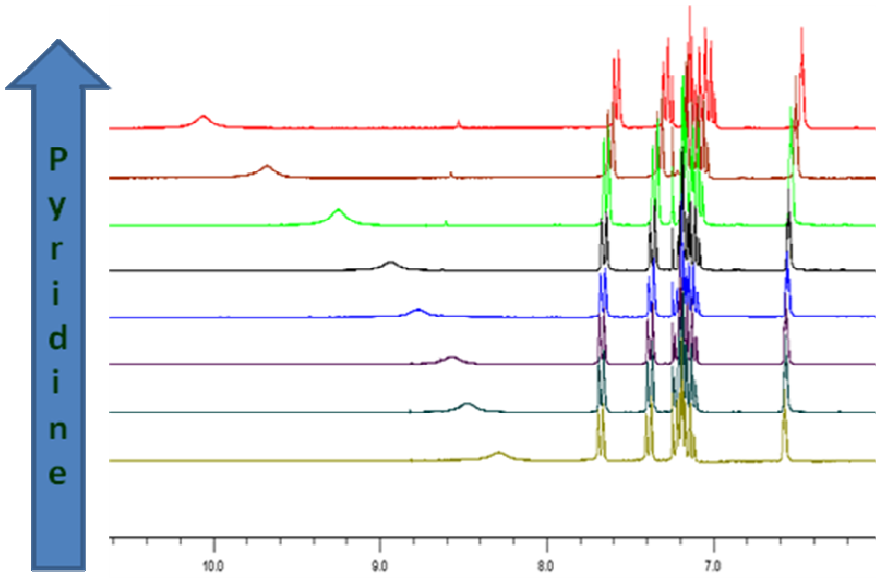

Figure 40: ^{1}H-NMR spectra of indole with increasing equivalents of *d5*-pyridine from 0.2 to 7 eq. Indole was dissolved at a concentration of 85.4 mM in CD_2Cl_2 and increasing equivalents of *d5*-pyridine ranging from 0.2 equivalent (1.71×10^{-2} M) to 7 equivalents (5.98×10^{-1} M) were added to the solution.

The values of δ_C, in function of *d5*-pyridine concentration are shown in **Table 2**.

Table 2: Values of the chemical shift of δ_{Hi} and the variation of chemical shift $\Delta\delta_{Hi}$ in function of the concentration of *d5*-pyridine in CD_2Cl_2 using ^{1}H-NMR (270 MHz). The chemical shifts are in ppm and relative to TMS (tetramethylsilane).

[*d6*-pyridine] (M)	δ_{Hi} in CD_2Cl_2(ppm)	$\Delta\delta_{Hi}$ (ppm) in CD_2Cl_2
0	8.15	0
1.71×10^{-2}	8.21	0.08
3.42×10^{-2}	8.28	0.15
6.83×10^{-2}	8.48	0.35
8.54×10^{-2}	8.57	0.44
1.28×10^{-1}	8.78	0.65
1.71×10^{-1}	8.94	0.81
2.56×10^{-1}	9.25	1.12
4.53×10^{-1}	9.67	1.54
5.98×10^{-1}	10.06	1.93

The values of the chemical shift of H_i displayed an increase as the concentration of deuterated pyridine was increased and the variation of chemical shift $\Delta\delta_{Hi}$ rose from 0.08 (0.2 equivalent) to 1.93 (7 equivalents).

The values of $\Delta\delta_{Hi}$ (cf **Figure 38**) were plot in function of the concentration of *d5*-pyridine and this is shown in **Figure 41**.

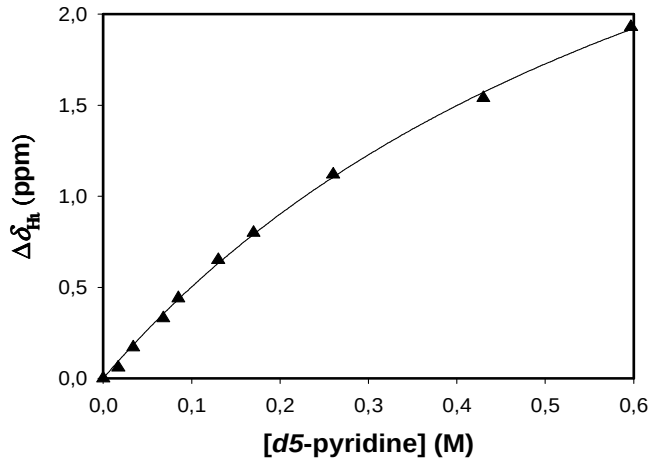

Figure 41: Plot of the variation of chemical shifts $\Delta\delta_{Hi}$ of the protons H_i, corrected from the value of the chemical shift of H_i of indole alone versus the concentration of *d5*-pyridine in CD_2Cl_2.

As well as in chloroform, a curvature after 1.5 equivalents of *d5*-pyridine could be noticed and this suggested an equilibrium in the formation of the complex between indole and pyridine. The light curvature of the plot displayed in **Figure 41** suggestedd a high value of the dissociation constant K_D and as a result a low value of the association constant K_{ass}, regarding **Eq 6**. The association constant K_{ass} of the system could be determined as explained in section 2.1.5.3 using **Eq. 6** that establishes the relationship between $\Delta\delta_{Hi}$ and *d5*-pyridine concentration. The data shown on **Figure 41** could be fitted into a hyperbola using a ligand binding model in Sigma plot 8.0 data analysis software.

$$y = \frac{B_{Max} \times x}{K_D + x} \qquad \textbf{(Eq. 7)}$$

Where y is the fraction of ligand bound, B_{Max} the maximal concentration of ligand, x the concentration of *d5*-pyridine, and K_D the dissociation constant of the complex.

This equilibrium could therefore be quantified and a binding constant K_{ass} of 1.76 M^{-1} was determined. This value, although relatively low, was in line with previous results on a similar system reported by Mataga *et al.*[148]. This constant K_{ass} also gave access to the percentage of template that was actually bound in the case of an equimolar preparation of indole and 4-vinylpyridine that was found to be around 50%.

Thus, the formation of a hydrogen bonding between the template molecule indole and pyridine was demonstrated in non-polar solvents through the nitrogen proton of indole H_i and the nitrogen of pyridine. It was expected that the same type of interactions would occur with the functional monomer 4-vinylpyridine, which differs from pyridine only by the presence of the vinyl functionality in *para* of the nitrogen atom.

The interactions between indole and 4-vynilpyridine were also investigated in polar solvents such as dimethylsulfoxide (DMSO), acetonitrile, and water. The same experiment as previously was performed. ^{1}H-NMR spectra of indole alone and in presence of deuterated pyridine were recorded. The values of δ_{Hi} obtained were compared with those in non-polar solvents and are shown in **Table 3**.

Table 3: Comparison of chemical shifts δ_{Hi} of the nitrogen proton of indole in presence of *d5*-pyridine in different non-polar solvents and polar solvents. Indole was dissolved in each of the corresponding deuterated solvents at a concentration of 85.4 mM and increasing equivalents of deuterated pyridine (from 0.2 equivalent (1.71×10^{-2} M) to 7 equivalents (5.98×10^{-1} M)) were added to the solution. The chemical shifts are in ppm and relative to the one of TMS.

		Chemical shift (δ_{Hi}, ppm)		
Solvent		**Indole**	**Indole + *d5*-pyridine (1:1)**	$\Delta\delta_{Hi}$
$CDCl_3$	H_i	8.13	8.42	0.29
CD_2Cl_2	H_i	8.15	8.57	0.42
Toluene-d8	H_i	6.70	7.15	0.45
DMSO-d6	H_i	11.06	11.07	0.01
Acetonitrile-d3	H_i	9.28	9.32	0.04
D_2O	H_i	12.50	12.51	0.01

The proton H_i in polar solvents such as DMSO, acetonitrile and D_2O displayed a higher value of chemical shift δ_{Hi} (11.06, 9.28 and 12.5 respectively) than in non-polar solvents, where the value was found to be around 8.13 in chloroform, 8.15 in methylene chloride and 6.70 in toluene. The value of δ_{Hi} was found to be greater in D_2O and DMSO than in acetonitrile. This shift variation down field could be explained by the formation of a hydrogen bond between indole and H_2O, acetonitrile and DMSO. The phenomenon was more important in D_2O and DMSO, which are a more polar solvent. This hydrogen bond between indole and the molecules of solvent prevented therefore the formation of the complex between indole and pyridine. This gave rise to a chemical shift value δ_{Hi}, which remained unchanged after addition of pyridine.

2.1.5.5 Study of indole-pyridine interaction at high temperature

The procedure employed to prepare the nanogels required heating up the pre-polymerisation mixture containing the template/ functional monomer complex to 70°C for four days. The interactions between indole and 4-vinylpyridine had been studied previously in non-polar solvents at room temperature. Thus, it was necessary to evaluate the interactions between indole and 4-vinylpyridine at temperatures similar

to the one used for the polymerisation process to insure that the complex remained stable, allowing the functional groups to position themselves correctly in the polymer matrix.

It is known that the position of the chemical shift of a proton in an amine or hydroxyl function is inclined to move depending on the environment or interactions such as hydrogen bonding or also the temperature[163]. NMR studies at different temperatures than room temperature have been investigated. It was reported the use of NMR spectroscopy to study the effect of temperature on protein structures and conformations with notably the use of solid state mode NMR[164]. More recently, Sharif and co-workers reported the use of NMR to study hydrogen bonding between water molecules and heterocyclic bases such as pyridine or pyridine derivatives at low temperature around 170 K[165]. In this work, hydrogen bonded species were characterised in frozen water-pyridine mixtures experimentally by ^{15}N-NMR. When the heterocyclic bases were in excess, it was demonstrated that molecules of water were symmetrically bonded to two pyridine molecules with a bond length of 1.82 Å as suggested in **Figure 42**.

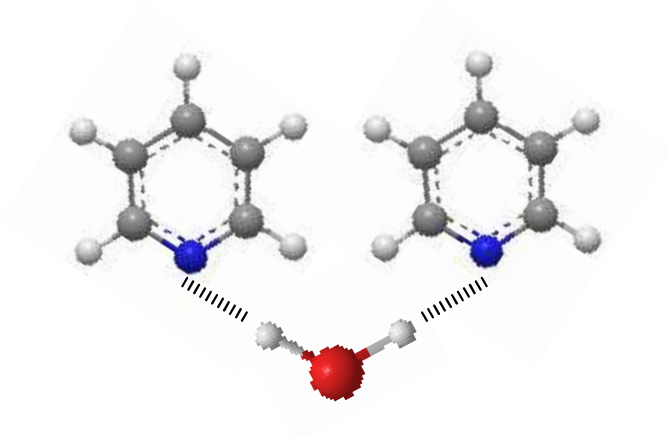

Figure 42: Hydrogen bonds between the protons of the water molecule and the nitrogen of the pyridine molecules where r(NH) is found to be 1.82 Å[165]

Not only have these studies allowed the determination of the nature of interaction between the two molecules but also their geometrical arrangements.

In our system, the use of ^{1}H-NMR was used to investigate the strength of the interaction linking the template molecule indole and the functional monomer 4-vinylpyridine together and to evaluate if this interaction is able to withstand a temperature of 70°C, which was the polymerisation temperature. In section 2.1.5.4, the NMR studies at room temperature demonstrated complex formation between the template indole and the functional monomer 4-vinylpyridine in non-polar solvents. The formation of the hydrogen bond between the two compounds was characterised by the fact that the chemical shift of the nitrogen proton of indole moved down field. Therefore, similar experiments were carried out at high temperature up to 70°C. For this purpose, non-polar solvents with a boiling point higher than 70°C were required such as 1,2-dichloroethane or toluene. The boiling point of 1,2-dichloroethane is found to be around 84°C and the one of toluene around 110°C. These two solvents are similar in polarity, although 1,2-dichloroethane displays a higher dielectric constant (around 10.5) compared to the one of toluene (around 2.38). The hydrogen bonds formed in 1,2-dichloroethane are expected to be stronger than in toluene.

The first set of experiments was performed in *d8*-toluene. The same procedure as that of at room temperature was applied, using deuterated pyridine instead of 4-vinylpyridine. This facilitated the reading and the monitoring of the chemical shift of the indole proton H_i shown in **Figure 43**.

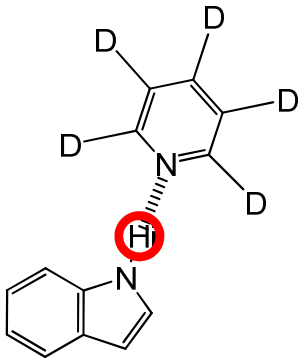

Figure 43: Non-covalent interaction via hydrogen bonding between the nitrogen proton of indole H_i and the nitrogen from pyridine-*d5*.

Prior the investigation of the chemical shift of H_i when indole is bonded to the pyridine molecule as a function of temperature, the spectra of indole in toluene-*d8*

alone at 340K was recorded and the chemical shift δ_{Hi} was compared to one obtained at room temperature 300K. This control experiment would allow a reliable comparison between the spectra of indole bonded to pyridine and free indole at 340K. The spectra are shown in **Figure 44**.

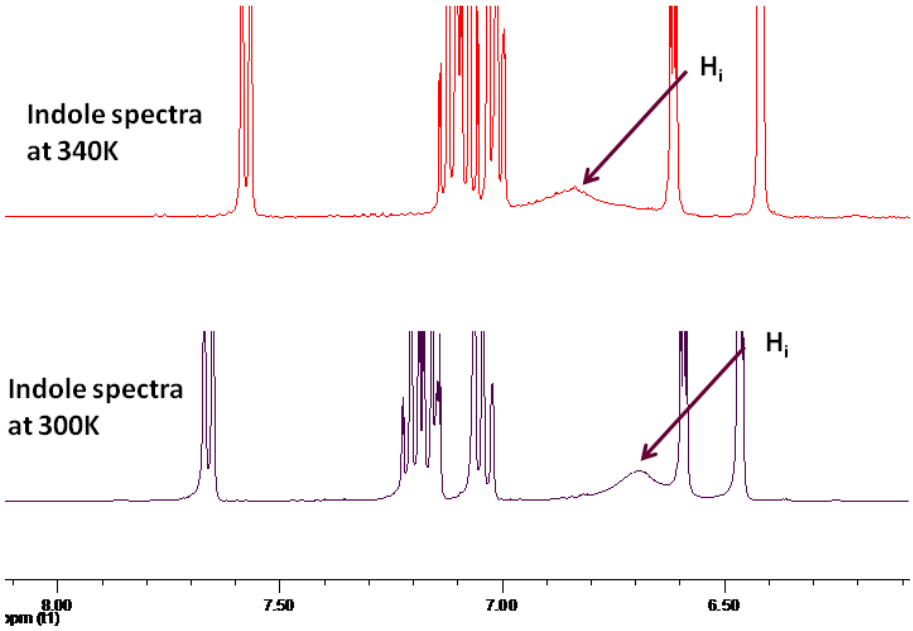

Figure 44: ^{1}H-NMR spectra of indole in toluene-d8 at 300K and at 340K.

With increasing temperature from 300K to 340K, the chemical shift of H_i was shifted down field from 6.7 to 6.9 ppm. The increase of temperature appeared to have an effect on the chemical shift of the nitrogen proton of indole.

The stability of the hydrogen bond between indole and *d5*-pyridine was then investigated with increasing temperature from 300K to 340K. The results are summarised in **Table 4**.

Table 4: Values of the chemical shifts of the indole nitrogen proton Hi in presence of d5-pyridine and in function of temperature. A solution of indole in *d8*-toluene was prepared at a concentration of 85.4 mM and one equivalent of *d5*-pyridine was added. ^{1}H-NMR spectra were recorded at different temperatures 300K, 310K, 320K, 330K, and 340K and the chemical shift δ_{Hi} was monitored for each spectra.

		Chemical shift (δ_{Hi}, ppm)	
Temperature (K)		**Indole**	**Indole + *d5*-pyridine (1:1)**
300	H_i	6.70	7.16
310	H_i	-	7.15
320	H_i	-	7.13
330	H_i	-	7.11
340	H_i	6.90	7.11

The chemical shifts of Hi of indole alone and in presence of *d5*-pyridine were found to be different at 340K around δ 6.9 and δ 7.11 respectively. The slight decrease in the chemical shift of H_i from 7.16 at 300K to 7.11 at 340K might be due to a decrease in the hydrogen bond stability with the increase of temperature. This demonstrated the stability of the complex formed between indole and pyridine at 70°C.

The interactions studies have demonstrated the formation of a complex between the template, indole, and the functional monomer, 4-vinylpyridine, via a hydrogen bond linking the nitrogen proton of the indole molecule to the nitrogen from 4-vinylpyridine in non-polar solvents at room temperature. There was no evidence of complex formation in polar solvents. This information limited the range of solvents that could be employed for the synthesis of the imprinted nanogels to only non-polar solvents such as methylene chloride or chloroform. Furthermore, it was demonstrated with ^{1}H-NMR studies that the interactions were stable at high temperature such as 70°C, which was the polymerisation temperature. This was a good indication that, during the polymerisation process the template molecule - functional monomer complex was stable, allowing a good organisation of the functional group in the polymer matrix. This was an essential feature for the formation of specific cavities with good properties of molecular recognition.

The establishment of a procedure for the synthesis of imprinted nanogels in non-polar solvents was required as the preparation of imprinted nanogels using high

dilution radical polymerisation technique in non-polar solvents has not been reported in the literature. The next section focuses on the preparation of imprinted nanoparticles in the suitable non-polar solvent.

2.1.6 Polymer preparation

2.1.6.1 High dilution radical polymerisation

In the group where this work was done, the focus was on the generation of particles that could behave as colloidal suspensions. Therefore, standard techniques of polymerisation such as 'bulk' polymerisation or precipitation polymerisation that give rise to insoluble particles were not considered. There are several techniques available in the literature for the generation of nanoparticles with colloidal behaviour and among them stands the emulsion polymerisation that leads to the formation of spherical gel-type particles (**Figure 45**), or solution polymerisation.

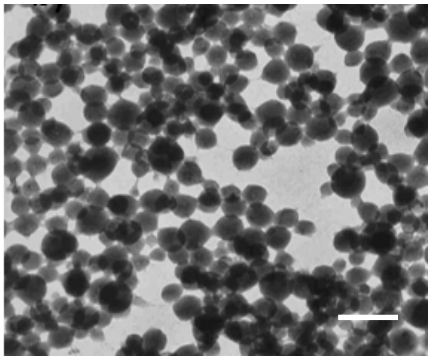

Figure 45: T.E.M picture of particles obtained by emulsion polymerisation (scale bar: 100 nm) [166].

Emulsion polymerisation is a method, where a water-soluble mixture of monomers is dispersed in an organic solvent in the presence of a surfactant. A water-soluble initiator is added into the mixture to start the polymerisation. Each micelle homogeneously dispersed in the emulsion behaves like a mini-reactor that contains all the active components such as monomers, radicals and initiators. Aggregation between droplets is avoided by addition of the surfactant that stabilises the droplets, ensuring the formation of polymer beads. The particle diameter reached during this process typically ranges from 50 nm to 500 nm[166]. At high surfactant concentration, the polymerisation is called micro-emulsion polymerisation, where smaller particles are obtained and range from 50 nm to 100 nm. This latter method appeared in a single

paper in 1973 by Pr. Ugelstad[167]. Although very sophisticated and leading to the formation of mono-dispersed particles, this technique requires the use of a high amount of surfactant and/or monomeric co-stabiliser. Furthermore, the use of aqueous media for our system seems compromised by the non-covalent approach of our imprinting process. Water tends to break the hydrogen bonding between the template indole and 4-vinylpyridine disrupting the interaction between the two molecules.

An alternative to generate nano/microgel particles without using an aqueous media was the solution polymerisation or high dilution radical polymerisation. This approach is based on the fact that in an appropriate solvent, it should be possible to obtain microgels or nanogels without the appearance of macrogelation. If the phenomenon of macrogelation occurs anyway, it would be through the prior formation of microgel particles. This method was introduced first by Graham and co-workers in 1998[124]. In other words, in an appropriate solvent-monomer system, soluble microgel and nanogel formation should always take place. Good solvating power of the solvent strongly influences the appearance of macrogelation and it was reported by Matsumoto *et al.* that in certain cases macrogelation could be delayed[168]. The high dilution radical polymerisation is therefore a polymerisation technique that does not require the use of surfactant; the polymer particles formed are stabilised via steric hindrance, which can be strong depending on the solvating power of the solvent. This is called '*auto-steric stabilisation*' effect[169]. If the solvent selected is a good solvent for the polymer chains located at the surface of the particles, they will therefore swell leading to strong repulsive forces between the individual particles. In the case of a poor solvent, these chains will be shrunken and the repulsive force will be weak as described in **Figure 46**. This last situation generally gives rise to intermolecular cross-linking and subsequently to macrogelation. Thus, the choice of solvent is crucial for this type of polymerisation.

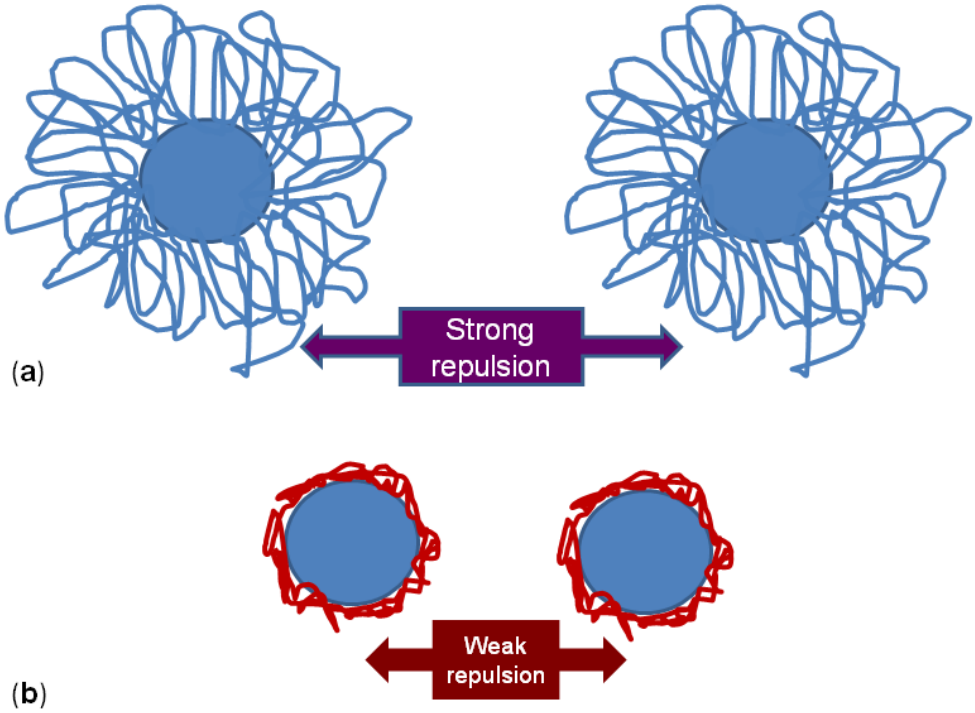

Figure 46: Schematic representation of auto-steric stabilisation effect in (**a**) good solvent and (**b**) poor solvent

The overall monomer concentration C_M is also an important parameter for the high dilution radical polymerisation. This concentration should be lower than a critical gelation concentration for the solution also called Critical Gelation Concentration (CGC), the value of which is experimentally determined. The latter represents by definition the highest value of monomer concentration at which microgels and nanogels can be obtained as a stable solution. In correlation with the variation of microgel structure with polymerisation parameters such as cross-linker content, nature of monomers, amount of initiator or temperature, CGC will also be dependent on these parameters and particularly on the polymerisation solvent.

This elegant way of forming microgel particles was applied to the molecular imprinting approach and developed by Biffis *et al.* in 2001[170]. In this work, the preparation of EGDMA-based microgels was investigated in different types of solvents since the polymerisation of divinylbenzene and methylenebis(acrylamide) was already established[120, 171]. This consisted in determining mainly the gelation point, at which macrogelation occurs, in different solvent systems. Thus, standard monomer mixtures

of EGDMA/MMA (70/30 wt.-%) were heated up to 80 °C in the presence of AIBN as initiator in a number of solvents with different Hildebrand solubility parameters δ. This parameter is a measure of the attractive strength between molecules of the material. These studies allowed the determination of CGC of EGDMA-based microgels in solvents of different nature. Subsequently, the observed CGC were plotted in function of the Hildebrand solubility parameters δ and a phase diagram could be established showing the formation of macro/microgels. This is described in **Figure 47**.

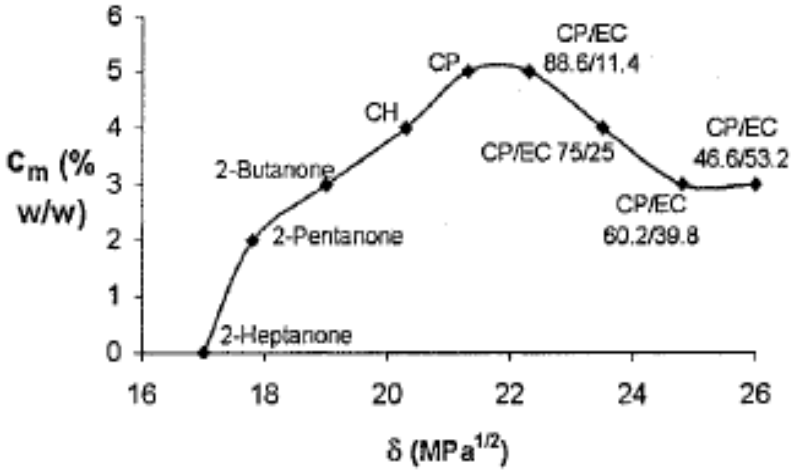

Figure 47: Plot of the observed CGC versus the Hildebrand solubility parameter of different ketonic solvents where CH is cyclohexanone, CP cyclopentanone, EC ethylene carbonate and the number is the volume fraction of the two components in the solvent mixture. The curve establishes the limit in monomer concentration C_M above which macrogelation occurs[170].

High yields of microgels were obtained of around 90% of conversion for the highest concentrations and falling to 80% for the lowest. Other types of solvents such as dimethylformamide (DMF) or dialkylamide were tested as well as polymerisation solvent. The influence of cross-linking degree was also investigated. It was reported that by increasing the cross-linking degree from 70 to 95 wt.-%, a decrease of CGC from 5 to 2 wt.-% was noticed. The microgels were then characterised using different techniques including Gel Permeation Chromatography (GPC), membrane osmometric and viscometry. The molecular weight was found to increase in accordance with the increase of monomer concentration. The resulting imprinted microgels could be re-dissolved in the polymerisation solvent after isolation.

With this work, Biffis *et al.* marked an important step in the preparation of imprinted polymers applied to catalysis allowing the use of microgel matrix, which is more suitable for the development of "*artificial enzymes*". This protocol was further optimised in our group while developing imprinting microgels with hydrolase-type activity, with an average particle size of around 50 nm following a high dilution radical polymerisation procedure[2]. The preparation of these microgels was achieved by using a monomer mixture of acrylamide/ethylene bisacrylamide at a low monomer concentration of 0.5 wt.-% and 80% of cross-linker in DMSO after determining experimentally the critical monomer concentration of this system. More recently, imprinted nanogels with an average size of around 20 nm could be prepared using a similar protocol of high dilution polymerisation in DMF[3].

These studies on the synthesis of imprinted nanogels confirmed the hypothesis that there is a direct relationship between the size of the micro/nanogels formed via high dilution radical polymerisation and the C_M used. It appears that when decreasing the monomer concentration C_M, the dimensions of the resulting particles are smaller. Other variations to the high dilution radical polymerisation have been investigated such as the 'post-dilution' technique recently developed by Wulff et al.[128]. This technique consists in starting the polymerisation process at values of C_M above the CGC but avoiding macrogelation to occur by diluting the mixture after a set period of time in order to reach standard values of C_M ranging from 0.5 wt.-% to 0.1 wt.-%. The size of the latter nanogels was determined at around 22 nm. More details about this new protocol will be discussed later in 2.2.3.

In our system, the choice of the experimental parameters for the synthesis of imprinted nanogels such as the selection of a suitable solvent and the corresponding C_M to obtained nanogel particles remained to be evaluated. The next section focuses on the determination of these polymerisation parameters and on the establishment of a general procedure to prepare imprinted and non-imprinted nanogels for the catalysis of the Kemp elimination.

2.1.7 Determination of polymerisation conditions

2.1.7.1 Selection of the polymerisation solvent

The choice of a suitable polymerisation solvent is an essential feature for the preparation of imprinted polymers. The nature of the solvent selected could have indeed a significant impact on the success of the imprinting process as it is able to favour or reduce the interactions between template and functional monomers. The choice of solvent for our system was greatly inspired by the result of the interaction studies between indole and 4-vinylpyridine and was directed towards non-polar solvent with relatively high boiling points such as toluene or 1,2-dichloroethane, which boiling points are 111°C and 84°C respectively. The use of toluene as polymerisation solvent was discarded as it contains an aromatic ring, which could interact with 4-vinylpyridine by π-stacking reducing the indole/4-vinylpyridine interaction. In order to exclude any possibility of interaction with the solvent, 1,2-dichloroethane was chosen as polymerisation solvent. This solvent is structurally related to chloroform and methylene chloride, in which interaction between indole and 4-vinylpyridine were proven, with a higher boiling point. It presents a similar polarity as toluene insuring indole/4-vinlypyridine complex formation at 70°C.

2.1.7.2 Selection of polymerisation parameters

Subsequently to the solvent selection, the choice of the backbone monomers and especially of a cross-linker soluble in 1,2-dichloroethane was also of great importance. As described in section 2.2.1, the nature of solvent can be rationalised by a useful parameter called Hildebrand solubility parameter, δ. This value can be determined for both, solvent and polymer[172] and a comparison of these two values allows a prediction of the solubility of the material in the solvent. Generally, in absence of strong interactions such as hydrogen bonding between the monomers and the solvent, a good solubility can be expected when the difference between δ_{sol} and δ_{pol} is lower than 3.5 or 4. In our system, the best candidates as backbone monomers including cross-linker in 1,2-dichloroethane, were methyl methacrylate and ethylene

glycol dimethacrylate (EGDMA) (**41**) as cross-linker; the difference between the two solubility parameters is lower than 3.5 (δ_{DCE}: 9.8 and δ_{EGDMA}, δ_{MMA} ~9.5). This result confirmed our interest in using EGDMA as cross-linker, since it was already found to be the best candidate regarding the interaction studies. The use of co-monomer such as methyl methacrylate was however discarded since it creates a potential competition with 4-vinylpyridine (functional monomer) for the interaction with the template and as a consequence it can reduce the imprinting efficiency of our nanogels (cf section 2.1.4.1).

The choice of polymerisation parameters such as the content of cross-linker, monomer concentration type and amount of initiator, polymerisation length and temperature, was largely inspired by the previous studies carried out in the group on the preparation of imprinted nanogels described in the previous section[2-3]. The cross-linker content must reach a value of at least of 70% for a good rigidity of the matrix for the preservation of the cavity shape. However, cross-linker content above 90% is inappropriate for the creation of an enzyme mimic due to an important lack of flexibility limiting the swelling of the particles in the suitable solvent. An optimal content was found to be at 80%. The initiator used was AIBN (**44**) and its content was fixed at 1% of the amount double bonds available in the pre-polymerisation mixture. This initiator is known to decompose at 60°C to give radical entities that are able to start the polymerisation process, as described in **Figure 48**. The structures of the initiator and cross-linker are displayed in **Figure 48**. The polymerisation procedure was based on standard high dilution radical polymerisation procedures employed in the group, consisting in heating the mixture to polymerise for four days at 70°C.

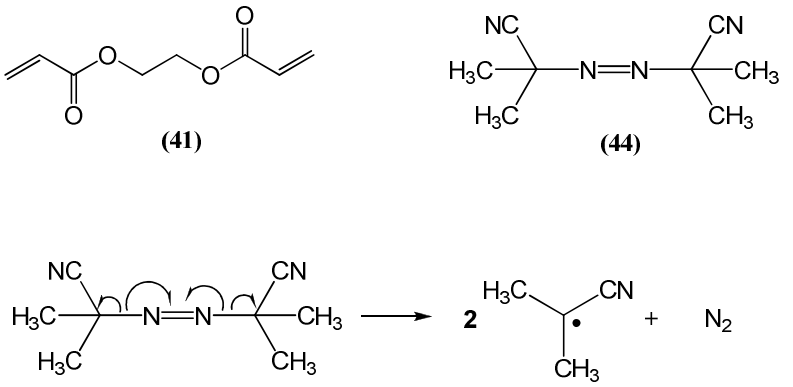

Figure 48: Structures of the cross-linker (EGDMA) (**41**), the initiator azobisisobutyronitrile (AIBN) (**44**) and its mechanism of decomposition at 60°C.

2.1.7.3 Determination of the monomer concentration C_M

The determination of the CGC in 1,2-dichloroethane was performed experimentally by preparing a set of nanogels in presence of 4-vinylpyridine and EGDMA without indole, at the different monomer concentrations C_M ranging from 0.1% to 1.5% leaving all the other parameters such as cross-linker content (80% in mole), temperature, initiator content (1% of double bonds present in the mixture) fixed. The nanogels were prepared by heating the polymerisation mixture at 70°C during 4 days. Unlike the other polymerisation methods, high dilution radical polymerisation generates nanoparticles that remain soluble in the polymerisation solvent even after completion of the reaction. This is an important feature of this method and macrogelation can be spotted easily with the aspect of the resulting solutions. Clear solutions are the evidence of nano/microgel particles; whereas the presence of a precipitate is the attestation that the macrogelation point has been reached. After completion of 4 days of polymerisation, the polymer mixtures were removed from the oven and **Table 5** summarises the results obtained after four days.

Table 5: Determination of the Critical Gelation Concentration for nanogels prepared in 1,2-dichloroethane.

Polymer preparation	Monomer concentration C_M (%)	Product
AS168	0.1	**Soluble microgels**
AS167	0.2	**Soluble microgels**
AS166	0.3	**Soluble microgels**
AS165	0.4	**Soluble microgels**
AS164	0.5	**Soluble microgels**
AS184	1.0	Macrogels
AS185	1.5	Macrogels
AS186	2.0	Macrogels

As reported in **Table 5**, above a value of C_M equal to 0.5%, macrogelation seems to occur and this was characterised by a solid powder lying at the bottom of the flask. Below this value, solutions without precipitates were obtained. The CGC appeared to be between 0.5% and 1%. It is expected that at a low C_M, the size of the particles is decreased. However the yields obtained under these conditions are also found to be decreased. Thus, in order to maximize the yield of material obtained, the C_M selected to synthesise the imprinted nanogels 0.5%.

2.1.7.4 Choice of template/functional monomer ratio

For an optimal interaction between indole and 4-vinylpyridine in the pre-polymerisation mixture, the addition of a co-monomer such as methyl methacrylate was discarded. This also reduces any risk of competition between the two monomers in term of reactivity with the cross-linker EGDMA that could limit the incorporation of 4-vinylpyridine in the polymer matrix. The choice of monomer/template ratio is a significant parameter as it has a considerable effect on the imprinting efficiency of the polymers. In previous preparations of catalytic imprinted nanogels, different template/functional monomer ratios were reported. Generally a ratio 1/1 is employed for the preparation of catalytic imprinted polymers when strong interactions between the template and the functional monomer are reported. However, it is not unusual to

find catalytic imprinted polymers prepared with an excess of functional monomer compared to the template especially when the interactions between the template and the functional monomer are weak. This has for aim to increase the strength of these interactions. In the work of Mosbach et al. on the catalysis of the Kemp elimination, an excess of 6.55 of 4-vinylpyridine compared to indole quantity was used[107].

Furthermore, several functional monomers can be used to create a tight complex with the template. This was seen in the hydrolase-type catalytic imprinted nanogels by Resmini *et al.*[2], where is also two different types of functional monomers were utilised, one polymerisable tyrosine and one polymerisable arginine. This functional monomer selection was based on previous results on the hydrolytic activity of polyclonal antibody preparations[126]. Another example of using several type of functional monomers was reported notably for the preparation of peroxidase-type catalytic imprinted polymers[131]. In this work, three types of functional monomers were used: 4-vinylpyridine, acrylamide, and a polymerisable Fe^{2+}-porphyrin. The design of this system was inspired by natural metallo-enzyme peroxidase. The interactions with the template molecule were found to be strong with multiple hydrogen bonds and one metal-coordination based bond.

Regarding the results of the interaction studies, an equilibrium was reached in methylene chloride after 2 equivalents of functional monomer. However, in order to limit the creation of non-specific binding sites that cause the decrease of the imprinting efficiency, the monomer/template ratio chosen was 1/1. The variation of this ratio and its impact on the imprinting efficiency of the nanogels is studied in details later in section 2.5.2.

2.1.8 Nanogel preparation – Establishment of a general procedure

The results of the interaction studies that led to the identification of the polymerisation solvent, the subsequent selection of cross-linker and the choice of C_M allowed the determination of the conditions for the preparation of imprinted nanogels. The addition of template in the polymerisation mixture was expected not to

change the value of the CGC of the system. Therefore, the polymerisation parameters were kept the same for the synthesis of the imprinted and non-imprinted polymers.

For each preparation of polymers, a set of two polymers were synthesised, an imprinted nanogel and the corresponding non-imprinted nanogel, synthesised under the same conditions as the imprinted nanogel but without the template. The non-imprinted nanogel that contains only the catalytic pyridine moieties but no cavity would serve as a control for the kinetic studies and other characterisations. The pre-polymerisation mixture constituted of the template indole (or not for the non-imprinted preparation), functional monomer, 4-vinylpyridine, cross-linker EGDMA, initiator and the appropriate quantity of 1,2-dichloroethane for a monomer concentration of 0.5 wt.-% were heated at 70°C for four days. The polymer preparations as well as polymerisation conditions are gathered in **Table 6**.

Table 6: Polymer preparations for the catalysis of the Kemp elimination

Polymer preparation [a)]	Indole (mg)	4-VP[b)] (mg)	EGDMA (mg)	Solvent (ml)	AIBN (mg)	C_M (%)	Cross-linker content (%)
MIP AS199	20	18.0	135	24.3	2.5	0.5	80
NIP AS200	-	18.0	135	24.3	2.5	0.5	80
MIP AS205	50	45.7	338	61	6.3	0.5	80
NIP AS206	-	45.7	338	61	6.3	0.5	80
MIP AS207	60	54.9	406	73.2	7.6	0.5	80
NIP AS208	-	54.9	406	73.2	7.6	0.5	80
MIP AS230	90	82.4	610	110	11.4	0.5	80
NIP AS231	-	82.4	610	110	11.4	0.5	80

a) MIP: imprinted polymer; NIP: non-imprinted polymer; b) 4-VP: 4-vinylpyridine; Polymerisation was carried out at 70°C for 4 days

After 4 days of polymerisation, the polymers were removed from the oven and the solvent was evaporated. The nanogel residues were dissolved in a mixture of acidified water and methanol in order to extract the template molecule. The mixture of acidified water and methanol was indeed expected to disrupt the hydrogen bond that linked the template to the polymer matrix allowing the dissociation of the complex between indole and the pyridine moieties. The latter solution was then dialysed against distilled water for two days, during which period the water was

changed twice a day. The pore size of the dialysis membranes was around 12- 14 kDa, insuring the removal of all molecules under this molecular weight. The dialysis of the aqueous polymer solutions was an important step in the isolation of the nanogels. It allowed in fact not only the removal of the residual template molecules stocked inside the polymer matrix but also the extraction of the remaining unreacted monomers and initiator from the mixture as well. The molecular weight of the imprinted nanogels was expected to be greater than the cut-off weight of the membrane so that the material was not lost in during this purification process. The dialysed solutions of nanogels were then freeze-dried and fluffy pale yellow solid are recovered.

The yields of the nanogels were calculated with mass %, taking into consideration the total mass of all monomers added in the pre-polymerisation mixture and the mass of polymer recovered after freeze-drying. This is explained in **Eq 8**.

$$\%Yield = \frac{Mass_{Polymer}}{\sum Mass_{Monomer}} \times 100 \qquad \textbf{(Eq 8)}$$

The yields obtained for several polymer preparations are gathered in **Table 7**.

Table 7: Yields obtained for the dried nanogels recovered after freeze-drying (C_M =0.5 wt.-% and 80% of cross-linker)

Nanogel preparations	Polymer mass (mg)	Yields (%)
MIP AS199	66.5	43
NIP AS200	60.4	39
MIP AS205	131.3	34
NIP AS206	134.2	34
MIP AS230	237.7	34
NIP AS231	147.7	21

The yields of the recovered nanogels were relatively low and ranged from 21% to 43%. Aside the low yield obtained for NIP AS231, there was no significant difference between the different preparations suggesting a relatively good reproducibility in the nanogel synthesis. The values of yields observed were in the range of yields generally obtained in imprinted nanogels. Yields around 20% were reported by Wulff et al. for

hydrolase-like catalytic imprinted nanogels synthesised with a monomer concentration C_M of 0.1 wt.-%[128]. Thus, this relatively low yield could explained by the low monomer concentration C_M of 0.5 wt.-%. The lower the monomer concentration is, the lower the yield. Unfortunately, the C_M could not be increased as macrogelation occurs above a C_M value of 1%. However, the yield could possibly be improved by altering certain parameters such as initiator content or cross-linker content. These alterations could have an effect on the particles morphology and as a consequence on the catalytic efficiency and needed to be investigated. It is worth noticing that the presence of template did not have an effect on the polymerisation process since the values of yield for imprinted and non-imprinted nanogels were found to be similar. It has been reported in previous work on imprinted nanogels that the template molecule could inhibit the polymerisation leading to low yields of imprinted polymers compared to the non-imprinted one[3].

2.1.9 Polymer solubility

The solubility of the dry nanogels was a determining step in the synthesis. The advantageous feature of using nanogels as polymer matrix resides in their ability to swell in the appropriate solvent and as a result to behave like '*soluble macromolecules*'. Soluble macromolecules can be characterised conveniently using standard instruments HPLC, NMR, UV-Visible spectrometry or GPC among others and this presents a main advantage compared to insoluble polymers. Good solubility allows nanogel particles to function the same way as their natural counterparts, enzymes. The identification of a solvent in which the nanogels are soluble would determine the ideal solvent to perform all the polymer characterisations and the kinetic assays.

Previous studies on the preparation on imprinted micro/nanogels demonstrated that there was a correlation between the cross-linking density of the nanogel and their solubility properties. Wulff and co-workers with establishing a new protocol for preparing imprinted nanogels successfully generated nanogels that were able to be re-dissolved in most organic solvents[128]. This outcome was correlated to the

compact structure of the particles obtained after using the '*post-dilution*' method. It was previously established that the maximum cross-linking density that nanogel particles could acquire during the polymerisation process was just prior macrogelation to occur[129]. Thus, from this finding, the basic principle of the '*post-dilution*' was to stop the reaction just prior the macrogelation point and to dilute extensively the system in order to reach low monomer concentration. In this manner, soluble nanogels with highest degree of cross-linking and more rigid structures could be prepared. This was proven to considerably increase the solubility of the nanogel.

Other parameters seem to have an effect on the solubility of nanogel particles. Nanogels prepared with high monomer concentrations usually display greater dimensions than those synthesised at low concentration and also present limited solubility properties. In the group where this work was carried out, imprinted microgels synthesised at a concentration of 0.5 wt.-% in DMSO at fixed cross-linking content (70% and 80%) could be re-dissolved in the latter solvent while those prepared at 1.0% or 1.5% could not. The same trend was observed with the cross-linker content. Nanogels with 90% of cross-linker at C_M 0.5 wt.-% and 1 wt.-% were not soluble whereas those at 70% were able to be re-dissolved in the polymerisation solvent DMSO and mixtures of DMSO/water at the same C_M values[173].

Subsequently to the synthesis of the imprinted and non-imprinted polymers in 1,2-dichloroethane (80% cross-linker and C_M 0.5 wt.-%), the solubility of the dry nanogels recovered in different solvent systems was tested. A wild variety of solvents were selected with different types of polarity. Polymer solutions were prepared at a concentration of 1 $mg.ml^{-1}$ in each solvent. The results are summarised in **Table 8**.

Table 8: Solubility tests in different solvents on the nanogels. The tests were performed on different sets of inprinted and non-imprinted nanogels.

Solvents	Solubility [a)]
1,2-dichloroethane	Not soluble
Chloroform	Not soluble
DMSO	Not soluble
THF	Not soluble
Water	Cloudy solution
Acetonitrile	Partially soluble
Methanol	Cloudy solution

a) Polymer solutions were prepared at a concentration of 1 $mg.ml^{-1}$ in each solvent.

The dry nanogels could not be re-dissolved in 1,2-dichloroethane, the polymerisation solvent, neither in other non-polar solvents such as methylene chloride or chloroform. The nanogels were not soluble in solvents such as tetrahydrofurane (THF), DMSO, or only partially soluble acetonitrile; however they were found to be partially soluble in protic solvents such as water or methanol. This could be explained by the fact that the structure of the nanogels was composed of 80% EGDMA, which was likely to form hydrogen bonds in protic solvents.

The solubility of the dry nanogels in mixtures of organic/aqueous solvents was tested as well. Aqueous media was required to perform the kinetic assays as the rate of the Kemp elimination is dependent on the concentration of hydroxide ions as explained further in section 2.4.2.1. Acetonitrile was selected as organic solvent since it displays good miscibility properties with water. Tetrahydrofurane was discarded as the polymer particles were not soluble in this solvent. Thus, the polymers were dissolved in mixtures of acetonitrile in water at a concentration of 1 $mg.ml^{-1}$. The acetonitrile content was varied from 10% to 80%. The results are summarised in **Table 9**.

Table 9: Solubility tests on dry nanogels in mixtures of acetonitrile/ water.

Acetonitrile content in water (%)	Solubility[a)]
10	Cloudy solution
20	Cloudy solution
30	**Soluble**
40	**Soluble**
50	**Soluble**
60	**Soluble**
80	**Soluble**

a) Polymer solutions were prepared at a concentration of 1 $mg.ml^{-1}$

The nanogels displayed good solubility in acetonitrile/ water mixtures, although at low acetonitrile content the solubility was reduced. The data suggested that a minimum of 30% of acetonitrile was required for a total solubility of the nanoparticles. A similar trend was observed for the hydrolase-like catalytic imprinted microgels. These microgels, developed in our group, were found to be more soluble in pure DMSO and a mixture of 10% of water in 90% of DMSO. Water contents above 10 % induced the precipitation of the particles[173].

The optimal solvent system appeared to be mixtures of acetonitrile/ water with a minimum of acetonitrile content of 30%. This knowledge was of great importance for setting the conditions for the kinetic experiments and for the characterisations of the imprinted nanogels notably the determination of active sites.

2.1.10 Active site number determination

2.1.10.1 Introduction

In the previous section, it was described the careful attention that was put on the design of the system for the development of efficient imprinted nanogels with catalytic activity for the Kemp elimination. This led to the selection of a suitable template and functional monomer for the imprinting process, whose interactions via hydrogen bond were demonstrated. This also led to the identification of the most suitable solvent, in which to perform the polymerisation. Subsequently, soluble imprinted nanogels were successfully produced using high dilution radical polymerisation following the optimisation of important parameters including the monomer concentration C_M and the cross-linker content. The full characterisation of nanogel particles is discussed in section 2.7 that describes their physical-chemical properties. In this section, the focus is on the determination of active site concentration, an essential parameter for accurate kinetic studies.

The number of active sites is essential for assessing the catalytic activity of natural catalysts such as enzymes or enzyme mimics. The knowledge of this parameter would allow indeed an accurate determination of important kinetic parameters such as the rate constant of the catalysed reaction, k_{cat}. Whereas this step is systematic for the study of enzyme activity, it is rarely reported for the characterisation of the catalytic activity of imprinted polymers. This is generally due to limited means of determination of active residues inside a polymer matrix especially with insoluble materials. This gives rise to an uncertainty in the calculation of kinetic constant and prevents any accurate comparison not only within catalytic imprinted polymers but also with catalytic antibody and enzymes. A limited number of research groups that described the preparation of catalytic imprinted system have invested efforts in the determination of active site concentration.

The methods available for this type of characterisation are highly dependent on the functional units involved in the catalysis and turns out sometimes to be very

challenging[174]. The technique generally used in molecular imprinting is the calculation of binding sites that consists in re-binding the template molecule into the polymer matrix or using the properties of the catalytic centre. For instance, in the case of the preparation of imprinted polymers for the selective hydrolysis of diphenyl carbonate and diphenyl carbamate, where a metal was the catalytic centre, the use of redox properties of the metal for the determination of active site number was reported[109]. More recently, Allender et al. published the determination of binging sites of imprinted polymers by identifying the changes in coordination shell of the metal Co(II) using the EXAFS instrument[175].

For catalytic imprinted polymers, the theoretical concentration of functional monomer in the pre-polymerisation mixture is generally used to calculate k_{cat}. However, it is expected that the totality of functional monomer added in the mixture is certainly not incorporated inside the polymer matrix. This underestimates the value of the rate constant k_{cat}. The determination of active site concentration can be carried out in the same way as for binding polymers. It is however important to keep in mind that during the polymerisation process the repartition of the active units occurs randomly rather than in order and as a consequence all the active moieties are not necessarily located inside cavities. This generates different types of active sites displaying different reactivity and properties. Thus, these active sites can be separated into three classes: i) the '*catalytic*' sites C_C located inside the cavities, ii) the '*binding*' sites C_S that will be typically standing at the surfaces of the particles and in the worst case iii) the active units C_B blocked inside the polymer matrix or where a template molecule is still stocked inside a cavity, with no possibility of access for the template molecule or the substrate. The total concentration of active sites can be rationalised as in **Eq 9**.

$$C_{TOT} = C_C + C_S + C_B \qquad \textbf{(Eq 9)}$$

It is worth bearing in mind that although the '*binding*' sites C_S are not located inside the three dimensional cavity, they are able to react with the substrate and therefore to catalyse the reaction. So the concentration of active sites that can be measured will ineluctably represent the sum of the '*catalytic*' sites C_C and the '*binding*' sites C_S.

In the group where this work was performed, the determination of active sites was carried out for the imprinted nanogels with aldolase type I activity[3]. The way to measure the concentration was carried out by titrating the proline moieties inside the nanogel matrix using the irreversible acetylation of the proline nitrogen by 4-nitro-phenolacetate. The product of this reaction is the 4-nitrophenol, widely used in the kinetic analysis field due to its spectroscopic tremendous properties. This molecule possesses indeed strong absorbance in the visible region of the spectrum, even at low concentration. The basic principle of this titration is described in **Figure 49**.

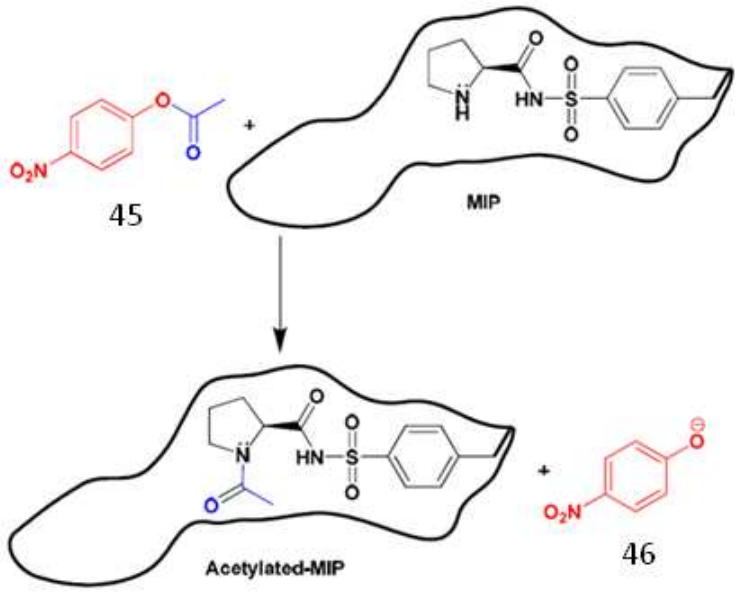

Figure 49: Aminolysis of 4-nitro-phenolacetate, (**45**), by proline moieties inside the nanogel matrix. The hydrolysis of (**45**) is irreversible resulting in the formation of 4-nitro-phenol, **(46)**.

The method consisted in monitoring the product formation by UV-Visible spectroscopy at a wavelength of λ = 319 nm. After completion of the reaction, the concentration of 4-nitro-phenol was measured by HPLC, after the establishment of a calibration curve of 4-nitro-phenol. The titration of the polymers was performed in 20% DMSO in DMF at a concentration of 0.25 $mg.ml^{-1}$. It was following this method possible to determine an accurate value of the concentration of active sites and a concentration of 79 µM was found for the imprinted nanogels and of 69 µM for the non-imprinted polymer. These experiments were found to be reproducible and

allowed a precise determination of the rate constant k_{cat} of the reaction catalysed by the nanogels.

2.1.10.2 Establishment of a titration procedure

In our system, the active moieties that are expected to catalyse the Kemp elimination are the pyridine residues resulting from the incorporation of the functional monomer, 4-vinylpyridine in the nanogel matrix. As explained in a previous section 4-vinylpyridine displays good basicity properties with a pK_a around 5.4 for the nitrogen of the aromatic cycle. Thus, our approach to titrate the pyridine moieties inside the nanogels was to use an acidic/ basic procedure. A direct titration of the pyridine residue was not envisaged because of the low pK_a and the risk of not being able to identify any equivalent point. Thus, the idea was to employ a back titration protocol by protonating all the pyridine residues in an excess of hydrochloric acid and then titrating the mixture of the remaining strong acid HCl and the pyridinium ions by a solution of a strong base for instance sodium hydroxide NaOH.

2.1.10.2.1 Titration of a strong and weak acids mixture

The basic principle of the titration of a mixture of two different acids, strong and weak, by a strong base remains quite similar as that of a di or triacid. Different equivalent points are observed depending on the value of pK_a of each species. However, the ability of identifying more or less accurately the two equivalent points depends strongly on the pK_a difference between both acids. Three cases ($\Delta pK_a > 2$, $\Delta pK_a = 2$, and $\Delta pK_a < 2$) needs to be distinguished.

- Case 1: $\Delta pK_a > 2$

In the case of a pK_a difference superior to 2 units, the identification of two distinct equivalent points is quite easy. The strong acid is titrated first, followed by the titration of the second acid, which is weak. Both acids are then titrated separately. The second equivalence is however easier to repair than the first one. The semi-equivalence of the

weak acid can be noticed where at this point the pH value becomes identical to the value of pK_a of the weak acid. The allure of a typical titration curve of a mixture of hydrochloric acid (0.1 $mol.l^{-1}$) and ethanoic acid (pK_a 4.9, 0.1 $mol.l^{-1}$) by a solution of NaOH (0.1 $mol.l^{-1}$) is shown in **Figure 50**.

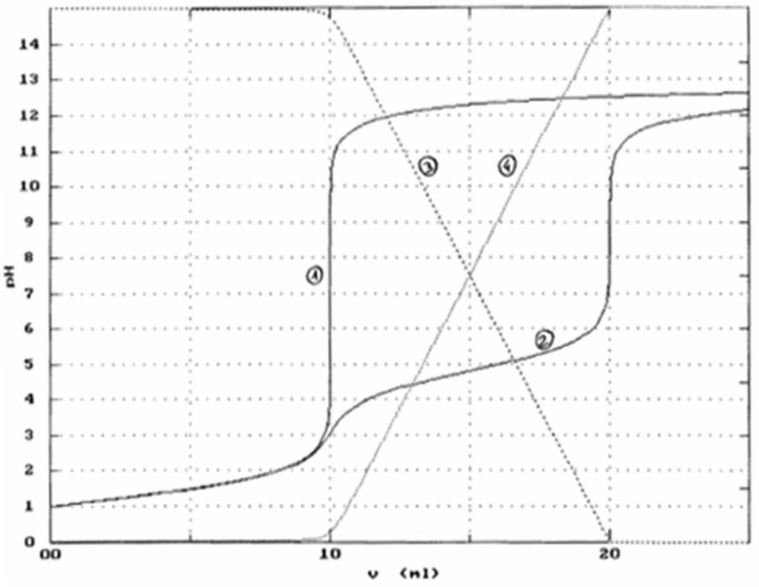

Figure 50: Example of titration curve of a mixture of a weak and a strong acids with a pK_a difference greater than 2 by a solution of NaOH (0.1 $mol.l^{-1}$). Two distinct equivalent points can be distinguished. The first equivalent point corresponds to the strong acid HCl (0.1 $mol.l^{-1}$) and the second corresponds to the weak acid, ethanoic acid (0.1 $mol.l^{-1}$).

- Case 2: $\Delta pK_a = 2$

With a pK_a difference equal to 2, the identification of two distinct equivalent points becomes more difficult. In fact, the first equivalent point is hardly observable. The two acids are not titrated separately; the weak acid starts being titrated before completion of the titration of the first acid. Surprisingly, the semi-equivalence of the two acids can be observed where at these points $pH = pK_{a1}$ and $pH = pK_{a2}$. At the semi-equivalence, by definition, the volume measured is equal to half of the volume that would be measured at the equivalence. Thus, knowing the ratio between both acids in the mixture at the beginning of the titration, the determination of the concentration of both acids is theoretically possible by using the semi-equivalence.

- Case 3: $\Delta pK_a < 2$

When the pK_a difference between both acids is less than 2, only one equivalent point can be observed. The different titrations are not occurring successively. The values of pH at the semi-equivalences do not correspond to pK_{a1} and pK_{a2} anymore. The determination of the concentration of both acids is impossible.

With regards to that was explained previously, in order to apply this technique to our system, the difference between hydrochloric acid and the pyridinium ions needed to be high enough to be able to observe two equivalent points leading to an accurate determination of pyridinium ions concentration. The pK_a value of the couple pyridinium/pyridine is around 5.4 marking a good difference with the usage of a strong acid such as HCl in the mixture. The back titration of the pyridine residues incorporated in the nanogels will be then similar to case 1.

2.1.10.2.2 Establishment of the protocol for back titration of pyridine

In order to apply a protocol of back titration for the detection of pyridine moieties it was essential to identify the optimal conditions under which these studies would be proceed. As explained in the previous section, the accurate determination of the pyridine residue concentration depends on the reading of the equivalent points subsequently to the titration. Although the distinction of two inflection points is highly dependent on the pK_a difference between the two acids to be titrated, the concentration of the respective acids is also expected to have a significant effect. In our system, the strongest acid in terms of pK_a (HCl) had to be in excess to insure the protonation of all the pyridine moieties and to be able to detect two equivalent points. However, the extent of the excess was of great importance as a low excess would not allow the identification of these inflection points.

Before titrating the pyridine residues inside nanogels, preliminary investigations on the back-titration of free pyridine were performed. This had for aim the identification of the optimal conditions, in which to carry out the titration of the active sites. This would also lead to an accurate evaluation of the pyridine residue

concentration using this method. As a result of the limited solubility of the nanogels, the nature of the solvent for the titration was reduced to the choice of mixtures of acetonitrile in water. Clear solutions of nanogels were obtained for mixtures with a minimum of 30% acetonitrile in water. As a consequence, it was decided to perform all the titrations in a mixture of 30% acetonitrile in water.

The first step was to establish the optimal concentration of HCl. For this purpose, a series of back-titration of free pyridine with different concentrations of HCl were performed. A solution of free pyridine in 30% acetonitrile in distilled water was prepared at a concentration of 2×10^{-3} M (4×10^{-5} mol in 20 ml). This concentration of pyridine was chosen in order to match the range of concentrations of pyridine moieties incorporated in the nanogels. The back-titration of this solution was performed using different equivalents of HCl from 0.5 equivalent to 2.5 equivalents. The titrant solution was kept the same for all titrations and was a solution of NaOH at a concentration of 1.5×10^{-3} M. The titration curves are shown in **Figure 51**.

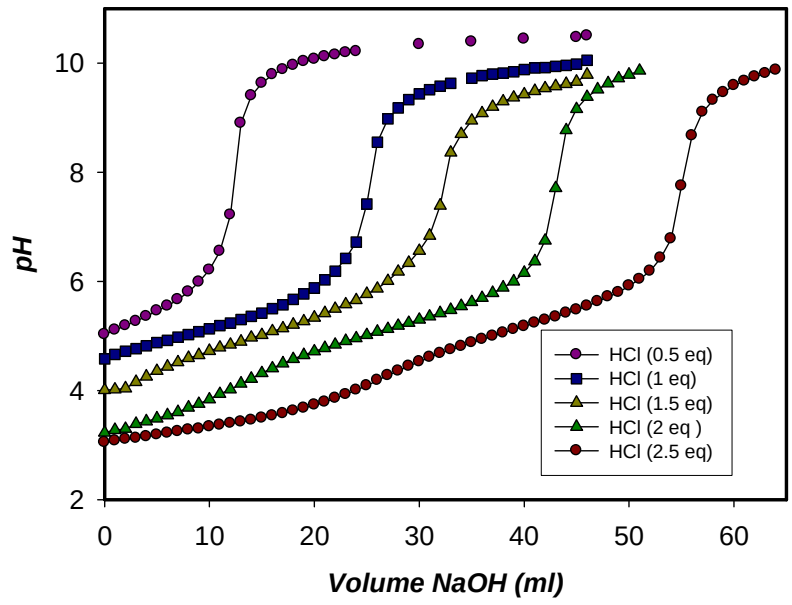

Figure 51: Back-titration curves of free pyridine (2×10^{-3} M in a 30% acetonitrile in distilled water) with different equivalents of HCl (● 0.5 eq, ■ 1 eq, ▲ 1.5 eq, ▲ 2eq, ● 2.5 eq) using a titrant solution of NaOH at a concentration of 1.5×10^{-3} M.

As described in **Figure 51**, the identification of two inflection points became evident for 1.5 eq of HCl. It can be noticed that the volume of NaOH corresponding to the first equivalent point moves from 2 ml (1.5 eq of HCl) to 13 ml (2 eq of HCl) and finally to 25 ml (2.5 eq of HCl) indicating the increase of the excess of HCl in the media. Furthermore, for these three titration curves the value of pH was found to be equal to the pK_a of pyridine (around 5.3) at the semi-equivalence. This confirmed that the conditions of titration were similar as case 1 explained in the previous section, where the pK_a difference between both acids is larger than 2.5.

The determination of the pyridine quantity was achieved using the value of NaOH volume at both equivalences, as specified in **Eq 10**.

$$n_{Pyr} = (V_{e2} - V_{e1}) \times C_{NaOH} \qquad \textbf{(Eq 10)}$$

Where n_{Pyr} is the quantity of pyridine in mol, V_{e1} and V_{e2} are the volume at the first and second equivalence respectively in litre and C_{NaOH} is the concentration of the titrant (NaOH) solution.

The calculation of the pyridine concentration following **Eq 10** for the three curves (1.5 eq, 2 eq and 2.5 eq of HCl) gave a pyridine quantity of 4.1×10^{-5} mol, which corresponded to the quantity of pyridine added initially in the mixture with a standard error of 2.5%. This implied that low concentrations of pyridine could be determined in a reliable way using this titration method.

These preliminary results confirmed that back-titration of pyridine in presence of an excess of HCl was a suitable method for the evaluation of active sites in the imprinted nanogels. The concentration of pyridine used previously matched the range of concentrations of pyridine moieties present in a reasonable quantity of nanogels. This assay could therefore be used to titrate pyridine moieties with a relatively low quantity of nanogels allowing the detection of reliable data.

2.1.10.3 Active sites number determination

The previous method was applied to several sets of imprinted and non-imprinted nanogels (MIP AS207/NIP AS208; MIP AS230/NIP AS231) following the same procedure as for free pyridine. Dry nanogels were dissolved in a mixture of 30% of acetonitrile in distilled water at a concentration of 1 $mg.ml^{-1}$. To the latter solution, 25 ml of a solution of HCL (2×10^{-3} M) are added in order to reach an excess of HCl around 2.5 equivalents compared to the theoretical quantity of pyridine residues inside the nanogels. After gentle stirring, the latter is titrated using a NaOH solution of 1.5×10^{-3} M. The titration curves of the polymers MIP AS230 and NIP AS231 are shown in **Figure 52**.

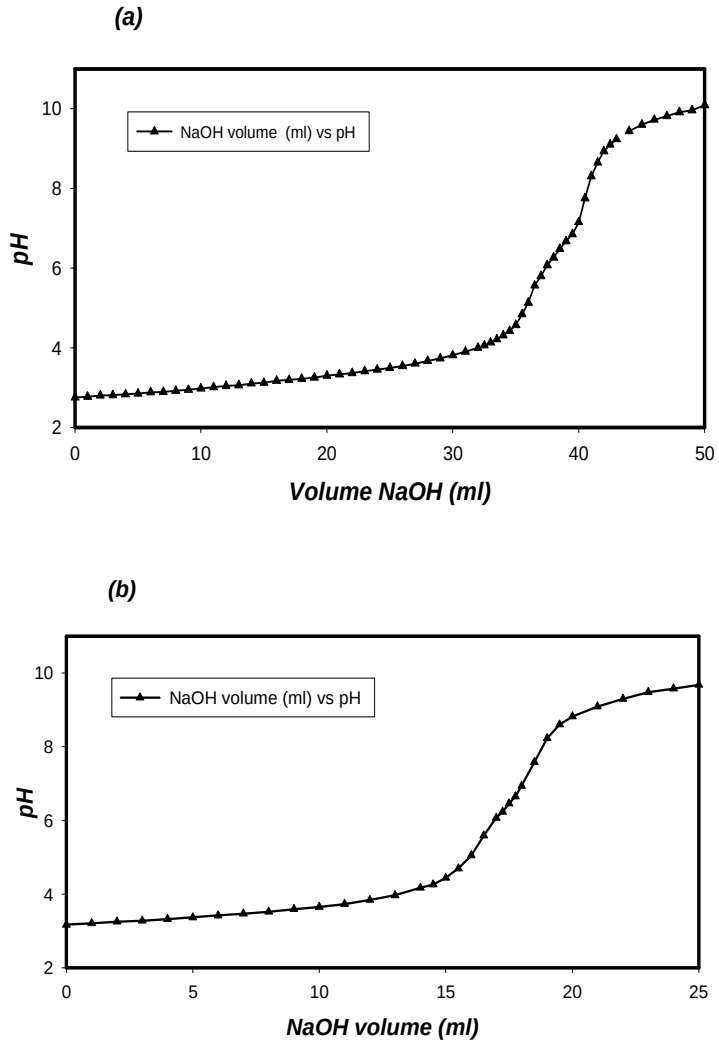

Figure 52: Titration curves of a) imprinted nanogels MIP AS230 and b) non-imprinted NIP AS231 nanogels using a solution of NaOH at a concentration of 1.5×10^{-3} M. Dry nanogels were dissolved in a mixture of 30% of acetonitrile in distilled water at a concentration of 1 $mg.ml^{-1}$. To the latter solution, 25 ml of a solution of HCL (2×10^{-3}

M) are added in order to reach an excess of HCl around 2.5 equivalents compared to the theoretical quantity of pyridine residues inside the nanogels.

As shown in **Figure 52** two equivalent points could be distinguished, although very closed from each other. This could be explained that the entity titrated was a polymer and therefore the determination of inflection point was more difficult. The value of pH at the semi-equivalence for both polymers MIP AS230 and NIP AS231 appeared to be the same, around 6.5. This value could be identified as the $pK_{a,app}$ of the pyridine incorporated in the nanogel matrix and was different from that of free pyridine.

Assuming that the second equivalent point corresponded to the pyridine moieties, the quantity $n_{Pyr,Exp}$ of pyridine residues present in the polymer solution titrated was obtained according **Eq 10**. The active site number $n_{Pyr,Exp}$ obtained after titration of the polymers could be compared to the quantity n_{Pyr} of functional monomer, 4-vinylpyridine, theoretically present in the nanogel matrix. This value could be assimilated to the maximum concentration of pyridine moieties that can be incorporated in the nanogel matrix. This value could be evaluated by considering the quantity of 4-vinylpyridine present per mg of polymers calculated from the quantity of 4-vinylpyridine n_{FM} initially added into the pre-polymerisation mixture and the yield of polymerisation following the procedure explained below in **Eq 11**.

$$n_{Pyr}(mol/mg) = n_{FM} \times \frac{Yield}{Mass_{Polymer}} \qquad \textbf{(Eq 11)}$$

Where n_{Pyr} is the theoretical quantity of pyridine residue per mg of polymer and n_{FM} is the quantity of 4-vinylpyridine initially added in the pre-polymerisation mixture.

The ratio between both values gave rise to the percentage A_N of pyridine incorporated inside the polymer matrix and that are active as specified in **Eq 12**.

$$A_N = \frac{n_{Pyr,Exp}}{n_{Pyr}} \times 100 \qquad \textbf{(Eq 12)}$$

The molar quantities of active pyridine inside the nanogels were gathered along with the amount of functional monomer added in the pre-polymerisation mixture and the percentage of active pyridine residues in **Table 10**.

Table 10: Values of pyridine concnetrations $n_{Pyr,Exp}$ obtained after titration of imprinted polymers (MIP AS207, MIP AS230) and non-imprinted polymers (NIP AS208, NIP AS231), concentration of functional monomer n_{Pyr}, 4-vinylpyridine, added to the pre-polymerisation mixtures, and percentages A_N of active pyridine incorporated inside the nanogel matrix

Polymers	*Concentration of 4-vinylpyridine n_{Pyr} (µmol/mg)	Concentration of pyridine moieties $n_{Pyr,Exp}$ after titrations (µmol/mg)	A_N (%)
MIP AS207	1.10	0.24	22
NIP AS208	1.10	0.30	27
[a)]MIP AS230	1.10	0.24	22
[a)]NIP AS231	1.10	0.19	17

*The values were calculated following **Eq 11** and corresponded to the maximum quantity of pyridine residues available in the mass of dry nanogels used to generate the polymer solution of 1 $mg.ml^{-1}$ for the titration**.**

[a)] The titration of the imprinted and non-imprinted nanogels MIP AS230 and NIP AS231 respectively was performed 3 times in order to evaluate the reproducibility of assay. A standard error of 13% was found in both cases

As shown in **Table 10**, the values of active site concentrations ranged from 17% to 27% of the theoretical concentration of pyridine residues incorporated in the polymer matrix. In other terms, from the initial quantity of 4-vinylpyridine added in the pre-polymerisation, only a low amount would be actually incorporated inside the polymer matrix and catalytically active. Furthermore, the data suggested a high variability regarding pyridine incorporation and availability for polymers prepared under the same conditions. This could be justified by several factors. The first reason is that polymerisation process more specifically nanogel formation occurred rather randomly than in an organised way and as a consequence many pyridine residues could be blocked inside the polymer matrix making these active sites inaccessible. The assay probably carries some experimental errors and although it provided some indication of an order of magnitude of active site concentration, it could not still be very precise. Another reason of the low 4-vinylpyridine incorporation could be that the incorporation of 4-vinylpyridine during the polymerisation process can be limited by a difference of reactivity between EGDMA and 4-vinylpyridine. The reaction of

polymerisation between EGDMA molecules might occur faster than with 4-vinypyridine. As a result, some nanogel particles might be formed only by EGDMA molecules with no incorporation of 4-vinylpyridine.

The knowledge of active pyridine moieties was essential for an accurate determination of the catalytic efficiency of the imprinted nanogels as it required for the determination of important kinetic parameters such as the rate constant k_{cat} of the catalysed reaction. The next part focuses on the catalytic activity of the imprinted nanogels for the Kemp elimination.

KINETIC CHARACTERISATION

2.2 RESULTS AND DISCUSSION: KINETIC CHARACTERISATION

The main focus of this section is the kinetic investigations of the catalytic activity of the imprinted nanogels. The results obtained in section 2.3, including the determination of active site concentrations, can now be utilised for an accurate estimate of the kinetic parameters. The kinetic characterisations of the nanogels represent a very important part of this work as it evaluates the use of imprinted nanogels for the development of enzyme mimics and provides indications towards improving nanogel performance. The simplicity and versatility of the Kemp elimination permits a rapid construction of the kinetic profile of the nanogels, enabling a fast analysis of the nanogel activity with the view of observing enzyme-like kinetics.

Kinetic analysis is a vast area of research that spans a variety of catalysis approaches from protein-based catalysis and catalysis by organo-metallic complexes, to 'artificial enzymes'. Numerous methods for the measurement of catalytic efficiency are reported in the literature, depending on the physical-chemical properties of the catalysts and the nature of the reagents involved in the reaction.

The work discussed in the following section was performed using UV-Vis spectroscopy. This analytical technique allows the acquirement of reliable and accurate data in a relatively short period of time. The first part of this chapter focuses on the establishment of the optimal conditions to study the activity of the nanogels and their adherence to the Michaelis-Menten saturation model. This consisted in analysing the uncatalysed reaction altering the parameters that influence the rate of the reaction. In the second part, the catalytic efficiency of imprinted nanoparticles is investigated as well as the key parameters that have an effect on the nanogel catalytic performance.

2.2.1 Introduction to kinetic experiments

2.2.1.1 UV-Visible spectrometry for kinetic analysis

Different types of analytical instruments are available to carry out kinetic studies, either by monitoring product formation or substrate consumption. Examples of the most commonly used analytical instruments include UV-Vis spectroscopy, NMR, HPLC, or FTIR. In the Kemp elimination, the product of the reaction, 1,2-cyanophenol, is a chromophore with a maximum absorption peak at 325 nm, a wavelength that is distinct from the maximum absorption peak of the substrate at 270 nm as shown in **Figure 53.**

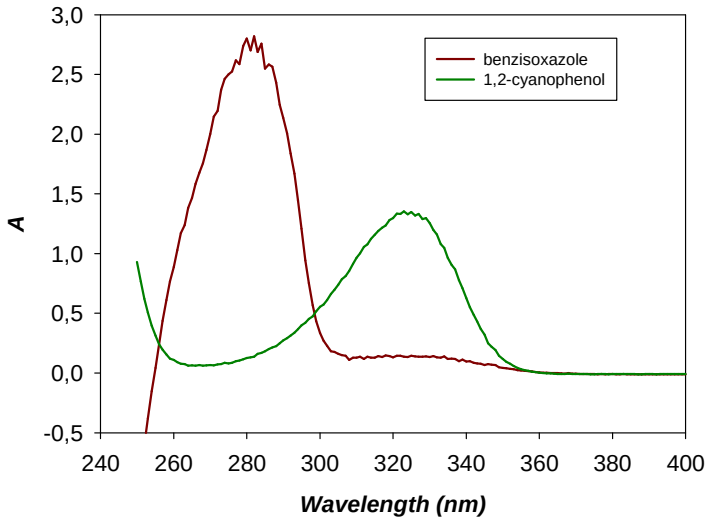

Figure 53: Absorbance spectra of benzisoxazole (**34**) and 1,2-cyanophenol (**35**).

The specific difference in absorbance peaks allows the use of UV-Vis spectroscopy for the kinetic characterisation of the catalyst, by monitoring product formation. This instrument is advantageous as it permits a collection of large quantities of data in a relative short period of time. The product formation is monitored by quantifying the increase in absorbance at a critical wavelength (325 nm for 1,2-cyanophenol) as a function of time. A typical progression curve of product formation by this method is shown in **Figure 54**.

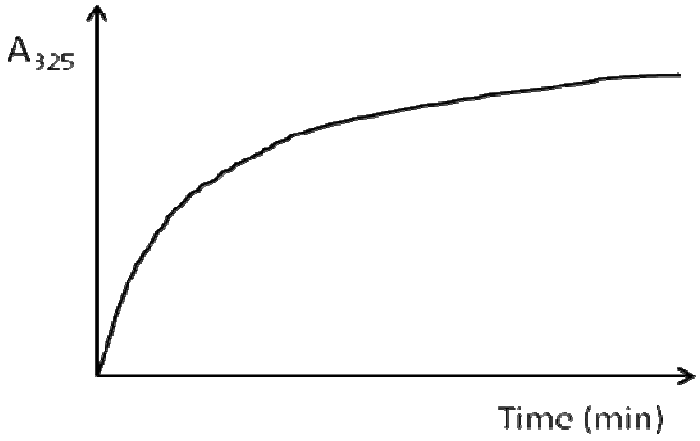

Figure 54: Example of a reaction progression curve: product formation is detected by the change in absorbance at 325 nm.

As the reaction proceeds, the concentration of substrate decreases in the media, provoking the decrease of the rate of the reaction, characterised by saturation in the progression curve. The linear part of the progression curve, where the rate can be considered as maximum represents usually the first percents of the reaction completion. This linear part is commonly used to study the kinetics of a reaction by determining the initial rates. Typically, the initial rate v_i are calculated within the first 5% of the reaction. The equation of the rate can be written like in the following equation.

$$\frac{d[P]}{dt} = v_i \qquad \textbf{(Eq 13)}$$

Using the Beer-Lambert law (shown in **Eq 14**), which establishes a relationship between absorbance and concentration of a given chromophore, the initial rate can be determined by the change in absorbance over a defined period of time.

$$A = \varepsilon l c \qquad \textbf{(Eq 14)}$$

Where A is the product absorbance, l the path length, ε the extension coefficient of the product and c the concentration of the product.

Using **Eq 14**, the determination of the initial rate becomes as in the following equation:

$$v_i = \frac{1}{\varepsilon}\frac{d[A]}{dt} = \frac{slope}{\varepsilon} \quad \textbf{(Eq 15)}$$

The determination of the initial rate v_i can be performed by calculating the slope of the linear portion of the curve divided by the extinction coefficient ε.

The value of the extinction coefficient ε is usually determined experimentally by establishing a reference line of the chromophore and using the Beer-Lamber law. This is discussed in the next sections.

2.2.1.2 Reaction medium for the kinetic assays

The Kemp elimination is a base-catalysed reaction, with a rate that is favoured by the presence of an aqueous media. However, the substrate, benzisoxazole, is a highly hydrophobic molecule because of the aromatic ring and therefore has a low solubility in water. In order to be able to work with a homogeneous solution, the presence of certain percentage of organic solvent was required. A range of organic solvents, miscible with water were evaluated including THF, DMF, DMSO and among them acetonitrile was found to be the most suitable, representing a good compromise in term of solubility and polarity. Given that the concentration in hydroxide ions plays an important factor in the reaction rates for the Kemp elimination, it became clear that a stable pH was required throughout the reaction. This is provided by the use of buffered solutions. The reaction solutions were therefore made as a combination of acetonitrile and aqueous buffers. The choice of buffers and the percentage of organic solvent are discussed in more details in section 2.4.3.2.

2.2.1.3 Reference line

In order to quantify product formation by correlating absorbance and concentration, the establishment of an accurate value of the extinction coefficient was required. This could be obtained by constructing a reference line correlating absorbance and concentration using the Beer-Lambert law to obtain ε. The value of

the extinction coefficient ε can be dependent on the pH of the solution, when protonation equilibrium is involved. A relationship exists between the extinction coefficient ε of a chromophore at a given pH, the pK_a of the product and the extinction coefficient obtained at pH 14, as specified in **Eq 16**.

$$\varepsilon_{pH} = \frac{\varepsilon_{\max}}{1 + \frac{10^{-pH}}{10^{-pKa}}} \qquad \textbf{(Eq 16)}$$

Where ε_{pH} is the extinction coefficient of a product with a certain pK_a at a certain pH, ε_{max} is the maximum value of the extinction coefficient.

The extinction coefficient ε of a compound can be calculated for a given pH as long as the value of ε_{max} is known.

The pK_a value of 1,2-cyanophenol is known and is equal to 6.9. The establishment of a reference line for 1,2-cyanophenol was carried out in concentrated NaOH at pH 14, a pH value that insured that 1,2-cyanophenol would be completely dissociated into its conjugate base leading to the determination of ε_{max}. Three different stock solutions of 1,2-cyanophenol were prepared at different concentrations (10 mM, 20 mM and 40 mM) by weight in concentrated NaOH (3M) using volumetric flasks. Each of these solutions were cross-diluted three times giving rise to 9 solutions of 1,2-cyanophenol in concentrated NaOH with concentrations ranging from 0.1 mM to 4 mM. The cross-dilution technique is based on the independent preparation of 3 stock solutions by weight. In this way it is possible to verify the actual concentration of the solution prepared and to spot any experimental mistake during the preparation of the solutions. The maximum absorbance (at 325 nm) of each solution was recorded and plotted against the corresponding 1,2-cyanophenol concentrations (**Figure 55**).

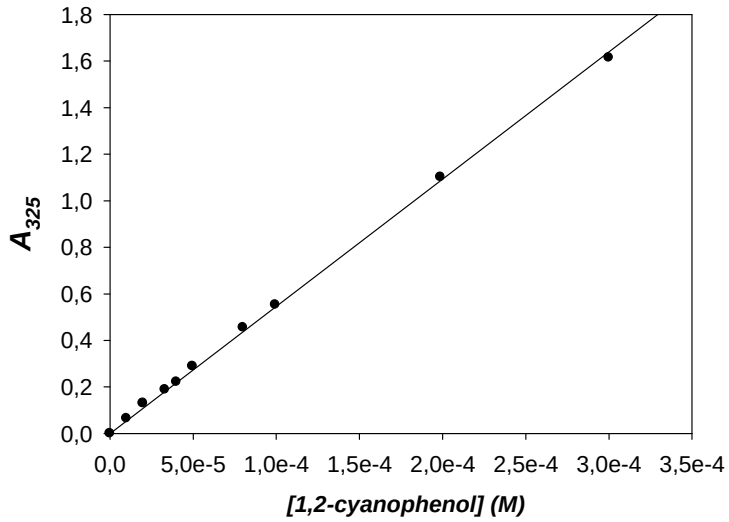

Figure 55: Reference line for 1,2-cyanophenol (**35**). The value for each concentration was obtained by cross-dilution.

This reference line allowed the determination of the extinction coefficient given by the slope, which coefficient ε_{max} was found to be 5383.8 ± 39.21 $M^{-1}cm^{-1}$ (S.E.) with a value of R^2 at 0.9997.

As a result, the concentration of product could be obtained over time using the Beer-Lambert law from the absorbance recorded with the UV-Visible spectrometer in combination with the value of extinction coefficient ε at the corresponding value of pH.

2.2.2 Enzyme-kinetics applied to the Kemp elimination

The investigation of the catalytic activity of the imprinted nanogels was carried out using the analytical methods employed for enzyme kinetics in the view of generating a true enzyme mimic inspired by the mechanism of the Kemp elimination. The following section describes briefly the theory of enzyme-like kinetics used in this work.

2.2.2.1 The Kemp elimination

Kemp and co-workers in 1973 reported that the mechanism of the isomerisation of bensisoxazoles was based on a concerted intermediate-less elimination type E2 rather than E1cB[176]. The mechanism of E1cB type elimination requires the presence of a resonance or an inductively stabilised anion[177]. In the paper of Kemp *et al.*, it was established that this elimination occurred in one concerted step, where both C-H and N-O bonds were cleaved at the rate-determining transition state as described in **Scheme 12**.

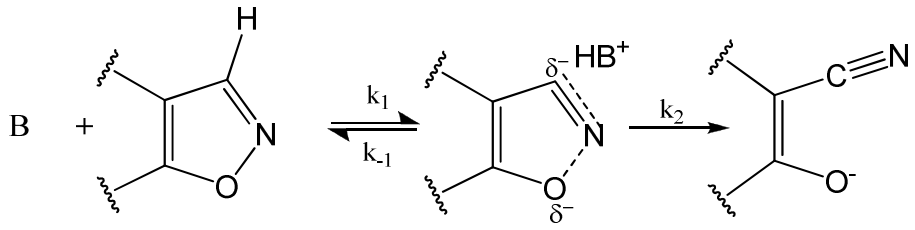

Scheme 12: Concerted Kemp elimination type E2 where both N-O and C-H bonds are cleaved at the rate-determining transition state.

Kemp and co-workers also reported that the rate of this reaction was dependant on the concentration of the base and the catalysis was shown to be involved only in removing the vicinal proton of the nitrogen. Thus, the Michealis and Menten model of enzyme kinetic could be applied easily since the Kemp elimination is a reaction without intermediate and no product inhibition.

2.2.2.2 The Michaelis-Menten model

Introduced in 1913 by Maud Menten and Leonor Michealis, the Michealis-Menten model described the kinetics of many enzymes. However, this kinetic model is relevant to situations where simple kinetic profiles such as single-substrate reactions can be assumed; more complex models are available for systems to which the Michaelis-Menten model cannot be applied. The Michealis-Menten model resides in an equation that relies on two key assumptions: i) the total enzyme concentration does not vary over time and ii) the concentration of the substrate-enzyme complex

does not change over time (quasi steady-state assumption). The establishment of this equation can be explained by the following explanations.

The enzymatic reaction is supposed to be irreversible and the product of the reaction does not bind the enzyme as specified in **Eq 17**.

$$E + S \underset{k_{-1}}{\overset{k_1}{\rightleftharpoons}} ES \xrightarrow{k_2} E + P \qquad \textbf{(Eq 17)}$$

Where E is the enzyme, S the substrate, ES is the substrate/enzyme complex and P the product of the reaction.

This first equilibrium characterised by the rate constants k_1 and k_{-1} describes the specific association between the substrate and the enzyme giving rise to the formation of the complex ES. The second reaction with the rate constant k_2 leads to the formation of the product and the regeneration of the enzyme. The global rate of the reaction is determined by the rate determining formation of the product P from the complex ES via the second reaciton as specified in **Eq 18**.

$$v = -\frac{d[S]}{dt} = \frac{d[P]}{dt} = k_2[ES] \qquad \textbf{(Eq 18)}$$

As explained earlier, in order to apply the Michaelis-Menten model, two key assumptions are required. The first approximation consists in considering the total concentration of enzyme constant over time. This can be illustrated by the following equation.

$$[E]_0 = [E] + [ES] \qquad \textbf{(Eq 19)}$$

The second assumption is that the complex concentration is also constant over time, which corresponds to the quasi steady state approximation. This can be expressed as follows:

$$\frac{d[ES]}{dt} = k_1[E][S] - k_{-1}[ES] = 0 \qquad \textbf{(Eq 20)}$$

From these two equations, the rate constant of the reaction can be expressed in function of the substrate concentration [S] and the total concentration of enzyme $[E]_0$.

These two approximations inherent to the Michaelis-Menten model limit their application to the 'initial' part of the reaction, where the substrate is in a large excess compared to the enzyme concentration and the enzyme presence is mostly materialised as its bonded form, substrate/enzyme complex ES. From this, the Michaelis-Menten equation is deducted and establishes a relationship between the initial rate constant of the reaction and the substrate concentration [S] as follows in **Eq 21**:

$$v_i = \frac{k_2[E]_0[S]}{\frac{(k_{-1}+k_2)}{k_1}+[S]} \qquad \textbf{(Eq 21)}$$

Where v_i is the initial rate of the reaction, [S] the substrate concentration and $[E]_0$ the total concentration of enzyme.

The condition of a 'rapid equilibrium' in the formation of the complex imposes a rate constant k_2, which corresponds to product formation P from the complex ES, to be much slower than that of complex dissociation back to the free enzyme E and the substrate S, k_{-1} ($k_2 << k_{-1}$). **Eq 21** becomes then **Eq 22** as follows:

$$v_i = \frac{k_2[E]_0[S]}{\left(\frac{k_{-1}}{k_1}\right)+[S]} \qquad \textbf{(Eq 22)}$$

These two last equations describe both the 'initial' phase of the reaction when the product formation is still negligible (1% - 3%) and the substrate concentration can be assimilated to its initial value $[S]_0$ and the $[E]_0$ is the total concentration of enzyme. The study of enzyme kinetics is performed through the introduction of different notations such as the rate constant of the catalysed reaction k_{cat} and the Michaelis-Menten constant K_M, as specified in the following equation.

$$v_i = \frac{k_{cat}[E]_0[S]_0}{K_M+[S]_0} \qquad \textbf{(Eq 23)}$$

This model establishes a hyperbolic relationship between the 'initial rate' and the concentration of substrate. The maximum velocity V_{max} is reached at very high or

infinite substrate concentrations and can be expressed as specified in **Eq 24**. This value is the asymptotic value of the velocity of the reaction when saturation is reached.

$$V_{\max} = k_{cat} \times [E]_0 \qquad \textbf{(Eq 24)}$$

The constant K_M is defined as the value of the concentration $[S]_0$ when the initial rate v_i has reached half of the maximum velocity V_M in a steady state conditions. In other terms, K_M is the value of substrate concentration $[S]_0$ when half of the enzyme active sites are occupied or at half saturation. A high value of K_M implies that a high concentration of substrate is required in order to saturate half of the enzyme active sites while a low value of K_M indicates that a small amount of substrates can bind half of the active sites. Thus, K_M could be considerate as a direct measurement of the binding affinity of the substrate towards the enzyme. These parameters are illustrated in an example of Michaelis-Menten saturation curve on **Figure 56**.

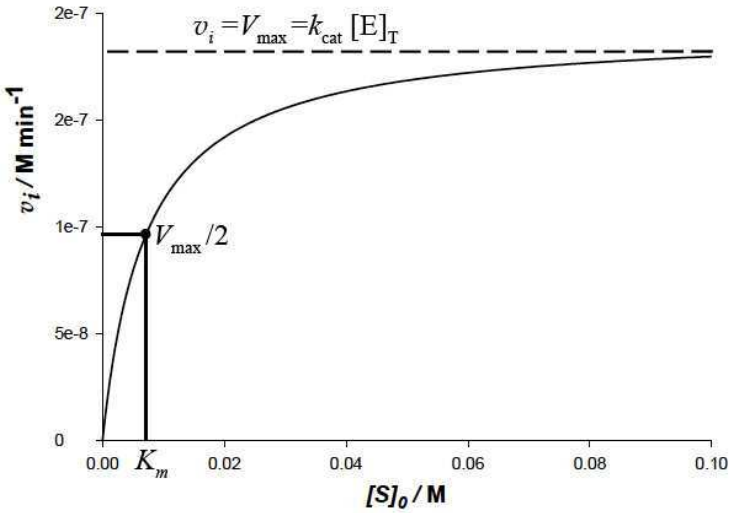

Figure 56: Example of Michealis-Menten saturation curve, where V_{max} is the maximum velocity and K_M the Michaelis-Menten constant

The other important parameter introduced in the Michaelis-Menten equation is the rate constant k_{cat}. This constant is defined from the model as the following ratio:

$$k_{\max} = \frac{V_{\max}}{[E]_0} \qquad \textbf{(Eq 25)}$$

The knowledge of k_{cat} allows a comparison of the catalytic activity between different catalysts as it describes the maximum velocity that can be obtained at a fixed enzyme

concentration and also the number of catalytic turnover events per units of time. The catalytic efficiency of an enzyme or 'artificial enzyme' defined by the ratio k_{cat}/K_M give information about how many molecules of substrates bound to an active site give rise to formation of product. It permits in practice to compare the effectiveness of the catalysts to generate product from substrate molecules[178].

The parameters introduced in the previous paragraph are of great importance for the study of the catalytic activity of the imprinted nanogels presented in this thesis. These values allow in fact a quantification of the activity of the active particles and permit a comparison of the efficiency with other 'artificial enzymes'. In view of establishing the best conditions for obtaining reliable kinetic data in a reasonable amount of time, a protocol for the kinetic assays needed to be optimised. This consisted in investigating the behaviour of the uncatalysed reaction under various conditions. This is the focus of the next section.

2.2.3 Development of a suitable analytical procedure

2.2.3.1 Determination of initial rate v_i of the reaction

One of the possible ways to determine the rate of a reaction is by studying product formation over time. In the case of UV-Vis spectroscopy, the progress of the reaction is characterised by an increase of the product maximum absorbance A_{max} over time. For an accurate determination of the rate, the kinetic conditions are set-up so that there is a linear relationship between product absorbance A_{max} and the time scale t used to evaluate the initial rate of the reaction. The slope of this curve (A = f(t)) is calculated by the instrument as specified in **Eq 15** and gives access to the initial rate of the reaction, v_i, by substituting the value of A by the product concentration calculated from the Beer-Lambert law with the value of the extinction coefficient ε as described in **Eq 25**.

$$s = \frac{(A_t - A_{t0})}{(t - t0)} \qquad \textbf{(Eq 26)}$$

Where A_t is the product absorbance recorded at t and A_{t0} is the initial product absorbance recorded at t0.

Subsequently, the rate constant is determined as follows:

$$v = \frac{s}{\varepsilon} \qquad \textbf{(Eq 27)}$$

Where v is the rate of the reaction, s the slope of the curve A=f(t), and ε the extinction coefficient.

2.2.3.2 Study of the uncatalysed reaction

As mentioned previously, the Kemp elimination is a base-catalysed reaction in which the formation of the product, cyanophenol, occurs through the removal of a proton concerted with the cleavage of N-O bond. This elimination is a second order reaction, where the rate limiting step of the reaction is the attack of the proton by the base. Thus, the rate of the reaction depends on the concentration of base in the media and of the substrate as specified in **Eq 28**.

$$\frac{d[P]}{dt} = k[B][S] \qquad \textbf{(Eq 28)}$$

Where P is the product, B the base and S the substrate.

Nevertheless, the study of the kinetics of the Kemp elimination were not done following a second order type of reaction as the reaction was occurring in a large excess of base. The reaction rate can be written in a different way as specified in **Eq 29**.

$$\frac{d[P]}{dt} = k'[S] \qquad \textbf{(Eq 29)}$$

In this last equation, where k' = k[B], the rate is only dependant on the concentration of substrate as k' is considered as the observed rate constant. The study of the background reaction allowed the determination of this constant k', also called k_{uncat} as specified in **Eq 30**. The reaction can be assimilated now as a pseudo-first order reaction.

$$k_{uncat} = k' = k[B] \qquad \textbf{(Eq 30)}$$

Where [B] is the concentration of base in the media.

As demonstrated by Kemp and co-workers, the Kemp elimination rate is highly dependent on the concentration and strength of base so that any increase of hydroxide ions concentration in the media would result in significant acceleration of the reaction[4]. This indicates that the uncatalysed reaction rate is not likely to be negligible and will have to be carefully taken into account when characterising the catalytic activity of the nanogels. As a result, the study of the change of k_{uncat} as a function of pH was required in order to evaluate the contribution of the background rate to the catalytic activity.

Thus, the initial rates of the background reaction were investigated as a function of pH at fixed substrate concentration in two different buffers in order to cover a broad range of pH values from 8.9 to 11.1. From pH 8.9 to pH 9.4, Tris buffer was selected as the stability of this buffer is found to be between pH 7.0 and pH 9.4. From pH 9.4 and pH 11.1, carbonate buffer was selected since its efficacy is found to be between pH 9.2 to pH 11.5. A stock solution of benzisoxazole (substrate) was prepared in acetonitrile at a concentration of 25 mM. All the background reactions were carried out inside the cuvette in a mixture of 10% of acetonitrile in buffer at fixed substrate concentration (0.1 mM) for different values of pH ranging from 8.9 to 11.12 and the initial rates (v_i) were plotted as a function of the concentration of OH^- as shown in **Figure 57**. As described in **Eq 28**, the rate of the Kemp elimination is dependent on the substrate concentration and on the concentration of base more specifically in this case of hydroxide ions concentration. Thus, at a fixed substrate concentration, it was expected to observe a linear relationship between the initial rate vi and the concentration of hydroxide ions. The low substrate concentration (0.1 mM) chosen to perform the experiments would allow an accurate determination of the initial rates at high pH values, as at high pH the reaction occurs too quickly leading to the loss of linearity in the progression curve. It was decided to work with 10% acetonitrile to minimise solvent effect.

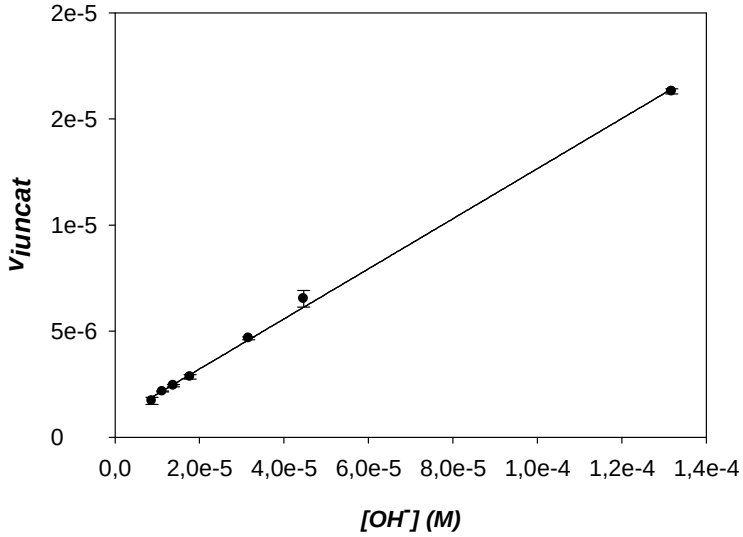

Figure 57: Variation of the initial rates of the reaction in function of the concentration of OH^- at a fixed substrate concentration (0.1 mM). The reactions were carried out inside the spectrophotometric cuvette in 10% acetonitrile and two different buffers depending on the pH: from pH 8.9 to pH 9.4, Tris buffer (50 mM) was used and from pH 9.4 to pH 11.1, carbonate buffer was used.

The data could be fitted to a linear regression using SigmaPlot 8.0 and the slope was found to be 0.12 ± 0.002 min^{-1} with R^2 of 0.9986. This was expected when considering **Eq 30**, where it was shown that k_{uncat} is dependant of the concentration of base. Under a pH value of 8.5 (concentration in hydroxide ions of 8.56×10^{-6} M), no meaningful quantity of product could be detected within the timeframe used for data collection implying that k_{uncat} was negligible.

The rate constant of the background reaction k_{uncat} at pH 8.9 was obtained by plotting the initial rates against the concentration of substrate. The curve of the initial rate v_{iuncat} versus substrate concentration is shown on **Figure 58**.

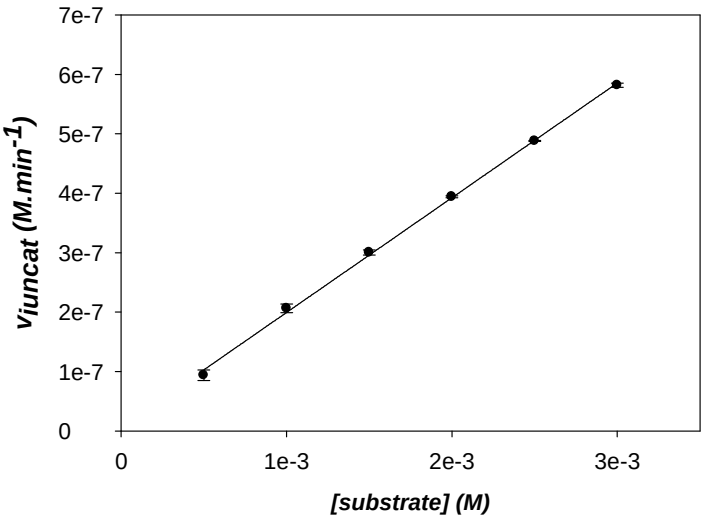

Figure 58: Plot of the initial rates v_i versus substrate concentrations at pH 8.9. The different v_i were determined at various substrate concentrations ranging from 500 µM to 3 mM in mixture of 10% of acetonitrile in Tris buffer at pH 8.9.The data could be fitted to a linear regression using SigmaPlot 8.0.

The rate constant k_{uncat} was found to be $1.93\times10^{-4}\pm 3.10\times10^{-6}$ min^{-1} (S.E.) at pH 8.9 with a value of R^2 of 0.99897. This value was in line with the values of k_{uncat} obtained previously in the literature[4] highlighting, along with the low standard deviation, the reliability of this method. The knowledge of k_{uncat} would allow a meaningful evaluation of the catalytic efficiency of the nanogels, as the values of initial rates v_i obtained with the nanogels would be corrected for the initial rates v_{iuncat}.

2.2.3.3 Preliminary studies on nanogel kinetics

Following the preliminary studies on the background reaction it was decided to investigate the catalytic activity of the imprinted nanogels at pH 8.9 in Tris buffer with 10% of acetonitrile. Stock solutions of imprinted nanogels and non-imprinted nanogels (MIP AS230 and NIP AS231) were prepared at a concentration of 2 $mg.ml^{-1}$ in a mixture of 50% acetonitrile in Tris buffer (pH 8.9, 50 mM) at which conditions the nanogel gave clear solutions. A stock solution of substrate (bensizoxazole) was prepared at concentration of 50 mM in acetonitrile. The experiments were carried out following a similar protocol as for the uncatalysed reaction. All the reactions were performed in 10% acetonitrile in Tris buffer (pH 8.9, 50 mM) and the imprinted and non-imprinted

nanogels, MIP AS230 and NIP AS231, concentration used for the kinetic experiments was fixed at 0.1 mg.ml^{-1} inside the cuvette. The range of substrate concentration used for the assay was from 1 mM to 6 mM. The initial rates for both polymers were corrected for background reaction and plotted versus substrate concentration as shown in **Figure 59**.

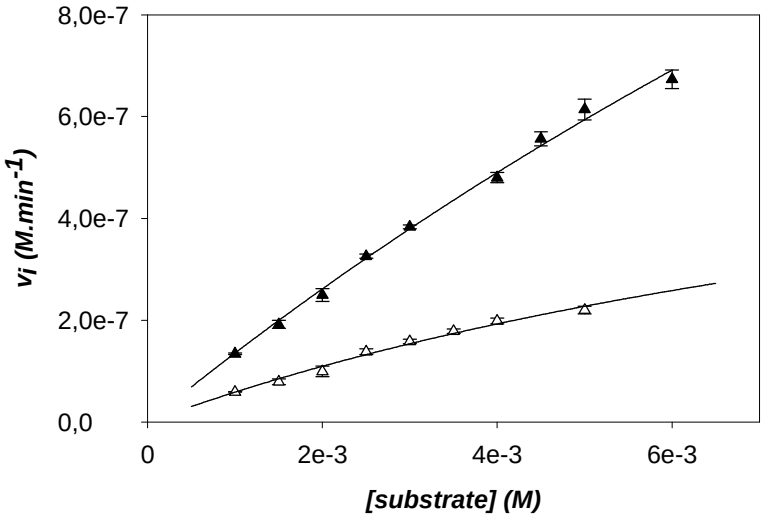

Figure 59: Initial rates (corrected for background reaction) versus substrate concentration: (▲) MIP AS230 (0.1 mg.ml^{-1}), (Δ) NIP AS231 (0.1 mg.ml^{-1}). All the reactions were performed in 10% acetonitrile in Tris buffer (pH 8.9, 50 mM). The range of substrate concentration used for the assay was from 1 mM to 6 mM.

Both polymers, MIP AS230 and NIP AS231 demonstrated catalytic activity toward the Kemp elimination. The data could be fitted using Sigma Plot 8.0 into a hyperbola in agreement with the Michaelis-Menten saturation model. From these curves, the kinetic parameters V_{max} and K_M could be extrapolated and they were found to be 3.86×10^{-6} (S.E. ± 8.47×10^{-7}) M.min^{-1} and 2.75×10^{-2} (S.E. ± 7.03×10^{-3}) M for MIP AS230, and 8.05×10^{-7} (S.E. ± 1.03×10^{-7}) M.min^{-1} and 1.27×10^{-2} (S.E. ± 2.21×10^{-3}) M for NIP AS231.

The active sites concentration was determined (cf section 2.3) for both polymers and was found to be 0.24 µmol.mg for MIP AS230 and 0.19 µmol.mg for NIP AS231 for a polymer solution at 0.1 mg.ml^{-1}. This polymer concentration was in agreement with the Michaelis-Menten requirement, and therefore inferior to 10% of the substrate concentration. Thus, the rate constants k_{catMIP} and k_{catNIP} of the imprinted

and non-imprinted nanogels could be determined using the active site concentration and were found to be 0.184 min^{-1} and 0.043 min^{-1} respectively. These values represented a 948-fold rate enhancement and 221-fold rate enhancement for the imprinted and non-imprinted nanogels respectively when compared to the uncatalysed reaction.

The value of K_M for both polymers was relatively high and this indicated a low affinity between the substrate molecule and the nanogels. The values of K_M reported for enzymes fall in the mM range or below[178]. It was reported for the catalysis of the Kemp elimination by serum albumins a K_M constant ranging from 0.4 mM to 2 mM[140] and with the catalytic antibodies K_M values ranging from 0.05 mM to 0.8 mM[179]. These values that were found to be 10 times to 100 times lower to the value of K_M observed with the imprinted nanogels, indicated a strong binding between the substrate and the catalyst. In the work presented here, the large value obtained for K_M was not surprising. The nanogels were indeed prepared using a non-covalent molecular imprinting approach where weak interactions were involved. This was demonstrated by the interaction studies in section 2.2 where a low value of K_{ass} (1.76 M^{-1}) for the template-monomer complex formation was found. Furthermore, it was reported that the high properties of molecular recognition displayed by resides not only to their well organised and strong interactions between the functional groups of the enzyme and the substrate molecule, but also to the number of interaction points. Ogston et al. in 1948 demonstrated that in order to reach optimal substrate specificity, a minimum of three points of interaction between the enzyme matrix and the substrate was required[180-181]. In the work presented here, there was only one point of interaction between the nanogel matrix and the substrate molecule as shown in the interaction studies in section 2.2. This might explained the low K_M values observed for the imprinted nanogels.

The catalytic efficiency defined by the ratio k_{cat}/K_M was calculated and was found to be 6.7 $M^{-1}.min^{-1}$ and 3.4 $M^{-1}.min^{-1}$ for MIP AS230 and NIP AS231 respectively. This parameter describes how often a substrate molecule bound to the nanogel matrix reacts to form a molecule of product. This value is often used to compare catalyst or

enzyme effectiveness to transform substrate into product. The catalytic efficiency values reported with the catalytic antibodies ranged from 100 to 10^4 $M^{-1}.min^{-1}$ [179]. The catalytic efficiency obtained with the imprinted nanogels was far lower than the one reported with the catalytic antibodies. This was expected as the imprinted approach used to synthesise the nanogels was based on a weak system with poor interactions. The kinetic parameters of MIP AS230 and NIP AS231 are gathered in **Table 11**.

Table 11: Kinetic parameters obtained for MIP AS230 and NIP AS231 in 10% acetonitrile in Tris buffer (50 mM, pH 8.9) after fitting the data to a Michealis-Menten model using Sigma Plot 8.0.

	V_M/ (M.min^{-1})	K_M/ (M)	[active sites] (µmol/mg)	k_{cat}/ (min^{-1})	k_{cat}/K_M
MIP AS230	3.86×10^{-6}	2.75×10^{-2}	0.34	0.184	6.7
NIP AS231	8.05×10^{-7}	1.27×10^{-2}	0.19	0.043	3.4

The imprinting efficiency of nanogels, which reports the difference of catalytic activity between the imprinted polymer and the non-imprinted polymer, is defined by the ration k_{catMIP}/k_{catNIP}. A high value of the imprinting efficiency implies that the catalysis of the reaction occurs via the specific cavities formed during the imprinting process. This parameter was therefore of great importance as it would ensure that even using with a non-covalent system with a poor template-monomer association, a specific cavity was formed leading to an enhanced catalytic activity. The value obtained for these studies around 4.31 was reasonably high especially when compared to other imprinting factors reported in the literature for catalytic imprinted polymers for hydrolytic reactions[104].

Given that the nanogel format is quite different from the 'bulk' format commonly used for imprinted polymers, these results were compared to the catalytic activity obtained by Mosbach *et al.* for the preparation of imprinted 'bulk' polymers for the Kemp elimination. This would provide further insight for possible area of improvement of nanogel performance. In this study reported by Mosbach and co-workers, it was reported a rate constant k_{cat} for the imprinted polymer of 0.205 min^{-1} and K_M was found to be around 0.484 mM[107]. The rate constant obtained previously

with the imprinted nanogels appeared to be lower than the rate constant obtained with the 'bulk' polymers. However, the data presented in this paper, which consisted of four points, were fitted into a Linweaver-Burke displaying a relatively high standard error. The active site concentration was not carried out in the studies of Mosbach and co-workers with the 'bulk' polymers preventing an accurate calculation of the rate constant k_{cat}. Furthermore, it is worth noticing that in this work, the concentration of polymer used for the kinetics was equal to 1.25 $mg.ml^{-1}$, which was 12.5 times higher than the concentration of catalysts used with the imprinted nanogels. As a result, the catalytic activity of the imprinted 'bulk polymers' could not be accurately compared to the one obtained with the nanogels.

The initial preliminary kinetic data obtained with the imprinted and non-imprinted nanogels demonstrated that the nanoparticles were catalytically active towards the Kemp elimination with an enzyme-like behaviour. The catalytic activity and efficiency were found to be far lower than the one obtained with the catalytic antibodies or compared to the performance of enzymes. However, given the weak interactions involved in the imprinting process, the nanogels demonstrated a proof of concept displaying rate enhancement, enzyme-like behaviour and a relatively good imprinting efficiency.

2.2.4 Optimisation of the catalytic and imprinting efficiency

With the aim of improving the performance of the imprinted nanogels, it was decided to study the effect of external stimuli such as pH and acetonitrile content on the catalytic activity of the nanomaterials. It is worth remembering that these types of studies have not yet been reported in the development of enzyme-mimics using imprinted materials. The next section focuses on two main parameters: first the investigation of the effects of pH and buffer on the imprinting and catalyst efficiency, and the effect of the addition of organic solvent in the media on the catalytic activity of the nanogels.

2.2.4.1 Effect of pH

As it was explained in section 2.4.3.2, pH has an important effect on the rate of the Kemp elimination. Earlier experiments had also established that at pH below 8.5, the reaction rate could be considered as negligible. It was therefore interesting to investigate how this effect on the rate of the reaction could have an impact on the catalytic activity and imprinting efficiency of the polymers.

Before investigating the effect of pH on the activity of the imprinted nanogels, the extinction coefficient of the product of the Kemp elimination, 1,2-cyanophenol, was measured in presence of the nanogels in order to verify that the presence of nanogels did not affect the exctinction coefficient of 1,2-cyanophenol. This phenomenon was observed in previous work where the presence of nanogels affected the extinction coefficient of the chromophore[173]. No significant change in the exctinction coefficient value was noticed with varying the acetonitrile content in the reaction mixture.

A similar experiment to the one carried out in section 2.4.3.2 for the uncatalysed reaction was performed with the imprinted and non-imprinted nanogels. The reactions were performed in 10% acetonitrile in two different buffers in order to reach a wider range of pH values. Tris and carbonate buffers, were used at pH ranging from 8.9 to 9.4 and from 9.4 to 11.12 respectively. A detailed study of the effect of pH on the catalytic activity of the nanogels would have required the determination of a full kinetic profile for each value of pH. However, this was not considered for a preliminary study and the determination of the initial rate at different pH was only carried out at a single substrate concentration. The substrate concentration was fixed at 1 mM because for this value, the portion of the curve v_i as a function of substrate concentration established in section 2.4.3.3 was linear and there was a clear difference between the activity of imprinted polymer and the non-imprinted polymer. The concentration of polymers was decreased to 0.01 $mg.ml^{-1}$ (previously 0.1 $mg.ml^{-1}$) in order to determine accurately the initial rates and to avoid the curvature of the progression curve as shown in **Figure 60**.

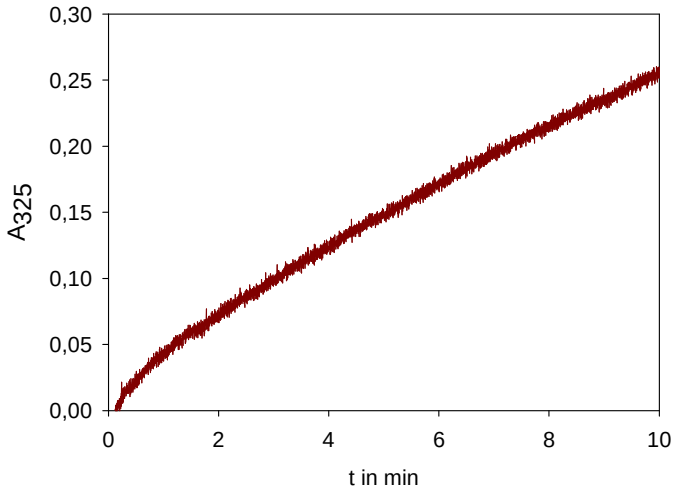

Figure 60: Example of a progression curve where the reaction occurs too quickly and curvature is obtained since the first minutes of monitoring product formation preventing an accurate determination of the initial rate. Product formation was monitored at 325 nm, a wavelength where the absorbance of cyanophenol is maximal. The reaction was performed inside the cuvette in 10% acetonitrile in Tris buffer (50 mM) at pH 9.2. Polymer concentration is 0.1 $mg.ml^{-1}$.

The values of the initial rates v_i obtained with the polymers were corrected for background reactions. The apparent rate constant k_{app} defined by the ratio of the initial rate at one substrate concentration (1 mM) and the value of the active site concentration was calculated using the active site concentration determined in section 2.3 for MIP AS230 and NIP AS231 at a concentration of 0.01 $mg.ml^{-1}$. The values of the active sites concentration were found to be 2.1 µM for MIP AS230 and 1.9 µM for NIP AS231. The plot of the apparent rate constants k_{app} for both polymers against pH is shown on **Figure 61**.

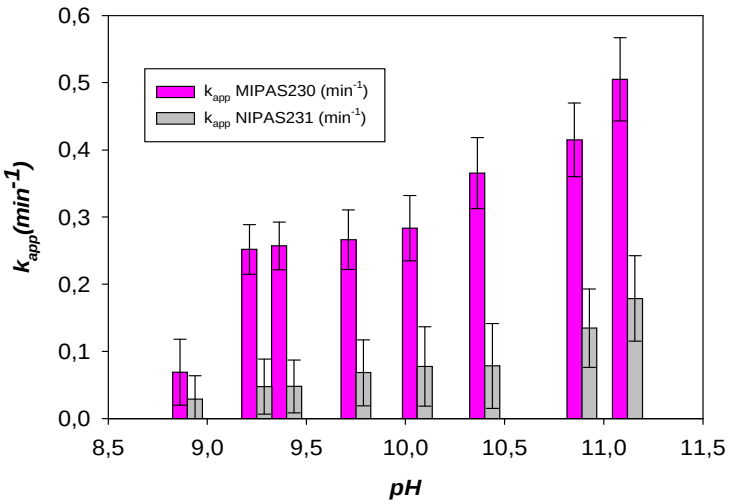

Figure 61: Apparent rate constants k_{app} of the reaction with MIP AS230 and NIP AS231 at a polymer concentration of 0.01 $mg.ml^{-1}$. The initial rates of MIP AS230 and NIP AS231 were corrected for background reaction before the calculation of k_{app} at a substrate concentration of 1 mM in 10% acetontrile in Tris buffer (50 mM) from pH 8.9 to pH 9.4 and carbonate buffer (50 mM) from pH 9.4 to pH 11.12.

In a similar manner as for the background reaction, the values of v_i for both polymers MIP AS230 and NIP AS231 were increased from 0.07 min^{-1} to 0.50 min^{-1} for the imprinted nanogels and from 0.03 min^{-1} to 0.2 min^{-1}, as the pH of the solution increased. The maximum values of v_i were obtained at the highest pH. The values of v_i were corrected for the values of v_i of the background reaction, as a consequence the trend observed in the case of both polymers was the effect of pH on the activity of the polymers. The increase of activity of the nanogels could be explained by the fact that the increase of pH insured better dissociation of the pyridine residues from pyridinium ions to pyridine (pKa around 6.4 cf active site number section 2.3) inside the polymer matrix and therefore increased the number of active sites available for the substrate molecule.

The activity of MIP AS230 was found to be higher than NIP AS231 at all pH. In order to visualise better this difference of catalytic activity between MIP AS230 and NIP AS231 in function of pH, the apparent imprinting factor I_{app}, which was defined by the ratio between the apparent rate constant obtained with the imprinted nanogels and the one of the non-imprinted nanogels, was calculated. These values were plotted against pH and are shown in **Figure 62**.

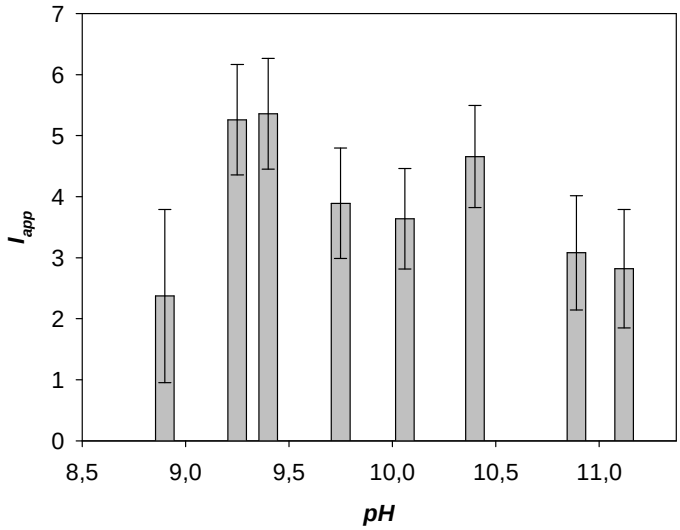

Figure 62: Variation of the apparent imprinting factor in function of pH. The apparent imprinting factor is defined by the ratio between the apparent rate constant of the reaction obtained for the imprinted polymer MIP AS230 and the initial rate of the reaction obtained for the non-imprinted polymer NIP AS231. The reactions were performed inside the cuvette at 1 mM substrate concentration in 10% acetontrile in Tris buffer (50 mM) from pH 8.9 to pH 9.4 and carbonate buffer (50 mM) from pH 9.4 to pH 11.12

It appeared to have some variability in the values of the apparent imprinting factors but overall there was no major difference. The values of I_{app} ranged from 2.62 to 5.92 and the maximum value was found to be at pH of 9.4. However, the standard deviation was found to be quite important preventing an accurate determination of the pH where I_{app} was maximal. The fluctuations of the values of I_{app} could be due to minor experimental errors related to the high sensitivity of monitoring product formation with UV-Vis spectroscopy especially at high pH values, the contribution of the background reaction was significant.

Although the catalytic activity appeared to be the highest for a pH of 11.12, the imprinting efficiency was a more important criterion to take into account in order to identify the best conditions to carry out a full kinetic profile of the nanogels. Considering the data obtained with the apparent imprinting factor I_{app}, the imprinting efficiency appeared to be the greatest at pH 9.4 at fixed substrate concentration of 1 mM, although there was found to be significant standard errors. Nevertheless, it was

decided to consider this approach at fixed substrate concentration and to investigate the kinetics of the nanogels at pH 9.4.

2.2.4.2 Effect of acetonitrile content

The solvent system used for the kinetic assays was as described in section 2.4.2 is a mixture of acetonitrile and buffered solutions. So the next obvious step was a study of the effect of organic solvent content on the kinetic parameters. A content of 10% of acetonitrile used previously in the kinetic assays ensured the formation of clear homogeneous solutions, as the substrate molecule is quite hydrophobic. Furthermore, the results of the solubility tests for the nanogels (section 2.2) demonstrated that a solution of water and acetonitrile provided clear colloidal solutions. The purpose of this work was to evaluate the effect of acetonitrile content on the kinetic parameter with a view to optimising catalytic activity and imprinting efficiency.

Before investigating the effect of acetonitrile content on both, background reactions and reactions in the presence of the imprinted nanogels, the extinction coefficient of the product of the Kemp elimination, 1,2-cyanophenol, was measured at different acetonitrile content in order to verify that the value did not change significantly as a function of acetonitrile. No significant change in the exctinction coefficient value was noticed with varying the acetonitrile content in the reaction mixture.

Preliminary experiments on the background reactions were carried out, where the content of acetonitrile was varied from 5% to 30%. The reactions were performed at a single substrate concentration in order to have an insight of the effect of acetonitrile content on the activity of the particles. For similar reasons as for the pH studies on the background reactions, a substrate concentration of 1 mM was selected. The initial rates of the reactions were calculated and plotted against the acetonitrile content, as shown in **Figure 63**.

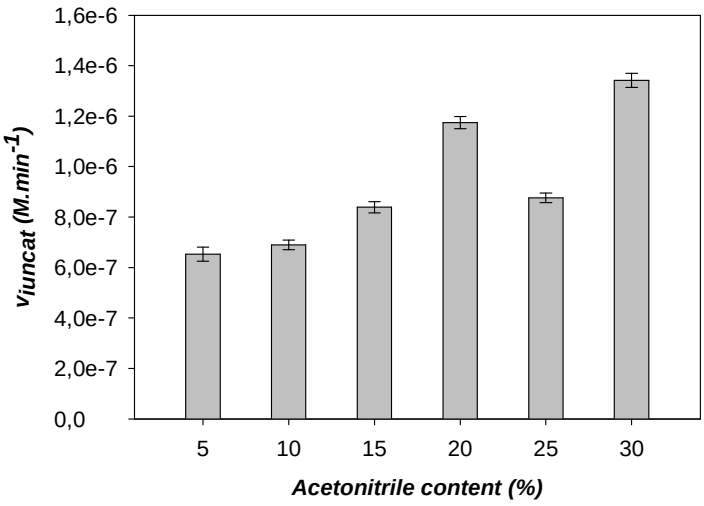

Figure 63: Variation of the initial rates v_{iuncat} of the uncatalysed reaction in function of the content of acetonitrile. All the reactions were carried out in carbonate buffer (50 mM, pH 9.4) at different content of acetonitrile.

There was no significant variation in the initial rates of the reaction when the acetonitrile was increased from 5% to 30%. The values of v_{iuncat} appeared to increase slightly from 6.52×10^{-7} M.min^{-1} at 5% of acetonitrile to 1.34×10^{-6} M.min^{-1} at 30%. This could be explained by a better solvatation of the substrate molecule, benzisoxazole that is not very soluble in water, in higher content of acetonitrile. The higher solubility of the substrate in the media increased the number of molecules that could react and led to higher initial rates.

Following these preliminary results, the same experiment was repeated with the imprinted and non-imprinted nanogels MIP AS230 and NIP AS231. The reactions with different content of acetonitrile ranging from 5% to 30% were performed at fixed substrate concentration, the same concentration used for the studies with the uncatalysed reaction. The concentration of the polymer solution was decreased to 0.02 mg.ml^{-1} in order to accurately determine the initial rates of the reaction at pH 9.4. At a polymer concentration of 0.1 mg.ml^{-1} (concentration used in the preliminary studies at pH 8.9 in section 2.4.3.3), the reaction occurred too rapidly to be monitored and a curvature of the progression curve was observed. In a similar as for the investigation with the variation of pH, the apparent rate constants of the polymers were calculated using the active site concentration for a polymer concentration of 0.02

mg.ml^{-1} (0.24 µmol/mg for MIP AS230 and 19 µmol/mg for NIP AS231) and they were plotted against acetonitrile concentration, as shown in **Figure 64**.

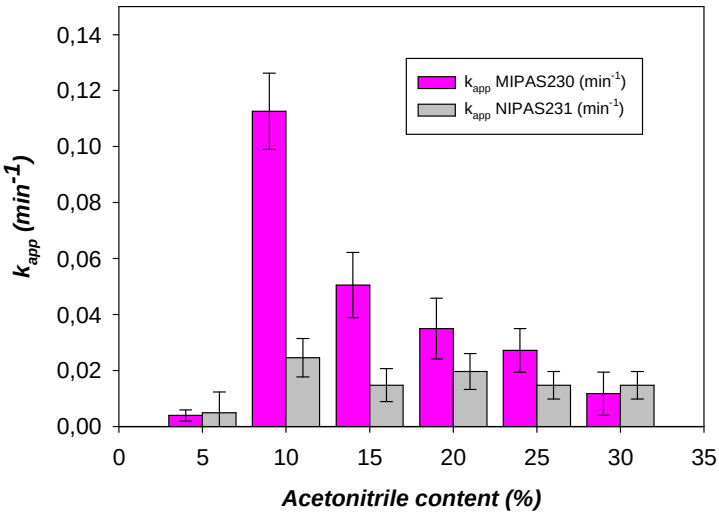

Figure 64: Variation of the apparent rate constant k_{app} for MIP AS230 and NIP AS231 in function of the content of acetonitrile using the active site concentration for a polymer concentration of 0.02 mg.ml^{-1}. All the values of initial rates were corrected for background reactions prior the calculation of the apparent rate constants. The reactions were carried out using a concentration of 0.02 mg.ml^{-1} of polymers in carbonate buffer (50 mM) at pH 9.4 varying the content acetonitrile from 5% to 30% at fixed substrate concentration (1 mM).

The values of k_{app} ranged from 0.004 min^{-1} to 0.11 min^{-1} for MIP AS230 and from 0.005 min^{-1} to 0.02 min^{-1} for NIP AS230. For the imprinted polymer, a significant decrease in k_{app} was noticeable above a content of 10% of acetonitrile, while for the non-imprinted polymer NIP AS231 was not significant. The low values of k_{app} at 5% of acetonitrile for both polymers could be explained by a low solubility of the polymers at such low acetonitrile content giving rise to cloudy solutions. This lack of nanogel solubility prevented a good exposure of all active sites of the polymer matrix to the substrate limiting the rate of the reaction. The decrease was found to be more significant between 10% and 15% of acetonitrile for the imprinted polymer MIP AS230 where the initial rate of MIP AS230 was decreased by half. Above 15 %, the effect of the content of acetonitrile is not very significant and might be due to minor experimental errors or the increase of the contribution of the uncatalysed reaction.

Overall, high content of acetonitrile seemed to reduce the catalytic activity of the imprinted polymer, while leaving unchanged the activity of the non imprinted polymer. This suggested that increasing the concentration of this solvent in the reaction mixture reduced the exposure of active sites to the substrate solutions since the decrease was also occurring with the non-imprinted nanogels. This might be explained by possible aggregation of the nanogel particles or a change in their morphology leading to a reduced activity. A detailed physical-chemical characterisation of nanogel particles in different content of acetonitrile is discussed in section 2.7 focusing on the characterisation of the nanogels.

Solvent effect on the activity of imprinted polymers was reported in previous work on binding imprinted polymers for capillary electrochromatograhy applications[182]. In this work, the effect of the nature of the organic solvent and the content on the chiral recognition properties of the imprinted polymer was investigated. It was demonstrated that the nature of organic solvent used for the elution was of great importance. The interactions between the template molecule and the imprinted polymer were mainly based on non-covalent hydrogen bond, so the use of protic solvents such as methanol prevented a good re-binding process. The use of aprotic solvents such as acetonitrile and DMSO led to better recognition properties, however acetonitrile was found to be a much better candidate due to its reduced polarity compared to DMSO. The polarity index of acetonitrile is found to be 5.8 and the one of DMSO 7.2[183]. The content of acetonitrile was also studied and it was shown that higher acetonitrile contents led to an enhanced chiral recognition and resolution in the chromatogram. This was explained by the fact that hydrogen bonds are found to be stronger in hydrophobic environments.

From the preliminary results obtained with the nanogels at different pH and acetonitrile contents at fixed substrate concentration, it was decided to investigate the catalytic activity of the nanoparticles was at a pH 9.4, and at an acetonitrile content of 10% for different substrate concentration in order to determine the kinetic parameters under these conditions and to be able to compare them to the one obtained in the

preliminary studies in section 2.4.3.3. The next section focuses on the determination of the full kinetic profile of the nanogels at pH 9.4 and at 10% of acetonitrile.

2.2.4.3 Nanogel kinetic with optimised conditions

Following these preliminary results, the determination of a complete kinetic profile was then carried out and the kinetic parameters were determined in order to compare this new kinetic profile with the preliminary one obtained earlier (section 2.4.3.3).

Stock solutions of imprinted nanogels and non-imprinted nanogels (MIP AS230 and NIP AS231) were prepared at a concentration of 2 $mg.ml^{-1}$ in a mixture of 50% acetonitrile in Carbonate buffer (pH 9.4, 50 mM). A stock solution of bensisoxazole was prepared in acetonitrile at a concentration of 10 mM prior to the kinetic assays. The imprinted and non-imprinted nanogel solutions were prepared at a concentration of 0.02 $mg.ml^{-1}$, which was the concentration used for the preliminary studies on the effect of acetonitrile content at pH 9.4 (section 2.4.4.2). In order to avoid the reaction to become too fast to be monitored at this pH, careful attention was put on the range of substrate concentration selected to determine the kinetic parameters. Curvature of the progression curves were observed for substrate concentrations of and above 1 mM preventing the determination of the initial rates. The range of substrate concentration used for the kinetic assay was therefore from 0.1 mM to 1 mM. The initial rates for both polymers were corrected for the background reaction and plotted versus substrate concentration as shown in **Figure 65**.

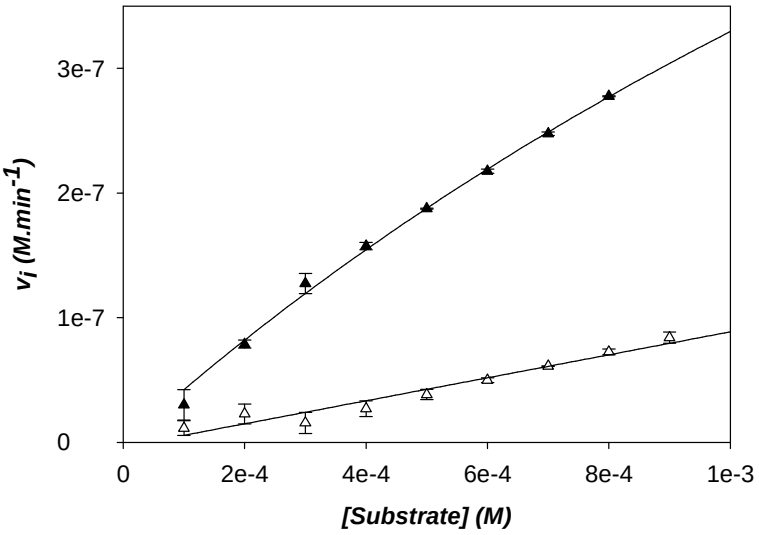

Figure 65: Initial rates v_i of (▲) MIP AS230 and (Δ) NIP AS231 in function of substrate concentration in 10 % acetonitrile in carbonate buffer (50 mM, pH 9.4). All the reactions were carried out using polymer concentration of 0.02 mg.ml^{-1}. All the values of v_i were corrected for background reactions. All the reactions were performed inside the cuvette using the appropriate amount of acetonitrile and buffer in order to respect the content of 10% acetonitrile in carbonate buffer (pH 9.4, 50 mM).

For MIP AS230 the data could be fitted using Sigma Plot 8.0 to the hyperbola in agreement with the Michaelis-Menten saturation model. In the case of the non-imprinted polymer NIP AS231 there was a major difference with the data presented in section 2.4.4.3, the data could not be fitted into a Michaelis-Menten model and appeared to be a linear regression. One possible explanation was that K_M was very large for the non-imprinted polymer so that the curvature of the plot of v_i as a function of substrate concentration was not detectable within the range of substrate concentrations used for the kinetics. For MIP AS230, the kinetic parameters V_{max} and K_M could be extrapolated and they were found to be 1.35×10^{-6} (S.E. ± 6.72×10^{-7}) M.min^{-1} and 3.08×10^{-3} (S.E. ± 2.13×10^{-4}) M respectively. The rate constant k_{cat} of the reaction was calculated using the active site concentration obtained in section 2.3, which for MIP AS230 at a polymer concentration of 0.02 mg.ml^{-1} was found to be 4.2 µM. The value obtained was 0.321 min^{-1}. The apparent rate constant $k_{cat,app}$ for the non-imprinted that was defined by the slope of the linear curve and was found to be 9.22×10^{-5} (S.E. ± 3.31×10^{-6}) min^{-1}.

The rate constant k_{cat} obtained at pH 9.4 in carbonate buffer (0.321 min^{-1}) increased about two fold compared to the one obtained at pH 8.9 in Tris buffer (0.187 min^{-1}). This could be correlated to the results obtained with pH studies in section 2.4.4.1, where the apparent imprinting efficiency I_{app} was increased from 2.62 at pH 8.9 to 5.92 at pH 9.4. This confirmed the trend obtained with the preliminary studies for the initial rates as a function of pH (section 2.4.4.1) performed at one single substrate concentration (1 mM). Therefore, it was decided that a more detail study on the effects on pH on the catalytic activity of the nanogels at more substrate concentrations was not necessary.

It is worth remembering that the range of substrate concentration used for the kinetics was much lower at pH 9.4 than the one at pH 8.9 since at pH 9.4 higher substrate concentrations provoked a curvature of the progression curve. Furthermore, the polymer concentration used at pH 9.4 was also lower (0.02 $mg.ml^{-1}$) than at pH 8.9 (0.01 $mg.ml^{-1}$) for similar reasons, an accurate reading of the initial rates. With the view of comparing the catalytic activity of the polymers for a same range of substrate concentrations, the values of the apparent rate constant defined by the ratio of the initial rates v_i with the active site concentration for each polymers were calculated from the curves for substrate concentration ranging from 100 µM to 800 µM, and the values are shown in **Table 12**.

Table 12: Values of k_{app} for MIPAS230 and NIPAS231 obtained at pH 8.9 (Tris buffer, 50 mM) and pH 9.4 (carbonate buffer, 50 mM) at polymer concentration of 0.1 $mg.ml^{-1}$ and 0.02 $mg.ml^{-1}$ respectively rationalised with the active site concentration for both polymers. The values of v_i were corrected for background reaction.

[S] (mM)	k_{app}(MIPAS230) $\times 10^2$ pH 8.9 (Tris buffer) (min^{-1})	k_{app}(NIPAS231) $\times 10^2$ pH 8.9 (Tris buffer) (min^{-1})	k_{app}(MIPAS230) $\times 10^2$ pH 9.4 (carbonate buffer) (min^{-1})	k_{app}(NIPAS231) $\times 10^2$ pH 9.4 (carbonate buffer) (min^{-1})
0.10	0,06	0,03	0,63	0,30
0.20	0,13	0,07	1,6	0,60
0.30	0,20	0,10	2,7	0,41
0.40	0,26	0,13	3,3	0,71
0.50	0,33	0,16	3,9	1,0
0.60	0,39	0,19	4,5	1,3
0.70	0,46	0,23	5,2	1,6
0.80	0,52	0,26	5,8	1,9

The apparent rate constant values in **Table 12** clearly demonstrated that at pH 9.4 the catalytic activity of the polymers was much higher than at pH 8.9. The values of the rate constants at pH 9.4 were found to be around 10 fold the one at pH 8.9. These values correlated to the value of apparent rate constant k_{app}, which was found to be 8 times higher at 9.4 than at pH 8.9 in the preliminary studies in section 2.4.4.1.

The value of K_M for MIP AS230 at pH 9.4 was found to be lower than the one at pH 8.9. The value of K_M was decreased by 9 times from pH 8.90 to pH 9.4. This suggested a much higher affinity between the polymer matrix and the substrate molecule at pH 9.4. In other terms, in order to achieve half of the maximal velocity V_{max} (1.93×10^{-6} $M.min^{-1}$), a substrate concentration of 27.5 mM at pH 8.9 was required, while only a concentration of 3.08 mM was needed at pH 9.4 to achieve half of the maximum velocity, which was 6.75×10^{-7} $M.min^{-1}$. The catalytic efficiency, which is defined by the ratio k_{cat}/K_M, describes how often a substrate molecule bound to the nanogel matrix reacts to form a molecule of product. This value is often used to compare catalyst or enzyme effectiveness to transform substrate into product. This value was found to be 104 $M^{-1}.min^{-1}$ at pH 9.4 for the imprinted polymer MIP AS230, a value that was 15.5 times higher than the one obtained at pH 8.9 in section 2.4.3.4 (6.9

$M^{-1}.min^{-1}$). This indicated a significant improvement in the performance of the imprinted nanogels at pH 9.4.

It was interesting to compare the imprinting efficiency of the nanogels at both pH at several substrate concentrations. Since the non-imprinted nanogel kinetic data could not be fitted to the Michaelis-Menten model, the apparent imprinting factors I_{app} defined by the ratio of the apparent rate constant calculated previously between MIP AS230 and NIP AS231 for several substrate concentrations at pH 8.9 and pH 9.4 were calculated in order to compare the imprinting efficiency of the nanogels for both pH. The values of the apparent imprinting factors I_{app} for substrate concentrations ranging from 0.5 mM to 0.8 mM are presented in **Table 13**.

Table 13: Comparison of the values of the apparent imprinting factor I_{app} at pH 8.9 and at pH 9.4 for substrate concentration ranging from 0.5 mM to 0.8 mM.

[substrate] (mM)	I_{app} pH 8.9	I_{app} pH 9.4
0.5	2,0	3,9
0.6	2,0	3,5
0.7	2,0	3,2
0.8	2,0	3,1

Overall, the apparent imprinting factor I_{app} was found to be higher at pH 9.4 for the different substrate concentrations with an enhancement of around 1.75 fold. These results confirmed the results obtained in the preliminary studies in section 2.4.4.3 for the imprinted polymer, where an enhancement of around 2 fold was found between the apparent imprinting factor at pH 8.9 and the one at pH 9.4.

The kinetic parameters V_M and K_M obtained at pH 8.9 were obtained with a significant standard error of around 22% and 26% respectively for the imprinted polymer MIP AS230 and around 15% and 13% respectively for the non-imprinted polymer NIP AS231, while at pH 9.4 the standard errors was far lower around 5% for V_M and 7% for K_M for MIP AS230 and 7% for V_M and 3% for K_M for NIP AS231. The deprotonation of a higher number of pyridine moieties at pH 9.4 generating a greater number of active sites available could explain the higher catalytic activity and the better fitting to the Michaelis-Menten model for the imprinting polymer and the linear

regression for the non-imprinted polymer. The pK_a of pyridine incorporated inside the nanogels was found to be around 6.5 in the determination of active site number in section 2.3.

The value of K_M for MIP AS230 at pH 9.4 was found to be lower than the one at pH 8.9. The value of K_M was decreased by 9 times from pH 8.90 to pH 9.4. This suggested a much higher affinity between the polymer matrix and the substrate molecule at pH 9.4. This effect was previously reported on imprinted polymers for capillary electrochromatography application[182]. In this work, it was demonstrated an enhancement in the chiral recognition ability of the (S)-nanproxen imprinted polymers towards a racemic mixture of naproxen for a low pH around 2 - 3. This was explained by the fact that at this pH the monomer methylmethacrylic acid (MAA) was not dissociated into its ionic form. The pKa of the couple MAA-*co*-EGDMA is found to be around 9. This had for consequence an increase in the chiral recognition abilities of the imprinted polymer.

The work presented so far demonstrated that the molecular imprinting approach was successfully used for generating polymeric catalysts with enzyme-like activity for the Kemp elimination. The hydrogen bond interaction between template and functional monomer is sufficiently strong to provide a significant imprinting efficiency. The performance of the nanogels could be improved by tuning some experimental conditions such as pH and organic solvent content. In the second part of the project, the work concentrated on the evaluation of surfactant effect on the catalytic activity of the nanogels and on the variation of polymerisation parameters such as initiator content and template-monomer ratio and their effect on the nanogel performance.

2.2.5 Use of surfactant

The use of surface-active molecules, also called surfactants, to stabilise colloidal suspensions is well known and it is widely employed in various area of industrial

production. Stabilisation of colloidal dispersions is, for example of significant importance in the paint, petroleum, cosmetic, pharmaceutical and food industries[184-185]. Important economic waste was reported as the result of production of unstable foams or emulsions. This is why the physical and chemical properties of surfactants have attracted attention as it allows control of the stability of particle dispersions[186].

Surfactants molecules display characteristic chemical structures, which are composed of a molecular component that will have minor interactions with the surrounding environment (solvent or phase), called generally lyophobic group, and another part that will posses strong binding affinity with the media called lyophilic group. Since the vast majority of the scientific work is focusing on aqueous media and the interactions with a second phase, the term lyophilic is commonly replaced by hydrophilic and lyophobic by hydrophobic[187]. A scheme of a surfactant molecule is illustrated on **Figure 66**.

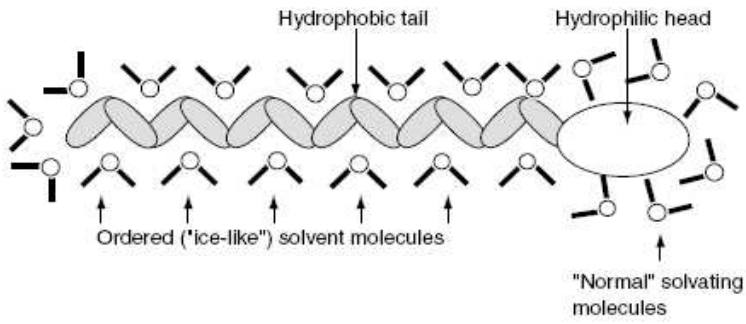

Figure 66: Basic molecular structure of surfactant molecule in water: a hydrophobic tail that will be "solvated" in the media with an ice-like structure of associated solvent molecules and a hydrophobic tail that will be solvated in the usual way[187].

In a general way, molecules that present chemical groups leading to surface-activity are referred as 'amphilphilic'. This means that they have affinity to two immiscible phases. In order to reduce their free energy, these types of molecules adsorb generally at the interfaces or undergo another type of distortion leading to the formation of micelles as described in **Figure 67**.

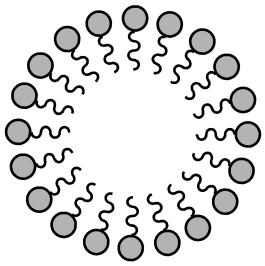

Figure 67: Example of micelle formation in an aqueous media where the hydrophilic head are oriented on the outside to interact with the solvent and the hydrophobic tail are confined to reduce the free energy of the system[187].

Within all the types of surface-active molecules, it exists a way of classifying surfactants. This can be done in many different ways but mainly depends on the areas of interests of the users. However, classifications according the physical chemical characteristics of the molecule can be established such as the degree of solubility in water or in oil, and the stability under harsh conditions. The simplest structural classification procedure is the one in which the nature of the solubilising group is the determining parameter. In aqueous systems that represent by far the largest number of applications, the hydrophobic group is generally a long alkene chain however surfactants with fluorinated or oxygenated hydrocarbon or siloxane chains are also being used. As a result, the classification of surfactants resides on the nature of the hydrophilic group. Thus, the four main classes are the following:

1. *Anionic*, where the hydrophilic group carries a negative charge. Examples include, carboxyl (CO_3^-, M^+), sulfonate (RSO_3^-, M^+), or sulphate ($ROSO_3^-$, M^+)

2. *Cationic*, where the hydrophilic group carries a positive charge such as quaternary ammonium halide (R_4N^+, X^-)

3. *Nonionic*, where the hydrophilic group does not carry any charge but display a very polar group such as polyoxyethylene, sugars or similar groups

4. *Amphoteric* (and zwitterionic), where the molecule possesses a negative and a positive charge on the principal chain

2.2.5.1 Colloidal stabilisation with surfactant

Colloids are found to be from different nature including proteins, inorganic or organic materials. In this thesis the focus was on the stabilisation of nanogels as lyophilic colloids (i.e polymer solutions) by the use of surfactant and its effect on their catalytic activity.

Interactions between surfactants and natural or synthetic polymers have generated a lot of interests within the scientific community. Numerous groups of research have investigated these interactions with varying degrees of success. Although the associations' surfactant-macromolecules are relatively well-established, a lack of knowledge and understanding remains especially for interactions at a molecular level. Surfactants are known to stabilise colloids by adsorbing onto their surface and forming one or a double layer around the particle as described in **Figure 68**. This gives rise to a protective layer that prevents aggregation between particles by steric hindrance.

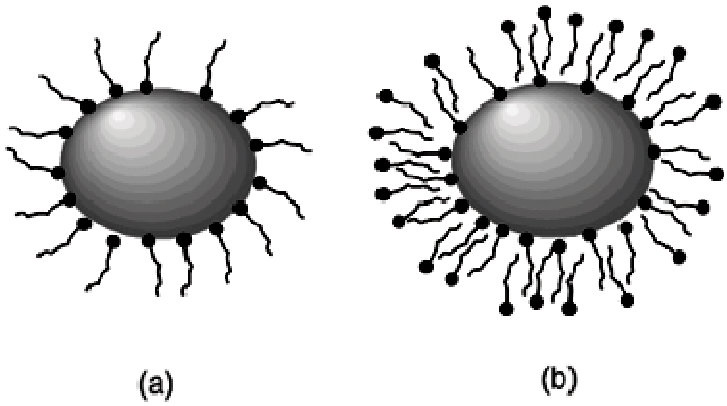

Figure 68: Basic scheme of surfactant adsorption onto the surface of a polymer particle forming (**a**) one layer or (**b**) a double layer around the particles.

The use of surfactants with molecularly imprinted polymers was reported for capillary electrochromatography (CEC) application[182]. In this work, the effect of employing three different types of surfactant, sodium dodecyl sulphate (SDS) (anionic surfactant), cetyltrimethylammonium bromide (CTAB) (cationic surfactant) and polyoxyethylene sorbitan monolaurate (Tween 20) (non-ionic surfactant) on the chiral

recognition of (S)-naproxen imprinted polymer was investigated. The chemical structures of these surfactants are shown in **Figure 69**.

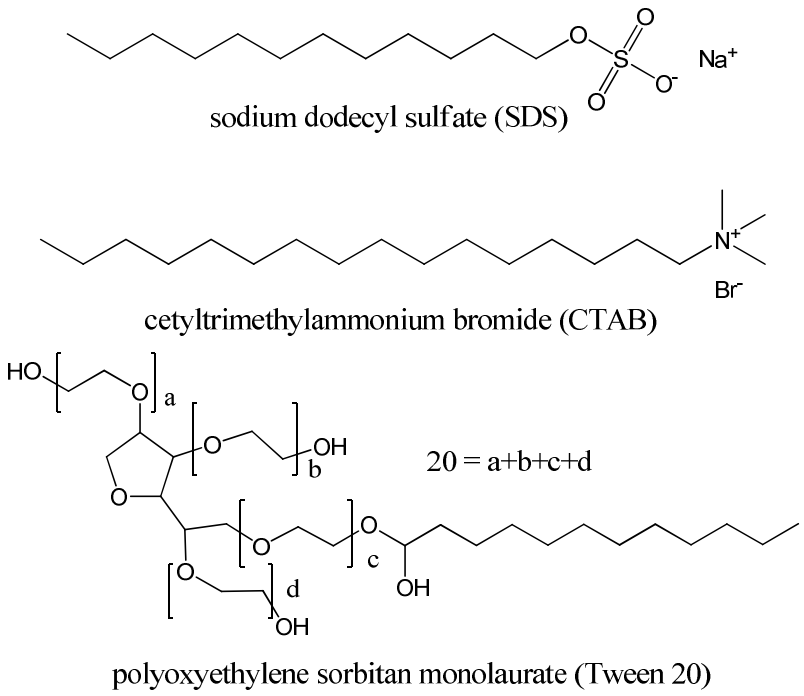

Figure 69: Chemical structures of SDS, anionic surfactant, of CTAB, cationic surfactant, and of Tween 20, non-ionic surfactant.

All these surfactants altered the chiral recognition of the polymers. Tween 20 and CTAB were found to improve the recognition efficiency, while SDS decreased it. This was explained by the fact the surfactant adsorbing onto the surface of the monoliths modified the surfaces of the particles. The anionic surfactant SDS weakened the binding affinity of the polymer matrix towards the substrate, acting as a competitor in the formation of the hydrogen bond.

2.2.5.2 Choice of surfactant

With regards to the ability of surfactant to prevent particle aggregation, it was interesting to study the effect of surface-active molecules on the catalytic activity of the imprinted nanogels. The Kemp elimination is a versatile reaction that requires aqueous medium and this allows surfactants to be used without having to change the reaction set-ups in order to investigate its effect on the polymer activity. The nature of

surfactants, anionic, cationic or non-ionic, could have different effects on the activity of the nanogels and this is why different types of surfactants were tested.

Preliminary kinetic studies were performed using different types of surfactants on the nanogels. Since SDS is widely used as surfactant in many applications, it was selected as anionic surfactant. Two different non-ionic surfactants were chosen as well, Tween 20 and Tween 80, to study the effect on the catalytic activity of the nanogels. These two surface-active molecules differ from each other by the length of the alkene chain. The use of cationic surfactants was discarded since the mechanistic route in the Kemp elimination involves proton removal favoured in presence of base. The presence of positive charges would interfere and prevent good interaction between the substrate molecule and the pyridine moieties from the nanogel matrix.

The effect of SDS, Tween 20 and Tween 80 were investigated at fixed substrate concentration 1 mM using the finalised conditions established in section 2.4.4.3 (10% acetonitrile in carbonate buffer 50 mM, pH 9.4). The reactions were carried out with MIP AS230 and NIP AS231 at a concentration of 0.02 $mg.ml^{-1}$, same polymer concentration as in the previous studies in section 2.4.4.3. In previous work on surfactant effect on polymeric materials the quantity of surfactant used ranges commonly between a minimum of 0.01 % in volume and 2% in volume depending of critical micellar concentration (cmc) of the surfactant[187]. Therefore, arbitrary concentrations of SDS and Tween 20 ranging from 0% to 1% in volume were used for the kinetic assays. These concentrations of surfactant were carefully chosen in order to be inferior to the cmc that is found to be around 8.3 mM for SDS and around 0.06 mM for Tween 20 in pure water[188]. The cmc of Tween 80 is found to be around 0.02% in volume in pure water. Therefore the range of concentration investigated for Tween 80 ranged from 0% to 0.02% in volume. However, several factors are known to influence the cmc of a surfactant such as organic solvent content, concentration of salt and temperature. It was reported in previous studies on surfactants an increase of cmc with increasing the content of acetonitrile in the media[189-190]. As a result, it could be assumed that the presence of 10% acetonitrile would increase the cmc of all surfactants.

The initial rates v_i for each surfactant and for both polymers, MIP AS230 and NIP AS231 were corrected for the uncatalysed reaction. The apparent rate constants were calculated using the active site concentration for the polymer concentration used and were plotted against the concentration of surfactant for SDS, Tween 20 and Tween 80, as shown in **Figure 70**.

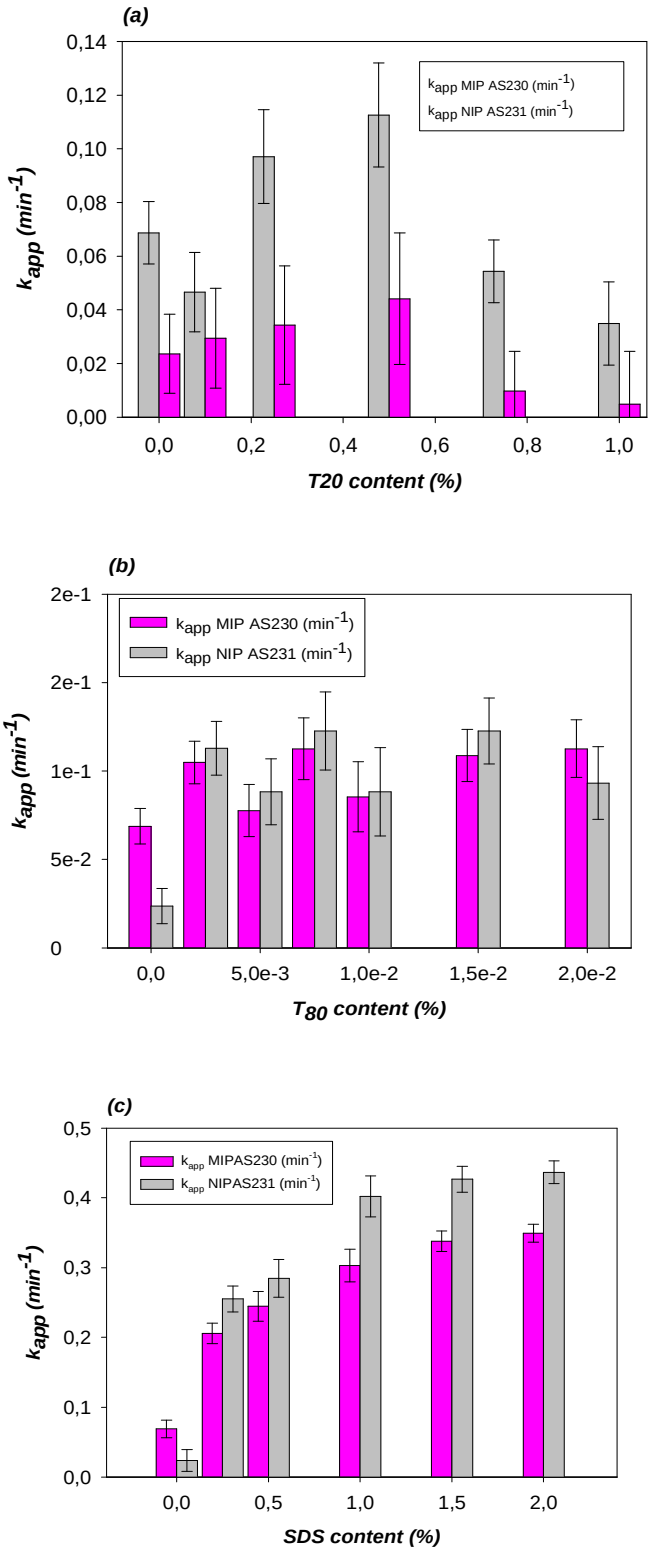

Figure 70: Apparent rate constants k_{app} of MIP AS230 and NIP AS231 in function of (**a**) Tween 20 content, (**b**) Tween 80 content and (**c**) SDS content in %. All reactions were performed in 10% acetonitrile in carbonate buffer (50 mM, pH 9.4) at 1 mM substrate concentration and the concentration of polymer used was 0.02 mg.ml^{-1}. All v_i values were corrected for background reaction.When the surfactant is used with the

nanogels the values of vi have been corrected for the background reaction under the same conditions.

The three surfactants appeared to have an effect on the catalytic activity of the nanogels as the values of v_i were varied with adding surfactant.

In the case of SDS, which is an anionic surfactant, an increase of the nanogel activity was observed. The values of the rate constant k_{app} for both imprinted and non-imprinted reached a plateau above a concentration of 0.75% with a maximum k_{app} of 0.44 min^{-1}. Barreiro-Iglesias et al. reported in previous studies on SDS adsorption onto microgel particles that this enthalpy-driven hydrophobic adsorption was only observed for a SDS concentration between 0.05% and 0.08%. For a concentration above 0.6%, there was no SDS adsorption observed. These concentrations were corresponding to the critical aggregation concentration (cac) of SDS, which is found to be much lower than the cmc (around 8.3 mM in pure water) and to the saturation binding concentration respectively[188]. The phenomenon of saturation binding concentration leading to micelle formation could explain the plateau observed after 0.75% of SDS in the media. It is worth noticing that the rate constants for both polymers were found to be much higher when SDS was added compared to the non-ionic surfactants. This could be explained by the fact that SDS is charged negatively and this favoured the proton transfer responsible of product formation during the Kemp elimination.

The imprinting efficiency of the imprinted nanogels seemed to be inhibited with the presence of SDS as the values of the rate constants for the non-imprinted polymers were found to be about the same as for the imprinted polymer. This could indicate that the surfactant adsorbing onto the surface of the nanogels prevented the access of the substrate molecule to the imprinted cavity. The presence of negative charges or of the counter ions Na^+ could prevent the interactions between the substrate benzisoxasole with the polymer matrix.

In the case of Tween 80, non-ionic surfactant a longer alkyl chain, the activity of the nanogels was slightly increased by adding surfactant, however the catalytic activity did not show any significant improvement above a Tween 80 concentration of 0.001%. The apparent rate constant k_{app} of the imprinted polymers ranged from 0.07 min^{-1}

without Tween 80 to 0.11 min^{-1} at 0.001% after which concentration a plateau was reached. An important standard error was observed as the concentration of Tween 80 increased, limiting the identification of the effect of Tween 80 on nanogel activity. The plateau observed at concentration of Tween 80 above 0.001% could be explained by a surfactant-surfactant interaction leading to the formation of micelles. The imprinting efficiency of the imprinted nanogels also seemed to be inhibited in presence of Tween 80. This could be for the same reasons as for SDS with regards to the fact that Tween 80 displays a long alky chain that when adsorbed onto the surface of the nanoparticles could prevent the acces of the substrate molecule to the imprinted cavity.

In the case of Tween 20, which is a non-ionic surfactant with a smaller alkyl chain than Tween 80, the activity of the nanogels was improved with adding surfactant and the maximum catalytic activity was found to be at a concentration of 0.5%. The apparent rate constants for the imprinted nanogels increased from 0.03 min^{-1} without surfactant to 0.11 min^{-1}. This increase could be related to the fact that nanogels are stabilised by the adsorption of Tween 20 molecules onto the surface of the particles via non-covalent hydrophobic-hydrophobic interactions[188]. As a consequence, more active sites are exposed to the substrate molecules and subsequently the velocity of the reaction is increased. The decrease of v_i for a concentration above 0.5% could be explained by micelle formation in the media that could prevent the access of the substrate molecule towards the active sites, as the concentration approached the cmc of Tween 20.

The imprinting efficiency of the nanogels was also altered in function of Tween 20 content The apparent imprinting factors I_{app}, which is the ratio between the initial rates of the imprinted nanogels and the non-imprinted nanogels were calculated for Tween 20. The maximum value $I_{app,max}$ was found to be 3.75 at a concentration of 0.5%. Tween 20 seemed to give the best results regarding the imprinting efficiency. Tween 20 appeared to favour the access of the substrate molecules towards the imprinted cavity while for the other surfactants appeared to decrease it.

Although the addition of SDS gave the highest apparent rate constants for both polymers, the use of this surfactant was not considered as it reduced dramatically the imprinting efficiency. With regard to an optimal imprinting efficiency, it was decided to investigate the effect of Tween 20 by determining a full kinetic profile of the nanogels in presence of this surfactant. Tween 20 demonstrated an enhanced catalytic activity for both polymers that was found to be maximal for a content of 0.5% at fixed substrate concentration (1 mM). Thus, the catalytic activity and efficiency of the nanogels was studied at 0.5% of Tween 20 in 10% acetonitrile and carbonate buffer (50 mM, pH 9.4).

2.2.5.3 Effect of surfactant on the active site concentration

Prior the determination of the kinetic parameters in the presence of 0.5% of Tween 20, it was important to investigate the effect of adding Tween 20 to the concentration of active sites. This would allow a good comparison between the rate constant of the Kemp elimination catalysed by the nanogels with and without surfactant. A similar protocol of back-titration of pyridine residues inside the polymers, which was established in section 2.3, was used. The surfactant Tween 20 (130 µl) was added at a concentration of 0.5% in volume to the polymer solution before titration. After gentle stirring, the latter is titrated using a NaOH solution of 1.5×10^{-3} M. The titration curves of the polymers MIP AS230 and NIP AS231 in presence of Tween 20 and without Tween 20 are shown in **Figure 71**.

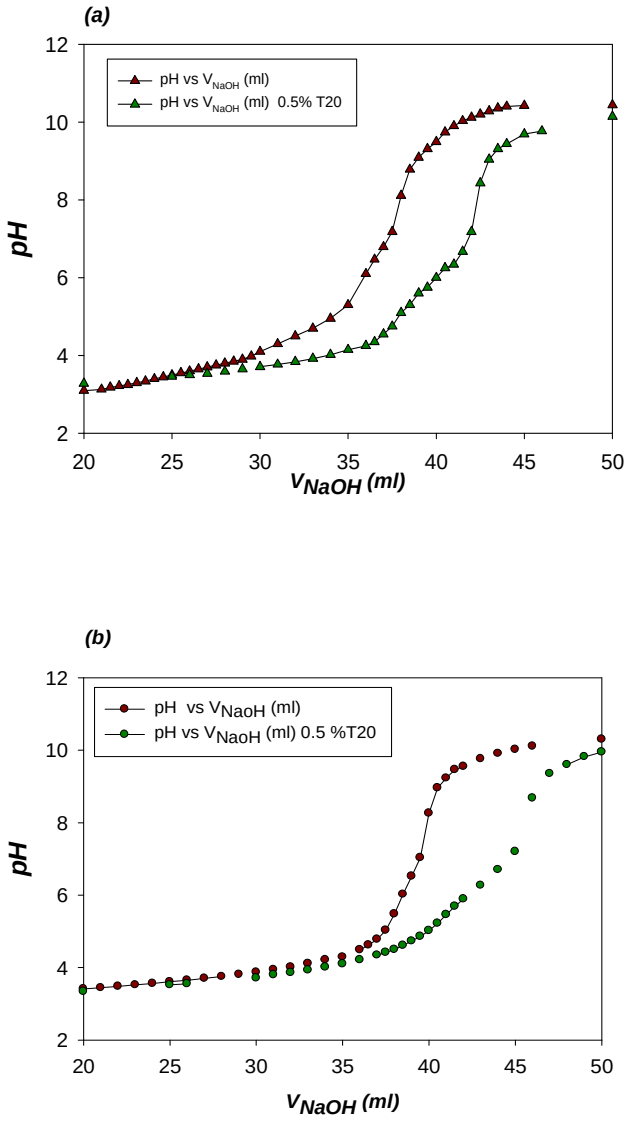

Figure 71: Back-titration curves of a 1 mg.ml^{-1} solution (a) MIP AS230 (▲) in presence of 0.5% of Tween 20 and (▲) without Tween 20 and (b) (●)in presence of 0.5% of Tween 20 and (●) without Tween 20 using NaOH solution at 1.5×10^{-3} M.

In both cases, MIP AS230 and NIP AS231, two equivalent points were observed. In presence of surfactant, the position of the equivalent points appeared to move slightly up toward higher volumes of NaOH. The determination of pyridine concentration was carried out by calculating the different of volume between the first and the second equivalent point. The concentrations of active sites for both polymers are summarised in **Table 14**.

Table 14: Values of pyridine concentrations, $n_{Pyr,Exp}$, obtained after titration of imprinted polymers MIP AS230 and non-imprinted polymers NIP AS231 with Tween 20 (0.5% in volume) and without Tween 20, concentrations of functional monomer n_{Pyr}, 4-vinylpyridine, added in the pre-polymerisation mixtures, and percentages A_N of active pyridine incorporated inside the nanogel matrix

	*Concentration of 4-vinylpyridine n_{Pyr} (µmol/mg)	Concentration of pyridine moieties $n_{Pyr,Exp}$ after titrations (µmol/mg)	A_N (%)
MIP AS230 with Tween 20 (0.5%)	1.10	0.28	24.4
MIP AS230	1.10	0.24	22.0
NIP AS231 with Tween 20 (0.5%)	1.10	0.42	36.0
NIP AS231	1.10	0.19	17.0

*The values were calculated following **Eq 11** and corresponded to the maximum quantity of pyridine residues available in the mass of dry nanogels used to generate the polymer solution of 1 $mg.ml^{-1}$ for the titration**.**

The values of the active site concentrations of both polymers with 0.5% in volume of Tween 20 were found to be higher than without surfactant. The presence of surfactant in the mixture appeared to have increased the amount of active pyridine residues available inside the polymer matrix. This evidence supported the hypothesis that Tween 20 stabilised nanogel suspensions, preventing aggregation between particles. As a result, more active sites were exposed to the substrate molecule and this explained the higher initial rates in presence of surfactant.

The knowledge of the active site concentration with 0.5% Tween 20 in buffer would allow the determination of the rate constant k_{cat} of the reaction in the presence of surfactant. This would also allow the verification of whether the use of surfactant increased the catalytic activity by stabilisation of the colloidal suspension or by improving the binding properties between the substrate molecule and the nanogels. The next step was then to establish a full kinetic profile of the imprinted and non-imprinted nanogels in the presence of 0.5% Tween 20.

2.2.5.4 Effect of surfactant on the nanogel catalytic activity

In order to allow a reliable comparison between the kinetic profiles of the polymers, the same conditions as in section 2.4.4.3 were applied: 10% of acetonitrile in carbonate buffer (50 mM) at pH 9.4. A carbonate buffer solution at a concentration of 50 mM was prepared adding 0.5% in volume of Tween 20 and then was allowed to stir for few minutes. Stock solutions of polymers MIP AS230 and NIP AS231 at 2 $mg.ml^{-1}$ were prepared in a mixture of 50% of acetonitrile in carbonate buffer at pH 9.4 containing 0.5% in volume of Tween 20. A stock solution of benzisoxazole (substrate) was prepared at 10 mM in acetonitrile. The initial rates were calculated and corrected for the background reaction. The kinetic profiles obtained with and without surfactant (section 2.4.4.3) are shown in **Figure 72**.

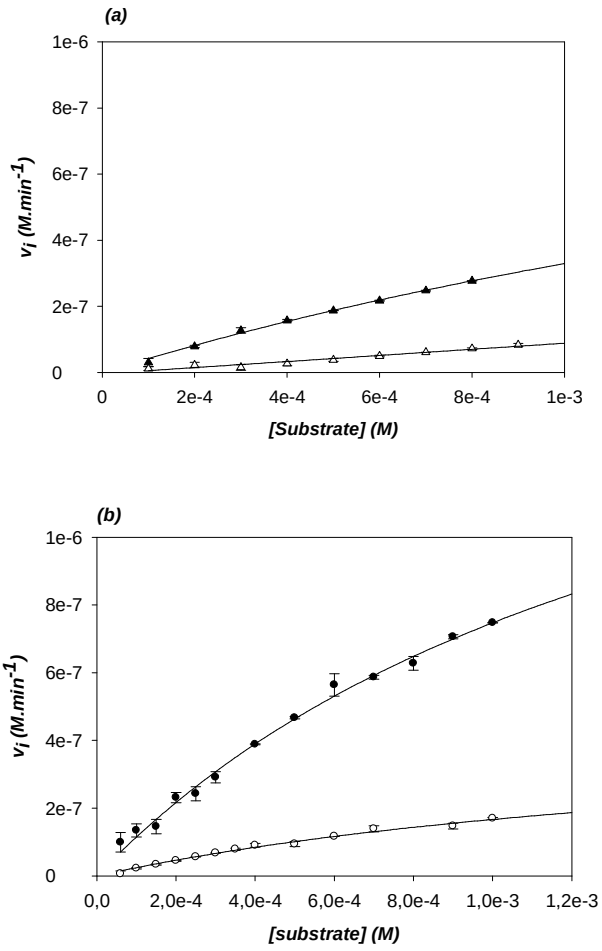

Figure 72: Initial rates v_i of (a) (▲) MIP AS230 and (Δ) NIP AS231 in function of substrate concentration in 10 % acetonitrile in carbonate buffer (50 mM, pH 9.4)

without Tween 20 and (b) MIP AS230 (●) and NIP AS231 (o) with 0.5% of Tween 20. The substrate concentration ranged from 0.1 mM to 1 mM. All the reactions were carried out using polymer concentration of 0.02 $mg.ml^{-1}$. All the values of v_i were corrected for background reactions.

For both polymers MIP AS230 and NIP AS231, the data could be fitted to a Michaelis-Menten saturation model. There were major differences between the kinetic profiles with and without surfactant. The first major difference was the fact that the data for the non-imprinted polymer in presence of 0.5 % Tween 20 could be fitted to a Michaelis-Menten saturation curve while the data obtained without surfactant could not be fitted to the hyperbola. Furthermore, the catalytic activity of both nanogels appeared to much higher in presence of surfactant for both polymers.

The kinetic parameters V_{max} and K_M for MIP AS230 could be extrapolated from the plot using Sigma Plot 8.0 and they were found to be 1.93×10^{-6} (S.E. ± 8.11×10^{-8}) $M.min^{-1}$ and 1.58×10^{-3} (S.E. ± 1.08×10^{-4}) M respectively and 4.71×10^{-7} (S.E. ± 2.75×10^{-8}) $M.min^{-1}$ and 1.83×10^{-3} (S.E. ± 1.65×10^{-4}) M for NIP AS231. The value of V_M of MIP AS230 with 0.5% Tween 20 displayed an enhancement of around 1.5 fold compared to the one obtained without surfactant (1.35×10^{-6} (S.E. ± 6.72×10^{-7}) $M.min^{-1}$). This was consistent with the preliminary data observed at one single substrate concentration (1 mM) with increasing the concentration of Tween 20 (section 2.4.5.2) where the rate constant of MIP AS230 with 0.5 % Tween 20 (0.11 min^{-1}) was 1.8 times higher that without surfactant (0.06 min^{-1}).

The values of active site concentration for both polymers were determined in the previous sections and were found to be 0.28 $\mu mol.mg^{-1}$ for MIP AS230 and 0.42 $\mu mol.mg^{-1}$ for NIP AS231. The rate constant of the reaction could be then calculated and was found to be 0.357 min^{-1} for MIP AS230 and 0.059 min^{-1} for NIP AS231. These values are gathered in **Table 15** and compared to the one obtained in section 2.4.4.3 without surfactant.

Table 15: Values of initial rates v_i, active site concentration, apparent rate constant, Michaelis-Menten constant K_M, and imprinting factor for MIP AS230 and NIPAS231 at 0.7 mM of substrate concentration with 0.5% of Tween 20 and without Tween 20. The kinetic parameters were obtained after fitting the data in a Michaelis-Menten model using SigmaPlot 8.0.

Polymers	Surfactant	V_{MAX} ($M.min^{-1}$)	[active sites] [$\mu mol.mg^{-1}$]	K_M [M]	k_{cat} [min^{-1}]	k_{cat}/K_M
MIP AS230	NO	1.35×10^{-6}	0.24	3.08×10^{-3}	0.320	104
MIP AS230	YES	1.93×10^{-6}	0.28	1.58×10^{-3}	0.357	226
*NIP AS231	NO	-	0.19	-	-	-
NIP AS231	YES	4.71×10^{-7}	0.42	1.83×10^{-3}	0.059	32

*The data obtained for NIP AS231 in 10% acetonitrile in carbonate buffer (50 mM, pH 9.4) could not be fitted into a Michaelis-Menten saturation model but into a linear fitting.

As it can be seen, the catalytic activity of the polymers, characterised by the rate constant k_{cat} of the reaction, was not significantly increased by the addition of surfactant. The increase of the initial rates v_i was mainly due to an increase of active site concentration as a result of the stabilising effect of the surfactant on the colloidal suspension.

Nevertheless, it could be noticed a significant change in the value of K_M, the Michaelis-Menten constant, from 3.08×10^{-3} M to 1.58×10^{-3} M. This constant is a good indication of the binding affinity of the catalyst towards the substrate molecule. A low value of K_M implies a strong interaction between the substrate and the polymer matrix. The fact that the value of K_M decreased when Tween 20 was added to the media, suggests that the presence of surfactant improved the binding affinity of the nanogel matrix towards the substrate molecule. This enhancement of binding affinity could be similar to the one reported by Schweitz et al., where the chiral recognition abilities of imprinted polymers for capillary electrochromatography (CEC) were improved by addition of Tween 20 in the media[190]. This phenomenon, in this paper, was explained by considering Tween 20 absorbing onto the polymer and modifying its binding

properties. As a result of this surface modification the affinity between the polymer particles and the substrate was enhanced.

As a consequence of a lower K_M in presence of Tween 20, the catalytic efficiency of the nanogels, which is defined by the ratio of the rate constant k_{cat} of the reaction and K_M, was found to be much higher (226 $min^{-1}.M^{-1}$) than the one obtained without surfactant (104 $min^{-1}.M^{-1}$). This parameter is of great interest as it describes how often a substrate molecule bound to the nanogel matrix reacts to form product. This value is often used to compare catalyst or enzyme effectiveness to transform substrate into product. The presence of surfactant appeared to have improved the catalytic efficiency of the polymer particles.

Since the data for the non-imprinted nanogels NIP AS231 without Tween 20 could not be fitted to the Michaelis-Menten saturation model using Sigma plot 8.0 for the range of substrate concentration used for the kinetics, it was impossible to compare the imprinting factor I defined by $k_{cat}(MIP)/k_{cat}(NIP)$. Instead the apparent imprinting factor I_{app}, using the ratio of the initial rate at a fixed substrate concentration (0.7 mM) was employed. The values were gathered in **Table 16**.

Table 16: Values of initial rates v_i, active site concentration, apparent rate constant, Michaelis-Menten constant K_M, and imprinting factor for MIP AS230 and NIPAS231 at 0.7 mM of substrate concentration with 0.5% of Tween 20 and without Tween 20.

Polymers	Surfactant	v_i [$M.min^{-1}$]	[active sites] [$\mu mol.mg^{-1}$]	K_M [M]	k'_{app} [min^{-1}]	$k'_{app,MIP}/k'_{app,NIP}$
MIP AS230	NO	2.48×10^{-7}	0.24	3.08×10^{-3}	0.059	3.1
MIP AS230	YES	5.87×10^{-7}	0.28	1.58×10^{-3}	0.109	6.4
NIP AS231	NO	6.11×10^{-8}	0.19	-	0.017	-
NIP AS231	YES	1.39×10^{-7}	0.42	1.83×10^{-3}	0.019	-

The apparent imprinting factor was found to be higher in presence of Tween 20 than without surfactant. In fact the value was double in presence of Tween 20 (I_{app} 6.4) compared to that without Tween 20 (I_{app} 3.1). The presence of surfactant appeared to increase catalytic efficiency with a 2 fold enhancement. This also confirmed the preliminary results obtained at a single substrate concentration (1 mM) with varying the concentration of Tween 20 in section 2.4.5.2, where approximatively 2 fold enhancement in the catalytic activity and efficiency was observed.

Overall, the presence of surfactant improved the catalytic and imprinting efficiency of the nanogels. This was notably characterised by a drop by half of the value of the Michaelis-Menten constant K_M for both polymers. Nevertheless, it was necessary to verify if the saturation observed in the kinetic profile of the polymers was due to the saturation of the active sites as a true enzyme mimic or due to a mass transfer and diffusion phenomenon. This is usually carried out by verifying the linear relationship between the initial velocities and the concentration of catalyst, as discussed in the next section.

2.2.5.5 Relationship between initial rates v_i and polymer concentration

Chemical transformation of molecules can occur in a wide variety of systems, manmade or natural[191]. The rate and effectiveness of these chemical reactions are governed by the availability of the reagents and catalysts. As the transformation progresses, the initial concentration of reagents is depleted and these holes in concentration distribution created are almost always filled up by some process of diffusion. Thus the speed of the reaction is dependent on the relative competition between the reactivity and the diffusion capability of the reagents or catalysts in the relevant part of the system or mass transfer that is characterised by the transport of atoms or molecules from high concentrations towards the low concentrations. The observed rate of chemical reactions is generally the rate of the '*slowest*' or '*rate-determining*' step. Diffusion controlled reactions are reactions that occur so quickly that the reaction rate becomes the rate of transport of the reagents in the medium.

Reactions where activated complexes form relatively easily and product formation occurs very rapidly are more likely to be limited by diffusion control. This phenomenon was observed in reaction where enzymes were supported onto large surfaces[192]. A schematic representation of enzyme mechanism of action is shown in **Figure 73**.

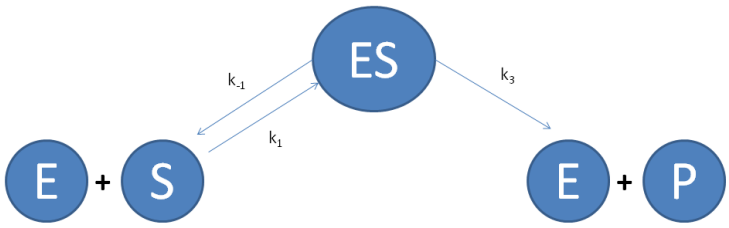

Figure 73: Schematic representation of enzyme E mechanism of action towards a substrate molecule S to give product P, where k_1 and k_{-1} are the rate constant of binding and dissociation of the enzyme - substrate complex respectively and k_3 is the rate constant of product formation.

In the scheme displayed on **Figure 73**, if product formation occurs very quickly and therefore the value of k_3 becomes much higher than the value of k_{-1}, the rate constant of the complex dissociation, the reaction would become diffusion limited and the rate of the reaction would become the rate of complex dissociation that depends on the concentration of both substrate and catalysts.

When investigating the catalytic activity of enzyme-mimics, it is essential to identify the contribution or action of the catalyst and, if any, the effect of other phenomena that might lead to saturation in the kinetic profile such as diffusion and mass transfer. Diffusion and mass transfer could be the cause of a rate decrease and the saturation observed could entirely be the results of these phenomena. In order to eliminate this hypothesis, it is important to study the relationship between the initial velocities of the reactions and the concentration of polymers. If a saturation curve is obtained for the plot of the initial rates as function of nanogel concentration at fixed substrate concentration, this would suggest that at high concentration of nanogel the reaction becomes diffusion controlled. This would also imply that the saturation curve observed for the plot of the initial rates as function of substrate concentration at fixed nanogel concentration was the result of diffusion control.

These experiments were performed at lower and higher concentrations of polymer used for the kinetic assays first without Tween 20. Initial rates v_i were calculated from the slopes of the product absorbance versus time with a polymer concentration ranging from 0.01 mg.ml^{-1} and 0.08 mg.ml^{-1} and at a fixed substrate concentration of 1 mM. This substrate concentration was selected since the curvature in the kinetic profile with the polymers started at 0.5 mM as described in section 2.4.4.3 without Tween 20. The initial rates were corrected for background reaction and plotted against the concentration is shown in **Figure 74**.

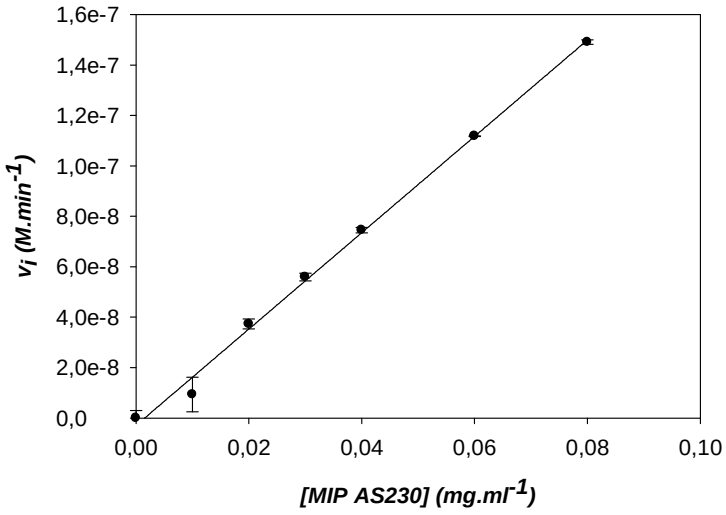

Figure 74: Plot of the initial rates v_i versus MIP AS230 concentration ranging from 0.01 mg.ml^{-1} to 0.08 mg.ml^{-1}. All the reactions were performed inside the spectrophometric cuvette in 10% of acetonitrile in carbonate buffer (50 mM, pH 9.4). The initial rates were corrected for background reaction.

A linear relationship was observed between the initial velocities and MIP AS230 concentration and the slope was found to be $1.91\times10^{-6} \pm 5.06\times10^{-8}$ M.min^{-1}.mg.ml^{-1} with a value of R^2 of 0.9963. No sign of saturation was noticed even at high polymer concentration. This suggested that there was no phenomenon of diffusion or mass transfer in this range of polymer concentration.

The same experiment was repeated in the presence of 0.5% in volume of Tween 20. A stock solution of MIP AS230 at a concentration of 2 mg.ml^{-1} was prepared in 50% of acetonitrile in carbonate buffer (50 mM, pH 9.4, 0.5% in volume of Tween 20). Initial rates v_i were calculated from the slopes of the product absorbance versus

time with a polymer concentration ranging from 0.01 mg.ml^{-1} and 0.08 mg.ml^{-1} and at two substrate concentrations, 0.5 mM and 1 mM. These substrate concentrations were chosen since the curvature in the kinetic profile of MIP AS230 with 0.5% in volume of Tween 20 started at a substrate concentration of 0.4 mM and the dependence of v_i versus catalyst concentration needs to be linear throughout the substrate range analysed. The plot of the initial rates against the concentration is shown in **Figure 75**.

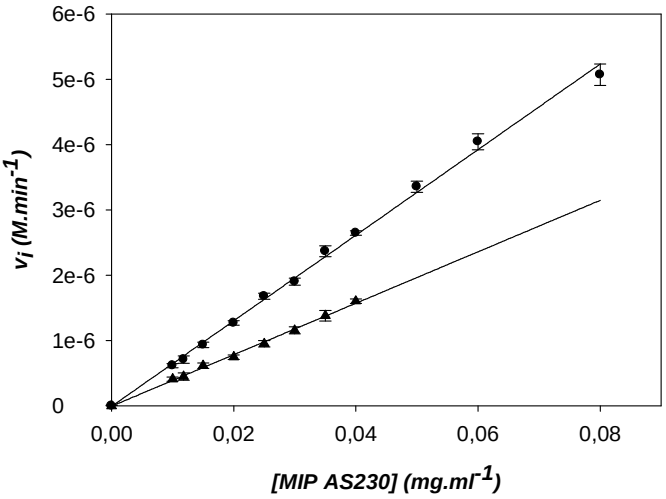

Figure 75: Plot of the initial rates v_i versus MIP AS230 concentration ranging from 0.01 mg.ml^{-1} to 0.08 mg.ml^{-1} at two substrate concentrations, 0.5 mM and 1mM. All the initial rates were corrected for background reaction. All the reactions were performed inside the spectrophotometric cuvette in 10% acetonitrile in carbonate buffer (50 mM, pH 9.4) with 0.5% in volume of Tween 20.

The data clearly indicated that in presence of Tween 20, no sign of deviation from the linear regression was observed for the two substrate concentrations in this range of polymer concentration. These data could be fitted to a linear regression with a slope of $6.56\times10^{-5}\pm0.10\times10^{-5}$ M.min^{-1}.mg.ml^{-1} for a substrate concentration of 1 mM and $3.94\times10^{-5}\pm0.034\times10^{-5}$ M.min^{-1}.mg.ml^{-1} for a substrate concentration of 0.5 mM with a low standard deviation and the value of R^2 for both curves was closed to 1 (0.9964 at 1 mM and 0.9975 at 0.5 mM). This indicated that the saturation observed for both kinetic profiles in presence of Tween 20 and without Tween 20 was the result of the saturation of active sites and not the outcomes of diffusion and mass transfer.

2.2.6 Influence of polymerisation parameters

The previous sections demonstrated the importance of carefully choosing external parameters for the nanogel kinetics such as pH, organic solvent content, or the use of surfactant, as they seemed to have a significant effect on the catalytic activity of the polymer particles. This effect was believed to be partially caused by a change in the morphology of the nanogel particles. Therefore, it appeared interesting to investigate the influence of polymerisation parameters such as initiator content, or functional monomer/template ratio on the activity of the nanogels. It was expected that these parameters would have a direct influence on the polymer morphology or concentration of active site and therefore would alter the activity of the nanoparticles. These studies are of great interest as the outcomes could possibly lead to the development of new strategic synthetic routes for catalysts with enhanced activity and specificity. The first parameter examined, discussed in the first part of this section was the content of initiator added in the pre-polymerisation mixture. In the second part of the section the alteration of the template/monomer ratio and their effect on the catalytic activity of the nanogels are discussed.

2.2.6.1 Initiator content

As described in section 2.1.4.3, the initiator selected for the synthesis of the imprinted and non-imprinted nanogels was AIBN. This initiator is widely used to start free radical polymerisation as it produces radicals that are stabilised due to the presence of two nitrile groups. Other initiators can be used to activate free radical polymerisation such as peroxides however they are found to be unstable and are known to be of an explosive nature. The AIBN molecule is found to decompose at a temperature of 60°C and its decomposition mechanism is shown on **Scheme 13**.

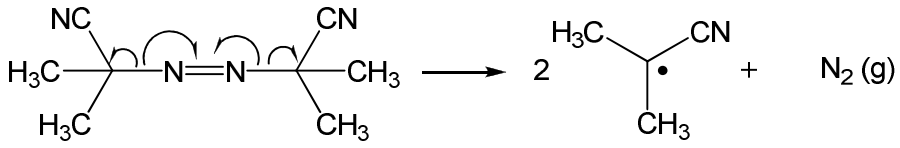

(44)

Scheme 13: Decomposition mechanism of the initiator AIBN (**44**) at 60°C

Initiators such as AIBN activate the polymerisation process by forming radicals that would be able to attack a monomer molecule present in the media. The resulting radical reacts with another monomer molecule allowing the growth of the polymer chain. The active polymer chain resulting from successive reactions between monomer molecules can eventually stop growing due to termination phenomena, which are characterised by the reaction between two radicals together forming an inactive molecule. This termination process cannot be controlled unless another type of polymerisation technique is used called living radical polymerisation. For the generation of cross-linked polymers, the polymerisation process is similar using monomers with higher functionalities or monomers with several insaturations called cross-linkers as described in **Figure 76**.

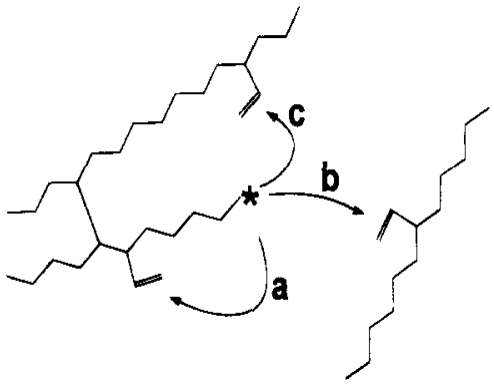

Figure 76: Cross-linking process between molecules with several insaturations by a) cyclisation, b) intermolecular cross-linking and c) intramolecular cross-linking.

The amount of initiator introduced in the pre-polymerisation mixture has a direct effect on the amount of radicals present in the media that would be able to react with a monomer molecule. In other terms, the number of active radical molecules or growing particles generated is closely related to the quantity of initiator introduced in the pre-polymerisation mixture.

Sometimes, when using a high dilution radical polymerisation, as in this project, the yields observed after recovery of the polymers are found to be relatively low, less than 30%. This could be due to the low monomer concentration C_M that is required in order to generate micro/nanogels and to avoid macrogelation occurring. The amount

of initiator commonly employed with high dilution radical polymerisation is generally between 1% and 5% of the quantity of double bonds in the mixture. For the preparation of the imprinted and non-imprinted nanogels for the Kemp elimination, the amount of AIBN used was equal to 1% of the quantity of double bonds in the pre-polymerisation mixture. It was therefore interesting to investigate the effect of initiator on the catalytic activity of the nanogels.

2.2.6.2 Effect of initiator content on nanogel yield

It was decided to study the influence of an increase of initiator content on the polymerisation and imprinting process. Three sets of two polymers, imprinted and non-imprinted polymers, were prepared using the same protocol described in section 1.2.3 (C_M 0.5% in mass and 80% of cross-linker) with initiator content equals to 1%, 2% and 3% of the quantity of double bonds in the pre-polymerisation mixture. Dry nanogels were recovered after the standard workup and the yields are presented in **Table 17**.

Table 17: Yields of imprinted and non-imprinted nanogels prepared with different AIBN contents

Nanogel preparations	Imprinted	AIBN (%)	Polymer mass (mg)	Yields (%)
MIP AS230	Yes	1	238	34
NIP AS231	No	1	148	21
MIP AS232	Yes	2	386	54
NIP AS233	No	2	307	43
MIP AS234	Yes	3	390	54
NIP AS235	No	3	230	>35

An increase in material recovered was observed from 34% for MIP AS230 and 21% for NIP AS231 synthesised with 1% of AIBN, to 54% for MIP AS234 and 32% for NIP AS235 synthesised with 3% of AIBN. The determination of the yield of NIP AS235 could only be estimated due to problems occurred during the recovery of the nanogels after free-drying. A higher yield of imprinted nanogels compared to the non-imprinted was

observed for each preparation. This could be due to the presence of remaining template indole in the imprinted polymer although no meaningful quantity of indole could be detected by fluorescence after two days of dialysis as described in section 2.2 that eliminated this hypothesis. This could also indicate that the template had an effect on the polymerisation process but in absence of other data, the difference of yield cannot be justified. The physical characterisation of the polymers with different initiator contents are discussed in section 2.7.

2.2.6.3 Effect on the active site concentration

Prior to the characterisation of the catalytic activity of the nanogels prepared with different initiator contents, it was necessary to evaluate the number of active sites in order to determine accurately the rate constant for each set of polymer. Using the same protocol as in section 2.3.3, the concentration of pyridine residues inside the polymer matrix was determined by back titration. Dry nanogels were dissolved in a mixture of 30% of acetonitrile in distilled water at a concentration of 1 $mg.ml^{-1}$. To the latter solution, 25 ml of a solution of HCL (2×10^{-3} M) were added in order to reach an excess of HCl around 2.5 equivalents compared to the theoretical quantity of pyridine residues inside the nanogels. After gentle stirring, the latter was titrated using a NaOH solution of 1.5×10^{-3} M. The titration curve of MIP AS232 and MIP AS234 are shown in **Figure 77**. Similar curves were obtained for NIP AS233 and NIP AS235.

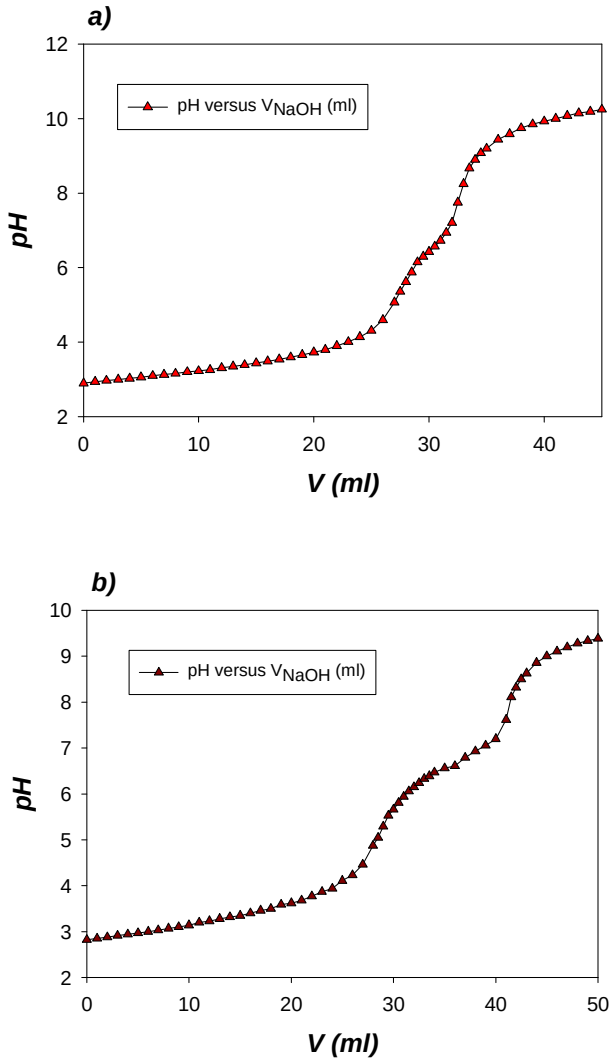

Figure 77: Titration curves of a) MIP AS232 and b) MIP AS234 using a solution of NaOH solution at a concentration of 1.5×10^{-3} M.

The determination of the concentration of pyridine moieties was performed using the difference of NaOH volume observed at the equivalent points. The values of active site concentration are gathered in **Table 18**.

Table 18: Values of pyridine concentrations $n_{Pyr,Exp}$ obtained after titration of imprinted polymers (MIP AS230, MIP AS232, MIP AS234) and non-imprinted polymers (NIP AS231, NIP AS233, NIP AS235), concentrations of functional monomer n_{Pyr}, 4-vinylpyridine, added in the pre-polymerisation mixtures, and percentages A_N of active pyridine incorporated inside the nanogel matrix

Polymers	AIBN (%)	*Quantity of 4-vinylpyridine n_{Pyr} (µmol/mg)	Quantity of pyridine moieties $n_{Pyr,Exp}$ after titrations (µmol/mg)	A_N (%)
MIP AS230	1	1.10	0.24	22
NIP AS231	1	1.10	0.19	17
MIP AS232	2	1.10	0.28	25
NIP AS233	2	1.10	0.26	23
MIP AS234	3	1.10	0.52	47
NIP AS235	3	1.10	0.64	58

*The values were calculated following **Eq 11** and corresponded to the maximum quantity of pyridine residues available in the mass of dry nanogels used to generate the polymer solution of 1 $mg.ml^{-1}$ for the titration**.**

A slight increase of the active site concentration was observed from at 1% of AIBN to at 3% of AIBN. The knowledge of the active site number at different initiator contents was of great interest as these values of active site numbers, when compared to the chemical yields of the nanogels allow an estimation of the pyridine incorporation yield as a function of initiator and a comparison of this incorporation between the different nanogels.

For the polymers MIP AS232 and NIP AS233 prepared with 2% of AIBN, similar values of active site number than the polymer synthesised with 1% of AIBN (MIP AS230 and NIP AS231) were obtained. These values, when compared with the chemical yields of for MIP AS230 (34%) and NIP AS231 (21%), and for MIP AS232 (54%) and NIP AS233 (43%), indicated that the incorporation of 4-vinylpyridine in the polymer matrix was less effective with 2% of AIBN than with 1% of AIBN. This also suggested that there was a higher content of cross-linker EGDMA in the polymers MIP AS232 and NIP AS233 than in the polymers MIP AS230 and NIP AS231. This low incorporation of 4-vinylpyridine could be explained by the difference in reactivity between the two

monomers used in the pre-polymerisation mixture, EGDMA and 4-vinylpyridine. The low value of the relative reactivity of these monomers (1.9) compared to other sustems such as styrene vinylacetate (100) that can be found in the literature[172] suggested a higher affinity of EGDMA monomers for EGDMA than for 4-vinylpyridine.

For the polymers MIP AS234 and NIP AS235, higher values of active site numbers were obtained around 47% of pyridine incorporated and available for MIP AS234 and around 58% for NIP AS235. These yields of active pyridine residues compared to the chemical yield of the nanogels suggested a higher incorporation of 4-vinylpyridine inside the polymer matrix than for MIP AS232 and NIP AS233 but similar to the 4-vinylpyridine incorporation in MIP AS230 and NIP AS231 (prepared with 1% of AIBN).

Although the amount of active pyridine residues inside the nanogels appeared to increase slightly with increasing initiator content, it was however difficult to draw any conclusion regarding the effect of initiator content on the yield of pyridine incorporation when compared to the chemical yield of nanogels.

2.2.6.4 Determination of the catalytic activity

Following the evaluation of the number of active sites, the determination of the kinetic parameters of the polymers was carried out. The reactions were performed in 10% acetonitrile and Tris buffer (50 mM) at a pH 8.9. These conditions were the preliminary conditions used in section 2.4.3.3 before tuning the pH and acetonitrile content in order to obtain an improved catalytic and imprinting efficiency. These conditions were chosen in order to accurately compare the effect of the initiator content on the catalytic activity of the nanogels with the effect of pH and acetonitrile content under the same conditions. The concentration of polymers used was the same as in section 2.4.3.3 such as 0.1 $mg.ml^{-1}$. Tween 20 was also used at a concentration of 0.5% in volume in order to identify accurately the effect of initiator content on the Michaelis-Menten constant K_M and on the binding affinity of the nanogels. In the presence of surfactant, the nanogels were found to exhibit enhanced binding

properties towards the substrate molecule at pH 9.4 resulting from a lower value of K_M. It would therefore be interesting to evaluate the effect of an increase of initiator content in presence of surfactant on K_M. The initial rates for the three sets of polymers were corrected for background reaction and plotted versus substrate concentration as shown in **Figure 78**.

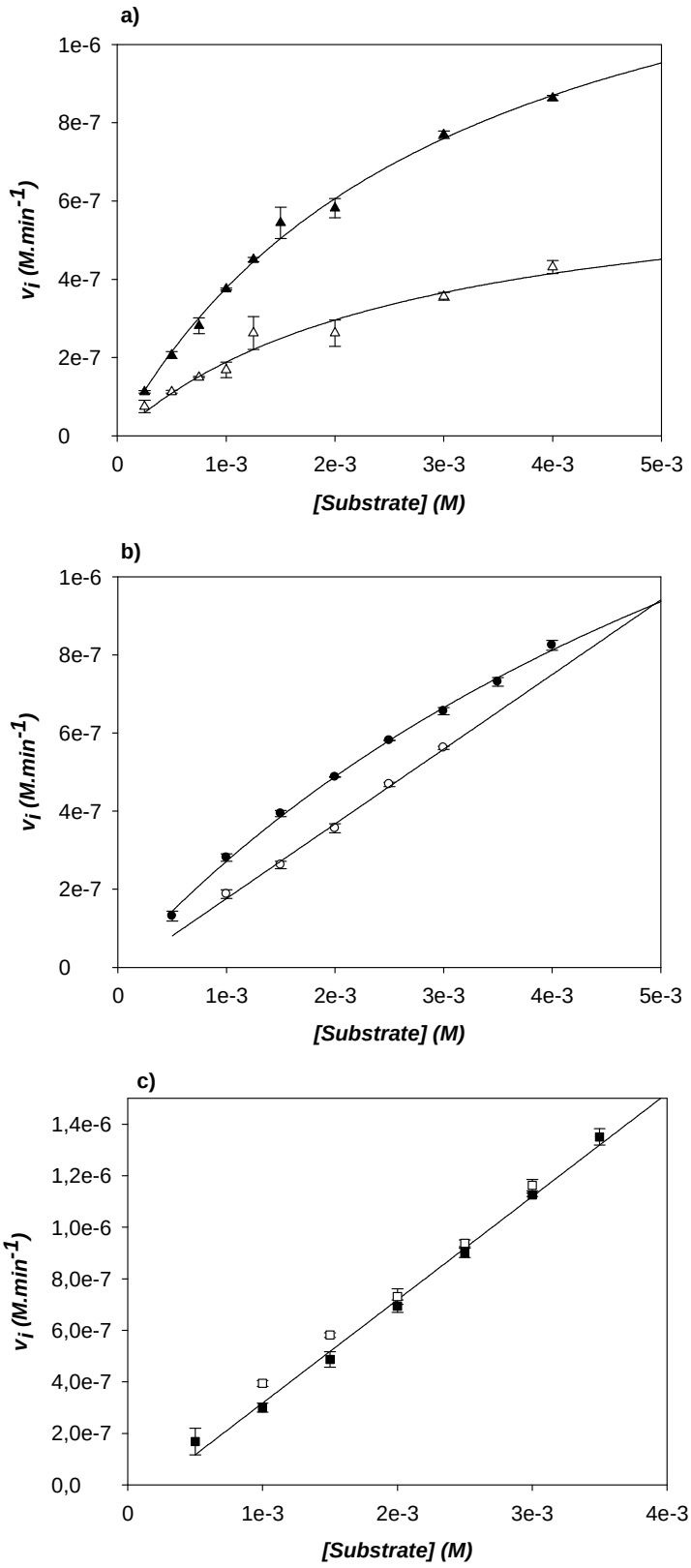

Figure 78: Initial rates v_i of a) (▲) MIP AS230 and (Δ) NIP AS231; b) (●) MIP AS232 and (o) NIP AS233; c) (■) MIP AS234 and (□) NIP AS235 in function of substrate concentration. All the reactions were performed in 10% acetonitrile in Tris buffer (pH 8.9, 50 mM) in presence of 0.5% of Tween 20 inside the spectrophotometric cell and

the polymer concentration used for the kinetic experiments was fixed at 0.1 $mg.ml^{-1}$. The range of substrate concentration used for the assay was from 0.5 mM to 4 mM.

As it could be noticed in **Figure 78**, the content of initiator had an effect on the kinetic profile of the nanogels. In the case of the nanogels MIP AS230 and NIP AS231, synthesised with 1% of AIBN, the data could be fitted into a Michelis-Menten saturation model using SigmaPlot 8.0. The kinetic parameters could be extrapolated and V_{max} and K_M were found to be 1.54×10^{-6} (S.E ± 5.22×10^{-8}) $M.min^{-1}$ and 3.08×10^{-3} (S.E ± 2.08×10^{-4}) M respectively for MIP AS230 and 6.92×10^{-7} (S.E ± 7.56×10^{-8}) $M.min^{-1}$ for V_{max} and 2.67×10^{-3} (S.E ± 4.64×10^{-4}) M for K_M for the non-imprinted nanogels NIP AS231.

In the case of the nanogels MIP AS232 and NIP AS233, synthesised with 2% of AIBN, only the data for the imprinted polymer MIP AS232 could be fitted into a hyperbola in agreement with the Michaelis-Menten model and the kinetic parameters were found to be V_{max} 2.41×10^{-6} (S.E ± 7.56×10^{-8}) $M.min^{-1}$ and K_M 7.88×10^{-3} (S.E ± 3.87×10^{-4}) M. For NIP AS233, synthesised with 2% of AIBN, the data could not be fitted into a hyperbola but into a linear regression with a slope of 1.91×10^{-4} (S.E ± 3.87×10^{-6}) min^{-1}.

For MIP AS234 and NIP AS235 synthesised with 3% of AIBN, the data did not show any difference between the imprinted nanogels and the non-imprinted nanogels. For both polymers, the data could not be fitted to a Michealis-Menten model but to a linear regression and the slope was found to be 4.0×10^{-4} (S.E ± 5.1×10^{-6}) min^{-1}.

Since NIP AS233, MIP AS234 and NIP AS235 did not display a saturation curve in the range of substrate concentration investigated, it was not possible to determine kinetic parameters such as the rate constant k_{cat} and catalytic efficiency k_{cat}/K_M for these polymers. In an effort to compare the nanogels with different AIBN content, the values of apparent rate constant k_{app} and the apparent imprinting factor were calculated for a single substrate concentration (2 mM) and the values are gathered in **Table 19**. This substrate concentration was selected since at this value, significant difference between imprinted and non-imprinted polymers was noticeable and saturation was observed for MIP AS230 and MIP AS232.

Table 19: Values of initial rates v_i, active site concentration, apparent rate constant, and apparent imprinting factor for MIP AS230 and NIP AS231, MIP AS232 and NIP AS233, MIP AS234 and NIP AS235, at 2 mM of substrate concentration with 0.5% of Tween 20 and without Tween 20.

Polymers	*AIBN content*	v_i [µM.min^{-1}]	active site number [µmol.mg^{-1}]	k'_{app} [min^{-1}]	$k'_{app,MIP}$/ $k'_{app,NIP}$
MIP AS230	1	0.61	0.24	2.95×10^{-2}	1.82
NIP AS231	1	0.30	0.19	1.62×10^{-2}	-
MIP AS232	2	0.49	0.28	0.85×10^{-2}	1.06
NIP AS233	2	0.37	0.26	0.80×10^{-2}	-
MIP AS234	3	0.70	0.52	1.21×10^{-2}	0.55
NIP AS235	3	0.73	0.64	2.19×10^{-2}	-

As suggested in **Table 19**, there was no clear trend in catalytic activity for the different nanogels as a function of initiator content. However, the values of the apparent rate constants obtained were in correlation with the pyridine incorporation of the different polymers. The low catalytic activity observed for MIP AS232 and NIP AS233 was in agreement with the low pyridine incorporation observed in section 2.5.1.2. It was interesting to notice the decrease of the apparent imprinting factor value from I_{app} 1.82 (1% of AIBN) to I_{app} 0.55 (3% of AIBN). By adding more initiator, the imprinting efficiency of the nanogels was found to be lower. This suggested that the increase of initiator gave rise to a higher number of non-specific binding sites, characterised by the decrease of the imprinting efficiency.

2.2.7 Variation of the template/monomer ratio

The investigation of the complex formation between the template molecule, indole, and the functional monomer, 4-vinylpyridine was described in section 2.2. It was demonstrated that the association of both molecules resulted from a non-covalent hydrogen bond between the nitrogen proton of indole and the nitrogen of the 4-vinylpyridine. These interactions were found to be stronger in non-polar solvents

such as chloroform, methylene chloride or 1,2-dicloroethane. Furthermore, the formation of the complex was governed by an equilibrium, with a constant found to be relatively low, around 1.76 M^{-1} in methylene chloride. The formation of specific cavities during the imprinting process is dependent on the interaction strength between the template molecule and the functional monomer. Tight and strong interactions would lead to the formation of well-defined three dimensional cavities, where the functional groups are in the desired place in order to catalyse the reaction. In the case of a non-covalent imprinting approach, it is often difficult to control the interactions and the resulting shape of the imprinted cavities and their homogeneity.

In an effort to further optimise the preparation of the imprinted nanogels with enhanced activity and imprinting efficiency, it was decided to alter the ratio template/monomer and to study the effect on the catalytic activity and on the imprinting factor. This ratio is indeed very important with respect to the number and the recognition properties of the active sites. The idea was to change the template/monomer ratio in a way to push the association of these molecules towards complex formation with the aim of creating more specific cavities. The first case investigated was the effect of synthesising the nanogels in presence of an excess of template and this id discussed in the first part of this section. The second part of the section describes the preparation of imprinted nanogels using an excess of functional monomer.

2.2.7.1 Excess of template

The first case was to investigate the kinetic profile and the subsequent catalytic activity of the nanogels synthesised in an excess of template. Two sets of imprinted and non-imprinted nanogels (MIP AS250, NIP AS251 and MIP AS252, NIP AS253) were prepared with 2 and 5 equivalents of indole compared to 4-vinylpyridine respectively. The polymers preparations are summarised in **Table 20**.

Table 20: Polymer preparations using a template excess: two sets of imprinted and non-imprinted nanogels were prepared with 2 equivalents of template (MIP AS250 and NIP AS251) and 5 equivalents of template (MIP AS252 and NIP AS253). NIP AS251 and NIP AS253 were prepared under the same conditions as MIP AS250 and MIP AS252.

Polymer preparations a)	Indole (mg)	4-VP[b)] (mg)	EGDMA (mg)	Solvent (ml)	AIBN (1%) (mg)	C_M (%)	Cross-linker content (%)
MIP AS250	160	71.8	544	98	10.1	0.5	80
NIP AS251	-	71.8	544	98	10.1	0.5	80
MIP AS252	400	71.8	544	98	10.1	0.5	80
NIP AS253	-	71.8	544	98	10.1	0.5	80

a) MIP: imprinted polymer; NIP: non-imprinted polymer; b) 4-VP: 4-vinylpyridine; The solvent used was 1,2-dichlorethane; polymerisation was carried out at 70°C for 4 days.

The nanogels were prepared using the standard protocol for high dilution radical polymerisation in 1,2-dichloroethane, similar to one used for all the previous preparations. Dry nanogels were recovered after isolation and the yields obtained are presented in **Table 21**.

Table 21: Yields obtained for the dried nanogels recovered after freeze-drying (C_M =0.5 wt.-% and 80% of cross-linker)

Nanogel preparations	**Polymer mass (mg)**	**Yields (%)**
MIP AS250	130	21
NIP AS251	139	23
MIP AS252	179	29
NIP AS253	174	28

The yields were similar to the one obtained for the nanogels prepared with 1 equivalent of template, which was around 34% for MIP AS230 and 21% for NIP AS231. This implied that the excess of the template molecule did not inhibit the polymerisation process. This phenomenon was observed in previous studies reported by Carboni *et al.* for the preparation of imprinted nanogels with catalytic activity for the cross-aldol reaction[3]. In this work, the imprinted approach was performed using a covalent complex template-monomer, which structure is shown on **Figure 79**.

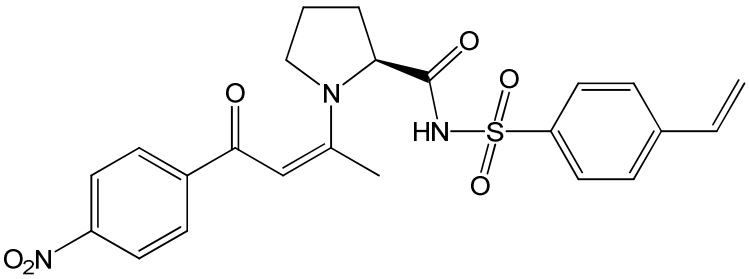

Figure 79: Structure of the covalent template/monomer complex.

The presence of this complex decreased dramatically the yield of nanogels recovered for the imprinted polymers (around 10%) compared to the non-imprinted and control nanogels (65% and 75% respectively). This was explained by the fact that the template/monomer complex was quenching the radicals giving rise to an inhibition of the polymerisation process.

In order to identify if the excess of template had an effect on the number of active sites, the determination of active site concentration was performed on MIP AS250, NIP AS251, MIP AS252 and NIP AS253. The determination of active site concentration of these new polymers was carried out following the same back-titration protocol established in section 2.3. The concentration of pyridine residues was calculated by the difference of the volume observed at the 2 equivalents points. The values are summarised in **Table 22**.

Table 22: Values of pyridine concentrations $n_{Pyr,Exp}$ obtained after titration of imprinted polymers (MIP AS230, MIP AS250, MIP AS252) and non-imprinted polymers (NIP AS231, NIP AS251, NIP AS253), concentrations of functional monomer n_{Pyr}, 4-vinylpyridine, added in the pre-polymerisation mixtures, and percentages A_N of active pyridine incorporated inside the nanogel matrix. The titrations were repeated three times and the standard deviation was calculated.

Polymers	Template equivalent	*Quantity of 4-vinylpyridine $n_{Pyr,0}$ ($\mu mol.mg^{-1}$)	Quantity of pyridine moieties $n_{Pyr,Exp}$ after titrations ($\mu mol.mg^{-1}$)	A_N (%)
MIP AS230	1	1.10	0.24 (S.E 15%)	22
NIP AS231	1	1.10	0.19 (S.E 15%)	17
MIP AS250	2	1.10	0.58 (S.E 20%)	53
NIP AS251	2	1.10	0.45 (S.E 22%)	41
MIP AS252	5	1.10	0.38 (S.E 13%)	35
NIP AS253	5	1.10	0.45(S.E 25%)	41

*The values were calculated following **Eq 11** and corresponded to the maximum quantity of pyridine residues available in the mass of dry nanogels used to generate the polymer solution of 1 $mg.ml^{-1}$ for the titration**.**

The number of active sites seemed to have slightly increased with adding an excess of template. This increase was not significant and could be due to minor experimental errors in the manual determination of the equivalent points. These results however gave an indication of the range of active site concentration and also allowed the determination of the kinetic parameters.

Following the evaluation of the number of active sites, the determination of the kinetic parameters of the polymers was carried out. All the reactions were performed in 10% acetonitrile in carbonate buffer (pH 9.4, 50 mM) in presence of 0.5% of Tween 20 and the polymer concentration used for the kinetic experiments was fixed at 0.02 $mg.ml^{-1}$. In this kinetic assay, the conditions used were the same as for the optimised systems in section 2.4.4.3. This would allow a good comparison of the imprinting efficiency observed for the nanogels prepared with an excess of template with the one of the nanogels synthesised without an excess of template under conditions when the imprinting efficiency was optimised and to its highest value I_{app} 6.4 (section 2.4.4.3).

The range of substrate concentration used for the assay was from 0.1 mM to 0.8 mM. The initial rates for the three sets of polymers the polymers were corrected for background reaction and plotted versus substrate concentration as shown in **Figure 80**.

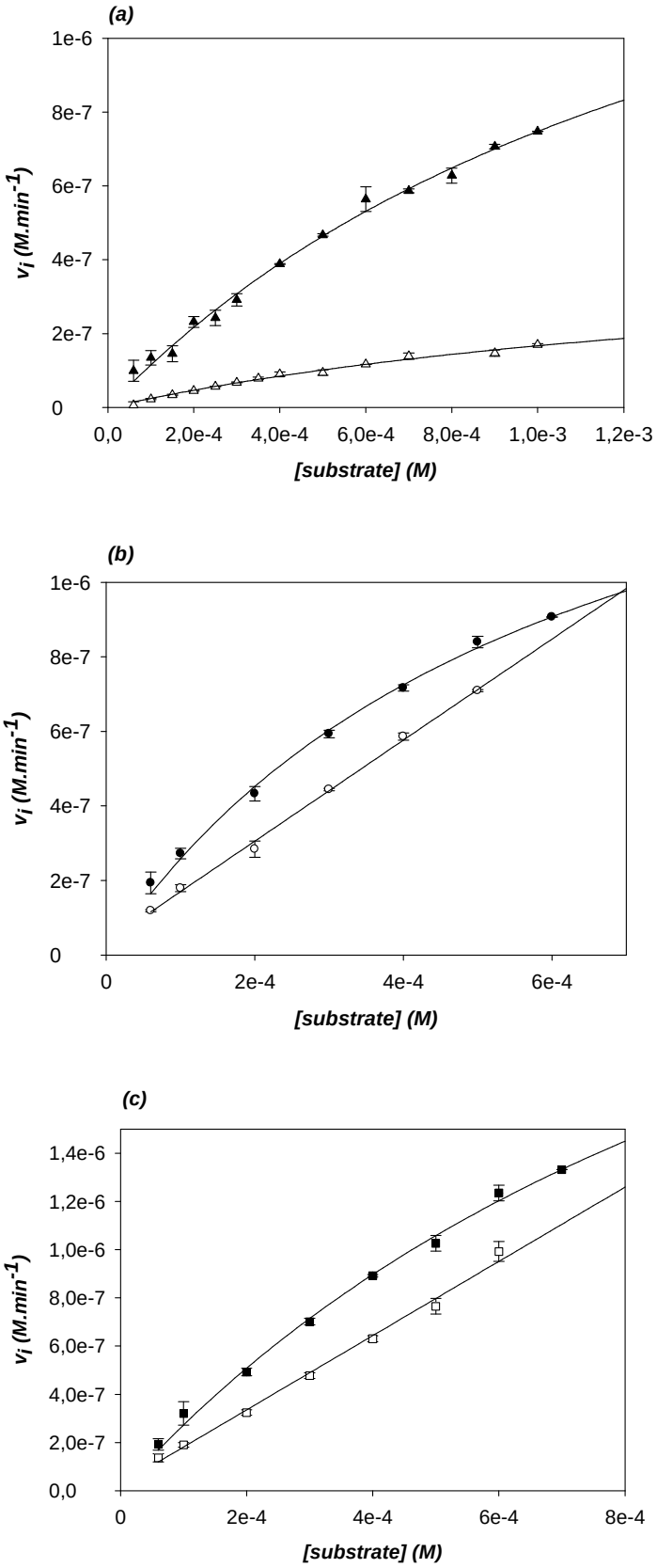

Figure 80: Initial rates v_i of a) (▲) MIP AS230 and (Δ) NIP AS231 (1 eq. of indole); b) (●) MIP AS250 and (o) NIP AS251 (2 eq of indole); c) (■) MIP AS252 and (□) NIP

AS253 (5 eq of indole) in function of substrate concentration in 10 % acetonitrile in carbonate buffer (50 mM, pH 9.4 with 0.5% of Tween 20). All the reactions were carried out using polymer concentration of 0.02 $mg.ml^{-1}$. All the values of v_i were corrected for background reactions.

For MIP AS250 and MIP AS252 synthesised with 2 and 5 equivalents of indole, the data could be fitted into a Michaelis-Menten saturation curve using SigmaPlot 8.0. In the case of the non-imprinted nanogels NIP AS251 and NIP AS253, the data could not be fitted to an hyperbola within the range of substrate concentration investigated but could be fitted to a linear regression. This result was also observed for NIP AS233 and AS235 (section 2.5.2), where the data for these two polymers could not be fitted to a hyperbola within the range of substrate concentration studied. The kinetic parameters of the three different sets of nanogels are summarised in **Table 23**.

Table 23: Kinetic parameters of the imprinted and non-imprinted nanogels synthesised with 1, 2 and 5 equivalents of template indole obtained after fitting the data using SigmaPlot 8.0.

Polymers	Template equivalents	V_{max} [$\mu M.min^{-1}$]	active site number [$\mu mol.mg^{-1}$]	K_M [mM]	k_{cat} [min^{-1}]
MIP AS230	1	1.93 ± 0.08	0.24 (S.E 15%)	1.58	0.359
NIP AS231	1	-	0.19 (S.E 15%)	-	-
MIP AS250	2	1.82 ± 0.03	0.58 (S.E 20%)	0.61	0.246
NIP AS251	2	-	0.45 (S.E 22%)	-	-
MIP AS252	5	3.79 ± 0.10	0.38 (S.E 13%)	1.27	0.341
NIP AS253	5	-	0.45(S.E 25%)	-	-

There was no significant improvement in the catalytic activity of the imprinted nanogels when adding more indole was added to polymerisation mixture. The rate constant k_{cat} obtained for MIP AS250 (0.246 min^{-1}) and MIP AS252 (0.341 min^{-1}) were not significantly different from the one obtained for MIP AS230 (0.359 min^{-1}). This was not a surprising result, as the addition of template molecules should not affect or have an influence on the active site concentration that is related to the incorporation of 4-vinylpyridine into the polymer matrix. The effect expected by adding an excess of template was the proportion of specific cavities, which was assumed to be higher

leading to an enhanced imprinting efficiency. An excess of indole would be expected to push the equilibrium towards the complex formation increasing the amount of specific cavities formed during the imprinting process. The polymers MIP AS250 and MIP AS252 did not show any enhancement in imprinting efficiency compared to the one exhibited by MIP AS230 (nanogels synthesised with one equivalent of template) but instead a decrease in the imprinting efficiency.

A similar template effect on the selectivity of imprinted polymers was reported in previous studies by Mosbach et al. for the generation of binding 'bulk' nicotine-imprinted polymers[193]. In this work, it was demonstrated that an excess of template during the polymerisation process was clearly unfavourable with regard to selectivity. This was explained by the formation of different complex states II and III that were favoured in excess of nicotine template over the complex IV, as shown in **Figure 81**. This led to the generation of cavities with high heterogeneity and therefore the decrease of the imprinting efficiency.

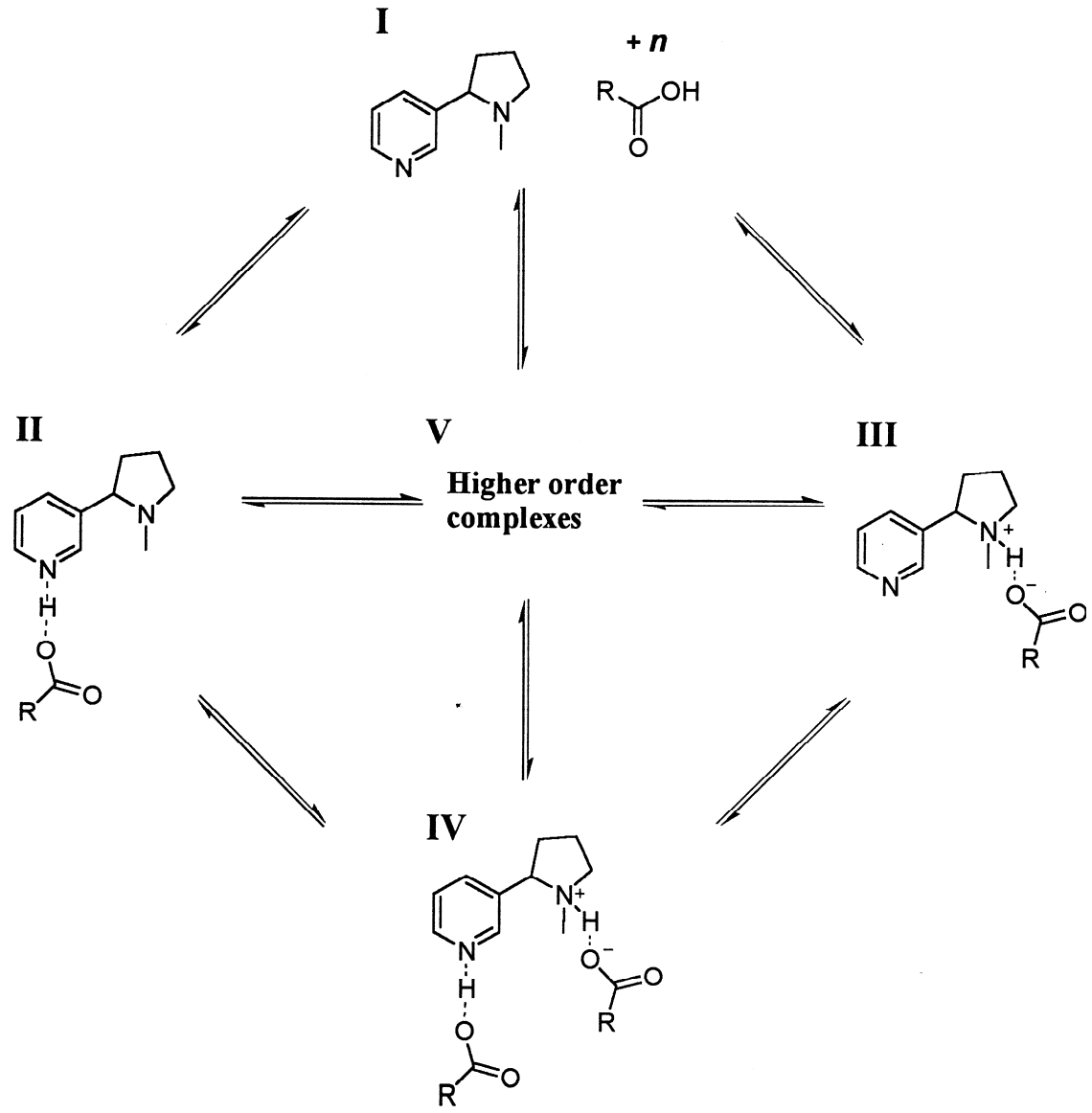

Figure 81: Hypothetical model of the template-monomer complex states in the pre-polymerisation mixture[193].

In the work presented in this thesis, the template indole displayed only one point of interaction through the proton attached to the nitrogen atom that limited the amount of other possible complexes between indole and 4-vinylpyridine. An excess of indole in the pre-polymerisation mixtures could however favour template-template association via intermolecular hydrogen bonding. The polymerisation solvent, 1,2-dichloroethane is known to be a non-polar solvent with a relatively high dielectric constant around 10.7. The nature of the solvent 1,2-dichloroethane could favour the

formation of hydrogen bonding between template molecules that could compete with template-monomer association decreasing the number of specific binding sites.

2.2.7.2 Excess of functional monomer

The effect of using an excess of functional monomer compared to the template indole was also investigated in this project. A similar attempt was done by Mosbach *et al.* with 'bulk' imprinted polymer with catalytic activity for the Kemp elimination although the results were very contradictive and non conclusive[107].

In this project, it was decided to study the effect of an excess of 4-vinylpyridine in the preparation of imprinted nanogels for the Kemp elimination. One set of imprinted and non-imprinted nanogels (MIP AS242 and NIP AS243) were prepared with 7 equivalents of 4-vinylpyridine compared to indole at a C_M of 0.5% and 80% of cross-linker, which resulted in having less template in the pre-polymerisation mixture, but with the same polymer composition. The standard protocol of high dilution radical polymerisation (see section 2.2.3) was applied. After 4 days of polymerisation, dry nanogels with a yield of 12% (60 mg) for MIP AS242 and of 11% (56.3 mg) for NIP AS243 were recovered. This yield was found to be relatively low compared to the one obtained for the polymers prepared with a template-monomer ratio of 1 (MIP AS230, 34% and NIP AS231, 21%). This could be explained by the higher content of 4-vinylpyridine (7 equivalents) in the pre-polymerisation mixture. This could suggest that 4-vinylpyridine has an inhibitory effect on the polymerisation.

In order to identify if the excess of 4-vinylpyridine had an effect on the number of active sites, the determination of active site concentration was performed on MIP AS242, NIP AS243. The determination of active site concentration of these new polymers was carried out following the same back-titration protocol established in section 2.3. The concentration of pyridine residues was calculated by the difference of the volume observed at the 2 equivalents points and compared to the quantity n_{Pyr} of 4-vinylpyridine added in the pre-polymerisation mixture that was found to be 1.16 $\mu mol.mg^{-1}$. The active site concentration obtained from the back-titration was found to

be 0.36 µmol.mg^{-1} (31% of pyridine incorporation) for MIP AS242 and 0.38 µmol.mg^{-1} (33% of pyridine incorporation) for NIP AS243. The active site concentration for MIP AS242 and NIP AS243 was found to be slightly higher than the one obtained for MIP AS230 (prepared with a template-monomer ratio of 1), found to be 0.24 µmol.mg^{-1} and 0.19 µmol.mg^{-1} for NIP AS231. This was expected since higher quantities of 4-vinylpyridine (7 equivalents) were added in the polymerisation mixture. However, the incorporation of pyridine remained quite low characterised by the fact that there was not a ratio of 7 between the active site concentration observed for both polymers MIP AS242 and NIP AS243 compared to the polymers MIP AS320 and NIP AS231.

The kinetic profile of the polymers MIP AS242 and NIP AS243 was determined. Similar conditions as the one used in the investigation of the effect of an excess of template in the previous section were applied. Tween 20 was used in carbonate buffer since the use of surfactant seemed to enhance the binding affinity of the polymer matrix as decribed in section 2.4.5.4. This would allow the study of the effect of an excess of monomer on the catalytic activity of MIP AS242 and NIP AS243 when the affinity of the polymer matrix towards the substrate is maximum. Stock solutions of imprinted nanogels and non-imprinted nanogels (MIP AS242, NIP AS243) were prepared at a concentration of 2 mg.ml^{-1} in a mixture of 50% acetonitrile in carbonate buffer (pH 9.4, 50 mM with 0.5% of Tween 20). The initial rates of the reactions with MIP AS242 and NIP AS243 as well as the background reaction were plotted versus substrate concentration as shown in **Figure 82**.

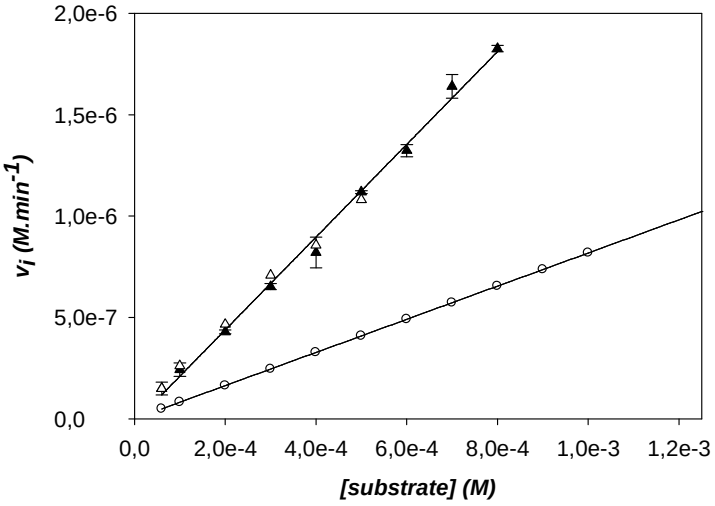

Figure 82: Initial rates v_i of a) (▲) MIP AS242 and (Δ) NIP AS243 (7 eq. of 4-vinylpyridine) non corrected for background reaction and (o) background reaction. All the reactions were carried out using polymer concentration of 0.02 mg.ml^{-1} in 10% acetonitrile in carbonate buffer (50 mM, pH 9.4, 0.5% in volume of Tween 20). The range of substrate concentrations used for the assay was from 0.1 mM to 0.8 mM.

As it can be seen in **Figure 82**, MIP AS242 and NIP AS243 demonstrated catalytic activity towards the Kemp elimination when compared to the background reaction. The value of the rate of the uncatalysed reaction k_{uncat} was found to be $8.18\times10^{-4} \pm 1.03\times10^{-21}$ min^{-1}. However, the data could not be fitted to a Michaelis-Menten saturation curve within the range of substrate concentration investigated but instead they could be fitted to a linear regression. The determination of active site concentration was not carried out as it was not relevant for the determination of the kinetic parameters. The apparent rate constant $k_{cat,app}$, could be indeed considered as the slope of plot of the initial rates versus substrate concentration and was found to be $2.19\times10^{-3} \pm 5.70\times10^{-5}$ min^{-1}; the value of R^2 was found to be 0.999. The activity of the nanogels AS242 and NIP AS243 was found to be higher than MIP AS230 and NIP AS231 (nanogels synthesised with only one equivalent of 4-vinylpyridine) under the same conditions. This increase of activity could be explained by the higher content of pyridine residues present in MIP AS242 and NIP AS243 resulting from the excess of monomer in the pre-polymerisation mixture. There was however no significant difference between the catalytic activity of MIP AS242 and that of NIP AS243. This suggested that there was a high number of non-specific binding sites. This could be

explained by the fact that adding a large excess of 4-vinylpyridine pushed the equilibrium towards the indole/4-vinylpyridine complex formation; however the remaining molecules of monomer could still be polymerised and incorporated inside the polymer matrix and allowing the generation of non-specific binding sites capable of catalysing the reaction. This was also in agreement with what was also reported by Andersson et al. in the preparation of binding 'bulk' nicotine-imprinted polymers[194], where an excess of methacrylic acid led to a decrease of the selectivity of the polymers.

2.2.8 Selectivity of the nanogel matrix

An important criterion in the development of enzyme mimics is the ability of these tailor-made catalysts to specifically recognise a substrate molecule and, in a similar way as enzymes, to form a complex and generate the product of the targeted reaction. One of the advantageous features of the molecular imprinting approach is the possibility of forming a conformational complement to a target molecule into a polymeric network, which allows the specific recognition of this molecule similarly to the "lock and key" complement[195]. This trait makes molecular imprinted polymers a very useful tool for binding applications such as organic scavengers, chromatography or enantiomeric separation, where good properties of molecular recognition are required.

Selectivity studies are commonly performed to evaluate the molecular recognition abilities of imprinted polymers. In the case of binding polymers, this type of characterisation allows to show the existence of a specific three dimensional cavity complementary in shape and size to the template molecule used to imprint the matrix with[104].

In the case of catalytic imprinted polymers this step is performed in order to give evidence that the catalytic activity of the imprinted polymers is mainly due to the imprinting effect and the presence of specific cavities in the polymer matrix. In the

group where this work was carried out, the specificity of imprinted microgels for the carbonate hydrolysis was tested by using a substrate analogue with a nitro group in *ortho* position instead of *para* position[2]. The results demonstrated a slight rate enhancement for both polymers but with no significant difference between the imprinted and non-imprinted microgels. Furthermore, the data could not be fitted into a Michealis-Menten saturation curve and were fitted instead by linear regression. Substrate selectivity was evaluated and the catalytic activity of the microgels for the '*para*' substrate demonstrated an 8.6-fold enhancement compared to the activity of the microgels for the '*ortho*' substrate. This provided the evidence that a three dimensional cavity with substrate selectivity was generated during the imprinting process and that the catalysis was occurring through these specific sites.

In our system, the selectivity of the imprinted nanogels was investigated in two different ways. The first approach was by studying the catalytic activity of the indole-imprinted nanogels with a different substrate molecule, 5-nitrobenzisoxasole, which differs from the first substrate by the presence of the nitro group in *para*. The second approach was to imprint the nanogel matrix with a different template, 5-nitroindole, and to study the catalytic activity of the imprinted nanogels towards 5-nitrobenzisolxasole and benzisoxasole. The structure of 5-nitroindole and 5-nitrobenzisoxasole are shown in **Figure 83**.

(47) **(48)**

Figure 83: Structure of new template molecule (**47**) 5-nitroindole and new substrate molecule (**48**) 5-nitrobenzisoxasole.

2.2.8.1 Catalytic activity of the imprinted nanogels with 5-nitrobenzisoxasole as substrate

The first approach used to study the selectivity of the polymer matrix was to investigate the catalytic activity of the indole-imprinted nanogels using 5-nitrobenzisoxasole as substrate. The presence of an electro-withdrawing group such as a nitro group in *para* to the oxygen atom was expected to enhance the rate of the reaction due to the change in electron environment and distribution[4]. The removal of the proton was found to be more favoured in presence of electro-withdrawing groups.

The pK_a of the product of the reaction, 5-nitro-1,2-cyanophenol, is found to be around 4.1. This chromophore displays a maximum absorbance at 381 nm. A reference line for 5-nitro-1,2-cyanophenol was carried out at pH 14 by cross-dilution using the same protocol as the one of the 1,2-cyanophenol in section 2.4.1.3 in order to determine the value of ε_{max} that would allow the access to the extension coefficient ε at a given pH as explained in section 2.4. The value of ε_{max} was found to be 15550 ± 210 $cm^{-1}.M^{-1}$ (S.E) and the value of R^2 was to be 0.9977.

For the non-substituted benzisoxasole, the value of pH, below which no meaningful quantity of product could not be detected was found to be 8.9 (cf section 2.4.3.2). The presence of the nitro group in the 5-nitrobenzisoxasole substrate was expected to change these conditions as the reaction rate would be enhanced by the presence of this electro-withdrawing group and as a result, significant quantity of product could be observed at lower concentration of hydroxide ions. The establishment of the most suitable experimental conditions was carried out with the same approach as the one employed in section 2.4.3.2, by studying the change in rate constant for the uncatalysed reaction as a function of pH. The optimal pH for investigating the activity of the nanogels with 5-nitrobenzisoxasole as substrate was found to be at pH 5.88 in BisTris buffer that is an effective buffer between pH 5.8 to pH 7.3. The value of the extinction coefficient at this pH was found to be 15555 ± 210 $cm^{-1}.M^{-1}$ (S.E) with a R^2 constant of 0.9977, value calculated from ε_{max} using **Eq 11**.

Preliminary studies performed with the nanogels at different polymer concentrations at pH 5.88, with a substrate concentration of 1 mM indicated that, with a polymer concentration of 0.1 $mg.ml^{-1}$, the initial velocity v_i could be accurately determined as no curvature was observed in the progression curve and was found to be linear under these conditions. A detailed study of the kinetic profile of the nanogels with 5-nitrobenzisoxasole and benzisoxasole at several substrate concentrations was not considered at this stage of the investigation, as preliminary studies at one single substrate concentration could give some insight into the selectivity of the nanogel matrix.

Two kinetic experiments were performed at a single substrate concentration (1 mM) using the nanogels MIP AS230 and NIP AS231 (0.1 $mg.ml^{-1}$) with benzisoxasole and 5-nitrobenzisoxazole in order to compare the activity of the polymers towards the two different substrates. The reactions were performed in 10% acetonitrile in Bis-Tris buffer (50 mM) at pH 5.88 for nitro-substituted substrate and in Tris buffer (50 mM) at pH 8.9 for the non-substituted substrate with and without surfactant Tween 20. The initial rates were corrected for background reaction and the results are shown in **Figure 84**.

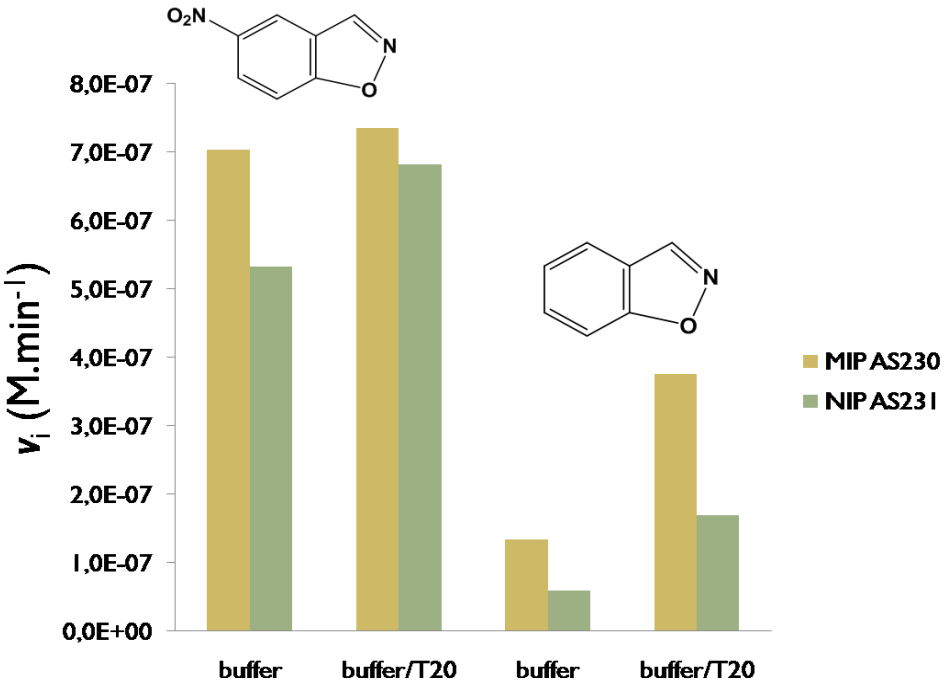

Figure 84: Initial rates of MIP AS230 and NIP AS231 (0.1 mg.ml^{-1}) with 5-nitrobenzisoxasole and benzisoxazole. The reactions were performed in 10% acetonitrile in Bis-Tris buffer (50 mM) at pH 5.88 for nitro-substituted substrate and in Tris buffer (50 mM) at pH 8.9 for the non-substituted substrate with and without surfactant Tween 20. The initial rates were corrected for background reaction.

The initial rates obtained with 5-nitrobenzisoxazole were found to be higher than with benzisoxasole substrate, as expected due to the presence of the electro-withdrawing group in *para* position of the oxygen atom that accelerated the reaction. The apparent imprinting factor I_{app}, defined in section 2.4.3 by the ratio between the apparent rate constants of the imprinted polymer over the apparent rate constant of the non-imprinted polymer, was compared for both substrates. These apparent rate constants were calculated using the active site concentration obtained in section 2.3, 0.24 µmol.mg^{-1} for MIP AS230 and 0.19 µmol.mg^{-1} for NIP AS231 without Tween 20 and 0.28 µmol.mg^{-1} for MIP AS230 and 0.42 µmol.mg^{-1} for NIP AS231 with 0.5% Tween 20. The results are summarised in **Table 24**.

Table 24: Apparent imprinting factors with the different substrates: 5-nitrobenzisoxasole and benzosixazole at fixed substrate concentration (1 mM).

Substrates	solvent	I_{app}
5-nitrobenzisoxasole	buffer	1.28
	Buffer/T20	1.05
benzisoxasole	buffer	2.05
	Buffer/T20	2.30

The values of the apparent imprinting factor around 2 observed with and without Tween 20 for the benzisoxazole demonstrated that the polymers MIP AS230 and NIP AS231 were selective in favour of the non-substituted substrate. The value of I_{app} obtained with 5-nitrobenzisoxasole around 1, indicated a very weak difference between the activity of the imprinted polymer and the one of the non-imprinted polymer. This implied that the catalysis of the reaction with the nitro-substituted substrate occurred via non-specific binding sites rather than inside the imprinted cavity and therefore this substrate could not access and/or enter the imprinted cavity probably due to the nitro group, which is relatively bulky. This also gave the evidence that three dimensional imprinted cavities were formed during the imprinting process and that they were selective to the substrate.

2.2.8.2 Catalytic activity of imprinted nanogels synthesised with 5-nitroindole

The second approach to investigate the selectivity of the imprinted nanogels was to imprint the polymer matrix with a molecule resembling to the 5-nitrobenzisoxasole. The best candidate in our system was 5-nitroindole. This molecule is structurally related to the previous template indole with the presence of the nitro group on the 5^{th} carbon of the aromatic group. Similarly to indole, this molecule displays only one single interaction point, limiting the formation of heterogeneous imprinted cavities. The pK_a of the nitrogen proton of 5-nitroindole is found to be around 14.75 in the same range as the one of indole (pK_a 16).

Before synthesising the nanogels, it was important to study if there was an interaction between 5-nitroindole and 4-vinylpyridine, the functional monomer. A non-

covalent hydrogen bonding between the nitrogen proton of the indole derivative and the nitrogen of 4-vinylpyridine was expected similarly to the one demonstrated in section 2.2 with the non-substituted indole. The interaction studies were carried out in a similar way using ^{1}H-NMR spectroscopy, studying the variation of chemical shift of the proton H_i', as specified in **Figure 85**.

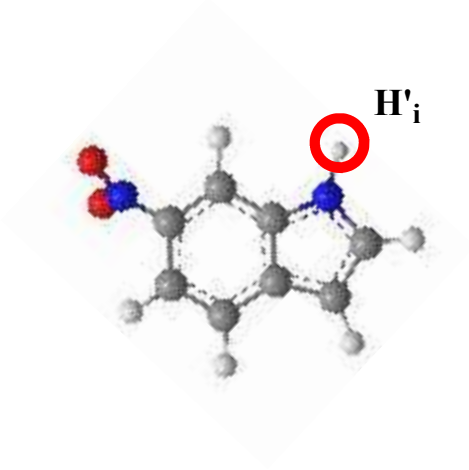

Figure 85: Structure of 5-nitroindole with the nitrogen proton H_i that is expected to form a hydrogen bon with the nitrogen atom of the 4-vinylpyridine.

A solution of 5-nitroindole was prepared at a concentration of 85.4 mM in CD_2Cl_2 and increasing equivalents of *d5*-pyridine ranging from 0.2 equivalent (1.71×10^{-2} M) to 7 equivalents (5.98×10^{-1} M) were added to the solution. The spectra of indole alone and for each equivalents of pyridine were recorded. The values of $\delta_{H'i}$ were collected and plotted against the concentration of *d5*-pyridine, as shown in **Figure 86**.

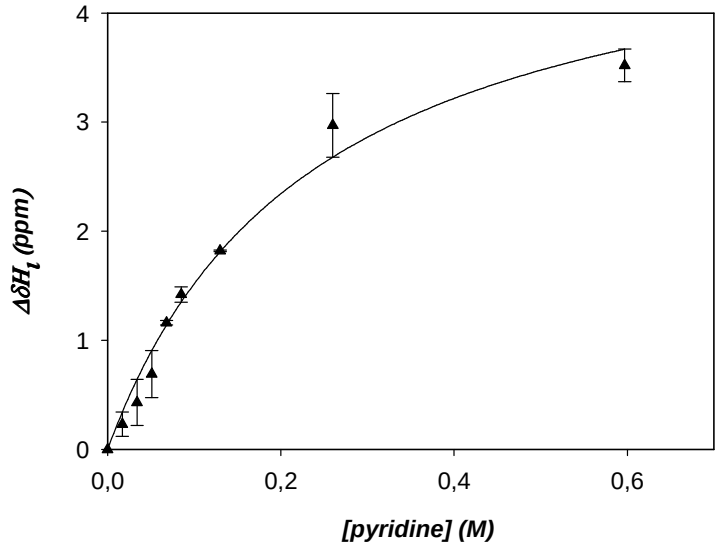

Figure 86: Plot of the variation of chemical shifts $\Delta\delta_{Hi}$ of the protons H_i, corrected from the value of the chemical shift of H_i of 5-nitroindole alone versus the concentration of *d5*-pyridine.

A variation of the chemical shift of H_i' from δ 8.76 to δ 12.3 was noticed, which confirmed the interaction via non-covalent hydrogen bond between 5-nitroindole and 4-vinylpyridine. The association constant K_{ass} was evaluated in the same way as in section 2.2 and was found to be around 4.20 M^{-1}. The interaction between 5-nitroindole and *d5*-pyridine was found to be slightly stronger than in the case of the non-substituted indole. This could be attributed to the presence of the nitro group that, as an electro with-drawing group, favoured the formation of a hydrogen bond through the nitrogen H_i in non-polar solvent. The interactions between 5-nitroindole and pyridine appeared to be stronger than in the case of indole. The interaction studies at high temperature (70°C) were therefore not considered, as it was demonstrated with indole template that the interactions with the *d5*-pyridine sustained at 70°C.

Thus, following the interaction studies, a set of imprinted and non-imprinted nanogels MIP AS238 and NIP AS239 were prepared with 5-nitroindole as template molecule, using the standard protocol of high dilution radical polymerisation established in section 2.3. Dry nanogels were recovered after 4 days of polymerisation with a yield of 40.2 % (179 mg) for MIP AS238 and of 37% (164.8 mg) for NIP AS239.

The determination of active site number was performed using the standard procedure of back-titration of pyridine residues established in section 2.3. The active site number obtained for MIP AS238 was found to be 0.20×10^{-6} µmol.mg^{-1} (18% of pyridine incorporation) and 0.18×10^{-6} µmol.mg^{-1} (16% of pyridine incorporation). These values were found to be within the range of active site concentrations obtained with previous polymers preparations (cf section 2.3).

The full kinetic profiles of 5-nitroindole-imprinted polymer MIP AS238 and the corresponding non-imprinted NIP AS239 were carried out with both substrates 5-nitrobenzisoxasole and benzisoxazole at several substrate concentrations. Stock solutions of imprinted nanogels and non-imprinted nanogels (MIP AS238, NIP AS239) were prepared at a concentration of 2 mg.ml^{-1} in a mixture of 50% acetonitrile in BisTris buffer (pH 5.88, 50 mM) for the kinetic studies with 5-nitrobenzisoxasole and in a mixture of 50% acetonitrile in carbonate buffer (50 mM, pH 9.40) for the kinetic studies with benzisoxasole. Stock solutions of both substrates were prepared at a concentration of 50 mM in acetonitrile. All the reactions were performed in 10% acetonitrile in carbonate buffer (pH 9.4, 50 mM) or Bis tris buffer (pH 5.88, 50 mM) depending on the substrate used, inside the spectrophotometric cell and the polymer concentration used for the kinetic experiments was fixed at 0.02 mg.ml^{-1}. The range of substrate concentration used for the assay was from 0.1 mM to 3 mM. The initial rates were corrected for background reaction for MIP AS242 and NIP AS243 and plotted versus substrate concentration as shown in **Figure 87**.

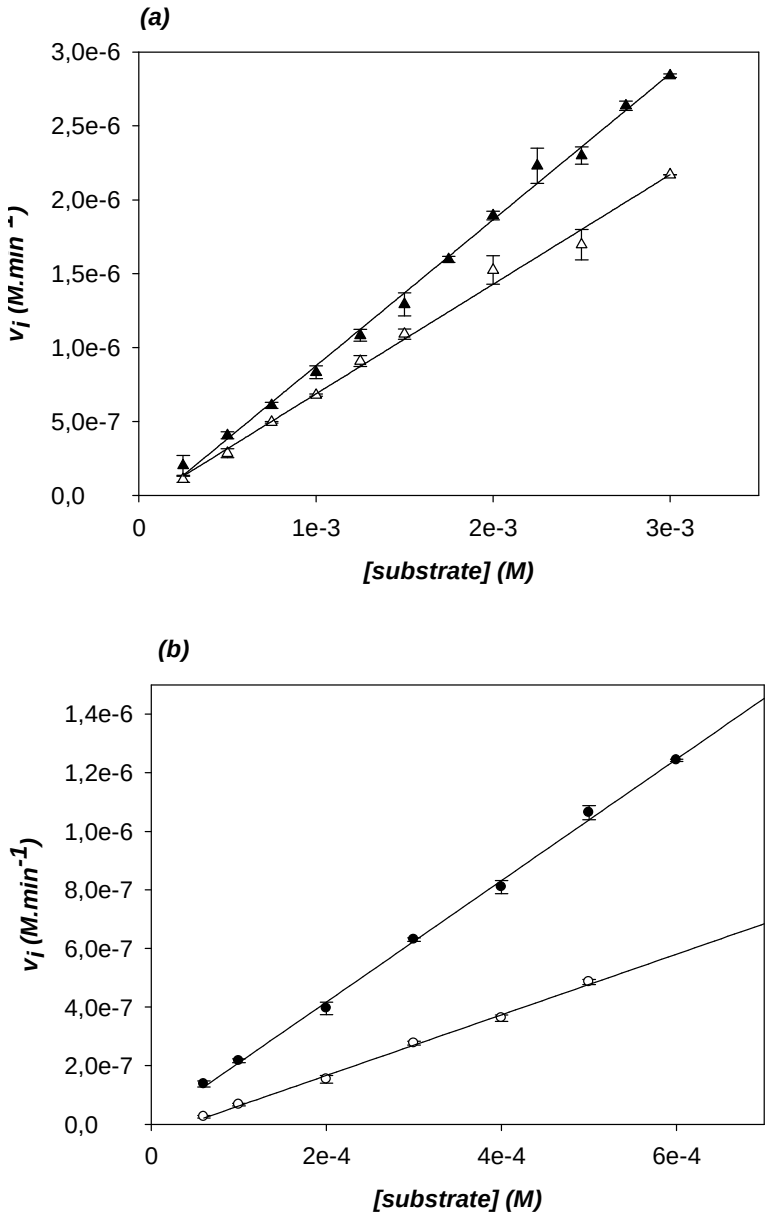

Figure 87: Initial rates v_i of a) (▲) MIP AS238 and (Δ) NIP AS239 (5-nitro-benzisoxazole) in 10% acetonitrile, Bis Tris buffer (50 mM, pH 5.88) for substrate concentration range from 0.5 mM to 3 mM; b) (●) MIP AS238 and (o) NIP AS239 (benzisoxazole) in 10 % acetonitrile in carbonate buffer (50 mM, pH 9.4) with substrate concentration range from 0.05 mM to 0.6 mM. All the reactions were carried out using polymer concentration of 0.02 $mg.ml^{-1}$. All the values of v_i were corrected for background reactions.

Both nanogels MIP AS238 and NIP AS239 demonstrated catalytic activity for the reaction with both substrates. In both cases, the data could not be fitted into a Michaelis-Menten saturation curve in the range of substrate concentration investigated, but instead they could be fitted to a linear regression. Thus, the apparent

rate constant of reaction k_{app}, defined by the ratio of the initial rate at one single substrate concentration over the active site concentration, was used to determine the apparent imprinting factor, which is defined by the ratio of k_{app} of MIP AS238 and k_{app} of NIP AS239. The substrate concentration selected to calculate the apparent rate constant was 3 mM, as at this value of substrate concentration the imprinting efficiency appeared to be high enough to be compared. The values of k_{app} and of the apparent imprinting factor were calculated and the values are summarised in **Table 25**.

Table 25: Kinetic parameters of the imprinted and non-imprinted nanogels (MIP AS238 and NIP AS239) synthesised with 5-nitroindole.

Substrates	Polymers	v_i [µM.min^{-1}]	Active site number [µmol.mg^{-1}]	$k_{app}\times10^2$ [min^{-1}]	$k_{app}MIP/k_{app}NIP$
5-benzisoxasole	MIP AS238	2.7	0.20	1.42	0.86
	NIP AS239	2.0	0.18	1.66	-
benzisoxasole	MIP AS238	0.80	0.20	0.42	1.4
	NIP AS239	0.37	0.18	0.30	-

The catalytic activity and the imprinting factor of the nanogels were found to be slightly higher for the reaction with the non-substituted benzisoxasole. The lower value of the imprinting factor of the nanogels towards 5-ntrobenzisoxasole indicated that the catalysis of the reaction occurred via non-specific binding sites located at the surface of the particles. The nitro-substituted molecule appeared to have difficulties to access and/or enter the imprinted cavities, characterised also by lower catalytic activity than for the other substrate. This was a surprising result considering that the polymer matrix was imprinted with 5-nitroindole. This could indicate that, even if the imprinted cavities were formed during the polymerisation process, they were still too small to fit the nitro-substituted substrate. A good alternative would be the investigation of the catalytic activity of the 5-nitroindole-imprinted polymer MIP AS238 and the corresponding non-imprinted polymer NIP AS239 with another substrate substituted with a less bulky and electro with-drawing group such as a methoxy group or substituted with a fluorine atom.

In the case of the reaction with the non-substituted substrate, benzisoxasole, a reasonable imprinting factor was found. The value of the imprinting factor was however half the value obtained for the indole-imprinted polymers MIP AS230 and NIP AS231 under the same conditions, where the apparent imprinting factor was found to be around 4. Thus, the nanogels MIP AS238 and NIP AS239 seemed to be more selective in favour to the benzisoxasole. This could be explained by the fact that this molecule is smaller than the nitro-substituted benzisoxasole and could therefore fit into the imprinted cavity. This was also a good indication of the presence of imprinted cavities in the polymer matrix of MIP AS238.

Overall, the imprinted nanogels demonstrated selectivity towards the nature of substrate used for the kinetics, characterised by a decrease of the imprinting efficiency for the reaction catalysis with the 5-nitrobenzisoxasole. The presence of imprinted cavities was proven by two different ways: the decrease of imprinting efficiency of the indole-imprinted nanogels with the nitro-substituted substrate and the catalytic activity with a relatively high imprinting factor of the 5-nitroindole-imprinted nanogels towards the substrate benzisoxasole.

POLYMER CHARACTERISATION

2.3 RESULTS AND DISCUSSION: POLYMER CHARACTERISATION

The tremendous growth witnessed over the past couple of decades in developing novel nanomaterials for innovative products and devices has been made possible with the development of improved methods of measurement, characterisation and manipulation[11]. To date, there are many characterisation tools available to study the morphology and behaviour of biological molecules or nanomaterials using different techniques. Scanning tunnelling spectroscopy provides important information on electronic structure and properties[7]. Computer-controlled scanning probe microscopy has become a useful tool for nanostructure manipulation in real time[196]. Nanomechanics carried out with atomic force microscopy (AFM) makes possible the study of single molecules making AFM a very useful technique for understanding folding and related problems in biological molecules[11].

The type of characterisation undertaken in this work was based on size and shape characterisation with the aim of understanding morphological changes of nanogel in response of external stimuli. For this purpose, the use of light scattering and electronic microscopy was envisaged. Another complex technique based on small angle neutron scattering (SANS) was used to complement the information obtained by the two latter techniques. The work carried out using the SANS technique was in collaboration with Dr. Zarbakhsh from Queen Mary University of London. The experiments were performed at ISIS Laboratories, Rutherford facilities, Didcot, UK.

The first part of this chapter is focussing on the size characterisation of the nanogels in response of external stimuli such as organic solvent content and presence of surfactant using mainly the zetasizer instruments and electron microscopy (T.E.M).

2.3.1 Size characterisation with Zetasizer instrument and electron microscopy

The first characterisation technique selected for the evaluation of the size of the nanogel particles was based on Dynamic Light Scattering (DLS) using the Zetasizer Nano ZS instrument[197]. The DLS technique also known as Photon Correlation Spectroscopy (PCS) gives access to the hydrodynamic radius of particles. This is achieved by measuring the Brownian motion of the particles and relating this motion to the size of the particles. In practice, this is achieved by illuminating the particles with a light source such as a laser and by analysing the fluctuations of intensity in the light scattered by the particles. Small particles (≤ 250 nm) scatter light in all directions when illuminated by a source of light with similar dimensions to the wavelength of light used. If, instead of one particle, there is a population of particles, the intensity of the light scattered will vary as a result of constructive or destructive interferences. As the particles in solution are not stationary but are in a state of constant motion, the light and dark fringes evolves over time by growing or diminishing leading to intensity fluctuations. A detector is kept at 90° to the sample position and the intensity is measured as a function of time. Given that the particles are moving randomly this leads to a broadening of the signal. The Zetasizer Nano ZS instrument measures the rate of these fluctuations of intensity and more precisely with the mean of a correlator (as described in **Figure 88**), the degree of similarity between two signals over a period of time τ (1 μs). An auto-correlation function G(τ)(a time shift version of the function) is defined as followed:

$$G(\tau) = G_0 e^{-DA\tau} \qquad \textbf{(Eq 31)}$$

Where D is the translational diffusion coefficient.

The measure of the fluctuation rate gives then good indication the size of the particles. The movement of particles is in fact correlated to the size, as small particles would move faster than big particles. The intensity of small particles will as a consequence fluctuate faster than in the case of big particles. The speed of fluctuation can be quantified by the translational diffusion coefficient (D) and its knowledge allows

the calculation of the hydrodynamic radius d(H) using the Stoke-Einstein equation, as specified in **Eq 32**.

$$d(H) = \frac{kT}{3\pi\eta D} \qquad \textbf{(Eq 32)}$$

Where k is the Boltzman constant, T the temperature in Kelvin, η the viscosity.

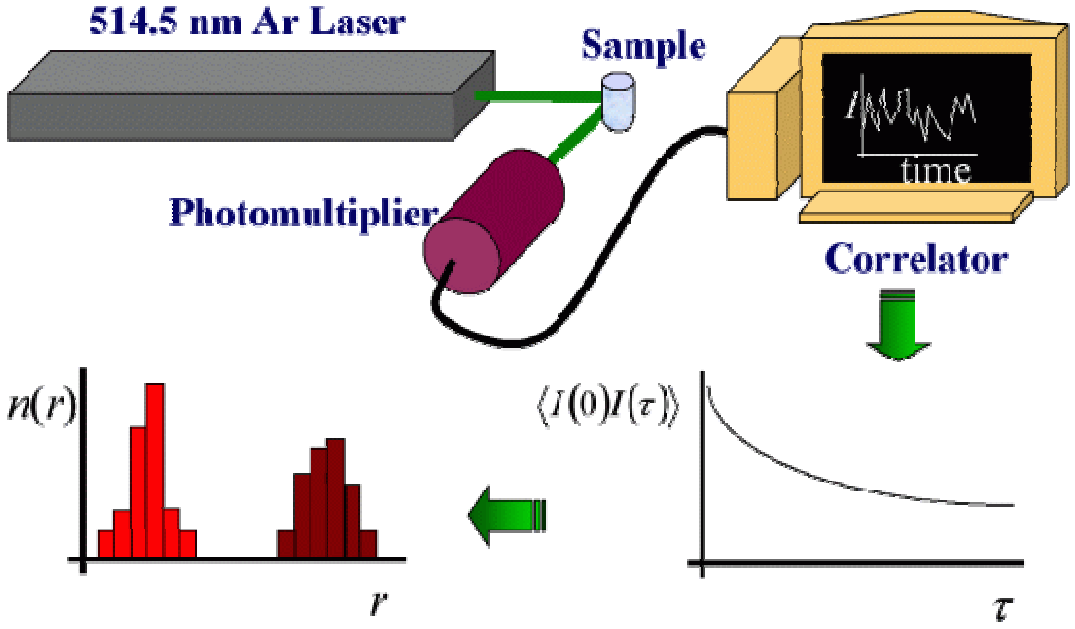

Figure 88: Process of the determination of the hydrodynamic radius d(H) via dynamic light scattering with the Zetasizer Nano ZS instrument.

It is important to remember that the hydrodynamic radius d(H) is not the accurate representation of the actual particle core size as it highly depends on the nature of the solvent used for the measurement, the way the particles swell in that particular solvent and the viscosity of the media. For this reason, it is not unusual to observe a size with the Zetasiser instrument that is different from the one obtained by other techniques such as electron microscopy. The hydrodynamic thickness (from zetasizer) is generally smaller than the steric thickness (from electronic microscopy) and considerably larger than the average thickness (obtained from SANS data).

Although the size distribution given by the zetasizer instrument is an intensity distribution, by the knowledge of parameters such as refraction index of the solvent or

of the polymer investigated, a distribution in volume can be obtained[198]. This distribution in volume can be converted further into a number distribution but this representation is of limited use, as small errors in data collection or correlation could lead to huge errors in the determination of the hydrodynamic radius. A simple way of describing the difference between the intensity distribution to the volume and number distribution is to consider a sample that contains two different populations of particles one of 5 nm and the other of 50 nm with an equal number of particles for each population. The size distribution of this sample would be represented very differently for a distribution in intensity, volume and number as shown in **Figure 89**.

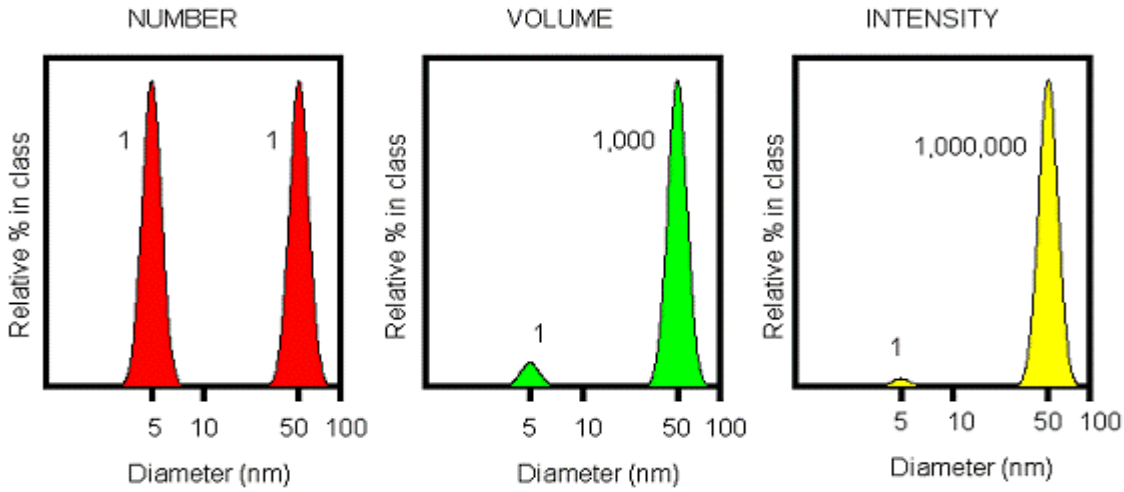

Figure 89: Number, volume and intensity distribution of a sample of two populations of particles with diameter of 5 nm and 50 nm[198].

For the number distribution, the graph will contain two peaks of equal intensity; for the volume distribution the peak corresponding to the particle population of 50 nm would be 1,000 times larger than the peak of the population at 5 nm. This is explained by the fact that the volume of a particle of 50 nm is 1000 higher than the one of a particle of 5 nm (volume of sphere: $4/3\pi r^3$). For the intensity distribution, the peak for the particle population at 50 nm would be 1,000,000 larger than the one for the particles with a 5 nm size. This is explained by the Rayleigh scattering equation, where the intensity of a particle is related to the diameter to the power 6 as described below:

$$I = I_0 \frac{1+\cos(\theta)}{2R^2}\left(\frac{2\pi}{\lambda}\right)^4\left(\frac{n^2-1}{n^2+2}\right)^2\left(\frac{d}{2}\right)^6 \quad \textbf{(Eq 33)}$$

Where λ and I_0 are respectively the wavelength and intensity of the beam of light, θ is the scattering angle, n is the refractive index of the particle, and d is the diameter of the particle.

As suggested in Rayleigh scattering equation, a particle with a diameter of 50 nm will scatter the light 10^6 times more than a particle with a diameter of 5 nm.

As the hydrodynamic radius d(H) is related to the behaviour of the particles in the solvent where the measurements are performed, it was interesting to use the zetasizer instrument to investigate the change of nanogel morphology in response to external stimuli such as organic solvent content or the use of surfactant. The outcomes of these studies would allow the establishment of a correlation between the morphology changes of nanogel particles with their catalytic behaviour and contribute to the development of new strategic synthetic routes for catalysts with enhanced activity and specificity.

2.3.1.1 Influence of acetonitrile content

The first external stimulus studied was the effect of acetonitrile content on the size of the nanogels. The results of the investigation on the effect of acetonitrile content on the catalytic activity of the nanogels in section 2.4.4.2 demonstrated a dramatic decrease of activity as the content of acetonitrile was increased from 10% to 30%. It was therefore interesting to investigate the effect of the increase of acetonitrile content on the size of the particle.

The first experiment that was carried out with the Zetasizer was to measure the size of the nanogels under the conditions used to the kinetic assays. Thus, the measurement of the size particles of MIP AS230 was performed in 10% acetonitrile in nanopure water. Stock solutions of nanogels were prepared at a concentration of 1 $mg.ml^{-1}$ and were diluted in order to reach a concentration of 0.05 $mg.ml^{-1}$. The average hydrodynamic radius was measured 3 times after filtration of the solutions

through PTFE filter with a pore size of 1 µm, in order to eliminate any particle dust. The graphs of size distribution in intensity and volume of MIP AS230 are shown in **Figure 90**.

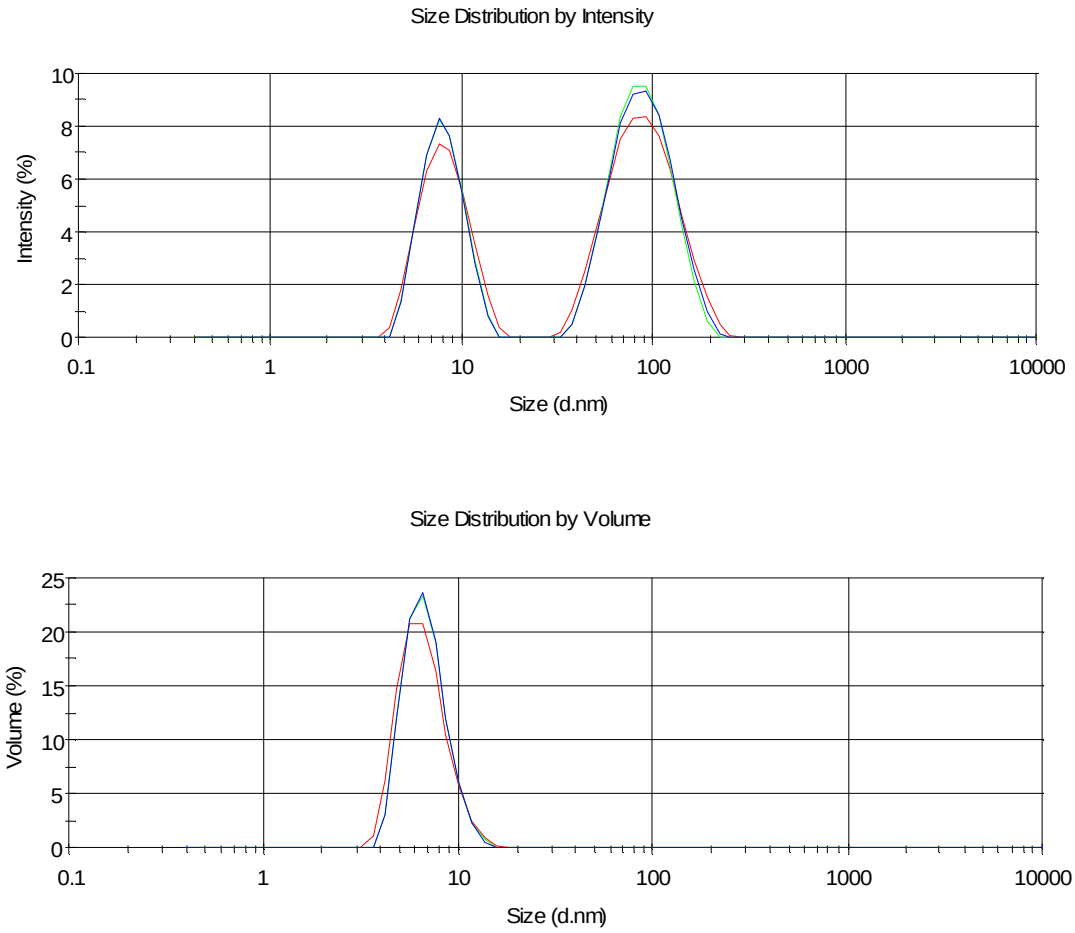

Figure 90: Size distribution in intensity and in volume of the nanogels MIP AS230

The average size of the particles of the particles was found to be around 9.1 ± 0.3 nm (S.E.) with a low polydispersity. As explained in the previous section, the size distribution in intensity displayed two particle populations, one at 9 nm and the other one at 90 nm, while the size distribution in volume only displayed one population of particles with an average particle size of 9 nm. This implied that the proportion of the particles with a hydrodynamic radius around 90 nm was quite low in comparison with the particles of a radius of 9 nm. The similar results obtained with the two types of distribution (intensity and volume) suggested that the measurements were reliable.

The size of the nanogels MIP AS230 was then measured with the Zetasiser instrument for different contents of acetonitrile ranging from 20% to 50%. Stock solutions of nanogels were prepared at a concentration of 1 $mg.ml^{-1}$ and were diluted in order to reach a concentration of 0.05 $mg.ml^{-1}$. The average hydrodynamic radius was measured 3 times after filtration of the solutions through PTFE filter with a pore size of 1 µm, in order to eliminate any particle dust. The graphs of size distribution in intensity of MIP AS230 are shown in **Figure 91**.

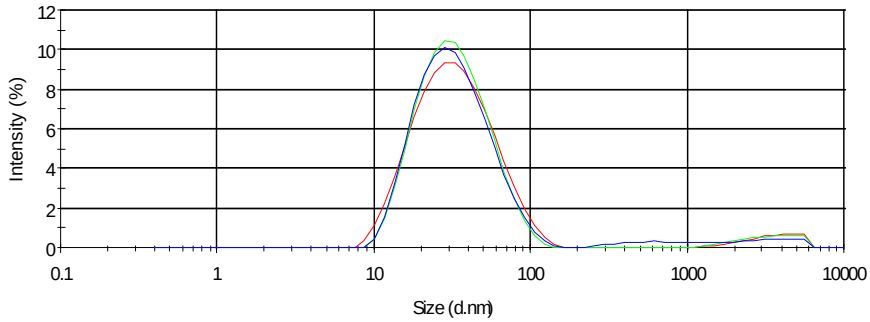

(a)

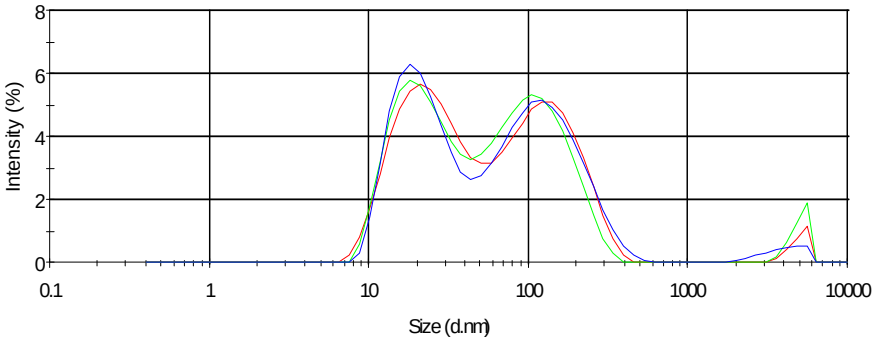

(b)

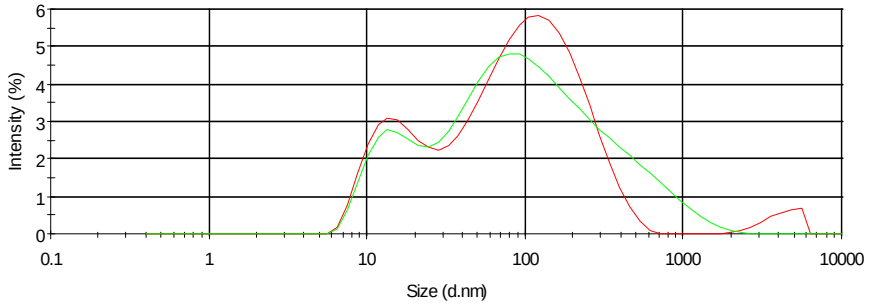

(c)

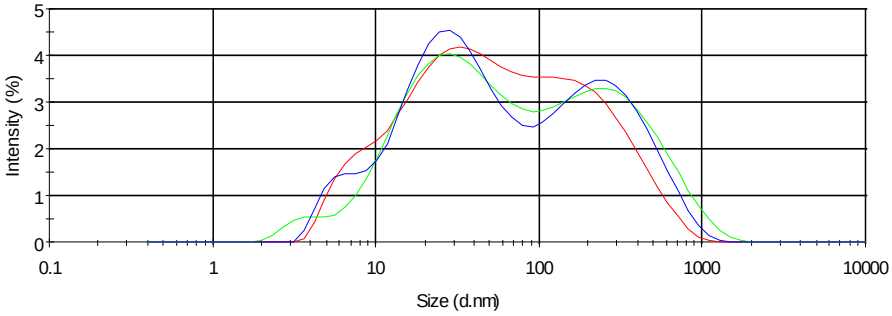

(d)

<u>Figure 91</u>: Size distribution in intensity of MIP AS230 at different acetonitrile content: **(a)** 20%, **(b)** 30%, **(c)** 40%, **(d)** 50%.

The graphs showed an increase of the polydispersity of the particles when the content of acetonitrile was increased, which was characterised by a broader peak at 20% of acetonitrile and the apparition of other peaks for higher acetonitrile contents. The apparition of the other peaks indicated the presence of several populations of particles. The broadening of the peak of size distribution and the presence of several populations of particles was interpreted as a sign of aggregation between the particles. The increase of acetonitrile content appeared to induce aggregation between nanogel particles. This could be explained by the fact that 80% of the nanogel matrix was composed of EGDMA that tend to form hydrogen bonds with the surrounding molecules in protic solvents such as water leading to a stabilisation of the colloidal suspension.

The average hydrodynamic radius d(H) of the nanogels were determined using the volume size distribution and the values were plotted as a function acetonitrile content, as shown in **Figure 92**.

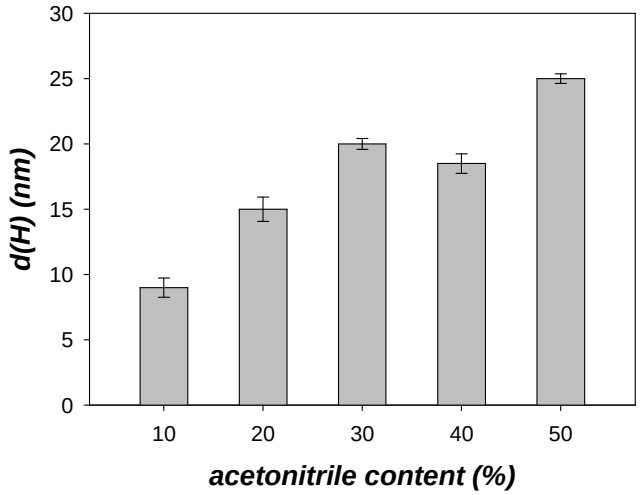

Figure 92: Average hydrodynamic radius d(H) of MIP AS230 as a function of acetonitrile content.

The size of the particles seemed to increase with the content of acetonitrile. This could be explained by aggregation between particles that lead to the formation of particles with a greater size in agreement with the graphs obtained.

2.3.1.2 Influence of initiator content on nanogel size

The zetasizer instrument was used to investigate the influence of initiator content on the size of nanogels. The chemical yields obtained for nanogels synthesised with 1%, 2%, and 3% of AIBN in section 2.5.1.1 revealed that more material was recovered in the case of imprinted nanogels than for the non-imprinted nanogels. The size characterisation with the zetasizer instrument would permit to identify if there is any correlation between the chemical yields observed and the size of the particles.

Stock solutions of nanogels were prepared at a concentration of 1 $mg.ml^{-1}$ and were diluted in order to reach a concentration of 0.05 $mg.ml^{-1}$. The average hydrodynamic radius was measured 3 times after filtration of the solutions through PTFE filter with a pore size of 1 µm, in order to eliminate any particle dust. The average diameters of the particles as a function of initiator content are shown in **Figure 93**.

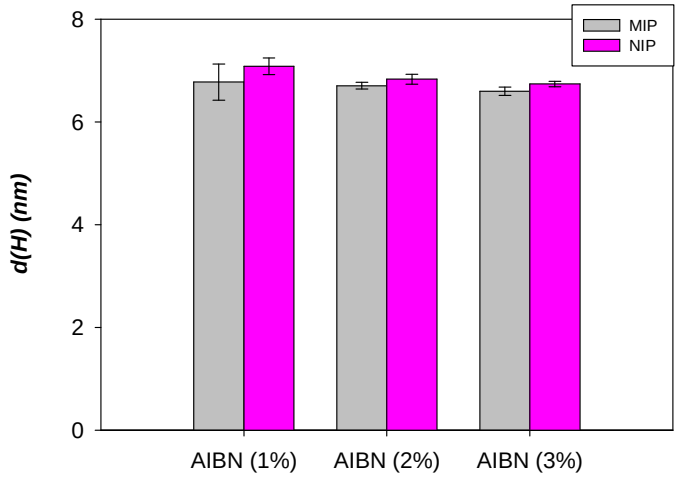

Figure 93: Average hydrodynamic radius d(H) of imprinted and non-imprinted nanogels as a function of AIBN content.

The average diameters of the particles were found to range from 6.4 ± 0.6 nm to 7.2 ± 0.6 nm. As shown in **Figure 93**, there was no significant difference between the size of imprinted and non-imprinted nanogels for any AIBN content. There was also no significant difference in size for the imprinted and non-imprinted nanogels when AIBN

content was increased from 1% to 3%. This suggested that the increase of AIBN content did not have an effect on the size of the particles.

The study of the chemical yields of the nanogels as a function of AIBN content in section 2.5.1.1 in correlation with the determination of active site number revealed different cross-linker content between the nanogels prepared with 1% of AIBN and, the one prepared with 2% of AIBN and the one prepared with 3% of AIBN. A study performed with the zetasizer alone did not permit to conclude on this effect of AIBN content on the cross-linker content, as this instrument only gives information on the apparent size of the particles and not on the density nor porosity. The use of techniques such as porosimetry or Gel Permeation Chromatography (GPC) for the determination of the molecular weight of the particles could help to study with more detail the effect of AIBN content of the nanogel matrix.

2.3.1.3 Influence of Tween 20 on nanogel morphology

The next experiment was to use the zetasizer instrument to investigate the effect of the surfactant Tween 20 on the particle morphology. The measurement of the size particles of MIP AS230 was performed in 10% acetonitrile in nanopure water with and without 0.5% in volume of Tween 20. Stock solutions of MIP AS230 and NIP AS231 were prepared at a concentration of 1 $mg.ml^{-1}$ and were diluted in order to reach a concentration of 0.05 $mg.ml^{-1}$. The results are shown in **Figure 94**.

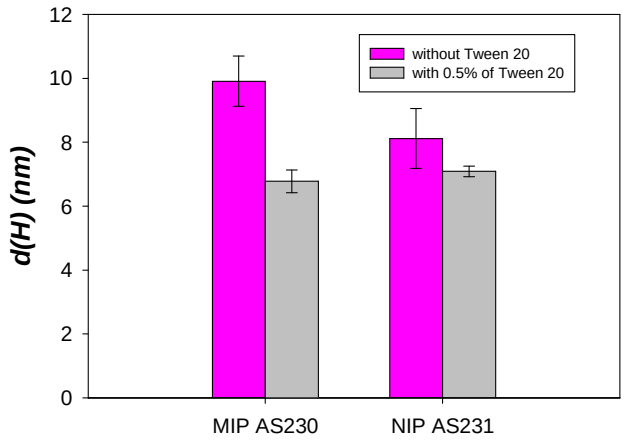

Figure 94: Average particle size of MIP AS230 and NIP AS231 with 0.5% of Tween 20 and without Tween 20.

The presence of surfactant seemed to decrease the particle size from 9.9 nm to 6.8 nm for MIP AS230 and from 8.1 nm to 7.1 nm for NIP AS231. This could be explained by the same phenomenon that was observed for the kinetic experiments. The surfactant Tween 20 adsorbingonto the surface of the nanogels particles stabilised the colloidal suspension and prevented aggregation between particles leading to the apparition of smaller particles.

Another phenomenon related to the surfactant adsorption onto the surface of acrylic acid-based microgels was reported by Barreiro-Iglesias and co-workers[188]. In this work, the effect of non-ionic surfactants such as Tween 80 and Pluronic F-17 on dispersion of acrylic acid-based microgels was investigated. A decrease of particle size with the adsorption of surfactant was noticed. The diminution of particle dimension was explained by the shrinking of the microgel matrix as the molecules of surfactant interacted with each other to form micelles, as described in **Figure 95**.

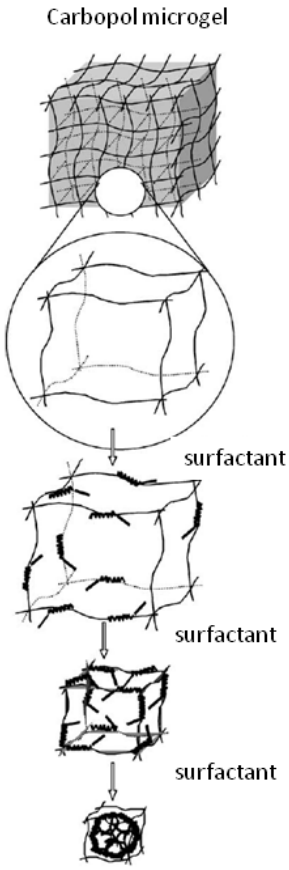

Figure 95: Schematic representation of the change in volume of acrylic acid-based microgels by surfactant adsorption[188].

The decrease of size observed for MIP AS230 and NIP AS231 in presence of 0.5% of Tween 20 could be also the result of the adsorption of the molecules of Tween 20 onto the polymeric network that by interacting and attempting to reduce surface energy gave rise to a shrinking of the nanogel matrix.

2.3.1.4 Study of the effect of surfactant by electron microscopy

In order to confirm the results obtained with the zetasizer instrument, the size characterisation of the nanogels was carried out by another technique the electron microscopy. Transition electron microscopy (TEM) is one of the most powerful techniques employed to characterise nanomaterials and has now become indispensable in the field of nanotechnology[199]. It was only with the appearance of the scanning probe microscopy that scientists could manipulate at the nanoscale.

Traditionally, TEM has been used for imaging, diffraction and chemical analysis of solid materials[200]. This technique permits to observe matter with the performance of an optical microscope with magnification in the order of more than 10000 times. The advantage of electron microscope to optical microscope resides in the ability of acquiring high resolution images using an electron beam instead of a light beam. The image arising from the electron beam is magnified by the use of electromagnetic lenses. These lenses by adjustment of the magnetic flux permit the electron beam to converge and focus on a detection surface that can be a fluorescent screen, a photographic film or a CCD camera.

The typical TEM images obtained are three dimensional images with light and dark areas as function of the amount of electrons transmitted through the sample. The combination of these dark and light areas gives rise to the generation of a TEM picture. The contrast of the image depends on the density of the sample analysed; particles with dense structures will give rise to images with a good contrast and subsequently good resolution. In the case of nanogels, in order to increase the contrast of the TEM image, it was to use a staining agent osmium tetroxide, which is commonly used to biological systems. This oxidant is known to darken polymeric particles by oxidising remaining double bonds at the surface.

Samples were prepared by adding 250 µl of a 4% wt/wt solution of osmium tetroxide to a 1 ml of 1mg.ml^{-1} nanogel solution in 10% acetonitrile in nanopure water. The solution are allowed to rest for an hour in order for the oxidant to react after which period of time the remaining oxidant molecules that can affect the image collection with TEM are removed by dialysis over night. The latter solution is then diluted 10 times and a drop is deposited onto a copper grid carbon coated for TEM analysis. This experiment was peformed with 0.5% of surfactant and without surfactant and the TEM pictures are shown in **Figure 96**.

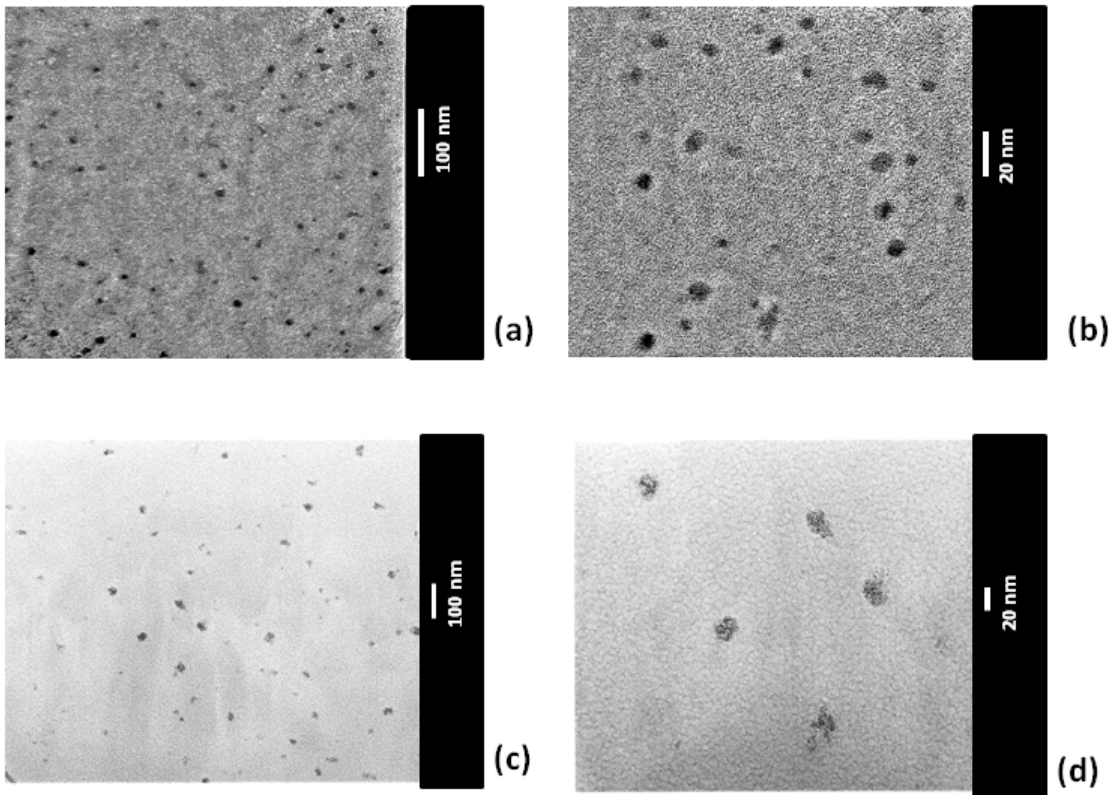

Figure 96: TEM images of nanogels for the Kemp elimination **a)** in presence of 0.5% Tween 20 displaying a small size distribution, scale bar: 100 nm and **b)** scale bar: 20 nm and without Tween 20 **c)** scale bar: 100 nm and **d)** scale bar: 20 nm. The particles were stained using osmium tetraoxide OsO_4.

The particle size displayed on the TEM pictures demonstrated a smaller particle size around 8-9 nm in presence of Tween 20 compared to the one without Tween 20 that was found to be around 15-20 nm. The decrease in particle size when adding surfactant in the media was also observed with the TEM pictures. It was also noticed a slight increase in particle size with the TEM pictures compared to the size obtained with the zetasizer. This could be due to the drying process in the preparation of the samples for TEM that could cause a flattening of the particles that therefore appeared larger than with the zetasizer analysis. The zetasier instrument is also known to underestimate the average size of nanoparticles in certain case so that it is recommended to use another technique to complement the results obtained with Zetasizer.

2.3.2 Characterisation using SANS

This part is focusing on the characterisation of the nanogels using the small angle neutron scattering (SANS) technique. This part of the project was done in collaboration with Dr. Zarbakhsh from Queen Mary University of London. The SANS experiments were carried out using the small angle neutron scattering instrument, LOQ, at the ISIS spallation neutron source, Rutherford Appleton Laboratory, Didcot, UK. The use of this novel technique was envisaged for characterising the nanogels at it permits a detailed structural characterisation of nanoparticles and gives access to information on the morphology such as size, shape and porosity. These studies would provide valuable information on nanogel structures and behaviour in different solvent systems and would contribute to the understanding on how physical-chemical properties of the polymer matrix affect the catalytic activity of these nanoparticles.

The first part of this section is introducing the principles and concepts of this technique and how to interpret and fit the data obtained from SANS analysis into the most suitable model. The following parts of this section are focusing on the characterisation of the nanogels and the investigation of the effects of acetonitrile content on the nanogel particles. The results from SANS are compared to the results obtained with the zetasizer instrument in section 2.7.2.3.

2.3.2.1 Introduction to the technique

The determination of molecular orientation in colloidal systems is an important parameter in the study of the relationships between the physical properties and molecular structures. Scattering techniques are the methods widely used to provide quantitative information on size, shape and structure of colloidal particles. These techniques are indeed based on interactions between incident radiations (e.g light, X-ray, or neutrons) and particles. In order to obtain valuable information of nanoparticles with a size that ranges from few Å to 10^4 Å, the incident wavelength used need to be comparable with these dimensions. Thus, micelles or micro-emulsion droplets or nanoparticles of approximately 100 Å would be analysed rather with X-ray

(0.5 Å – 2.3 Å) or neutron scattering (0.1 Å - 30 Å), while for larger colloidal particles light (4000 Å - 8000 Å) scattering is more appropriate[201].

It is a fundamental property of all waves to diffract on meeting an obstacle. This is true for X-rays or neutrons. X-rays scattering occurs via the electrons hence in the forward direction the resultant amplitude is proportional to atomic number. Neutron scattering however is from the nuclei and not electrons (except for magnetic samples), which act as scattering points. Neutron scattering amplitude is therefore isotropic, the sign and the magnitude change in an irregular fashion with atomic weight and varies between isotopes of the same element. As a result, in neutron scattering light atoms such as hydrogen or deuterium can be distinguished from heavier atoms. In the same way, neighbouring atoms in the periodic table can be distinguished from each other using neutron scattering. Equally, isotopes of a same atom can be differentiated by neutron scattering and therefore isotopic substitution can be used to identify different parts of molecules in a material.

Neutrons beams can be generated through two different ways: by nuclear fission in reactor-based neutron sources or by spallation in accelerator-based neutron sources. The first neutron reactor was built in the 1950's, although the application of neutron scattering for the study of condensed matter was reported only in the late 1970's. In the past 20 years, the use of neutron scattering has witnessed an exponential growth due to the development of more neutron production sites and neutron scattering has become an indispensable tool for particle characterisation. It was reported in the literature the successful application of neutron scattering for the study of micellation, micro-emulsion, molecular aggregates and liquid crystal structures.

In the case of the accelerator-based neutron source or pulsed neutron source (neutron source used in this project), the neutrons are released by spallation process, which consists in bombarding heavy metal targets such as Uranium, Tantalum or Tungsten with high energy particles such as protons from a high power accelerator. A beam of proton colloids hits the targeted nucleus that splinters into many smaller

particles of different kind including neutrons, which are very fast (high energy). Neutrons are also produced by excitation and relaxation of the nucleus as well, but these neutrons are much slower. The neutrons formed by the split of the nucleus heavy metals are then slowed down into a moderator, which can be water, before being used for diffraction. Adjusting the temperature of the moderator allows the tuning of the energy of the neutrons, as explained in Eq 32 to the size of the particles under investigation.

$$E = k\ T \qquad \textbf{(Eq 34)}$$

Where E is the energy of the neutrons in the moderator at a temperature T and k the Boltzman constant.

The advantageous features of neutrons reside in two main important points:

- Neutrons are not charged, which allow them to penetrate matter easily and they interact via strong short nuclear force with the nuclei of the materials studied
- The energy and wavelength of neutron can be adjusted depending on the nature of sample under investigation. This is due to de Bröglie equation that links the wavelength of the neutron to its velocity, as described in **Eq 35**:

$$\lambda = \frac{h}{mv} \qquad \textbf{(Eq 35)}$$

Where h is Planck's constant (6.63×10^{-34} Js) and v is the particle velocity.

The associated kinetic energy of the neutron is as specified in **Eq 36**:

$$E = \frac{1}{2}mv^2 \qquad \textbf{(Eq 36)}$$

The expression of the energy can be written as a function of λ and becomes as follow in **Eq 37**:

$$E = \frac{h^2}{2m\lambda^2} \qquad \textbf{(Eq 37)}$$

Since their wavelength and energy is related to their velocity, it is possible to adjust the wavelength of neutrons by the time-of-flight technique (determination of the time for the neutron to travel from the source to the sample).

In neutron scattering experiments, the intensity of scattered neutrons is measured as a function of Q the wave vector or *scattering vector* that depends on θ, the *scattering angle* and λ the wavelength, as specified in **Eq 38**.

$$Q = \frac{4\pi}{\lambda}\sin\theta \qquad \textbf{(Eq 38)}$$

Where λ is the neutron wavelength and θ is the scattering angle.

On a spallation source, polychromatic 'white' sources with different λ are used[202]. The energy analysis of the scattered beams can be achieved by using the 'time-of-flight' technique, which consists in determining the time for the neutron to travel from the source to the sample. The position of the detector is fixed so that, with the knowledge of the velocity of the neutron through the 'time-of-flight' technique, the wavelength of the neutrons can be calculated with **Eq 35**. The schematic representation of the instrument for neutron scattering with spallation source is shown in **Figure 97**.

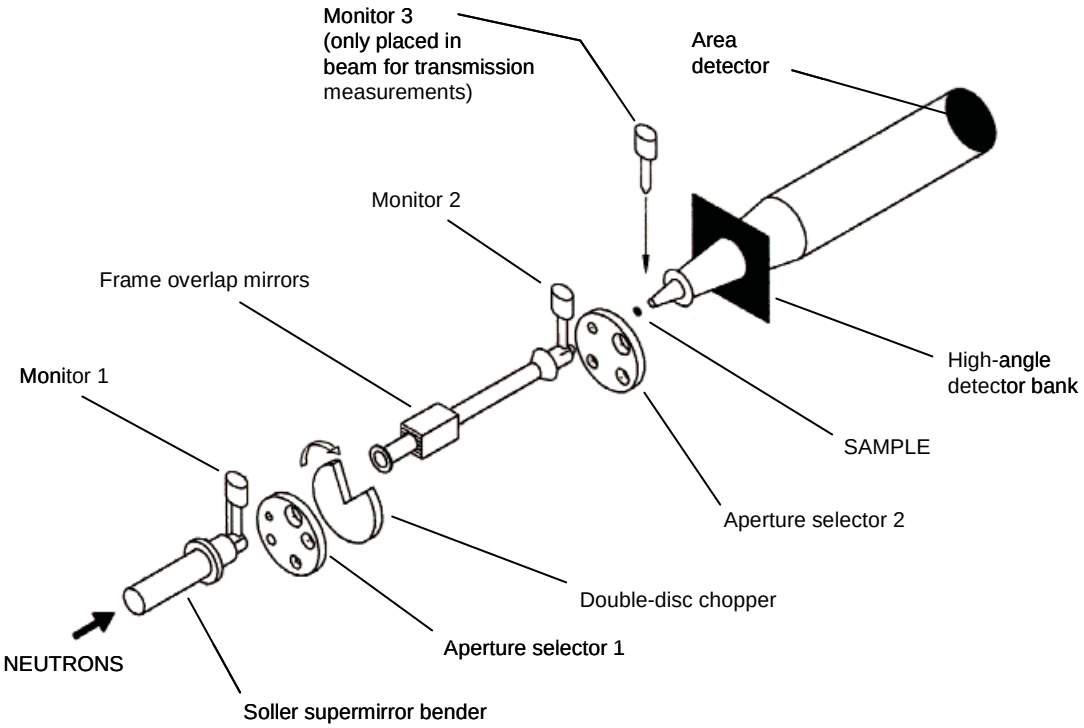

Figure 97: Schematic layout of the LOQ instrument, ISIS spallation source, Didcot (UK). After interaction with the sample (flux approximately around 2×10^{5} $cm^{-2}.s^{-1}$), the beam passes through a vacuum tube containing a ^{3}H gas filled detector placed at 4.5 m from the sample. Incident wavelengths range from 2.2 Å to 10 Å, and the scattering angle that is inferior to 7°, gives a useful Q-range of 0.009 Å to 0.249 Å[202].

Similar to light scattering studied with for instance the zetasizer instrument, neutron scattering events result from radiation-matter interactions and generates interference patterns that give information about spatial/or temporal correlations with the sample. Different modes of scattering can be seen: *elastic* scattering occurs when scattered neutrons possess the same energy as the incident neutrons, as opposed to *inelastic* scattering when a gain or loss of energy is observed. In addition, *coherent* scattering from ordered nuclei produces patterns of constructive and destructive interferences that contain structural information, while *incoherent* scattering arises from random events that provide dynamic information. In SANS, only elastic coherent scattering is considered and incoherent scattering that appears as background can be subtracted from the total scattering.

As mentioned earlier, neutrons interact with the nuclei of atom through short strong nuclear interactions around 10^{-15} m that are found to be smaller than the

incident neutron wavelength around 10^{-10} m. As a consequence, each nucleus acts as scattering point to the neutron beam. The strength of interaction between the free neutron and bound nucleus can be quantified by the *scattering length*, b, of an atom. In practice, the parameter used to quantify the strength of coherent scattering is ρ_{coh} or ρ, the *scattering length density*, which is more appropriate to quantify the scattering efficiency of the different components of the material. This parameter represents the sum of all the atomic contributions of the molecules and its expression is shown in **Eq 39**.

$$\rho_{coh} = \frac{1}{V_M}\sum_i b_{i,coh} = \frac{DN_a}{M_w}\sum b_{i,coh} \qquad \textbf{(Eq 39)}$$

Where $b_{i,coh}$ is the coherent scattering length of the ith atom of the molecule of a mass density D, and a molecular weight M_w. N_a is the Avogadro's constant.

The scattering length of most atoms such are known can be found in the literature[201]. Thus, the scattering length density of molecules can be calculated from **Eq 38**. The difference of the scattering length between hydrogen and deuterium is important and this feature is widely used in the contrast-variation technique to allow different region of molecular assemblies to be identified. For instance a molecular assembly of proton containing hydrocarbon type materials can be 'seen' by neutrons when dissolved in heavy water D_2O.

In practice, for SANS experiments, the intensity I scattered through the sample is measured as a function of the wave vector Q with the scattering angle fixed at of ≤10°. A SANS experiment is illustrated in **Figure 98**.

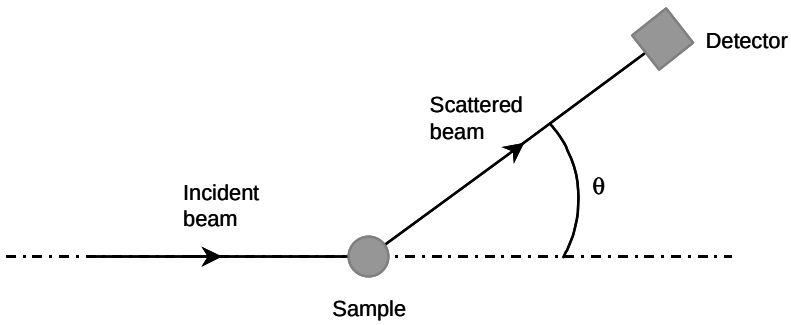

Figure 98: Schematic representation of a set-up of a SANS experiment. Sample-to-detector distance is usually from 1 m to 20 m and θ is lower than 10°.

The magnitude Q has the dimension of a reciprocal length and units are usually in Å. Large structures will scatter at low Q, while small structures scatter at higher Q values.

The scattered intensity I(Q) is the measured parameter in a SANS experiment and contains intra-molecules and inter-molecules information. For mono-dispersed spherical particles of radius R, volume V_p, number density n_p and coherent scattering length density ρ_p in a medium of density ρ_m, the normalised SANS intensity I(Q) (cm^{-1}) can be written as in **Eq 40**:

$$I(Q) = n_p \Delta\rho^2 V_p{}^2 P(Q,R) S(Q) \qquad \textbf{(Eq 40)}$$

Where $\Delta\rho$, the contrast is equal to $\rho_p - \rho_m$ (cm^{-2}).

The three first terms of **Eq 40** are not dependant on Q, the scattering vector. A scale factor can be defined as in **Eq 41**.

$$S_F = n_p (\rho_p - \rho_m)^2 V_p{}^2 = \phi \Delta\rho^2 V_p \qquad \textbf{(Eq 41)}$$

Where ϕ is the volume fraction of the particles.

The scale factor S_F is a measure of the validity and consistency of the model used to when analysing the SANS data. The value obtained from model fitting can be compared to the theoretical value calculated from **Eq 41**.

The last two terms of **Eq 40** are functions dependant on Q, the scattering vector. The function P(Q,R) represents the single particle form factor that comes from intra-particle scattering. It describes the angular distribution due to the shape and size of the particles. The function S(Q) is the structure factor that comes from inter-particle interactions. To represents better the contribution of these two functions on the scattered intensity I(Q), two scattering profiles are displayed in **Figure 99** in the case of repulsive and attractive forces between interacting homogeneous spheres.

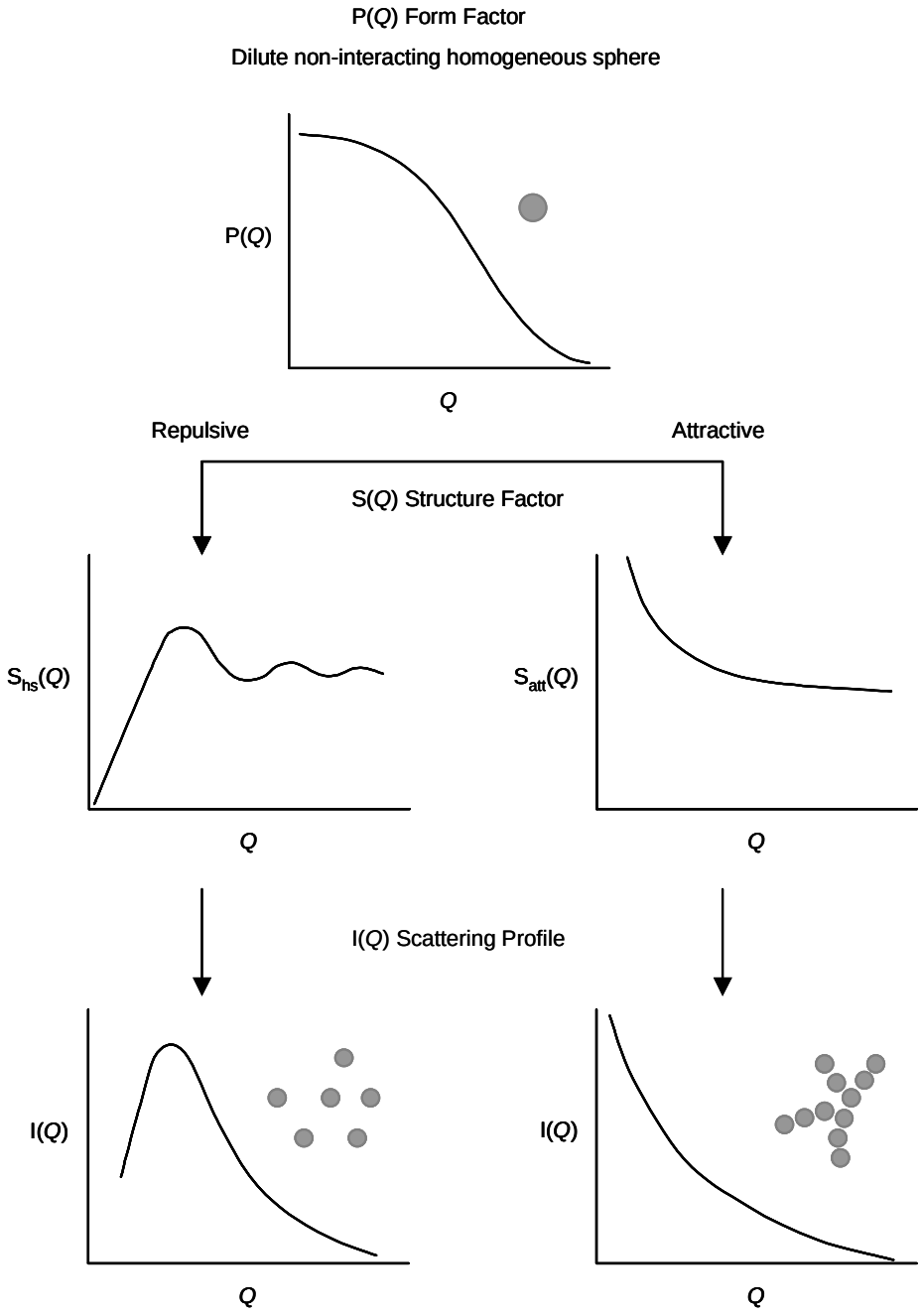

Figure 99: Schematic representation of the form factor function P(Q,R) and of the structure factor S(Q) for attractive and repulsive homogeneous interacting spheres and their contribution in the scattered intensity I(Q)[202].

2.3.2.2 Nanogels characterisation

The analysis of data obtained with the nanogels is discussed in this section. The first part of the section focuses on the characterisation the imprinted and non-imprinted nanogels in order to determine any structural difference between the two

nanoparticles. The next experiments concentrated on the effect of acetonitrile and temperature on the morphology of the nanogels.

The first SANS experiments carried out was the investigation of shape and size of the imprinted nanogels MIP AS236 and non-imprinted nanogels NIP AS237 in a similar solvent system as used for the kinetic characterisations, such as 10% acetonitrile in water. The polymers MIP AS236 and NIP AS237 were prepared in the same way and with the same formulation as for the nanogels MIP AS230 and NIP AS231 studied in the previous sections (CM 0.5%, 80% of cross-linker, 1% of double bonds of initiator, template-monomer ratio 1/1). Prior the SANS investigations on the nanogels, the determination of the scattering length density of the nanogels were calculated. This was required in order to evaluate the contrast of the nanogel particles in comparison with that of the solvent. The values of the coherent scattering length b of important atoms are shown in **Table 26**.

Table 26: Values of coherent scattering length b of important atoms

Nucleus	b [10^{-12} cm]
^{1}H	-0.3741
$^{2}H(D)$	0.6671
^{12}C	0.6646
^{16}O	0.5803
^{14}N	0.9380

From these values, the scattering length density ρ of the nanogels could be calculated knowing the atom composition of the particles. Considering that the nanogel structure is at 80% of EGDMA and 20% of 4-vinylpyridine, the scattering length density ρ obtained was 1.4919×10^{-10} cm^{-2}. The same calculations were also required for the solvent system, which was based on mixtures of acetonitrile and water in order to evaluate the contrast between the particles and the solvent. The values of the scattering length densities ρ of water, D_2O, acetonitrile and *d3*-acetonitrile are shown in **Table 27**.

Table 27: Values of the scattering length densities ρ of some solvents.

Solvent	ρ [10^{-10} cm^{-2}]
H_2O	-0.560
D_2O	6.356
acetonitrile	1.3421
d3-acetonitrile	4.8974

As mentioned earlier, there is a significant difference between ρ_{H2O} and ρ_{D2O}. This advantageous feature of D_2O is exploited by highlighting different parts of the materials investigated and revealing details of the structure. This can be achieved by varying the scattering length of the materials or of the solvent. There are two possibilities: dissolving the hydrogenated polymer particles in D_2O and/or deuterated solvents or investigating the structure of a deuterated material in a non-deuterated media (H_2O for example).

In order to characterise the nanogels with a maximum contrast, the particles were dissolved in a mixture of *d3*-acetonitrile, H_2O and D_2O. Water was added to the solvent system in proportions that would match the scattering length density of *d3*-acetonitrile. In this way, the particle structure would be investigated by contrast with a deuterated medium with a scattering length density different enough from the scattering length of the nanogel particles. This would allow the contrast required to correctly analyse the nanogels with SANS technique.

In data reduction on LOQ, the area detector is first divided into imaginary rings which are used in a radial average, summing over all distances from r+δr. The data in each ring are function of the wavelength λ, and are re-binned by choosing a suitable wavelength bin, as also are the monitor and the direct beam spectra. The fully normalised scattered intensity I(Q) corrected for detector efficiency and sample transmission are then plotted as a function of Q. A typical contour of SANS data is shown in **Figure 100**.

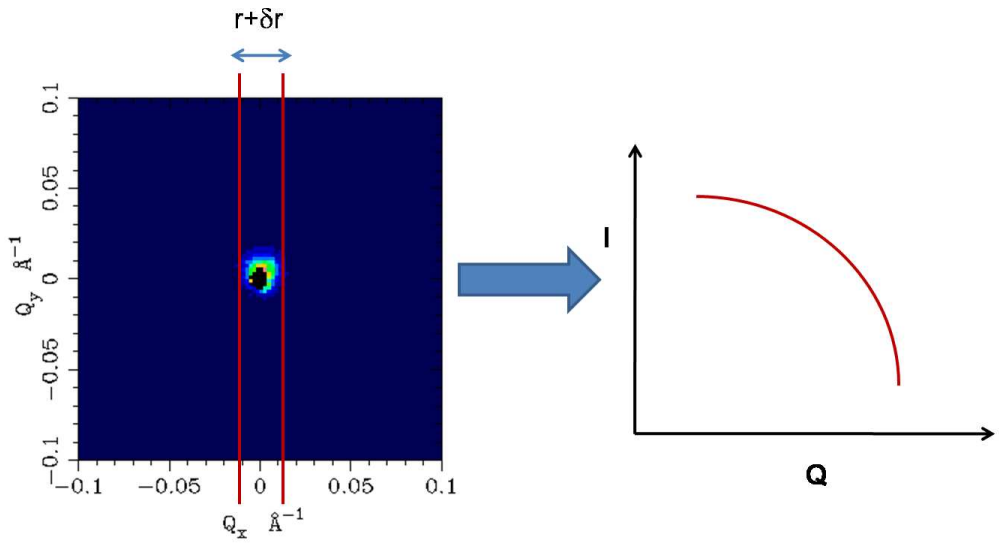

Figure 100: Typical contour plot obtained from SANS measurement. After integration of the intensity contained in the section defined between r and r + δr, a plot of the intensity as a function of Q is generated in a logarithmic scale.

Stock solutions of nanogels MIP AS236 and NIP AS237 were dissolved in 50% *d3*-acetonitrile and 50 % D_2O at a concentration of 5 mg.ml^{-1}. The latter solutions were dissolved in a mixture of water/D_2O to reach a concentration of 1 mg.ml^{-1} and then analysed using the LOQ instrument. The normalised scattered intensity I(Q) of the nanogel particles (MIP AS236 and NIP AS237) were plotted as function of Q on a logarithmic scale and are shown in **Figure 101**.

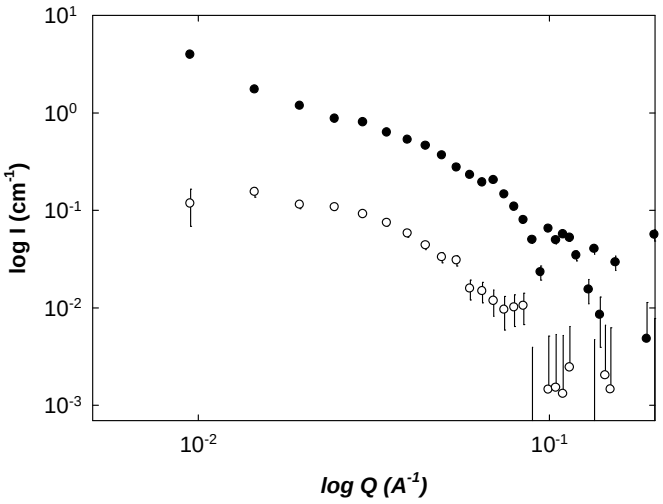

Figure 101: Logarithmic curves of the scattered intensity I(Q) of (●) MIP AS236 and (o) NIP AS237 as a function of Q. The plot of I(Q) for MIP AS230 was shifted up by a factor of 10 to improve the clarity of the graphs.

In order to determine the size and shape of nanogels, the data were fitted using a standard data analysis package FISH[203]. It was found that the data were best described using an ellipsoid oblate model (HSS) shown in **Figure 102**[203].

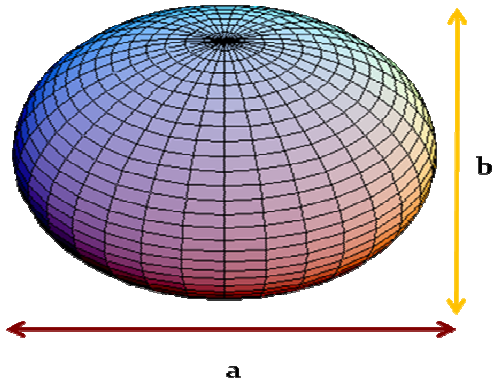

Figure 102: Representation of an ellipsoid oblate with two important radius a and b.

The fitted data are then fitted using this model and the fits to these data for MIP AS236 and NIP AS237 are shown in **Figure 103.**

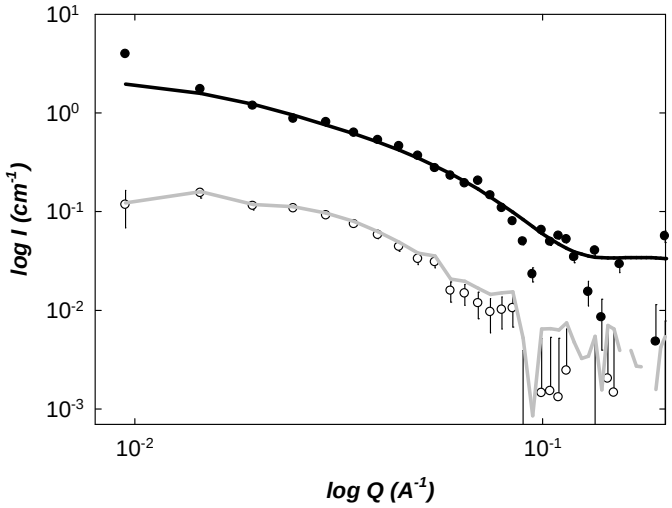

Figure 103: Logarithmic plot of the scattered intensity I(Q) of (●) MIP AS236 and (o) NIP AS237. The line represents the fit into an ellipsoid model using FISH software. The data for MIP AS230 were shifted up by a factor of 10 to improve the clarity of the graph.

From this fitting model the values of a and b are then determined for both nanogels and the values are summarised in **Table 28**.

Table 28: Values of a and b for MIP AS236 and NIP AS237 from the ellipsoid (HSS) fit obtained with FISH software.

Polymers	a (nm)	b (nm)	Scale factor S_F
MIP AS236	22 ± 1.20	3.2 ± 0.20	0.27 ± 0.04
NIP AS237	6.7 ± 0.08	4.1 ± 0.20	0.14 ± 0.01

The data suggested that there was a shape difference between the imprinted nanogels MIP AS236 and the non-imprinted nanogels NIP AS237. The imprinted nanogels appeared to be more elongated than NIP AS237. The value of the longitudinal radius a for MIP AS236 (14.7 nm) was found to be higher than the one of NIP AS237 (6.67 nm) as illustrated in **Figure 104**. This shape difference could be because of the presence of a cavity and the arrangement of the functional groups inside the imprinted cavity.

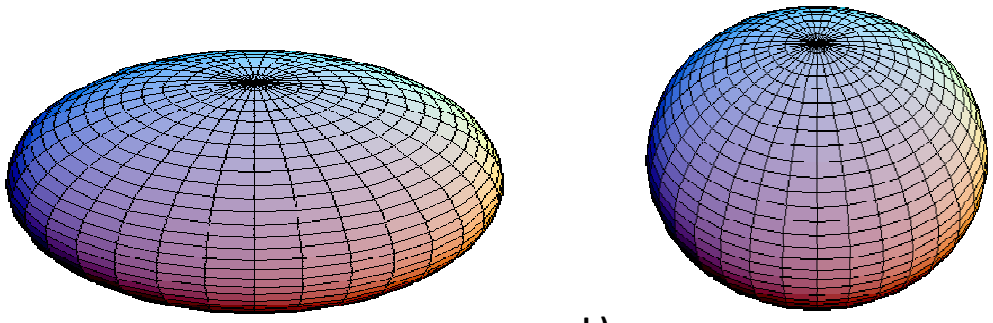

a) **b)**

Figure 104: Representation of the suggested shapes of **a)** MIP AS236 and **b)** NIP AS237 from the fitting model of an ellipsoid oblate from FISH software

The fact that the nanogels were found to be non spherical particles was not a surprising result. This has been reported in previous studies on the shape of microgel particles using SANS and other techniques[118], where it has been demonstrated that the internal structure of microgel was highly unlikely to be totally homogeneous and uniform in all directions as a result of the cross-linking density of the microgels.

2.3.2.3 Acetonitrile effect on particles

The effect of acetonitrile content in the media on the size and shape of the particles were also investigated with the SANS instrument. Stock solutions of MIP AS236 and NIP AS237 were prepared in 50% *d3*-acetonitrile and 50% D_2O. The latter solutions were then diluted in d3-acetonitrile and mixtures of water/D_2O in order to obtain nanogel solutions at a concentration of 2 $mg.ml^{-1}$, with d3-acetonitrile contents ranging from 20% to 60%. The scattered intensities I(Q) of the nanogel particles (MIP AS236 and MIP AS237) obtained at different *d3*-acetonitrile contents were plotted as function of the scattering vector Q**.** The data could be fitted into an ellipsoid (HSS) model using FISH software and the raw and fitted data are shown in **Figure 105**.

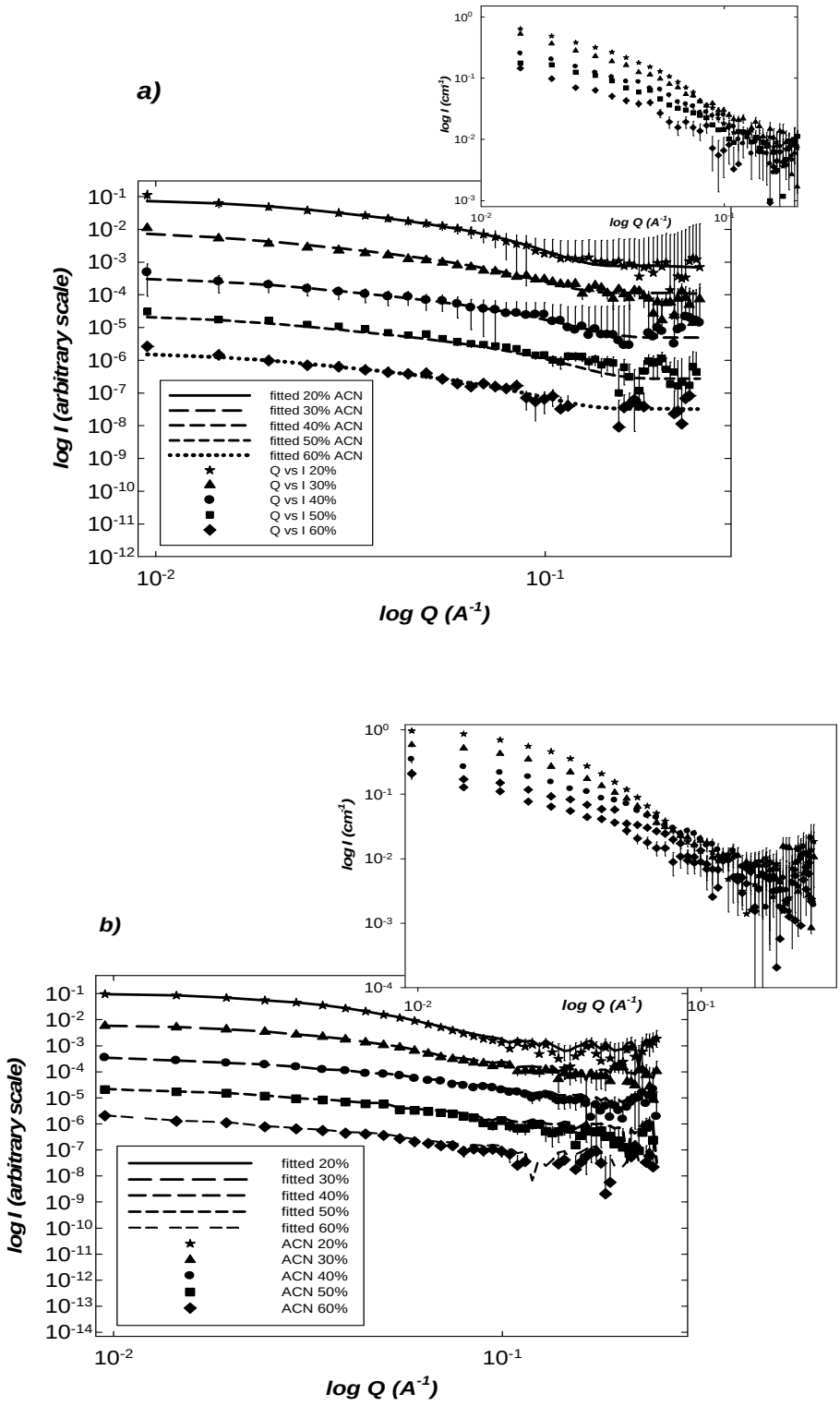

Figure 105: Logarithmic curves of the scattered intensity I(Q) of MIP AS236 and MIP AS237 are shown as an insert. The fitted data using an ellipsoid model are presented in the main graph. The data were shifted by a factor of 10 for clarity.

It could be noticed from the raw data, a slight variation of nanogel morphology for both imprinted and non-imprinted nanogels, depending of the acetonitrile content due to the slight variation of the curves obtained. From this data, the different values of the radius a and b could be extracted and the values are shown in **Table 29**.

Table 29: Values of a and b for MIP AS236 and NIP AS237 from the ellipsoid (HSS) fit obtained with FISH software at different acetonitrile content.

Acetonitrile (%)	a (nm)	b (nm)
20	MIP: 14.7 NIP: 12.7	2.83 3.64
30	MIP: 19.7 NIP: 13.0	2.75 3.45
40	MIP: 16.1 NIP: 15.8	2.25 2.26
50	MIP: 17.1 NIP: 15.8	2.25 1.96
60	MIP: 16.5 NIP: 20.1	2.59 2.92

The different values of radius a and b were plotted against the concentration of acetonitrile for MIP AS236 and NIP AS237 and this is shown in **Figure 106**.

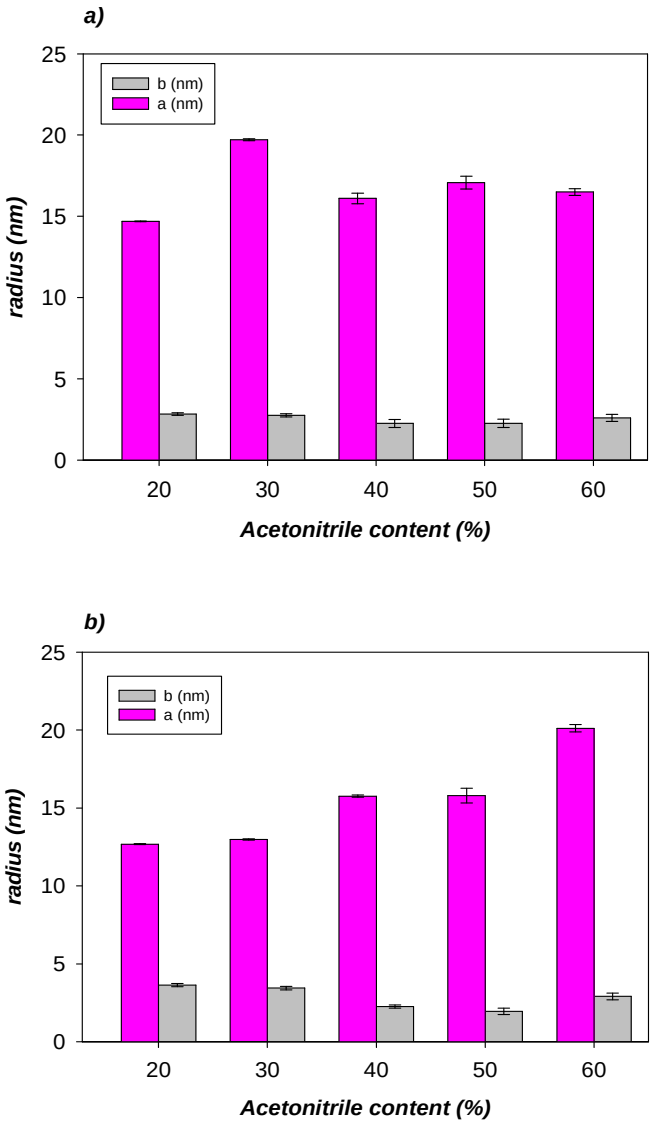

Figure 106: Values of the different radius a and b as a function of the content of acetonitrile in the media for a) MIP AS236 and b) NIP AS237.

As suggested in **Figure 106**, the content of acetonitrile appeared to have an impact on the shape and size of the particles more for the non-imprinted nanogel NIP AS237 than for the imprinted nanogel MIP AS236. In the case of NIP AS237, the increase of acetonitrile seemed to provoke the swelling of the polymer matrix in a privileged direction. The polymer was as a result elongated towards the direction of the longitudinal radius a. In the case of MIP AS236, the elongated structure observed did not seem to be significantly affected by the content of acetonitrile as no further elongation towards the direction of a was observed. This elongation of microgel particles as a result of a change of media was reported in previous work by Saunders *et*

al.[118]. In this paper, it was reported after the study of microgel particles with SANS instrument that the swelling of microgel particles would occurs uniformly in all direction as this would imply a uniform cross-link density. It was also demonstrated a decrease of cross-link density from the centre of the particles to the periphery. This was in agreement with the swelling in a privileged direction for the non-imprinted polymer NIP AS237. The presence of an imprinted cavity and the organised positions of the functional groups in the imprinted nanogels could explain the effect of acetonitrile that was not significant.

The diffraction figure obtained after full background subtraction from the particles confirmed the non-spherical shape of the nanogels. The diffraction figure of NIP AS237 at 60% of *d3*-acetonitrile is shown in **Figure 107**.

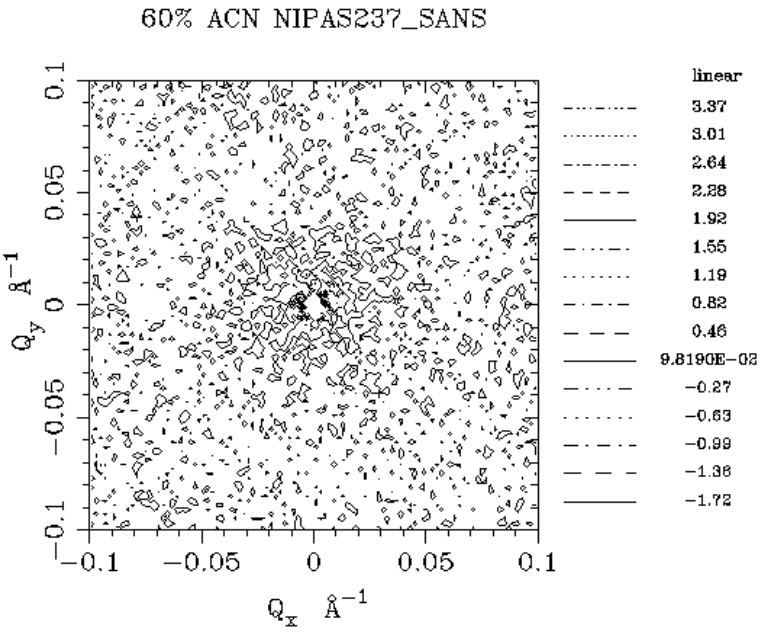

Figure 107: Diffraction figure obtained from NIP AS237 in 60% acetonitrile in a mixture of water/ D_2O. The diffraction figure was subtracted from background (solvent).

In order to compare the effects of the acetonitrile content on the size of the particles the values of the radius obtained with SANS and zetasizer were plotted in the same graph for NIP AS 237 and this is shown in **Figure 108**.

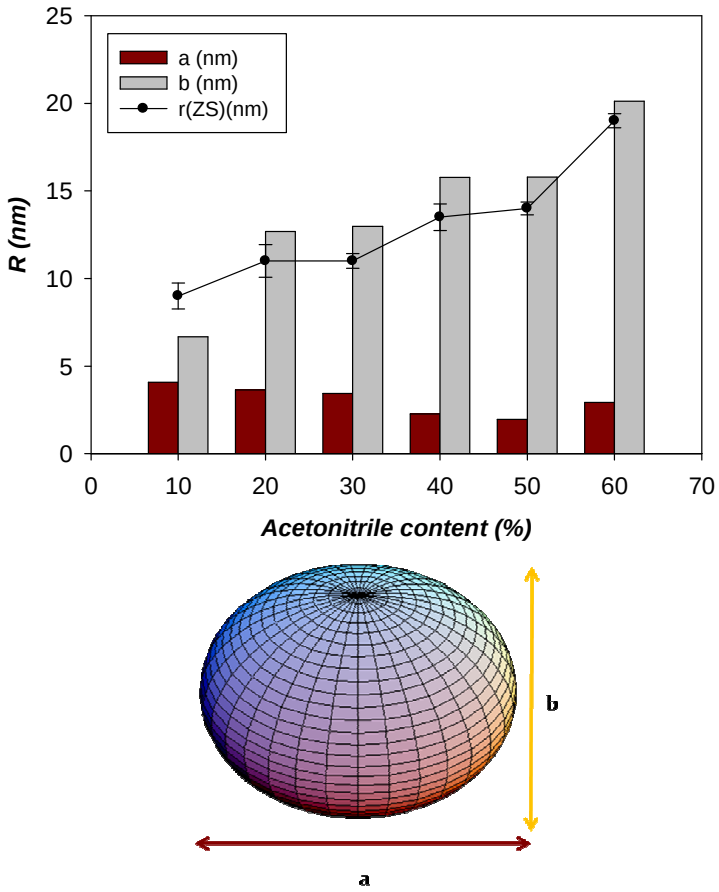

Figure 108: Values of radius as a function of the content of acetonitrile obtained with Zetasizer and with SANS instrument for NIP AS237.

The values of nanogel dimensions obtained by both techniques, Zetasizer and SANS were found to be in agreement. Nevertheless, it appeared that SANS instrument gave more information about the structure of the nanogels and the morphological changes due to the increase of acetonitrile. While the zetasizer instrument gave only an average of the size of the particles showing an increase of the average diameter of the particles, the SANS data indicated a non-uniform swelling of the nanogel matrix demonstrating an elongation towards one specific direction.

2.3.2.4 Effect of acetonitrile on the volume fraction of the particles

The study of aggregation between particles could be also investigated with the SANS instrument. It consisted in investigating the change in the volume fraction of the particles in the sample. As mentioned in the introduction of the SANS technique, the

volume fraction of the materials is a parameter that is independent from the scattering vector Q and that is contained in the scale factor S_F, as specified in **Eq 41**.

Following the fitting of the data with the ellipsoid (HSS) model using FISH software, the scale factor for the nanogels at different acetonitrile content could be extracted and the volume fraction of the particles in the sample could be calculated. The volume fractions of MIP AS236 and NIP AS237 were plotted as a function of the content of acetonitrile as shown in **Figure 109**.

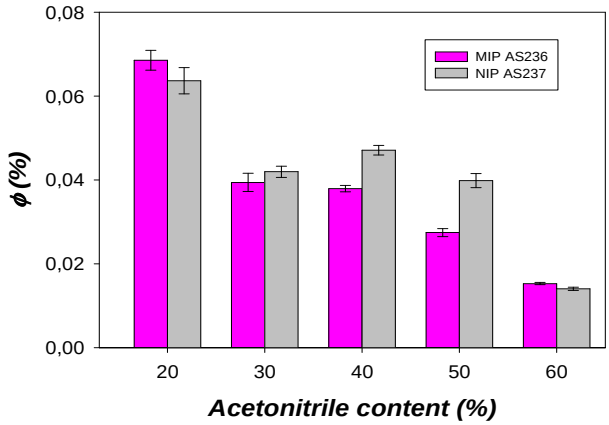

Figure 109: Volume fraction ϕ of the imprinted and non-imprinted polymer MIP AS236 and NIP AS237 as a function of acetonitrile content.

The volume fraction ϕ represents the volume occupied by the particles compared to the volume of the solution. As it could be seen in **Figure 109**, the volume fraction of the particles was found to be very low and ranged from 0.07% and 0.065% at 20 % of acetonitrile for MIP AS236 and IP AS237 respectively to 0.03% for both nanogels at 60% of acetonitrile. The volume fraction ϕ of the particles in the media appeared to decrease dramatically as the acetonitrile content was increased from 20 to 60%. This was a good indication of particles aggregation for both nanogels. The decrease of volume fraction demonstrated that the particles at high content of acetonitrile were aggregating at the bottom of the sample. This result was in correlation with the decrease of catalytic activity of the nanogel particles when the content of acetonitrile was increased from 10% to 30% described in section 2.4.4.2.

2.3.2.5 Temperature effect on particles

The effect of temperature on the nanogel matrix was also investigated with the SANS technique. Stock solutions of nanogels MIP AS236 and NIP AS237 were dissolved in 50% *d3*-acetonitrile and 50 % D_2O at a concentration of 5 $mg.ml^{-1}$. The latter solutions were dissolved in a mixture of water/D_2O to reach a concentration of 1 $mg.ml^{-1}$ and then analysed using LOQ instrument in ISIS Laboratories, Rutherford Facilities in Didcot Parkway. The scattered intensities I(Q) of the nanogel particles (MIP AS236 and MIP AS237) were plotted as function of the scattering vector Q and the curves are shown in **Figure 110.**

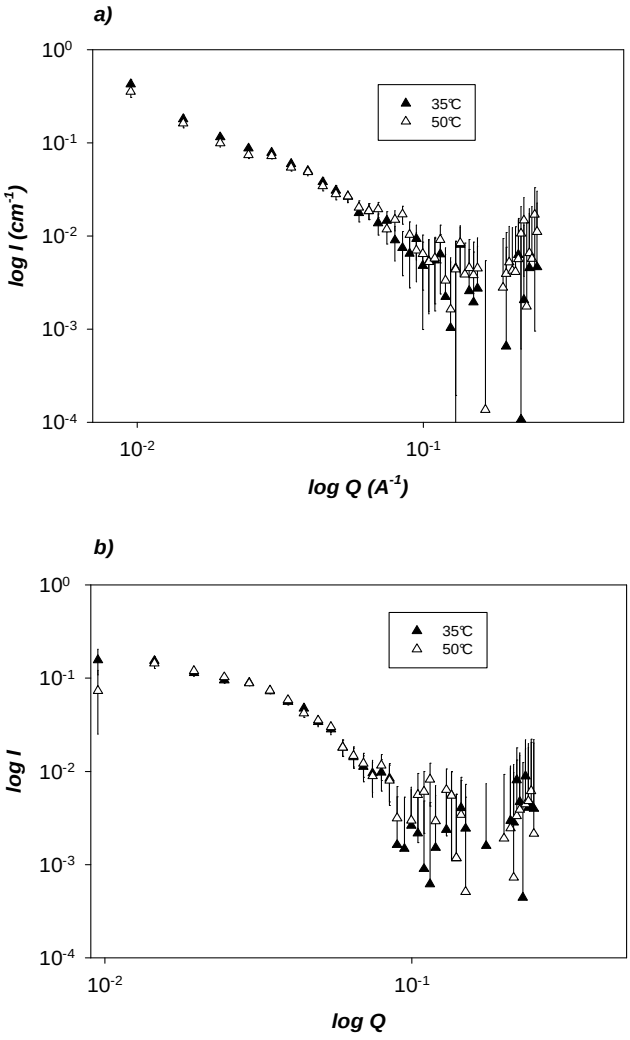

Figure 110: Logarithmic curves of the scattered intensity I(Q) at (▲) 35°C and (Δ) 50°C of **a)** MIP AS236 and **b)** NIP AS237 as a function of Q.

The raw data did not show any structural change at 35°C and 50°C for both polymers implying that temperature did not affect the polymer matrix. The data could be an ellipsoid (HSS) model using FISH software and the values of a and b obtained are summarised in **Table 30.**

Table 30: Values of a and b for MIP AS236 and NIP AS237 from the ellipsoid (HSS) fit obtained with FISH software

Temperature (°C)	Polymers	a (nm)	b (nm)	Scale factor S_F
35	**MIP AS236**	19.9 ± 1.44	2.65 ± 0.14	0.26 ± 0.02
	NIP AS237	6.90 ± 0.07	3.08 ± 0.18	0.15 ± 0.006
50	**MIP AS236**	31.15 ± 2.00	2.36 ± 0.15	0.32 ± 0.005
	NIP AS237	7.75 ± 1.30	3.37 ± 0.15	0.15 ± 0.01

The values of radius a and b indicated that the temperature did not have a strong effect on the polymer structure. There was in fact no significant difference the values obtained in section 2.7.7.2 for MIP AS236 and NIP AS237 and the one observed at high temperatures.

2.4 Conclusions

Imprinted methacrylate-based nanogels with catalytic activity for the Kemp elimination were successfully prepared using the high dilution radical polymerisation technique. Although the interaction studies between the template molecule indole and the functional monomer 4-vinylpyridine demonstrated weak interactions via hydrogen bond, the nanogels displayed an enzyme-like behaviour with a high imprinting efficiency that revealed the presence of specific imprinted cavities. This established further the reliability of the molecular imprinting approach combined with the use of nanogels for the generation of enzyme mimics.

Optimisations of the catalytic and imprinting efficiency were achieved by tuning pH and acetonitrile content as these two external stimuli were found to have effects on the catalytic behaviour of the nanogels. The use of surfactant marked a definite improvement in the catalytic activity of the nanogels as it was found to not only increase the activity of the nanogels for the catalysis of the Kemp elimination but also to enhance the affinity between the substrate molecule and the polymer matrix.

The effects of the parameters was also confirmed by a detailed physical characterisation of the nanogel particles that demonstrated the significant effect of acetonitrile content and the presence of surfactant on the aggregation of the nanogel particles. The investigations carried out using the powerful SANS technique also gave further insights on the size of the nanoparticles and additionally a model of the shape of the nanogels. These studies permitted to observe with more details the effect of acetonitrile content on the swelling properties of nanogel particles and especially confirmed the idea that the degree of cross-linking in the nanogel particles prepared with high dilution radical polymerisation was highly heterogeneous.

The work presented in this thesis marked a significant progress in the understanding of imprinted nanogel behaviour in response of external stimuli and its consequences in the catalytic activity. These studies on the physical properties of

imprinted nanogels are of great importance for the generation of novel efficient catalysts with enzyme-like behaviour as they will permit the establishment of new strategic synthetic routes for the production of imprinted nanogels with enhanced activity and specificity. The outcomes of these findings would allow the generation of tailor-made catalysts that could be used in condition where enzymes are not available and for a wider range of reactions.

Future work will follow these encouraging results notably in characterisation of nanogel particles in presence of surfactant or a different pH using SANS technique.

CHAPTER 3

MATERIALS AND METHODS

3 Materials and Methods

3.1 Materials

3.1.1 Chemicals and materials for substrate and nanogel synthesis:

4-vinylpyridine (4-VP, 95%), ethyleneglycol dimethacrylate (EGDMA, 98 %), indole (98%)and 5-nitroindole (98%), hydroxylamine hydrochloride (98%, A.C.S. reagent) were purchased from Aldrich Chemical Co. (Gillingham, Dorset, UK). 4-vinylpyridine and EGDMA were purified by vacuum distillation before use. 2,2'-azobisisobutyronitrile (AIBN, 98%) was purchased from Acros Fisher Scientific UK (Loughbrough, Leicestershire) and (Loughbrough, Leicestershire) and recrystallised from methanol before use. 2-hydroxy-5-nitrobenzaldehyde (97%) was purchased from Fluka (Gillingham, Dorset, UK). Anhydrous 1,2-dichloroethane (DCE, 99%) was purchased from Aldrich Chemical Co. (Gillingham, Dorset, UK). Dialysis membranes were purchased from Medicell International Ltd, 12000-14000/2 size, 22.0-mm diameter, molecular weight cut-off 12000-14000 Daltons.

3.1.2 Chemicals for interaction studies via 1H-NMR (270 MHz):

All the deuterated solvents for NMR studies were purchased from Cambridge Isotope Laboratories. Inc. Other solvents used for polymerizations or analytical experiments were of analytical grade.

3.1.3 Chemicals for the kinetic assays:

3.1.3.1 Chemicals:

BisTris, Tris and sodium carbonate were purchased from BDS. Benzisoxazole (BZO, 98%) was purchased from Aldrich Chemical Co. (Gillingham, Dorset, UK).

3.1.3.2 Micro-pipettes:

Eppendorf micropipettes with volumes ranging from 10-200 µl, 100-1000 µl and 2-20 µl were used to measure volumes for the kinetic assays. The accuracy of the volume measured was verified by weight and the standard error was found to be ± 1%.

3.1.4 Instruments

3.1.4.1 NMR Spectroscopy:

Proton (^{1}H NMR), Carbon (^{13}C NMR) were recorded at 270 MHz on a *J*eol *J*NM-EX270 spectrometer. Chemical shift (δ) were given in part per million (ppm) and coupling constants (J) were given in Hertz (Hz). The proton spectra were reported as follow δ/ppm (number of protons, multiplicity, coupling constant J/Hz, assignment). 1H-NMR peak multiplicity were reported as follow: s(singlet), d(doublet), t(triplet), q (quartet), m(multiplet).

3.1.4.2 UV-Vis Spectroscopy:

UV-Vis samples were analysed using a Varian Cary 300 BIO UV-Vis spectrophotometer, equipped with an internal thermostat.

3.1.4.3 Freeze-dryer:

Edwards, Super Modulyo

3.1.4.4 Data analysis software for the kinetic assays:

Sigmaplot 10.0 from SPSS Inc.

3.1.4.5 Dynamic Light Scattering (DLS) Zetasizer:

The measurements were performed in the department of materials and engineering in Queen Mary University of London with a Malvern Zetasizer Nano ZS. The solutions were filter prior analysis using a PTFE filter with a pore size of 1 µm.

3.1.4.6 Transmission electron Microscopy (TEM):

Images of the OsO_4-stained nanogels particles were obtained using a JEOL 1200EX (120kV) with a beam at 90° with 300mesh copper grid coated with a thin carbon layer.

The experiments were performed at the department of materials and engineering at Queen Mary University of London.

3.1.4.7 Small Angle Neutron Scattering (SANS):

The experiments were carried at ISIS Laboratories, Rutherford Facilities in Didcot Parkway, Oxfordshire under the supervision of Sarah Rogers using spallation source LOQ instrument. After interaction with the sample (flux approximately around 2×10^5 $cm^{-2}.s^{-1}$), the beam passes through a vacuum tube containing a 3H gas filled detector placed at 4.5 m from the sample. Incident wavelengths range from 2.2 Å to 10 Å, and the scattering angle that is inferior to 7°, gives a useful Q-range of 0.009 Å to 0.249 Å. The measurements were performed using round glass-wares of 2 mm width.

3.2 Methods

3.2.1 Interaction studies via NMR

3.2.1.1 Indole template:

Proton (^{1}H NMR) spectra were recorded at 270 MHz on a *J*eol *J*NM-EX270 spectrometer. Stock solutions of indole and 5-nitroindole were prepared in different deuterated solvent systems such as d6-DMSO, d3-acetonitrile, CD_2Cl_2, $CDCl_3$, d8-toluene and D_2O at a concentration of 85.4 mM. Spectra of indole in these different solvents were recorded. Increasing quantities of *d5*-pyridine from 0 to 7 equivalents were added to the indole solutions and the spectra of indole and *d5*-pyridine at different equivalents were recorded. The chemical shift variation $\Delta\delta_H$ of the proton bound to the indole nitrogen was calculated and plotted against deuterated pyridine concentration. The data obtained could be fitted using Sigma plot 8 software into a hyperbola and the binding constant was then determined using the ligand binding equation as follow:

Determination of the binding constant by NMR-titration:

$$\Delta\delta_H = \frac{A * x}{K_D + B * x} \qquad \text{(Eq 42)}$$

Where $\Delta\delta_H$ is the variation of chemical shift of the nitrogen proton of indole, x the concentration of d5-pyridine, K_D is dissociation constant of the complex formation and, A and B are constants.

3.2.1.2 5-nitroindole template:

The same procedure as for indole was applied to 5-nitroindole.

3.2.2 Synthesis:

3.2.2.1 Substrate Synthesis:

3.2.2.1.1 Synthesis of the substrate 5-nitrobenzisoxazole:

First step: Synthesis of 5-nitrosalicylaldoxime

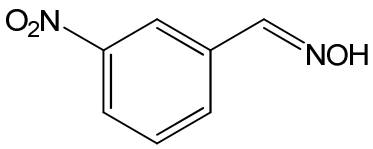

Aqueous sodium acetate (1.2 ml, 4.8 10-3 mol, 1.9 eq.) was added to a warm solution of 5-nitrosalicyladehyde (472 mg, 2.5 10-3 mol, 1.0 eq.) and hydroxylamine hydrochloride (350 mg, 5.0 10-3 mol, 2.0 eq.) in a mixture of acetonitrile/water (60% acetonitrile, 6 ml). The clear solution was heated at reflux for 3 hours. The clear orange solution was cooled down to room temperature and 3 ml of water were added to the mixture. The solution was then kept at 4°C in an ice bath. The formation of light yellow needles was observed. The solid was filtered off, washed with water and then dried under vacuum for few hours. Yield 76.4%.

^{1}H-NMR (270 MHz, CDCl3): δ 6.99 (1H, d, J = 33.6 Hz), 8.11 (1H, dd, J1 = 33.9 Hz, J2 = 10 Hz), 8.24 (1H, d, J = 10 Hz), 8.29 (1H, s)

Second step: synthesis of 5-nitrobenzisoxazole

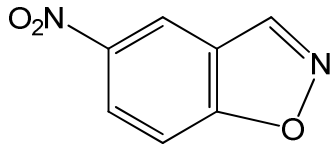

The oxime (410 mg, 2 mmol) was dissolved in anhydrous THF (5 ml) and 2 ml of a solution of trichloroacetyl isocyanate in THF (2 M, 4 mmol) was added under anhydrous conditions. The solution was stirred for 10 min before anhydrous potassium carbonate (286 mg, 2.7 mmol) was added. The mixture was stirred for 30 minutes before adding 7 ml of a mixture of water and diluted hydrochloric acid. The solution was stirred for an additional 10 minutes. THF was then evaporated and the organic phase was extracted with dichloromethane. The combined organic phases were dried with magnesium sulfate. After evaporation of the dichlormethane, a light yellow solid was recovered. The compound was recrystallized twice with acetonitrile and water. A mass of 163.2 mg of a white solid was recovered. Yield 44%.

m.p: 127°C-128°C (lit: 126.5°C- 127.5°C); UV-Vis: λ_{max} in acetonitrile: 281 nm; ^{1}H-NMR (270 MHz, CDCl3): δ 7.74 (1H, dd, JM = 0.97 Hz), 8.49 (1H, dd, J1 = 9.15 Hz, J2 = 2.24 Hz), 8.71 (1H, dd, J1 = 2.24, J2 = 0.5 Hz), 8.88 (1H, d, J = 0.97 Hz)

3.2.2.1.2 Synthesis of the 5-nitrocyanophenol (product of the Kemp elimination with 5-nitrobenzisoxazole):

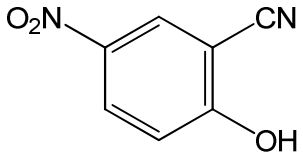

A solution of 5-nitrobenzisoxazole (0.3 g, 1.8 mmol) in 5 ml of acetonitrile and 5 ml of water was mixed with 15 ml of a solution of 3 M NaOH and was allowed to stir for 10 min. Concentrated HCl was added drop-wise to the latter solution to bring down the pH to 1. The solution was extracted three times with 10 ml-portions of dichloromethane and the extracts were combined and dried over magnesium sulphate. The solvent was evaporated and the solid residue was re-crystallised with acetonitrile. The re-crystallised solid was dried under vacuum overnight and stored in foil-wrapped vials in the freezer. A UV-Vis spectrum was recorded in order to test the

purity of the compound. Maximum absorbance was recorded at a wavelength of 381 nm in agreement with the literature.

3.2.2.2 General procedure of the nanogel synthesis:

3.2.2.2.1 Nanogel synthesis:

Indole-imprinted polymers (MIP) and non-imprinted polymers (NIP) were prepared using the standard protocol of high dilution radical polymerisation. The non-imprinted polymer was synthesized under the same conditions as the imprinted polymer but without the addition of template. The monomer concentration C_m was fixed at 0.5% (in weight) and cross-linker content at 80% (in mol). The quantity of initiator 2,2'-azo-bis(isobutyro)nitrile (AIBN) used was 1%, 2% or 3% of moles of total double bonds depending on the preparation. Indole (60 mg, 5.12 10^{-4} mol, 1 eq.), 4-vinylpyridine (55.8 µl, 5.12 10^{-4} mol, 1 eq.), EGDMA (386.4 µl, 2.05 10^{-3} mol) and AIBN (7.57 mg, 4.61 10^{-5} mol) were dissolved in 1,2-dichloroethane (91.7 mg, 73.2 ml) in 125 ml Wheaton glass serum bottles. The solutions were flushed with nitrogen for few minutes and then heated up to 70°C for 4 days.

3.2.2.2.2 Nanogel recovery:

After polymerization, the solvent was evaporated and the solid residue was dissolved in a mixture of 50% acidified water in methanol. The resulting solution was dialyzed against distilled water for 2 days, the water being changed 2 times a day using a dialysis membrane with a pore size of 12000 – 14000 Da. The presence of indole template was characterised by analysing the water from the dialysis by fluorescence. After 2 days of dialysis no meaningful quantity of indole was detectable by fluorescence. The dialyzed solutions were frozen with liquid nitrogen and then freeze-dried. Fluffy light yellow solids were recovered.

3.2.3 Determination of active sites

3.2.3.1 Determination of a general procedure: Pyridine back-titration

The determination of active sites was performed by back-titration of pyridine moieties inside nanogels using a Mettler Toledo MP 220 pH meter (Mettler Toledo ltd., Halstead, Essex, UK). Pyridine in a mixture of acetonitrile and distilled water was first titrated using back-titration technique. The latter solvent mixture was chosen as a result of the solubility tests on the polymers. A solution of pyridine in 20% acetonitrile in distilled water ($C_o = 2.0\times10^{-3}$ M, $V_o = 20$ ml) was prepared. The previous solution was then mixed with HCl solutions at different concentrations (0.5 eq., 1 eq., 1.5 eq., 2 eq., 2.5 eq.). The latter solutions were then titrated by NaOH solution at a concentration of 1.5×10^{-3} M and pH values were recorded every milliliter. The pH values versus the volume of NaOH solution added was plotted and the equivalent point was determined manually. The volume at equivalence was the mean of three measurements. Two equivalent points were observed for solutions of pyridine with an excess of HCl (1.5 eq., 2 eq. and 2.5 eq.), while for the two other solutions with HCl as limited reagents (0.5 eq. and 1 eq.) only one equivalent point was observed. As a result, the optimal condition (used as standard) to titrate accurately pyridine and therefore the nanogels was found to be by back-titration with light excess of HCl: 25 ml of HCl solution (2×10^{-3} M) was added to a 20 ml of pyridine solution (2×10^{-3} M) and the resulting solution was titrated by a NaOH solution (1.5×10^{-3} M).

3.2.3.2 Pyridine residues inside nanogels titration

A 20 ml solution of imprinted nanogels was prepared at a concentration of 1 $mg.ml^{-1}$ in 20% acetonitrile in distilled water. To the latter was added 15 ml of HCL solution at a concentration of 4×10^{-3} M. The mixture was then allowed to stir for few minutes and the pH of the solution was recorded. The resulting nanogel solution was titrated using a NaOH solution at a concentration of 1.5×10^{-3} M. The pH was recorded every milliliter and half milliliter around the equivalent points area and the values were plotted against the volume of NaOH solution. The equivalent points were determined

manually and the volume at the equivalence was determined as the mean from 3 measurements. The exact same procedure was applied to the non-imprinted nanogel. The concentration of pyridine moieties C_{Py} were determined by the volume difference between the 2 equivalent points and the knowledge of the titrant (NaOH) concentration C_{NaOH} as explained in the following equation:

$$C_{Py} = \frac{(V_{e2} - V_{e1}) \times C_{NaOH}}{V} \qquad \textbf{(Eq 43)}$$

Where V_{e1} and V_{e2} are the volume at the first and second equivalent point respectively and V is the volume of the polymer solution before titration.

3.2.4 Kinetic experiments

3.2.4.1 Calibration curves

3.2.4.1.1 Calibration curve of 2-cyanophenol and 5-nitro-2-cyanophenol at pH 14

Concentrations of the 2-cyanophenol and 5-nitro-2-cyanophenol formed during the kinetic experiments were evaluated by mean of calibration curves established using UV-Visible spectroscopy. Three stock solutions of 2-cyanophenol and 5-nitro-2-cyanophenol at concentration of 10 mM, 20 mM, and 40 mM, prepared independently by weight in acetonitrile. The latter solution was cross-diluted to generate 10 solutions with different concentrations ranging from 100 µM to 4 mM. 10 µl of each sample were diluted in a NaOH solution (4 M) in order to reach a volume of 1 ml (maximum volume inside the spectrophotometric cuvette). The maximum absorbance was recorded by UV-Visible spectroscopy at 325 nm for 2-cyanohenol and at 381 nm for 5-nitro-2-cyanophenol and was then plotted against product concentration (recalculated taking into account the dilution in the cuvette). The data could be fitted into a linear regression starting from the origin using Sigma plot 8.0. The determination of extinction coefficient ε_{max} at pH 14 was determined using the Beer-Lambert law, defined by the following equation:

$$A = \ell \, \varepsilon \, c \qquad \textbf{(Eq 44)}$$

Where A is the maximum absorbance, ε is the extinction coefficient, l the length of the cuvette (1 cm) and c the concentration inside the cuvette.

The extinction coefficient at pH 14 ε_{max} was obtained by determination of the slope of the linear curve obtained. The determination of the extinction coefficient at a given pH was then performed using the following equation:

$$\varepsilon_{pH} = \frac{\varepsilon_{\max}}{\left(1+\frac{10^{-pH}}{10^{-pKa}}\right)} \qquad \textbf{(Eq 45)}$$

Where ε_{pH} is the extinction coefficient at any pH, and ε_{max} is the extinction coefficient at pH 14.

3.2.4.2 Determination of substrate stock solution

A stock solution of substrate, benzisoxazole, was prepared in acetonitrile (stored under nitrogen atmosphere and away from light) at a concentration of 5 mM. A standard procedure was then adopted in order to determine accurately the stock concentration of substrate and to assess the reproducibility of the measurements. Three different volumes of benzisoxazole acetonitrile stock solution (C_{stock}) (20 µl, 10 µl, and 5 µl) were taken and dissolved in 980 µl, 990 µl anf 995 µl of NaOH 4M solution respectively. In this way the complete hydrolysis of the substrate was ensured and yellow solutions were obtained. Five absorbance measurements of each sample were performed and the absorbance was read at 325 nm (ε_{max} = 5382 $cm^{-1}.M^{-1}$) at 25°C, using 1 cm path length cells and NaOH 4M solutions as blanks. The substrate stock concentration was calculated considering the average value between the five calculated in the following way.

$$A = \varepsilon l c \Rightarrow c = \frac{A}{\varepsilon l} \qquad \textbf{(Eq 46)}$$

Where A is the absorbance, ε is the extinction coefficient in $M^{-1}.cm^{-1}$, l length path in cm, and c the concentration in M.

The exact same procedure was applied for the determination of the stock concentration of the other template 5-nitrobenzisoxazole, where the maximum absorbance was found to be at 381 nm (ε_{max} = 15 381 $cm^{-1}.M^{-1}$) at 25°C.

3.2.4.3 Determination of the rate constant for the uncatalysed reaction:

A stock solution of substrate was prepared in acetonitrile and the concentration was determined using the standard procedure described previously. Several reactions were performed using different substrate concentrations. The solvent was composed by acetonitrile in Tris [tris(hydroxymethyl)methylamine] buffer solution at pH 8.9: percentages of buffer and its concentration were varied accordingly to the aim of experiments. The reactions took place inside spectrophotometric cells (1 cm path length, 1 ml volume capacity) so that the absorbance of the released 1,2 cyanophenol in solution could be detected at the appropriate wavelength in function of time. The Tris stock volume and acetonitrile relative amount were injected in the cell, and when the instrument was in the start position, the substrate was quickly added and the absorbance collection began. The final absorbance for every reaction gone to completion (that is when all the 1,2 cyanophenol has been released) was calculated and reactions were followed in the first period until the absorbance value was reached 5% of the final one, in order to calculate the initial rate. The value of the slope (dA/dt, min^{-1}) of the initial linear segment of the curve absorbance versus time was calculated by the spectrophotometer software. Then Sigmaplot 8.0 software was used to plot the values of the initial rates against the substrate concentration in molarity. The slope of the best line fitting the experimental points was found to be the rate constant of the uncatalyzed reaction k_{uncat} (min^{-1}).

3.2.4.4 Determination of the rate constant for the substrate uncatalyzed hydrolysis in presence of surfactant Tween 20:

The determination of the rate constant for the substrate uncatalyzed hydrolysis in presence of surfactant was performed in the same way as described previously but adding 0.5% in volume of Tween 20 in the buffer solution. For a buffer solution of 250

ml, 1.25 ml of Tween 20 was added. The mixture was allowed to stir for few minutes and the pH of the solution was adjusted again to the desired pH.

3.2.4.5 Determination of the rate constant of the reaction in presence of the nanogels:

Once the rate of the uncatalyzed reaction of the Kemp elimination was determined, the effect of the imprinted and non-imprinted polymers on the rate of the reaction could be studied. Solubility tests were previously performed on the polymers and it was found that the optimal solvent system was a mixture of acetonitrile and water (1/1). Imprinted and non-imprinted stock solutions were prepared for each set of experiments, weighting the relative amounts of microgels and dissolving them in the appropriate volume of acetonitrile, and then the buffer solution (50 mM) at a fixed pH was added to give a clear solution.

Reactions were run inside the spectrophotometric cuvette (1 cm path length, 1 ml volume capacity) adding aliquots of polymer stock, then the appropriate amount of acetonitrile and buffer solution, and finally the substrate stock aliquot.

Kinetics were followed for the first 5% of the reaction; absorbance was collected as function of time at the appropriate wavelength depending on the substrate used, at room temperature.

As it was shown earlier, the value of the slope (dA/dt, min^{-1}) of the initial linear segment of the curve absorbance versus time was calculated by the spectrophotometer software. This value was then divided by ε, the extinction coefficient, in order to determine the initial rate $v_{i,total}$ ($M.min^{-1}$) of the reaction catalyzed by the polymers. The background rate $v_{i,uncat}$ ($M.min^{-1}$), which was determined previously for the same reaction was substracted from $v_{i,total}$ ($M.min^{-1}$) to obtain $v_{i,cat}$ ($M.min^{-1}$), which represents the net contribution due to the catalyzed reaction as shown in **Eq 47**:

Determination of $v_{i,cat}$ the net contribution of the catalyzed reaction

$$v_{i,cat} = v_{i,total} - v_{i,uncat} \qquad \textbf{(Eq 47)}$$

Values of the parameters V_{MAX} and K_M for the microgel catalyzed reactions of the Kemp elimination, for different substrates, were determined using the weighted non-linear regression program in Sigmaplot 8.0. The adherence of the initial rate $v_{i,cat}$ versus substrate concentrations data to the Michaelis-Menten equation was verified by the linearity of the plot of [substrate]/$v_{i,cat}$ versus [substrate]. The rate constant of the reaction was obtained from the following equation:

$$k_{cat} = \frac{V_{\max}}{[activesites]} \qquad \textbf{(Eq 48)}$$

3.2.4.6 Determination of initial rates in function of catalyst concentration:

A stock solution of imprinted nanogel AS 230 was prepared by weighing the relative amount dry nanogel and dissolving it in a mixture of acetonitrile/buffer solution (50 mM at a fixed pH) (1/1) in order to obtain a clear solution at a concentration of 2 $mg.ml^{-1}$.

Reactions were run inside the spectrophotometric cuvette (1 cm path length, 1 ml volume capacity) adding increasing aliquots of polymer stock from (0.01 $mg.ml^{-1}$, 0.0118 $mg.ml^{-1}$, 0.015 $mg.ml^{-1}$, 0.020 $mg.ml^{-1}$, 0.025 $mg.ml^{-1}$, 0.030 $mg.ml^{-1}$, 0.035 $mg.ml^{-1}$, 0.04 $mg.ml^{-1}$, 0.045 $mg.ml^{-1}$, 0.05 $mg.ml^{-1}$, 0.06 $mg.ml^{-1}$, 0.08 $mg.ml^{-1}$ at a fixed substrate concentration (1 mM). This experiment was also performed using 0.5 mM of substrate concentration. As it was done previously, the value of the slope (dA/dt, min^{-1}) of the initial linear segment of the curve absorbance versus time was calculated by the spectrophotometer software. This value was then divided by ε, the extinction coefficient, in order to determine the initial rate $v_{i,total}$ ($M.min^{-1}$) of the reaction catalyzed by the polymers. The background rate $v_{i,uncat}$ ($M.min^{-1}$), which was determined previously for the same reaction was substracted from $v_{i,total}$ ($M.min^{-1}$) to obtain $v_{i,cat}$ ($M.min^{-1}$). The data could be fitted to a linear regression of $v_{i,cat}$ versus catalyst concentration using Sigma Plot 8.0.

3.2.5 Polymer characterisations:

3.2.5.1 General procedure for size characterisation using Zetasizer:

The nanogels were dissolved in 50% acetonitrile in nanopure water, at a concentration equal to 1 mg/ml. The solutions were then diluted 20 times in the appropriate volume of acetonitrile and nanopure water to obtain solutions at a concentration of 0.05 $mg.ml^{-1}$ with acetonitrile content ranging from 10% to 50%. The samples were analyzed after filtration with a PTFE filter with a pore size of 1 µm, in order to eliminate any dust or aggregates that could disturb the measurements and induce a large error. Size distribution in intensity were obtained with calculating the refractive index of the mixture of solvent (acetonitrile n_D^{25} 1.341 and water n_D^{25} 1.33). Volume and number distribution were obtained with adding the refractive index of polymethacrylate selected as reference from literature around n_D^{25} 1.4914 and $dn/d\lambda$ -0.0575.

3.2.5.2 General procedure for imaging the nanogels using Transmission Electron Microscopy (TEM)

One milliliter of nanogel solution of 1 mg/ml is prepared and 250 µl of 4% wt OsO_4 solution was added to the latter. The mixture was allowed to rest for 1 hour and then dialyzed overnight to remove excess of oxidant, which could interfere with particle detection by T.E.M. The solutions are then diluted by 10 and a drop was deposited to 300 mesh copper grids coated with carbon and allow to dry for 10 min. Images of the nanogel particles were then recorded with a JEOL 1200EX (120kV) with a beam at 90°.

3.2.5.3 General procedure for characterisation using Small Angle Neutron Scattering (SANS)

The preparation of nanogel solution of MIP AS236 and NIP AS237 was carried in a mixture of non-deuterated and deuterated solvents in order to match the scattering length density ρ of the acetonitrile of a value of 4.90×10^{10} cm^{-2}. The resulting solvent system with a scattering length density of 4.90×10^{10} cm^{-2} was composed of *d3*-acetonitrile in a mixture of H_2O and D_2O (24% of H_2O, 76% of D_2O).

Stock solutions of nanogels MIP AS236 and NIP AS237 at a concentration of 5 $mg.ml^{-1}$ were prepared by dissolving 50 mg of dry nanogels in 5 ml of *d3*-acetonitrile and 5 ml of D_2O. The samples were then prepared by diluting the nanogel stock solutions in *d3*-acetonitrile and H_2O/D_2O with a H_2O content of 24% and D_2O content of 76% to generate 0.5 ml nanogel solutions of a concentration of 2 $mg.ml^{-1}$ in different acetonitrile contents. The details of the sample preparations are explained in **Table 31**.

Table 31: Preparation of the samples for S.A.N.S. of a volume 0.5 ml (Concentration: 2 $mg.ml^{-1}$, volume: 0.5 ml (acetonitrile-d3/D_2O mixed with water (5.26 g of water in 21.77 g of D_2O))

Samples	**Volume of polymer stock solution in ml (5 $mg.ml^{-1}$: 50% *d3*-acetonitrile and 50% D_2O)**	**Volume of d3-acetonitrile in ml**	**Volume of mixture of H_2O/D_2O in ml (24% H_2O and 76% D_2O)**
10% acetonitrile (sample concentration 1 $mg.ml^{-1}$)	0.1	-	0.4
20% acetonitrile	0.2	-	0.3
30% acetonitrile	0.2	0.05	0.25
40% acetonitrile	0.2	0.1	0.2
50% acetonitrile	0.2	0.15	0.15
60% acetonitrile	0.2	0.2	0.1

4 Bibliography

1. G. Wulff, *Chem. Rev.*, 2002, **102**, 1-27.
2. P. Pasetto, S. C. Maddock and M. Resmini, *Anal. Chim. Acta*, 2005, **542**, 66-75.
3. D. Carboni, K. Flavin, A. Servant, V. Gouverneur and M. Resmini, *Chem.-A Eur. J.*, 2008, **14**, 7059-7065.
4. M. L. Casey, D. S. Kemp, K. G. Paul and D. D. Cox, *Journal Of Organic Chemistry*, 1973, **38**, 2294-2301.
5. F. Hollfelder, A. J. Kirby and D. S. Tawfik, *J. Am. Chem. Soc.*, 1997, **119**, 9578-9579.
6. *Nanosciences and nanotechnology: Opportunities and Uncertainties*, Accessed 2009, 2004.
7. D. M. Eigler and E. K. Schweizer, *Nature*, 1990, **344**, 524-526.
8. A. J. Heinrich, C. P. Lutz, J. A. Gupta and D. M. Eigler, *Science*, 2002, **298**, 1381-1387.
9. M. Brust, J. Fink, D. Bethell, D. J. Schiffrin and C. Kiely, *J. Chem. Soc.-Chem. Commun.*, 1995, 1655-1656.
10. C. J. Kiely, J. Fink, M. Brust, D. Bethell and D. J. Schiffrin, *Nature*, 1998, **396**, 444-446.
11. C. N. R. Rao, Cheetham, A. K. , *J. Mater. Chem.*, 2001, **11**, 2887-2894.
12. R. P. Feynman, *Miniaturization*, Reinhold, New-York, 1961.
13. M. Schulz, *Nature*, 1999, **399**, 729.
14. M. A. Reed and J. M. Tour, *Sci.Am.*, 2000, **282**, 86-93.
15. B. Kane, *Nature*, 1998, **393**, 11.
16. P. Tambasco de Oliveira, Nanci A., *Biomaterials*, 1994, **25**, 403.
17. F. Rosei, *J. Phys.-Condes. Matter*, 2004, **16**, S1373-S1436.
18. G. Tegart, *Nanotechnology: The Technology for the 21st Century*, APEC Centre for Technology Foresight, 2002.
19. J. Grunes, J. Zhu and G. A. Somorjai, *Chem. Commun.*, 2003, 2510-2510.
20. R. Schlogl and S. B. Abd Hamid, *Angew. Chem.-Int. Edit.*, 2004, **43**, 1628-1637.
21. E. Roduner, *Chem. Soc. Rev.*, 2006, **35**, 583-592.
22. J. S. Bradley, *Clusters and colloids*, VCH, Weinheim, 1994.
23. L. Rapino, *J. Am. Chem. Soc.*, 1941, **63**, 2745-2746.
24. D. Y. Cha and Parravan.G, *J. Catal.*, 1970, **18**, 200-&.
25. M. Haruta, T. Kobayashi, H. Sano and N. Yamada, *Chem. Lett.*, 1987, 405-408.
26. M. Haruta, N. Yamada, T. Kobayashi and S. Iijima, *J. Catal.*, 1989, **115**, 301-309.
27. M. T. Reetz and W. Helbig, *J. Am. Chem. Soc.*, 1994, **116**, 7401-7402.
28. R. M. Crooks, M. Q. Zhao, L. Sun, V. Chechik and L. K. Yeung, *Accounts Chem. Res.*, 2001, **34**, 181-190.
29. L. N. Lewis, *Chem. Rev.*, 1993, **93**, 2693-2730.
30. J. D. Aiken and R. G. Finke, *J. Mol. Catal. A-Chem.*, 1999, **145**, 1-44.
31. A. Roucoux, J. Schulz and H. Patin, *Chem. Rev.*, 2002, **102**, 3757-3778.
32. M. T. Reetz, M. Winter, R. Breinbauer, T. Thurn-Albrecht and W. Vogel, *Chem.-Eur. J.*, 2001, **7**, 1084-1094.

33. www.azonano.com/details.asp?ArticleID=1332, 2009.
34. N. Toshima, in *Fine Particles Science and Technology - from Micro to Nanoparticles*, ed. E. Pelizzetti, Kluwer Academic Publ, Dordrecht, Editon edn., 1996, vol. 12, pp. 371-383.
35. T. Sanji, Y. Ogawa, Y. Nakatsuka, M. Tanaka and H. Sakurai, *Chem. Lett.*, 2003, **32**, 980-981.
36. M. Q. Zhao, L. Sun and R. M. Crooks, *J. Am. Chem. Soc.*, 1998, **120**, 4877-4878.
37. www.inkline.gr/inkjet/newtech/tech/dispersion/, 2010.
38. M. Moreno-Manas and R. Pleixats, in *Advances in Heterocyclic Chemistry*, ed. A. R. Katritzky, Academic Press, Inc.; Academic Press Ltd., Editon edn., 1996, pp. 73-129.
39. G. T. Crisp, *Chem. Soc. Rev.*, 1998, **27**, 427-436.
40. P. Baumeister, W. Meyer, K. Oertle, G. Seifert and H. Steiner, *Chimia*, 1997, **51**, 144-146.
41. J. McChesney, *Spec. Chem.*, 1999, **6**, 98-100.
42. I. Shinkai, A. O. King and R. D. Larsen, *Pure Appl. Chem.*, 1994, **66**, 1551-1556.
43. M. T. Reetz, R. Breinbauer and K. Wanninger, *Tetrahedron Lett.*, 1996, **37**, 4499-4502.
44. M. T. Reetz and G. Lohmer, *Chem. Commun.*, 1996, 1921-1922.
45. M. T. Reetz and E. Westermann, *Angew. Chem.-Int. Edit.*, 2000, **39**, 165-+.
46. S. Klingelhofer, W. Heitz, A. Greiner, S. Oestreich, S. Forster and M. Antonietti, *J. Am. Chem. Soc.*, 1997, **119**, 10116-10120.
47. K. Mori, K. Yamaguchi, T. Hara, T. Mizugaki, K. Ebitani and K. Kaneda, *J. Am. Chem. Soc.*, 2002, **124**, 11572-11573.
48. B. M. Choudary, S. Madhi, N. S. Chowdari, M. L. Kantam and B. Sreedhar, *J. Am. Chem. Soc.*, 2002, **124**, 14127-14136.
49. N. A. Dhas, H. Cohen and A. Gedanken, *J. Phys. Chem. B*, 1997, **101**, 6834-6838.
50. J. Le Bars, U. Specht, J. S. Bradley and D. G. Blackmond, *Langmuir*, 1999, **15**, 7621-7625.
51. N. Miyaura, K. Yamada and A. Suzuki, *Tetrahedron Lett.*, 1979, 3437-3440.
52. C. Rocaboy and J. A. Gladysz, *New J. Chem.*, 2003, **27**, 39-49.
53. M. Bartz, J. Kuther, R. Seshadri and W. Tremel, *Angew. Chem.-Int. Edit.*, 1998, **37**, 2466-2468.
54. G. C. Bond, P. A. Sermon, G. Webb, D. A. Buchanan and P. B. Wells, *J. Chem. Soc.-Chem. Commun.*, 1973, 444-445.
55. S. Galvagno and G. Parravano, *J. Catal.*, 1978, **55**, 178-190.
56. M. Haruta, S. Tsubota, T. Kobayashi, H. Kageyama, M. J. Genet and B. Delmon, *J. Catal.*, 1993, **144**, 175-192.
57. A. Haruta, *Chem. Rec.*, 2003, **3**, 75-87.
58. M. Haruta, *Catal. Today*, 1997, **36**, 153-166.
59. M. Okumura, K. Tanaka, A. Ueda and M. Haruta, *Solid State Ion.*, 1997, **95**, 143-149.
60. Y. Z. Yuan, A. P. Kozlova, K. Asakura, H. L. Wan, K. Tsai and Y. Iwasawa, *J. Catal.*, 1997, **170**, 191-199.
61. G. Hyett, M. A. Green and I. P. Parkin, *J. Am. Chem. Soc.*, 2007, **129**, 15541-15548.

62. J. D. Grunwaldt, C. Kiener, C. Wogerbauer and A. Baiker, *J. Catal.*, 1999, **181**, 223-232.
63. Y. Takita, T. Imamura, Y. Mizuhara, Y. Abe and T. Ishihara, *Appl. Catal. B-Environ.*, 1992, **1**, 79-87.
64. L. Lietti, *Appl. Catal. B-Environ.*, 1996, **10**, 281-297.
65. J. F. Jia, K. Haraki, J. N. Kondo, K. Domen and K. Tamaru, *J. Phys. Chem. B*, 2000, **104**, 11153-11156.
66. C. Mohr, H. Hofmeister, M. Lucas and P. Claus, *Chem. Ing. Tech.*, 1999, **71**, 869-873.
67. D. A. Landsman, *Handbook of fuel cell*, Wiley, New-York, 2003.
68. F. Raimondi, G. G. Scherer, R. Kotz and A. Wokaun, *Angew. Chem.-Int. Edit.*, 2005, **44**, 2190-2209.
69. *US Pat.*
70. C. J. Brinker, *Sol-Gel Sceince: THe physics and Chemistry of Sol-Gels processing*, Academic Press, New-York, 1990.
71. T. H. Adachi, *Sol-Gel production*, Trans. Tech. Publ., Vetikon-Zurich, 1998.
72. D. C. L. Vasconcelos, *Materials Science and Engineering*, 2002, **A234**, 53-58.
73. G. M. Pajonk, *Applied Catalysis*, 1991, **72**, 217-266.
74. M. A. Cauqui and J. M. Rodriguezizquierdo, *J. Non-Cryst. Solids*, 1992, **147**, 724-738.
75. W. F. Maier, Dordrecht, 1995.
76. G. G. Lenzi, M. K. Lenzi, M. L. Baesso, A. C. Bento, L. M. M. Jorge and O. A. A. Santos, *J. Non-Cryst. Solids*, 2008, **354**, 4811-4815.
77. M. P. Coles, C. G. Lugmair, K. W. Terry and T. D. Tilley, *Chem. Mat.*, 2000, **12**, 122-131.
78. M. V. Polyakov, *Zhur. Fiz. Khim.*, 1931, **2**, 799-805.
79. K. Flavin and M. Resmini, *Anal. Bioanal. Chem.*, 2009, **393**, 437-444.
80. P. F. Holmes, M. Bohrer and J. Kohn, *Prog. Polym. Sci.*, 2008, **33**, 787-796.
81. G. Wulff and A. Sarhan, *Angewandte Chemie-International Edition*, 1972, **11**, 341-&.
82. H. Lalo, C. Ayela, E. Dague, C. Vieu and K. Haupt, *Lab Chip*, 2010, **10**, 1316-1318.
83. S. C. Zimmerman, M. S. Wendland, N. A. Rakow, I. Zharov and K. S. Suslick, *Nature*, 2002, **418**, 399-403.
84. J. B. Beil and S. C. Zimmerman, *Chemical Communications*, 2004, 488-489.
85. Y. Y. Zhang, J. Zhang, H. B. Son, J. Kong and Z. F. Liu, *J. Am. Chem. Soc.*, 2005, **127**, 17156-17157.
86. C. G. Xie, Z. P. Zhang, D. P. Wang, G. J. Guan, D. M. Gao and J. H. Liu, *Anal. Chem.*, 2006, **78**, 8339-8346.
87. Y. Li, H. H. Yang, Q. H. You, Z. X. Zhuang and X. R. Wang, *Anal. Chem.*, 2006, **78**, 317-320.
88. H. J. Wang, W. H. Zhou, X. F. Yin, Z. X. Zhuang, H. H. Yang and X. R. Wang, *J. Am. Chem. Soc.*, 2006, **128**, 15954-15955.
89. I. S. Chronakis, A. Jakob, B. Hagstrom and L. Ye, *Langmuir*, 2006, **22**, 8960-8965.
90. K. Yoshimatsu, L. Ye, J. Lindberg and I. S. Chronakis, *Biosens. Bioelectron.*, 2008, **23**, 1208-1215.

91. K. Yoshimatsu, L. Ye, P. Stenlund and I. S. Chronakis, *Chemical Communications*, 2008, 2022-2024.
92. I. S. Chronakis, B. Milosevic, A. Frenot and L. Ye, *Macromolecules*, 2006, **39**, 357-361.
93. N. Perez, M. J. Whitcombe and E. N. Vulfson, *J. Appl. Polym. Sci.*, 2000, **77**, 1851-1859.
94. N. Perez, M. J. Whitcombe and E. N. Vulfson, *Macromolecules*, 2001, **34**, 830-836.
95. S. R. Carter and S. Rimmer, *Adv. Mater.*, 2002, **14**, 667-670.
96. M. A. Markowitz, P. R. Kust, G. Deng, P. E. Schoen, J. S. Dordick, D. S. Clark and B. P. Gaber, *Langmuir*, 2000, **16**, 1759-1765.
97. L. Ye, P. A. G. Cormack and K. Mosbach, *Analytical Communications*, 1999, **36**, 35-38.
98. L. Ye and K. Mosbach, *J. Am. Chem. Soc.*, 2001, **123**, 2901-2902.
99. P. Spegel, L. Schweitz and S. Nilsson, *Anal. Chem.*, 2003, **75**, 6608-6613.
100. G. Ciardelli, B. Cioni, C. Cristallini, N. Barbani, D. Silvestri and P. Giusti, *Biosens. Bioelectron.*, 2004, **20**, 1083-1090.
101. O. Ramstrom and K. Mosbach, *Curr. Opin. Chem. Biol.*, 1999, **3**, 759-764.
102. D. K. Robinson and K. Mosbach, *J. Chem. Soc.-Chem. Commun.*, 1989, 969-970.
103. A. Leonhardt and K. Mosbach, *React. Polym.*, 1987, **6**, 285-290.
104. C. Alexander, H. S. Andersson, L. I. Andersson, R. J. Ansell, N. Kirsch, I. A. Nicholls, J. O'Mahony and M. J. Whitcombe, *Journal Of Molecular Recognition*, 2006, **19**, 106-180.
105. K. Ohkubo, Y. Urata, S. Hirota, Y. Honda, Y. Fujishita and T. Sagawa, *J. Mol. Catal.*, 1994, **93**, 189-193.
106. S. C. Liu and K. Mosbach, *Macromol. Rapid Commun.*, 1997, **18**, 609-615.
107. X. C. Liu and K. Mosbach, *Macromol. Rapid Commun.*, 1998, **19**, 671-674.
108. J. Matsui, I. A. Nicholls, I. Karube and K. Mosbach, *J. Org. Chem.*, 1996, **61**, 5414-5417.
109. A. G. Strikovsky, D. Kasper, M. Grun, B. S. Green, J. Hradil and G. Wulff, *J. Am. Chem. Soc.*, 2000, **122**, 6295-6296.
110. K. M. Shokat, C. J. Leumann, R. Sugasawara and P. G. Schultz, *Nature*, 1989, **338**, 269-271.
111. J. V. Beach and K. J. Shea, *J. Am. Chem. Soc.*, 1994, **116**, 379-380.
112. R. Muller, L. I. Andersson and K. Mosbach, *Makromolekulare Chemie-Rapid Communications*, 1993, **14**, 637-641.
113. J. Q. Liu and G. Wulff, *J. Am. Chem. Soc.*, 2008, **130**, 8044-8054.
114. K. Morihara, S. Kurihara and J. Suzuki, *Bull. Chem. Soc. Jpn.*, 1988, **61**, 3991-3998.
115. J. Heilmann and W. F. Maier, *Angew. Chem.-Int. Edit. Engl.*, 1994, **33**, 471-473.
116. A. Suzuki, M. Tada, T. Sasaki, T. Shido and Y. Iwasawa, *J. Mol. Catal. A-Chem.*, 2002, **182**, 125-136.
117. M. Tada, T. Sasaki, T. Shido and Y. Iwasawa, *Phys. Chem. Chem. Phys.*, 2002, **4**, 5899-5909.
118. B. R. Saunders and B. Vincent, *Adv. Colloid Interface Sci.*, 1999, **80**, 1-25.
119. W. O. Baker, *Ind Eng Chem*, 1949, **41**, 511.

120. H. Staudinger, *Berichte der Bunsen-Gesellschaft fuer Physikalische Chemie*, 1935, **68**, 1618.
121. M. Antonietti and C. Rosenauer, *Macromolecules*, 1991, **24**, 3434-3442.
122. W. Funke, O. Okay and B. Joos-Muller, in *Microencapsulation - Microgels - Iniferters*, Editon edn., 1998, vol. 136, pp. 139-234.
123. N. B. Graham and C. M. G. Hayes, *Macromol. Symp.*, 1995, **93**, 293-300.
124. N. B. Graham and A. Cameron, *Pure Appl. Chem.*, 1998, **70**, 1271-1275.
125. S. C. Maddock, P. Pasetto and M. Resmini, *Chem. Commun.*, 2004, 536-537.
126. M. Resmini, R. Vigna, C. Simms, N. J. Barber, E. P. HagiPavli, A. B. Watts, C. Verma, G. Gallacher and K. Brocklehurst, *Biochem. J.*, 1997, **326**, 279-287.
127. V. A. Roberts, J. Stewart, S. J. Benkovic and E. D. Getzoff, *J. Mol. Biol.*, 1994, **235**, 1098-1116.
128. G. Wulff, B. O. Chong and U. Kolb, *Angewandte Chemie-International Edition*, 2006, **45**, 2955-2958.
129. Y. Y. Chiu and L. J. Lee, *J. Polym. Sci. Pol. Chem.*, 1995, **33**, 257-267.
130. Y. Li, *Appl Catal A: Gen*, 2007, **328**, 525-528.
131. Z. Y. Cheng and Y. Z. Li, *J. Mol. Catal. A-Chem.*, 2006, **256**, 9-15.
132. J. Wagner, R. A. Lerner and C. F. Barbas, *Science*, 1995, **270**, 1797-1800.
133. D. Astruc, F. Lu and J. R. Aranzaes, *Angew. Chem.-Int. Edit.*, 2005, **44**, 7852-7872.
134. J. Berg, Tymoczko, J., L., Stryer, L., *Biochemistry*, 2004.
135. S. Q. Liu, Z. H. Meng, Y. X. Fu and K. Q. Zhang, *J. Mol. Model.*, 2010, **16**, 17-28.
136. J. L. Gao, K. L. Byun and R. Kluger, in *Orotidine Monophosphate Decarboxylase: Mechanistic Dialogue*, Springer-Verlag Berlin, Berlin, Editon edn., 2004, vol. 238, pp. 113-136.
137. M. Resmini, S. Gul, S. Carter, S. Sonkaria, C. M. Topham, G. Gallacher and K. Brocklehurst, *Biochem. J.*, 2000, **346**, 117-125.
138. G. Boucher, B. Said, E. L. Ostler, M. Resmini, K. Brocklehurst and G. Gallacher, *Biochem. J.*, 2007, **401**, 721-726.
139. B. H. Tan, P. Ravi, L. N. Tan and K. C. Tam, *J. Colloid Interface Sci.*, 2007, **309**, 453-463.
140. F. Hollfelder, A. J. Kirby, D. S. Tawfik, K. Kikuchi and D. Hilvert, *J. Am. Chem. Soc.*, 2000, **122**, 1022-1029.
141. H. Shulman and E. Keinan, *Org. Lett.*, 2000, **2**, 3747-3750.
142. R. Muller, E. W. Debler, M. Steinmann, F. P. Seebeck, I. A. Wilson and D. Hilvert, *J. Am. Chem. Soc.*, 2007, **129**, 460-461.
143. D. Rothlisberger, O. Khersonsky, A. M. Wollacott, L. Jiang, J. DeChancie, J. Betker, J. L. Gallaher, E. A. Althoff, A. Zanghellini, O. Dym, S. Albeck, K. N. Houk, D. S. Tawfik and D. Baker, *Nature*, 2008, **453**, 190-U194.
144. C. Binet, S. Ferrere, A. Lattes, E. Laurent, J. D. Marty, M. Mauzac, A. F. Mingotaud, G. Palaprat and M. Weyland, *Analytica Chimica Acta*, 2007, **591**, 1-6.
145. L. Pauling, *Chem Eng News*, 1946, **24**, 1375.
146. T. R. Ward, *Angew. Chem.-Int. Edit.*, 2008, **47**, 7802-7803.
147. E. Yilmaz and Z. Kucukyavuz, *Polymer*, 1993, **34**, 145-149.

148. N. Ikeda, H. Miyasaka, T. Okada and N. Mataga, *J. Am. Chem. Soc.*, 1983, **105**, 5206-5211.
149. J. Hidalgo, A. Sanchez-Coronilla, M. A. Munoz, C. Carmona and M. Balon, *J. Lumin.*, 2007, **127**, 671-677.
150. Y. Tunc, N. Hasirci, A. Yesilada and K. Ulubayram, *Polymer*, 2006, **47**, 6931-6940.
151. J. Brandrup, *Polymer Handbook*, Jonh Wiley and Sons, New york, 2005.
152. G. Wulff, J. Vietmeier and H. G. Poll, *Makromolekulare Chemie-Macromolecular Chemistry and Physics*, 1987, **188**, 731-740.
153. M. Glad, P. Reinholdsson and K. Mosbach, *React. Polym.*, 1995, **25**, 47-54.
154. X. C. Dong, H. Sun, X. Y. Lu, H. B. Wang, S. X. Liu and N. Wang, *Analyst*, 2002, **127**, 1427-1432.
155. M. Kempe, *Anal. Chem.*, 1996, **68**, 1948-1953.
156. G. Wulff, W. Vesper, R. Grobeeinsler and A. Sarhan, *Makromolekulare Chemie-Macromolecular Chemistry And Physics*, 1977, **178**, 2799-2816.
157. A. G. Mayes and M. J. Whitcombe, *Adv. Drug Deliv. Rev.*, 2005, **57**, 1742-1778.
158. J. Q. Liu and G. Wulff, *J. Am. Chem. Soc.*, 2004, **126**, 7452-7453.
159. S. Subrahmanyam, S. A. Piletsky, E. V. Piletska, B. N. Chen, K. Karim and A. P. F. Turner, *Biosens. Bioelectron.*, 2001, **16**, 631-637.
160. Y. Yamamoto and A. Wakisaka, *J. Chem. Soc.-Faraday Trans.*, 1997, **93**, 1405-1408.
161. C. S. Wilcox, J. C. Adrian, T. H. Webb and F. J. Zawacki, *J. Am. Chem. Soc.*, 1992, **114**, 10189-10197.
162. B. A. Blight, A. Camara-Campos, S. Djurdjevic, M. Kaller, D. A. Leigh, F. M. McMillan, H. McNab and A. M. Z. Slawin, *J. Am. Chem. Soc.*, 2009, **131**, 14116-14122.
163. C. Ammann, P. Meier and A. E. Merbach, *J. Magn. Reson.*, 1982, **46**, 319-321.
164. A. E. Derome and S. Bowden, *Chem. Rev.*, 1991, **91**, 1307-1320.
165. S. Sharif, I. G. Shenderovich, L. Gonzalez, G. S. Denisov, D. N. Silverman and H. H. Limbach, *J. Phys. Chem. A*, 2007, **111**, 6084-6093.
166. F. J. Schork, Y. W. Luo, W. Smulders, J. P. Russum, A. Butte and K. Fontenot, in *Polymer Particles*, Springer-Verlag Berlin, Berlin, Editon edn., 2005, vol. 175, pp. 129-255.
167. J. Ugelstad, M. S. Elaasser and Vanderho.Jw, *Journal of Polymer Science Part C-Polymer Letters*, 1973, **11**, 503-513.
168. A. Matsumoto, in *Synthesis and Photosynthesis*, Springer-Verlag Berlin, Berlin 33, Editon edn., 1995, vol. 123, pp. 41-80.
169. J. S. Downey, R. S. Frank, W. H. Li and H. D. H. Stover, *Macromolecules*, 1999, **32**, 2838-2844.
170. A. Biffis, N. B. Graham, G. Siedlaczek, S. Stalberg and G. Wulff, *Macromolecular Chemistry And Physics*, 2001, **202**, 163-171.
171. Y. Huang, *Makromolekulare Chemie-Macromolecular Chemistry and Physics*, 1985, **186**, 273.
172. F. W. Billmeyer, *Textbook of Polymer Science*, Wiley and Sons, New-York, 1984.
173. P. Pasetto, Queen Mary University of London, 2005.
174. K. Brocklehurst, M. Resmini and C. M. Topham, *Methods*, 2001, **24**, 153-167.

175. C. J. Allender, O. K. Castell, P. R. Davies, S. Fiddy, J. Hedin-Dahlstrom and M. Stockenhuber, *Chem. Commun.*, 2009, 165-167.
176. D. S. Kemp and K. G. Paul, *J. Am. Chem. Soc.*, 1975, **97**, 7305-7312.
177. D. J. McLennan, *Quart. Rev Chem Soc*, 1967, **21**, 491.
178. R. A. Copeland, *Enzymes: A practical introduction to structures, mechanisms and data analysis*, Wiley VCH, New-York, 2000.
179. S. N. Thorn, R. G. Daniels, M. T. M. Auditor and D. Hilvert, *Nature*, 1995, **373**, 228-230.
180. A. G. Ogston, *Nature*, 1948, **163**, 963.
181. A. D. Mesecar and D. E. Koshland, *Nature*, 2000, **403**, 614-615.
182. Y. L. Xu, Z. S. Liu, H. F. Wang, C. Yan and R. Y. Gao, *Electrophoresis*, 2005, **26**, 804-811.
183. http://www.chemical-ecology.net/java/solvents.htm, Accessed 2010.
184. M. Dekker, *Encyclopedia of Emulsion Technology*, New-York, 1983.
185. S. S. Dukhin, *Dynamic of Adsorption at Liquid Interfaces*, Elsevier, Amsterdam, 1995.
186. E. Dickinson, *An introduction of Food Colloids*, Oxford Univ Press, 1992.
187. D. Myers, *Surfaces, Interfaces, and colloids: Principles and Applications*, John Wiley & Sons, Inc., 1999.
188. R. Barreiro-Iglesias, C. Alvarez-Lorenzo and A. Concheiro, *Int. J. Pharm.*, 2003, **258**, 179-191.
189. E. S. Ahuja and J. P. Foley, *J. Chromatogr. A*, 1994, **680**, 73-83.
190. L. Schweitz, L. I. Andersson and S. Nilsson, *Analyst*, 2002, **127**, 22-28.
191. P. B. Weisz, *Science*, 1973, **179**, 433-440.
192. K. Movagarnejad, M. Sohrabi, T. Kaghazchi and F. Vahabzadeh, *Biochem. Eng. J.*, 2000, **4**, 197-206.
193. H. S. Andersson, J. G. Karlsson, S. A. Piletsky, A. C. Koch-Schmidt, K. Mosbach and I. A. Nicholls, *Journal Of Chromatography A*, 1999, **848**, 39-49.
194. H. S. Andersson, J. G. Karlsson, S. A. Piletsky, A. C. Koch-Schmidt, K. Mosbach and I. A. Nicholls, *J. Chromatogr. A*, 1999, **848**, 39-49.
195. S. J. Li, X. Huang, M. X. Zheng and W. K. Li, *Anal. Bioanal. Chem.*, 2008, **392**, 177-185.
196. H. G. Craighead, *Science*, 2000, **290**, 1532-1535.
197. Malvern, ed. Malvern, Editon edn., 1997.
198. Malvern, *Zetasizer user manual*, Accessed November, 2009.
199. Z. L. Wang, *Adv. Mater.*, 2003, **15**, 1497-1514.
200. P. Buseck, Eyring, L., *High Resolution Transmission Microscope: theory and applications*, Oxford Univ Press, New-York, 1989.
201. G. E. Bacon, *Neutron Scattering in Chemistry*, London, 1977.
202. ISIS, *Isis world webpage*, Accessed April, 2010.
203. S. Rogers, Heenan, R., *A rough guide to FISH*, Isis, Didcot, 2008.